


# TARGETING THIOREDOXIN SYSTEM TO IMPROVE RADIOTHERAPEUTIC RESPONSE OF BRAIN CANCERS

**ANQI YAO**

**(MBBS, MMed)**

**Thesis submitted to the University of Nottingham for the degree of Doctor of Philosophy**

**June 2019**

# Abstract

Radiotherapy is often prescribed for brain cancer, particularly high-grade malignant gliomas. Efficacy is, however, often limited by radioresistance. The thioredoxin (Trx) system, a key antioxidant pathway in defence against oxidative stress, represents a potentially attractive target to overcome such resistance. Trx system alterations contribute to altered treatment response in a number of tumour types but information is lacking in brain tumours. The aim of the current study is to explore the potentially prognostic role of Trx system proteins in different types brain tumours; and investigate the chemotherapeutic and radiosensitising effects of a novel TrxR inhibitor IQ10 on brain cancer cells and the mechanisms underlying its action.

Expression of Trx system proteins was evaluated in four different brain tumour types by immunohistochemistry. A panel of five different brain cancer cell lines were used in this study: SNB19 (adult glioblastoma), SF188 and KNS42 (paediatric glioblastoma), and DAOY and UW228-3 (medulloblastoma); and a normal cell type, MRC5 lung fibroblasts, was used for comparing drug cytotoxicity. Professor Chris Moody's group (School of Chemistry, University of Nottingham) developed a series of Indolequinone (IQ) compounds that potently inhibited TrxR activity in pancreatic cancer cells. One of the most potent IQs, IQ10, was assessed for its inhibition of TrxR activity and Trx family expression in brain cancer cells using the insulin reduction assay and Western blotting respectively. The cellular cytotoxicity of IQ10 was evaluated using growth curves, resazurin reduction and clonogenic survival assays under both normoxic and hypoxic (1% $O_2$) conditions and in 2D *vs.* 3D spheroid cultures. Validation of TrxR as an important target for IQ10 in brain cancer cells was carried out using an siRNA approach. IQ10's role in regulating radioresponse of brain cancer cells was examined via clonogenic assays. In addition, intracellular ROS levels were determined by $H_2$DCFDA flow cytometry and γH2AX foci by immunofluorescence staining. Expression of genes associated with epithelial-mesenchymal transition was examined by RT$^2$ Profiler$^{TM}$ PCR Array.

The retrospective immunohistochemical study demonstrated that Trx system proteins were expressed to variable levels across a variety of brain tumour types, with high expression of cytoplasmic TrxR consistently correlating with a worse prognosis in all tumour types, suggesting that it is potentially a very important therapeutic target in brain cancers generally. *In vitro* results showed that IQ10 treatment significantly inhibited TrxR activity in a dose-dependent manner but did not affect the expression levels of Trx system proteins in brain cancer cells. IQ10 exhibited potent single agent anti-proliferative and cytotoxic effects against brain cancer cells under both normoxic and hypoxic conditions in 2D and 3D systems, with IC50s in the submicromolar/low micromolar range. IQ10 was up to ~1000 fold more potent than temozolomide, the agent used clinically to treat brain tumours and used as a comparator in the current study. IQ10 seemed to preferentially kill brain cancer cells but spare normal fibroblasts MRC5. More importantly, TrxR was found to be a promising radiobiological target in that inhibition of TrxR by IQ10 substantially sensitised both 2D and 3D cultured brain cancer cells to radiation (sensitiser enhancement ratio's ranging between 1.2 - 1.7), with such radiosensitising effect being due, in part, to functional inhibition of TrxR, which made cells less able to deal with oxidative stress, leading to oxidative DNA damage. In addition to its cytotoxic and radiosensitising effects, IQ10 showed potential to inhibit invasion/migration as treatment significantly downregulated EMT associated gene expression in brain cancer cells.

Collectively, although further confirmation is required both *in vitro* and *in vivo*, the current study highlights TrxR as a potential therapeutic target in brain cancers and suggests that IQ10 could be a promising agent, either single or combined with radiation, to improve patient outcome.

# Presentations and awards arising from this thesis

## Conference presentations

Oral presentation “Targeting redox homeostasis to improve radiotherapeutic response of brain cancer.” Radiation Research Society (RRS) Annual Meeting 2018, September 23-26, 2018, Chicago, USA.

Poster presentation “Targeting redox proteins to improve radiotherapeutic response of brain cancer.” The Association for Radiation Research (ARR) Annual Meeting 2017, June 26-28, Oxford, UK.

## Awards

2018 Radiation Research Society (RRS) SIT Travel Award.

2018 The British Association for Cancer Research (BACR) Student Travel Award.

2018 University of Nottingham School of Medicine Travel Prize.

2018 The Great Britain-China Educational Trust (GBCET) Chinese Students Award.

2018 The Henry Lester Trust Student Grant.

2017 University of Nottingham Graduate School Travel Prize.

2017 Association for Radiation Research (ARR) Travel Bursary.

# Acknowledgements

I would like to express my greatest gratitude to my supervisor, Prof. Stewart G. Martin, for his invaluable guidance, advice and support throughout this project. His kindness and patience are greatly appreciated.

I would like to thank the China Scholarship Council (CSC) and the University of Nottingham for funding my PhD program over the past 3 years. Also, I would like to thank the Great Britain-China Educational Trust (GBCET) and the Henry Lester Trust for their financial support/awards during my thesis pending time.

I am deeply grateful to Dr. Sarah J. Storr and Dr. Aula Ammar for their teaching, valuable discussions and help. Thank you to prof. Richard Grundy and Mr. Stuart Smith for providing brain tumour tissue microarrays and Dr. Beth Coyle for brain cancer cell lines. Also, I would like to thank Lisa Storer and Dr. Maria Estevez Cebrero for their assistance with the clinical data. A special big thank-you goes to everyone past and present in the Academic Unit of Clinical Oncology. Especially to Xuan Pu, Siwei Zhang, Khaled Alhadyan, Nurul Abdullah, Bhudsaban Sukkarn, Radhika Aiyappa, Richa Vasan, and Holly Nicholls for their motivation, support and friendship. In addition, I want to thank Tianhui Liu and Kuo Huang for their friendship and encouragement, and for making my life much easier, fun and colourful in Nottingham.

Last, but never least, I want to say thank-you to my parents and all my family members for their endless love and support throughout my life. I am also indebted to my husband, Zheng Wang, for his taking care, support and understanding over the past 8 years, for always standing by my side without doubt, for companying me all the time and filling every day of my life.

I dedicate this thesis to my grandmother, Yuping Zhu, who passed away last year and I will always miss her.

# Abbreviations

| | |
|---|---|
| 2D | two-dimensional |
| 2-DG | 2-deoxy-D-glucose |
| 3D | three-dimensional |
| 3D-CRT | 3D conformal radiotherapy |
| | |
| AF | auranofin |
| AIF | apoptosis-inducing factor |
| AP-1 | adaptor protein 1 |
| APL | acute promyelocytic leukaemia |
| ASK-1 | apoptosis signal-regulating kinase 1 |
| ATCC | American Type Culture Collection |
| ATM | ataxia telangiectasia mutated |
| ATO | arsenic trioxide |
| ATR | ataxia-telangiectasia and Rad3 related protein |
| | |
| BBB | blood-brain barrier |
| BCNU | 1,3-bis-(2-chloro-ethyl)-1-nitrosourea |
| BCRP | breast cancer related protein |
| BSA | bovine serum albumin |
| | |
| CA9 | carbonic anhydrase 9 |
| CBTRC | Children's Brain Tumour Research Centre |
| CBTRUS | Central Brain Tumour Registry of the United States |
| CDH1 | cadherin-1 |
| CDK | cyclin-dependent kinase |
| CI | confidence interval |
| CLL | chronic lymphocytic leukaemia |
| cm | centimetre |
| CNS | central nervous system |
| CSF | cerebrospinal fluid |
| CSI | craniospinal irradiation |
| CT | computerised tomography |
| | |
| DAB | 3, 3'-diaminobenzidine |
| DDR | DNA damage response |
| df | degree of freedom |
| $dH_2O$ | distilled water |
| DIPG | diffuse intrinsic pontine glioma |
| DMSO | dimethyl sulfoxide |
| DSB | double-strand break |
| DUOX | dual oxidase |
| | |
| ECACC | European Collection of Authenticated Cell Cultures |
| ECM | extracellular matrix |
| EDTA | ethylenediaminetetraacetic acid |

| | |
|---|---|
| EGFR | epidermal growth factor receptor |
| EMT | epithelial mesenchymal transition |
| EORTC | European Organisation for Research and Treatment of Cancer |
| ER | endoplasmic reticulum |
| ER | estrogen receptor |
| FACS | fluorescence-activated cell sorting |
| FAD | flavin adenine dinucleotide |
| FDA | Food and Drug Administration |
| FITC | fluorescein isothiocyanate |
| FL | fluorescent light |
| FSRT | fractionated stereotactic radiotherapy |
| GPx | glutathione peroxidase |
| GR | glutathione reductase |
| Grx | glutaredoxin |
| GSH | glutathione |
| GSSG | glutathione disulfide |
| GST | glutathione S-transferase |
| Gy | gray |
| $H_2$DCF-DA | 2',7'-dichlorodihydrofluorescein diacetate |
| $H_2O_2$ | hydrogen peroxidase |
| HDAC | histone deacetylase |
| H&E | haematoxylin and eosin |
| HGG | high-grade glioma |
| HIF-1α | hypoxia-inducible factor-1α |
| HNSCC | head and neck squamous cell carcinoma |
| HOCl | hypochlorous acid |
| HR | hazard radio |
| HRP | horseradish peroxidase |
| IC50 | half maximal inhibitory concentration |
| ICC | intraclass correlation co-efficient |
| IDH1/2 | isocitrate dehydrogenase 1/2 |
| IHC | immunohistochemistry |
| IMRT | intensity-modulated radiation therapy |
| IMS | industrial methylated spirit |
| IQ | indolequinone |
| IR | ionising radiation |
| IV2 | 1-methyl-1-propyl-2-imidazolyl disulfide |
| kDa | kilo dalton |
| KPS | Karnofsky Performance Status |
| LET | linear energy transfer |
| LGG | low-grade glioma |

| | |
|---|---|
| M | molar |
| MB | medulloblastoma |
| MET | mesenchymal-epithelial transition |
| MFI | median fluorescence intensity |
| MGd | motexafin gadolinium |
| MGMT | methylguanine-DNA-methyl transferase |
| mGy | milligrays |
| ml | millilitre |
| MLC | multi-leaf collimator |
| mM | millimolar |
| MMC | mitomycin C |
| MMP | matrix metalloproteases |
| MRI | magnetic resonance imaging |
| MRP1 | multidrug resistance protein 1 |
| N/A | not applicable |
| NADPH | nicotinamide adenine dinucleotide phosphate |
| NCCN | National Comprehensive Cancer Network |
| NCI-60 | National Cancer Institute-60 |
| ND | not determined |
| NF-1 | neurofibromatosis type 1 |
| NF-κB | nuclear factor kappa-light-chain-enhancer of activated B cells |
| NOX | NADPH oxidase |
| NQO1 | NADPH: quinone oxidoreductase 1 |
| Nrf-2 | nuclear factor-like 2 |
| OS | overall survival |
| PARP | poly-ADP-ribose polymerase |
| PBS | phosphate buffered saline |
| PCV | procarbazine, lomustine, and vincristine |
| PE | plating efficiency |
| PFS | progression free survival |
| PGP | p-glycoprotein |
| PQQ | pyrroloquinoline quinone |
| Prx | peroxiredoxin |
| PX-12 | 1-methyl-propyl-2-imidazolyl disulfide |
| qRT-PCR | quantitative reverse transcription polymerase chain reaction |
| Ref-1 | redox factor-1 |
| RNAi | RNA interference |
| ROS | reactive oxygen species |
| RTOG | Radiation Therapy Oncology Group |
| SACC | salivary adenoid cystic carcinoma |
| SCC | squamous cell carcinoma |
| SD | standard deviation |

| | |
|---|---|
| SDS-PAGE | sodium dodecyl sulfate poly-acrylamide gel electrophoresis |
| SEGA | subependymal giant cell astrocytoma |
| SER | sensitizer enhancement ratio |
| SF | surviving fraction |
| shRNA | short hairpin RNA |
| siRNA | small interference RNA |
| SMO | smoothened |
| SOD | superoxide dismutase |
| SP-1 | specificity protein 1 |
| SRS | stereotactic radiosurgery |
| SSB | single-strand break |
| STR | short tandem repeat |
| | |
| TBP2 | thioredoxin binding protein 2 |
| TBS | Tris buffered saline |
| TERTp | telomerase reverse transcriptase promoter |
| TMA | tissue microarray |
| TNFα | tumour necrosis factor α |
| TS | tuberous sclerosis |
| Trx | thioredoxin |
| TrxR | Trx reductase |
| TTFields | tumour-treating fields |
| TxNIP | thioredoxin-interacting protein |
| TXNL2 | redox protein thioredoxin-like 2 |
| | |
| ULA | ultra-low attachment |
| | |
| V | voltage |
| VEGF | vascular endothelial growth factor |
| VDUP1 | vitamin D3 up-regulated protein 1 |
| VMAT | volumetric-modulated arc therapy |
| | |
| WBRT | whole brain radiotherapy |
| WHO | World Health Organisation |
| | |
| µg | microgram |
| µg/mL | microgram per mililiter |
| µl | microliter |
| µM | micromolar |
| | |
| $\chi^2$ | Pearson Chi Square test of association |

# Table of Contents

**ABSTRACT**.....**I**

**PRESENTATIONS AND AWARDS ARISING FROM THIS THESIS** ..... **III**

**ACKNOWLEDGEMENTS** ..... **IV**

**ABBREVIATIONS**..... **V**

**LIST OF TABLES** ..... **XIII**

**LIST OF FIGURES**..... **XV**

**CHAPTER 1 GENERAL INTRODUCTION**..... **1**

*1.1 GENERAL INTRODUCTION TO BRAIN TUMOURS*..... *2*
1.1.1 Epidemiology and classification ..... 2
1.1.2 Prognostic and predictive factors ..... 8
1.1.3 Treatment strategies ..... 14
*1.2 ROS, REDOX HOMEOSTASIS, THE THIOREDOXIN SYSTEM AND CANCER*..... *21*
1.2.1 Antioxidants and redox protein families ..... 22
1.2.2 Role of Trx system in cancer ..... 31
*1.3 RADIOTHERAPY OF BRAIN TUMOURS*..... *35*
1.3.1 Basics of radiotherapy ..... 35
1.3.2 Radiotherapy options in brain tumours ..... 39
*1.4 HYPOTHESES AND AIMS* ..... *45*
1.4.1 Hypotheses ..... 45
1.4.2 Aims and objectives..... 46

**CHAPTER 2 CLINICAL IMPORTANCE OF THIOREDOXIN SYSTEM PROTEIN EXPRESSION IN BRAIN TUMOURS**.....**47**

*2.1 INTRODUCTION* ..... *48*
2.1.1 Challenging issues in brain tumours..... 48
2.1.2 Trx system and its association with clinical outcome in brain tumours ..... 49
2.1.3 Hypotheses and aims ..... 52
*2.2 MATERIALS AND METHODS*..... *52*
2.2.1 Cell lines and culture conditions ..... 52
2.2.2 Subculture ..... 53
2.2.3 Cryopreservation and cell recovery ..... 54
2.2.4 Cell lysis and protein extraction ..... 54
2.2.5 Western blotting ..... 55
2.2.6 Clinical samples ..... 56
2.2.7 Antibody optimisation..... 64
2.2.8 TMAs and Immunohistochemistry ..... 64
2.2.9 Immunohistochemical scoring ..... 66
2.2.10 Statistical analysis..... 68
*2.3 RESULTS* ..... *68*

2.3.1 Antibody specificity and IHC optimisation ..... 68
2.3.2 Staining pattern and frequency of Trx system expression in brain tumours ..... 71
2.3.3 Relationship of Trx system expression with clinicopathological variables and clinical outcome in the adult GBM cohort. ..... 77
2.3.4 Relationship of Trx system expression with clinicopathological variables and clinical outcome in the paediatric LGG cohort. ..... 79
2.3.5 Relationship of Trx system expression with clinicopathological variables and clinical outcome in the paediatric HGG cohort. ..... 81
2.3.6 Relationship of Trx system expression with clinicopathological variables and clinical outcome in the paediatric MB cohort. ..... 83
2.3.7 Comparison of protein expression between different regions in adult GBM patients ..... 85
2.3.8 Comparison of protein expression between different tumour types87
2.3.9 Comparison of protein expression between different tumour grades in paediatric gliomas..... 89
*2.4 DISCUSSION ..... 92*
*2.5 CONCLUSIONS..... 99*

**CHAPTER 3 *IN VITRO* DRUG SENSITIVITY OF THE TRXR INHIBITOR IQ10 IN BRAIN CANCER CELLS ..... 100**

*3.1 INTRODUCTION ..... 101*
3.1.1 TrxR inhibitors in cancer therapy ..... 101
3.1.2 Trx system and hypoxia ..... 107
3.1.3 Three-dimensional (3D) spheroid culture ..... 110
3.1.4 Hypotheses and Aims ..... 111
*3.2 MATERIALS AND METHODS..... 112*
3.2.1 Cell lines and culture conditions ..... 112
3.2.2 Drug preparation and treatments..... 112
3.2.3 Cell growth curves ..... 113
3.2.4 Clonogenic survival assay ..... 114
3.2.5 Protein concentration determination and insulin reduction assay (TrxR activity)..... 115
3.2.6 Western blotting ..... 116
3.2.7 TrxR siRNA experiments ..... 116
3.2.8 3D spheroids experiments..... 119
3.2.9 Statistical analysis..... 122
*3.3 RESULTS ..... 122*
3.3.1 Basic characteristics of brain cancer cell lines ..... 122
3.3.2 Role of IQ10 in regulating protein activity and expression..... 124
3.3.3 Cytotoxicity of IQ10 on brain cancer cells cultured in 2D..... 133
3.3.4 Cytotoxicity of IQ10 on brain cancer spheroids..... 143
3.3.5 Knockdown of TrxR using siRNA..... 148
*3.4 DISCUSSIONS ..... 151*

*3.5 CONCLUSIONS ..... 165*

**CHAPTER 4 EFFECTS OF THE NOVEL TRXR INHIBITOR IQ10 ON THE RADIORESPONSE OF BRAIN CANCER CELLS ..... 166**

*4.1 INTRODUCTION ..... 167*
4.1.1 Radiosensitisers in brain tumours ..... 167
4.1.2 Redox homeostasis modulators in radiotherapy ..... 173
4.1.3 Radioresponse of cells in 3D culture ..... 176
4.1.4 Hypotheses and Aims ..... 177
*4.2 METHODS ..... 177*
4.2.1 Cell irradiation ..... 177
4.2.2 Drug-radiation combination ..... 178
4.2.3 TrxR knockdown and irradiation ..... 179
4.2.4 Measurement of intracellular ROS levels ..... 179
4.2.5 Immunofluorescence ..... 180
4.2.6 Statistical analysis ..... 181
*4.3 RESULTS ..... 181*
4.3.1 Intrinsic radiosensitivity of brain cancer cell lines ..... 181
4.3.2 Effect of IQ10 on radiosensitivity of brain cancer cells ..... 184
4.3.3 Downregulation of TrxR protein expression radiosensitises brain cancer cells ..... 189
4.3.4 IQ10 induced ROS production ..... 191
4.3.5 IQ10 increases γH2AX formation alone and in response to radiation 193
*4.4 DISCUSSION ..... 194*
*4.5 CONCLUSIONS ..... 204*

**CHAPTER 5 EFFECT OF IQ10 ON EMT-RELATED GENE EXPRESSION ..... 205**

*5.1 INTRODUCTION ..... 206*
5.1.1 Epithelial-mesenchymal transition (EMT) ..... 206
5.1.2 Role of Trx system in EMT ..... 208
5.1.3 Hypotheses and Aims ..... 209
*5.2 MATERIALS AND METHODS ..... 209*
5.2.1 RNA isolation ..... 209
5.2.2 cDNA synthesis ..... 210
5.2.3 Real-time EMT PCR array ..... 210
5.2.4 Statistical analysis ..... 211
*5.3 RESULTS ..... 211*
*5.4 DISCUSSION ..... 221*
*5.5 CONCLUSIONS ..... 223*

**CHAPTER 6 GENERAL DISCUSSION ..... 224**

*6.1 GENERAL DISCUSSION ..... 225*
*6.2 LIMITATIONS AND SUGGESTIONS FOR FUTURE WORK ..... 232*
*6.3 FINAL CONCLUSIONS ..... 237*

**REFERENCES ……239**

**APPENDIX A: SUPPLEMENTARY INFORMATION FOR CHAPTER 2 .....294**

**APPENDIX B: SUPPLEMENTARY INFORMATION FOR CHAPTER 4 .....311**

# List of Tables

Table 1.1 Summary of cellular antioxidants. ..... 23
Table 2.1 List of antibodies used in Western Blotting. ..... 56
Table 2.2 Clinicopathological variables of the adult GBM cohort. ..... 59
Table 2.3 Clinicopathological variables of the paediatric LGG and HGG cohorts…….. ..... 61
Table 2.4 Clinicopathological variables of the MB patient cohort. ..... 63
Table 2.5 Intra-class correlation coefficient (ICC) analysis of Trx, TrxR and TxNIP scoring across different brain tumour cohorts. ..... 67
Table 2.6 X-tile cut points for stratification of TrxR, Trx and TxNIP expression in all four brain tumour cohorts. ..... 68
Table 2.7 The median scores and ranges of TrxR, Trx and TxNIP expression in brain tumour cohorts. ..... 76
Table 2.8 Multivariate Cox proportional hazards analysis for predictors of overall survival in medulloblastoma patients. ..... 85
Table 3.1 The procedure of siRNA transfection experiments. ..... 119
Table 3.2 Plating efficiencies of different cell lines. ..... 124
Table 3.3 Summary of the proliferation assay IC50 values of the brain cancer and fibroblast cells treated with IQ10 and TMZ. ..... 135
Table 3.4 Comparison of proliferation assay IC50 values (μM) of IQ10 between normoxia and hypoxia in DAOY and UW228-3 cells. ..... 139
Table 3.5 The clonogenic assay IC50 values (μM) of TMZ and IQ10 in various cell lines post 48 h drug exposure. ..... 141
Table 3.6 Comparison of clonogenic assay IC50 values (μM) of IQ10 between normoxia and hypoxia in DAOY and UW228-3 cells post 48 h drug exposure……. ..... 143
Table 4.1 Radiobiologic parameters of different brain cancer cell lines in 2D cultures……. ..... 182
Table 4.2 Radiobiologic parameters of brain cancer cells treated with IQ10 and/or radiation in 2D culture. ..... 186
Table 4.3 Radiobiologic parameters of brain cancer spheroids treated with IQ10 and/or radiation. ..... 189
Table 4.4 Radiobiologic parameters of brain cancer cells transfected with TrxR siRNA or negative siRNA control. ..... 191
Table 5.1 Reverse-transcription mix. ..... 210
Table 5.2 PCR components mix. ..... 211
Table 5.3 Profiler PCR array results (vehicle control UW228-3 cells vs. DAOY cells)……. ..... 213
Table 5.4 Profiler PCR array results for DAOY cells (IQ10-treated group vs. vehicle control group at two time points). ..... 216
Table 5.5 Profiler PCR array results for UW228-3 cells (IQ10-treated group vs. vehicle control group at two time points). ..... 219

Table 6.1 Results summary..... 238

# List of Figures

Figure 1.1 Redox proteins and ROS regulation..... 26
Figure 2.1 The specificity of anti-TrxR, anti-Trx and anti-TxNIP antibodies was determined in Western blotting by using various cell lines.. ..... 70
Figure 2.2 Representative photomicrographs of Trx, TrxR and TxNIP expression in adult GBM..... 72
Figure 2.3 Representative photomicrographs of Trx, TrxR and TxNIP expression in paediatric LGG.. ..... 73
Figure 2.4 Representative photomicrographs of Trx, TrxR and TxNIP expression in paediatric HGG.. ..... 74
Figure 2.5 Representative photomicrographs of Trx, TrxR and TxNIP expression in MB.. ..... 75
Figure 2.6 Kaplan-Meier survival curves of TrxR, Trx and TxNIP expression and OS in the adult GBM cohort (rim).. ..... 78
Figure 2.7 Kaplan-Meier survival curves of TrxR, Trx and TxNIP expression and OS in the paediatric LGG cohort. . ..... 80
Figure 2.8 Kaplan-Meier survival curves of TrxR, Trx and TxNIP expression and OS in the paediatric HGG cohort.. ..... 82
Figure 2.9 Kaplan-Meier survival curve of TrxR, Trx and TxNIP expression and OS in the MB cohort.. ..... 84
Figure 2.10 Box plots demonstrating the differences in expression of TrxR, Trx and TxNIP between core, rim and invasive regions of adult GBM tumours.. .. 86
Figure 2.11 Box plots of TrxR, Trx and TxNIP in different brain tumour types……. ..... 89
Figure 2.12 Box plots demonstrating the differences in expression of TrxR, Trx and TxNIP between different WHO grades of paediatric gliomas.. ..... 91
Figure 3.1 Chemical structures of Indolequinones..... 105
Figure 3.2 A proposed mechanism for the inhibition of TrxR by indolequinones.. ..... 106
Figure 3.3 Growth curves of SNB19, SF188, KNS42, DAOY, UW228-3 and MRC5 cell lines..... 123
Figure 3.4 Inhibition of TrxR activity across different brain cancer cells.. ... 125
Figure 3.5 Quantification of Trx system protein expression across different brain cancer cells.. ..... 126
Figure 3.6 Effect of IQ10 on the expression of Trx system proteins in brain cancer cells.. ..... 128
Figure 3.7 Effect of IQ10 on CA9 expression in brain cancer cells under normoxic and hypoxic conditions..... 129
Figure 3.8 Effect of IQ10 on TrxR, Trx and TxNIP expression in brain cancer cells under normoxic and hypoxic conditions.. ..... 130
Figure 3.9 Effect of IQ10 on P450, NQO1 and NQO2 expression in brain cancer cells under normoxic and hypoxic conditions.. ..... 132

Figure 3.10 Effect of TMZ on cell proliferation of brain cancer cells and the corresponding growth curves.. ..... 134
Figure 3.11 Effect of IQ10 on cell proliferation of brain cancer cells and the corresponding growth curves.. ..... 136
Figure 3.12 Effect of IQ10 on cell proliferation of brain cancer cells under normoxia and hypoxia.. ..... 138
Figure 3.13 CA9 expression in DAOY and UW228-3 cells following hypoxic incubation.. ..... 140
Figure 3.14 Effect of TMZ and IQ10 on cell survival under normoxic conditions.. ..... 140
Figure 3.15 Effect of IQ10 on clonogenic survival of brain cancer cells under both normoxic and hypoxic conditions.. ..... 142
Figure 3.16 Spheroids growth assay... ..... 144
Figure 3.17 PEs of DAOY and UW228-3 cells in 3D spheroids vs. 2D culture…….. ..... 145
Figure 3.18 Penetration of doxorubicin in DAOY and UW228-3 spheroids.. 146
Figure 3.19 Effect of IQ10 on cell viability of brain cancer cells whilst growing in 2D or 3D spheroid culture.. ..... 147
Figure 3.20 Effect of IQ10 on clonogenic survival of brain cancer cells whilst growing in 2D culture and 3D spheroids.. ..... 148
Figure 3.21 Transient siRNA-mediated knockdown of TrxR in DAOY and SF188 cells…….. ..... 149
Figure 3.22 The cytotoxicity of IQ10 on TrxR silenced DAOY and SF188 cells……. ..... 150
Figure 4.1 Survival curves of brain cancer cells after single dose irradiation…… ..... 182
Figure 4.2 Radiosensitivity of brain cancer cells under aerobic or hypoxic conditions.. ..... 183
Figure 4.3 Radiation response of DAOY (A) and UW228-3 (B) in 2D and 3D spheroid culture systems.. ..... 184
Figure 4.4 Effects of IQ10 on radiosensitivity of brain cancer cells in 2D culture…….. ..... 185
Figure 4.5 Effects of IQ10 on radiosensitivity of brain cancer cells in normoxic vs. hypoxic conditions.. ..... 187
Figure 4.6 Effects of IQ10 on radiosensitivity of brain cancer cells in 2D vs. 3D spheroid cultures.. ..... 188
Figure 4.7 TrxR knockdown enhances the radiosensitivity of DAOY and SF188 cells……. ..... 190
Figure 4.8 Effect of IQ10 on intracellular ROS levels of brain cancer cells... 192
Figure 4.9 Quantification of γH2AX foci in DAOY and UW228-3 cells following treatment with IQ10, radiation or combination of IQ10 plus radiation.. ..... 194
Figure 5.1 Outline of a typical EMT programme.. ..... 207

# Chapter 1 General introduction

## 1.1 General introduction to brain tumours

### 1.1.1 Epidemiology and classification

There are a variety of subject areas related to brain tumour epidemiology and classification. The sections below give an overview of the burden of brain tumours in populations, looking at the major subtypes, in addition to giving a summary of current views on possible risk factors.

#### 1.1.1.1 Incidence, mortality and survival

Although numbers are yet to be confirmed there was a predicted 18.1 million new cancer cases and 9.6 million cancer related deaths in 2018 worldwide, these numbers increased substantially compared with the 14.1 million new cases and 8.2 million deaths in 2012 (Ferlay et al., 2015, Bray et al., 2018). Globally, about 296,851 new brain and central nervous system (CNS) tumour cases and 241,037 deaths were estimated in 2018, accounting for about 1.6% of all newly diagnosed cancers and 2.5% of cancer deaths (Bray et al., 2018). According to the statistical report of the Central Brain Tumour Registry of the United States (CBTRUS), approximately two-thirds of brain and CNS tumours are non-malignant, and approximately half of these are non-malignant meningiomas. Most malignant tumours are gliomas, which represent ~80% of all malignant brain tumours and more than half of gliomas diagnosed are glioblastomas (GBMs) (Ostrom et al., 2017). The overall incidence of brain and CNS tumours is higher among female patients compared with male patients (Ostrom et al., 2017). Like most cancers, the incidence of all brain and CNS tumours increases with age, with the highest occurrence in adults aged 40 years and older. In this age group, the most common malignant brain tumours are gliomas, of which GBM represents the most frequent type. For children younger than 15 years old, brain tumours have been the primary solid tumours, with most being astrocytic tumours and medulloblastoma (MB) (Ostrom et al., 2015, Leece et al., 2017). Among adolescents and young adults (15-39 years), brain tumours are common with only breast and thyroid cancer occurring more frequently (Ostrom et al., 2016a). Generally, the rates of incidence and mortality for brain and CNS tumours vary markedly across the

globe; both rates are highest in the more-developed regions (e.g. Europe, Northern America and Australia/New Zealand) and lowest in Africa and the Pacific (Ferlay et al., 2015). It has been reported that the overall 1-year survival rate of malignant brain and CNS tumours was 56.6% between 2000 and 2010, and the 5-year survival rate was 32.1% in the US (Barnholtz-Sloan et al., 2018). By contrast, the survival rate of non-malignant brain tumours is significantly higher, with a 1-year survival rate of 94.5% and a 5-year survival rate of 90.8%. Among all brain tumours, GBM patients have the poorest survival, for which 1-year survival is 37.4% and 5-year survival is 4.9% (Barnholtz-Sloan et al., 2018).

In the UK, brain and CNS tumours are the 9$^{th}$ most common cancer (3% of all new cancer cases), with around 11,500 new cases in each year. Brain tumours are the 10$^{th}$ most frequent cause of cancer death (5,200 deaths per year), accounting for 3% of the total annual cancer deaths. Over the last decade, the incidence rate of brain tumours has increased by around a seventh (15%) in the UK; whilst the mortality rate has remained stable. Both the incidence and mortality rates for brain tumours in the UK are highest among people aged 85 to 89. The brain cancer survival rate has improved dramatically, doubling in the last 40 years in the UK. Around 19% of brain cancer patients in England and Wales survive at least 5 years; and the 10-year survival rate is about 14% (Cancer Research UK, 2016a). However, the survival rate is much lower in high-grade brain tumour patients, particularly GBM, the 5-year survival rate is only 5% (Cancer Research UK, 2016b).

#### 1.1.1.2 Risk factors

Brain tumours are a complex and heterogeneous group of diseases, many possible contributory risk factors for their development have been studied (Butowski, 2015). The most relevant risk factors are ionising radiation, family history and genetic factors, allergies, and cell phones (McNeill, 2016), which are described in detail as follows.

### Ionising Radiation

Ionising radiation is a well-established environmental risk factor for brain tumours, but contributes to only approximately <1% of brain and CNS tumour cases in the UK (Cancer Research UK, 2015). High-dose therapeutic ionising radiation to the head, administered for both benign conditions and cancer treatments, raises the risk of meningioma and glioma (Butowski, 2015). Between them, meningioma is more likely associated with radiation (Braganza et al., 2012). Apart from therapeutic radiation, diagnostic radiation exposure has also been identified as a potential contributing factor to brain tumour carcinogenesis (Prasad and Haas-Kogan, 2009). The risk of developing a brain tumour is nearly tripled in people who received 1-2 CT (computerised tomography) scans (cumulative x-ray doses of ~60 milligrays (mGy)) during childhood or adolescence (Pearce et al., 2012). People who have had dental x-rays (bitewing technique) taken from the sides of the head have doubled the risk of adult meningiomas (Claus et al., 2012). Linet et al. (2012) concluded that very low doses (i.e. 10-50 millisievert) of x- or γ-radiation from diagnostic imaging procedures is significantly associated with increased cancer risks in humans.

### Family history and genetic factors

Increased risk of developing a brain tumour appears to be associated with a family history of brain and CNS tumours. Having one parent with a brain tumour increases the individuals risk by ~70%, and having a sibling diagnosed presents a two-fold risk (Hemminki et al., 2009, 2010). Also, several genetic syndromes can increase the risk of developing CNS tumours with an estimated 5% of brain tumours being linked to hereditary syndromes (Barnholtz-Sloan et al., 2018). For example, neurofibromatosis type 1 (NF-1), represents the most common genetic syndrome that is associated with brain tumours (Williams et al., 2009b). Approximately 15% of NF-1 patients develop a glial tumour in their optic tract (optic pathway glioma) during their life (Boulanger and Larbrisseau, 2005, Singhal et al., 2002). Compared with NF-1, neurofibromatosis type 2 (NF2) is less frequent, occurring in 1:25,000-40,000

live births (Tonsgard, 2006). The hallmark feature of NF-2 is bilateral vestibular schwannomas with up to 50% of individuals developing multiple meningiomas, and 2-5% of patients developing ependymomas (McNeill, 2016). Another genetic syndrome, tuberous sclerosis (TS) is a rare multi-system genetic disease that causes tumours to grow in the brain and other vital organs. Approximately 5-15% of children with TS develop a low-grade type of brain tumour called a subependymal giant cell astrocytoma (SEGA) (Barnholtz-Sloan et al., 2018). Having TS also increases the risk of developing other brain tumours, such as malignant gliomas (Curatolo et al., 2008). In addition, patients with Gorlin syndrome or Turcot syndrome (a condition characterised by multiple adenomatous colon polyps) are at high risk of developing MB (Rood et al., 2004, Hottinger and Khakoo, 2007).

### *Allergies*

A number of epidemiologic studies have shown that allergic and atopic conditions such as asthma, hay fever, eczema, and food allergies reduce the risk of various brain tumours, including glioma, meningioma and vestibular schwannoma (Wigertz et al., 2007, McCarthy et al., 2011, Scheurer et al., 2011, Turner et al., 2013). Among those tumours, the link between allergies and the risk of glioma has been well studied. One large case-control study found that a history of allergic or autoimmune diseases is inversely correlated with glioma risk (Brenner et al., 2002). Other studies showed that total IgE levels were lower in glioma cases than controls (Wiemels et al., 2004, Calboli et al., 2011). Although the exact mechanism is unclear, increased tumour immunosurveillance in those with allergies and autoimmune diseases or brain tumour-related immune suppression has been proposed as possible mechanisms (Fisher et al., 2007).

### *Cell phones*

Since the introduction of cell phones in 1980s, there has been a growing public concern about whether cell phones might increase the risk of developing brain tumours (Samkange-Zeeb and Blettner, 2009). To address this concern, several large studies have tried to assess the association

between cell phone use and brain tumour risk, but inconsistent results have been reported (Frei et al., 2011, Hardell et al., 2013, Benson et al., 2013). On the one hand, a number of studies have suggested that heavy users of cell phones may be at higher risk of brain tumours with, as a result of this, radiofrequency fields produced by cell phones being considered as possible carcinogens to humans by the World Health Organisation (WHO) (Baan et al., 2011). On the other hand, several cohort studies found no evidence of an association between tumour risk and cell phone use (Ahlbom et al., 2004, Schuz et al., 2006). One of the largest case-control studies to date, the INTERPHONE study, also found no relationship between cell phone use and the increased risk of glioma or meningioma (INTERPHONE Study Group, 2010). The conflicting data between cell phone use and brain tumour risks needs further robust scientific investigation.

#### *Other risk factors*

Apart from the risk factors described above, a number of other risk factors for brain tumours have also been examined, including infection, diet, tobacco, alcohol, chemical agents, occupation and head trauma. However, the association between these factors and risk of brain tumours have not been well established.

### 1.1.1.3 Brain tumour classification

Historically, the WHO set out the most universally adopted classification system used in diagnosing brain tumours, which was primarily based on the consensus of histological features (Louis et al., 2007). Recently, with advances in molecular biology, the classification system has been updated to incorporate molecular parameters alongside histological characteristics (Louis et al., 2016). This combined histological and molecular genetic classification has generated new integrated diagnoses, where the histopathological name is followed by the genetic features (e.g. glioblastoma, IDH wild-type) (Louis et al., 2016). The addition of the genotypic parameters significantly improves the diagnostic objectivity and accuracy, and will probably lead to improved patient management and more accurate estimation of prognosis and

treatment response. Amongst all the brain tumours, the classification of astrocytic tumours and MB will be described in detail within this section, as the astrocytic tumours are the most frequently diagnosed brain tumours, and MB is the most common malignant brain tumour in childhood.

Astrocytic tumours are a type of glioma that arises from astrocytes. In the past, only astrocytic tumours were grouped together, but now all diffusely infiltrating gliomas (whether astrocytic or oligodendroglial) are classified together. This change is based not only on their growth patterns and behaviour, bus also more pointedly on the shared genetic driver mutations in IDH genes (Louis et al., 2016). Therefore in the 2016 WHO classification system these tumours are organised as either "diffuse astrocytic and oligodendroglial" or "other astrocytic" tumours. The diffuse astrocytic and oligodendroglial tumours include diffuse astrocytoma, anaplastic astrocytoma, glioblastoma (WHO grade II, III and IV, respectively), oligodendroglioma (grade II), and a new addition to WHO 2016, diffuse midline glioma, H3 K27M-mutant (grade IV). The "other astrocytic" tumours comprise pilocytic astrocytoma (PA), subependymal giant cell astrocytoma (SEGA) and pleomorphic xanthoastrocytoma (WHO grade I, I and II, respectively), they exhibit a more circumscribed growth pattern and a lack of IDH gene family alterations.

The two main types of embryonal tumours are MB and atypical teratoid/rhabdoid tumour. Both are defined as WHO grade IV malignant neoplasms because of their highly proliferative nature. Previously, based on histopathological features, the 2007 WHO classification system seperated MB into five subtypes: classic MB, desmoplastic/nodular MB, MB with extensive nodularity, large cell MB, and anaplastic MB. Patients with desmoplastic/nodular MB tend to have a good prognosis; while those with large cell/anaplastic MB have poorer outcomes (Louis et al., 2007). Currently, the classification of MB is based on molecular characterisation, but histological phenotypes are retained when the molecular analysis is not feasible or molecular results are not diagnostic (Dang and Phillips, 2017). The

molecular subgrouping of MB arises from large-scale genetic profiling studies that defines four subgroups: WNT-activated (10%), sonic hedgehog (SHH)-activated (30%), group 3 (20%) and group 4 (40%) (Taylor et al., 2012). WNT and SHH MBs are characterised by aberrations in the WNT and SHH signalling pathways, respectively. WNT MB has the best prognosis compared with the others, while SHH MB has an intermediate prognosis. The underlying signalling pathways associated with group 3 and group 4 MBs have not been identified. Group 3 MB is frequently associated with metastasis, resulting in a poor prognosis, while group 4 MB is sometimes associated with metastasis and has an intermediate prognosis. The molecular classification of MB redefines the risk stratification of MB patients, and has the potential to develop new therapeutic strategies for the treatment of MB (Kijima and Kanemura, 2016).

### 1.1.2 Prognostic and predictive factors

A prognostic factor is a patient-specific or tumour-specific trait that predicts clinical outcomes regardless of treatment. Unlike prognostic factors, predictive factors are able to identify patients who will benefit from specific treatment regimens (Johnson and Galanis, 2013). Although they can be separately classified, several factors in brain tumours have both prognostic and predictive strength. Measurement of prognostic and/or predictive factors can aid in clinical decision making and help select the appropriate treatments for individual patients. The following sections will review some important and commonly used prognostic and predictive factors in brain tumours.

#### 1.1.2.1 Clinical factors

Traditionally, the prognosis of patients with brain tumours has been largely based on clinical factors. In high-grade astrocytic tumours (i.e. anaplastic astrocytoma and GBM), the greater extent of tumour resection, lower tumour grade, younger age (<50 years), and good Karnofsky Performance Status (KPS) score are all favourable prognostic factors (de Groot, 2015). For anaplastic oligodendrogliomas (WHO grade III), treatment (for progression-free survival (PFS) only), younger age, confirmed absence of residual tumour on imaging,

frontal location and good performance status are independent factors that predict better PFS and overall survival (OS) (Gorlia et al., 2013a). While in adult low-grade gliomas (LGGs), older age ($\geqslant$ 40 years), astrocytoma histology, tumours larger than 5-6 cm in diameter, tumours crossing the midline and baseline neurological deficits are considered as unfavourable prognostic factors (Pignatti et al., 2002, Gorlia et al., 2013b). For patients with MB, age under 3 years, postoperative residual tumour more than 1.5 $cm^2$, metastasis at diagnosis and hydrocephalus have been identified as negative clinical prognostic factors. In contrast, good performance status, short neurologic symptoms duration, gross total resection, radiotherapy, lateral location of the tumour and desmoplastic/nodular phenotypes are associated with good prognosis (Rutkowski et al., 2010, Lai et al., 2012, Wong et al., 2015, Brandes and Paris, 2004, Kim et al., 2011).

#### 1.1.2.2 Molecular factors

Over the past decade, genetic alterations have been recognised as more powerful prognostic and predictive markers than histological appearance alone. Amongst the molecular markers, IDH1/2 (isocitrate dehydrogenase1/2) mutation, 1p/19q co-deletion, histone H3 gene mutations, methylguanine-DNA-methyltransferase (MGMT) promoter methylation status, epidermal growth factor receptor (EGFR) overexpression, TP53 mutation, telomerase reverse transcriptase promoter (TERTp) mutations and MYC/MYCN amplification are considered as relatively important prognostic and/or predictive factors. The functions and mechanisms of each marker are discussed in more detail below.

##### *IDH1/2 mutation*

IDH1 and IDH2 are key metabolic enzymes that convert isocitrate to α-ketoglutarate. IDH1/2 mutations are frequently observed in lower-grade tumours (>70% grades II-III astrocytomas and 100% oligodendrogliomas) and secondary GBMs that arise from lower-grade astrocytomas (about 85%) (Chan et al., 2015). However, these mutations rarely occur in primary GBMs (<1%) and the mutation rate in PAs, ependymomas, or other less common gliomas is

low or absent (Watanabe et al., 2009). For diffuse gliomas, patients with IDH1/2 mutations have a dramatically better prognosis than those with wild-type IDH genes (Yan et al., 2009b). The IDH mutation status, however, does not predict treatment specific responses in these patients (van den Bent et al., 2010). At present, the evaluation of IDH mutations is part of the WHO 2016 integrated diagnosis scheme for LGGs, anaplastic gliomas, and GBMs. The IDH mutation status serves as one of the most important prognostic factors in those tumours (Yan et al., 2009b, Gorlia et al., 2013a, 2013b, Hartmann et al., 2010).

### *Co-deletion of chromosome 1p/19q*

The 1p/19q co-deletion is a complete loss of the short arm of chromosome 1 (1p) and the long arm of chromosome 19 (19q), which results from an unbalanced centromeric translocation between the two chromosomes (Wesseling et al., 2015). This co-deletion is the hallmark molecular signature of oligodendrogliomas, as it is almost exclusively encountered in glial tumours with oligodendroglial morphology. The WHO 2016 classification integrates IDH mutations and 1p/19q co-deletion with histologic findings to classify grade II and III diffuse lower-grade gliomas (LGGs). Over 80% of LGGs are IDH-mutant; of those, 37%-50% harbour the 1p/19q co-deletion (Batchala et al., 2019). More importantly, the IDH-mutant 1p/19q co-deleted LGGs (oligodendrogliomas, IDHmut-Codel) demonstrate improved patient survival and enhanced responsiveness to PCV (procarbazine, lomustine, and vincristine) chemotherapy compared with IDH-mutant noncodeleted LGGs (astrocytomas, IDHmut-Noncodel). As a result, chromosome 1p/19q co-deletion is increasingly used in the routine diagnostic procedures of oligodendrogliomas, both as a diagnostic marker as well as a prognostic/predictive marker (Srebotnik-Kirbis and Limback-Stokin, 2016). Compared with oligodendrogliomas, the impact of 1p/19q co-deletion on WHO grade II and grade III astrocytic gliomas is less clear, but it appears to be a positive prognostic factor for OS (Mariani et al., 2006, Johnson and Galanis, 2013).

### *H3 K27M*

Diffuse midline glioma with histone H3 K27M mutation is a novel entity added to the 2016 update of the WHO classification of CNS tumours (Louis et al., 2016). The histone H3 K27M mutation is present in most paediatric gliomas arising in midline locations, including thalamus, brain stem and spinal cord. The mutations in H3 K27M occurs in either of two genes, H3F3A or HIST1H3B, which encode histone proteins H3.3 and H3.1, respectively (Aboian et al., 2017). This new group of gliomas are classified as WHO grade IV, regardless of the histological appearance. Among all diffuse gliomas, and within diffuse midline gliomas in general, the H3 K27M mutant tumours imply the worst prognosis (< 10% 2-year survival) (Louis et al., 2016). Within the H3 K27M-mutant category, H3.3 mutations have a poorer prognosis than those with H3.1 mutations, although additional research is required. Until now, no predictive value has yet been identified for H3 K27M mutations (Castel et al., 2015).

### *MGMT promoter methylation*

One of the most clinically relevant DNA methylation markers is the promoter of MGMT, which is a DNA repair enzyme that reverses the damage induced by ionising radiation or alkylating agents such as temozolomide (TMZ) (Hegi et al., 2005). Methylation of the MGMT promoter (MGMTp) induces MGMT gene silencing and increases the sensitivity of cells to alkylating agents. MGMTp is methylated in 73% of secondary (mostly IDH-mutant) GBMs, 30-50% of primary, IDH-wildtype, GBMs and in > 90% of oligodendrogliomas, but it is less commonly methylated in lower-grade astrocytomas (Zawlik et al., 2009, Lapointe et al., 2018). For GBM, MGMTp methylation can predict better treatment response from combined therapy of TMZ and radiation in both younger and elderly patients (Hegi et al., 2005, Stupp et al., 2005, Malmstrom et al., 2012, Wick et al., 2012, Perry et al., 2017). However, patients who lack methylated MGMTp also appear to benefit from TMZ, though the magnitude of benefit was larger in the methylated group. Because of this, alkylating chemotherapy should be the standard of care for all GBM patients and

MGMTp methylation status is best considered as a prognostic factor rather than a predictive biomarker of sensitivity to TMZ (Stupp et al., 2009).

### *EGFR and EGFR variant III (EGFRvIII)*

EGFR is a transmembrane glycoprotein belonging to the superfamily of receptor tyrosine kinases (Seshacharyulu et al., 2012). It controls key signalling pathways responsible for tumour cell growth, proliferation, migration, and survival (Chistiakov et al., 2017). EGFR is frequently active or overexpressed in GBM through EGFR gene amplification and/or the EGFRvIII deletion mutation (An et al., 2018). EGFRvIII is a constitutively active, oncogenic mutant EGFR variant resulting from deletions of exon 2-7 (Seshacharyulu et al., 2012). EGFR amplification is found in about 40% of all GBMs, with around 50% of these tumours also expressing the EGFRvIII (Felsberg et al., 2017). Both EGFR amplification and EGFRvIII have been linked to the invasive behaviour of GBM together with increased angiogenesis (Keller and Schmidt, 2017). Assessment of EGFR amplification is increasingly used for differentiating GBM from lower-grade gliomas and for stratifying patients in clinical trials and other studies. However, the prognostic value of EGFR amplification/EGFRvIII is controversial (Shinojima et al., 2003, Hartmann et al., 2013), and experimental therapies targeting EGFR in brain tumours have been largely disappointing to date (Bush and Butowski, 2017).

### *TP53 mutation*

TP53 is a typical tumour suppressor gene located in 17p13.1, which encodes the nuclear protein P53. The tumour protein p53 is a nuclear transcription factor that regulates the expression of a variety of genes involved in cell cycle, apoptosis, senescence, DNA repair, or metabolic changes in response to genotoxic or cellular stress (Park et al., 2017). TP53 is the most frequently mutated gene in human cancers and is often found mutated or lost in gliomas. To be specific, TP53 is mutated in the majority of IDH-mutant lower-grade astrocytomas, 60-70% of secondary GBMs and about 30% of primary GBMs (Brennan et al., 2013, Brat et al., 2015). However, these mutations are rare in oligodendrogliomas (13%), well-circumscribed astrocytic tumours,

ependymomas, and MB (except for the SHH type, p53-activated subgroup) (Shahpar et al., 2016, Park et al., 2017). Mutant TP53 is strongly associated with a poor prognosis in patients with GBMs and it may decrease the chemosensitivity of TMZ (Wang et al., 2014). For children with SHH MB, it is now clear that TP53 mutations harbour significant prognostic utility and comprise one of the highest risk subsets of MB (Ramaswamy et al., 2015).

### *TERTp mutations*

Human telomerase is a ribonucleoprotein that elongates the telomeric DNA by adding TTAGGG sequences to the end of chromosomes, therefore, it plays a crucial role in cellular immortalisation and tumourigenesis (Aldape et al., 2015). TERTp mutations are molecular hallmarks of gliomas, occurring in 77% of IDH-wildtype GBMs and 96% of oligodendrogliomas, but less frequently seen in astrocytomas (22%) (Pekmezci et al., 2017). Gliomas can be classified into five molecular groups on the basis of three alterations: TERTp mutations, IDH mutations and 1p/19q codeletion. Among patients with grade II/III gliomas, the molecular groups were independently associated with overall survival and patients with only TERTp mutations had poorer prognosis than other molecular groups (Eckel-Passow et al., 2015).

### *C-MYC and N-MYC amplification*

The MYC family (C-MYC, N-MYC and MYCL1) belongs to a group of genes known as proto-oncogenes, which controls cell cycle, cellular proliferation and differentiation (Bartlett et al., 2013). Amplification of MYC is found in many carcinomas, including MBs, in which 10% to 15% may show C-MYC/N-MYC amplification (Eberhart et al., 2004). Patients whose tumour exhibit overexpression or amplification of the MYC oncogenes usually have an extremely poor prognosis. Taking MB as an example, overexpression of C-MYC/N-MYC is significantly associated with poor clinical outcomes and the aggressive large-cell/anaplastic phenotypes (Herms et al., 2000, Eberhart et al., 2004). The MYC gene amplification has been observed in all four subgroups of MB, particularly group 3, which is characterised by recurrent MYC

amplification and approximately 20% cases of group 3 patients harbour the MYC amplification (Ramaswamy et al., 2016).

### 1.1.3 Treatment strategies

Optimal treatment strategies can prolong patient survival, prevent recurrence, control metastasis and improve quality of life. Surgery, chemotherapy, and radiation therapy have been longstanding treatment modalities in the management of brain tumours. The past decades have witnessed improved outcomes for patients with brain tumours due to the molecular advances and refinements in treatment regimens. The following sections summarise, by tumour type, the current treatment standards and the latest therapeutic advances for several of the most common primary brain tumour types.

#### 1.1.3.1 Pilocytic astrocytoma (PA) (WHO I)

PAs are the most common non-infiltrative LGGs. In general, the prognosis is excellent with overall 10-year survival reported to be over 90%, although survival significantly declines with increasing age and decreased extent of resection (Ostrom et al., 2017, Louis et al., 2016). Gross total resection is the standard of care, associating with the most favourable prognosis. The reported 10-year OS for patients with gross total resection is as high as 100%, as compared with 74% for those having subtotal resections (Louis et al., 2016, Forsyth et al., 1993). The use of adjuvant chemotherapy or radiotherapy for PA patients undergoing subtotal resection is still controversial (Brown et al., 2004, Kidd et al., 2006, Burkhard et al., 2003, Johnson et al., 2012) and the radiotherapy is only indicated at progression when surgical options no longer exist (Weller et al., 2017).

#### 1.1.3.2 Diffuse LGGs (WHO II)

Diffuse LGGs include WHO grade II diffuse astrocytomas and oligodendrogliomas. Early and maximal safe resection is the initial treatment for such patients (National Comprehensive Cancer Network, 2018, Weller et al., 2017, Jakola et al., 2017). Following surgery, treatment decisions are based on risk stratification, although the distinction between low- and high-

risk LGGs is highly variable among different studies (Gorlia et al., 2013a). According to the National Comprehensive Cancer Network (NCCN) guidelines 2018, low-risk patients are typically younger than 40 years with gross total resection and favourable prognostic molecular markers (i.e. IDH-mutant and ideally 1p/19q co-deleted) (National Comprehensive Cancer Network, 2018). In these patients, a "wait-and-see" approach is recommended based on the long-term results of the European Organisation for Research and Treatment of Cancer (EORTC) 22845 randomised trial, which found similar OS between early and deferred radiotherapy arms, although early postoperative radiotherapy significantly increased PFS. This study, therefore, suggested that radiotherapy might be deferred for LGG patients who are in a good condition, provided they are carefully monitored (van den Bent et al., 2005). Except adjuvant radiotherapy, the use of postoperative chemotherapy alone or in combination with radiotherapy remains investigational (van den Bent, 2003). Currently, there is a lack of data from randomised controlled trials regarding the clinical significance of chemotherapy for these patients.

LGG patients aged over 40 years and/or who underwent a subtotal resection are clinically defined as a high-risk group. Other high-risk factors that are sometimes taken into consideration are neurological deficits, tumour size >5 cm and tumour crossing the midline (Buckner et al., 2016, Baumert et al., 2016, Daniels et al., 2011). Additionally, IDH-wildtype LGGs are now also considered high-risk, as they have a poor survival comparable with primary GBMs and have been suggested to behave similarly (Larsen et al., 2017). IDH-wildtype LGGs are thus often treated like GBM (see Section 1.1.3.4), although no clinical trials have specifically evaluated this subgroup (Lapointe et al., 2018). For IDH-mutant high-risk LGGs, maximum safe resection is considered the best initial treatment. After surgery, the treatment standard is radiotherapy (45-54 Gy, 1.8-2.0 Gy/fraction) followed by 6 cycles of adjuvant PCV chemotherapy, based on the results of RTOG (Radiation Therapy Oncology Group) 9802 trial (Buckner et al., 2016). However, in current clinical practice, PCV is often replaced by lomustine alone due to fewer toxic effects

and that procarbazine has little efficacy, and that vincristine does not pass the blood-brain barrier (BBB) well. Moreover, TMZ is often preferred over PCV chemotherapy because of its favourable safety profile and ease of administration (Weller et al., 2017).

#### 1.1.3.3 Diffuse HGGs (WHO III)

Diffuse HGGs (WHO grade III) include anaplastic astrocytomas and anaplastic oligodendrogliomas. The current standard of care for patients with diffuse HGGs is maximal safe resection followed by chemoradiotherapy, based on the long-term results of three randomised trials (Wick et al., 2016, van den Bent et al., 2013, Cairncross et al., 2013) and on the interim results of the CATNON trial (van den Bent et al., 2017). The chemoradiotherapy consists of 59.4-60 Gy of radiotherapy with either six cycles of adjuvant PCV, or concurrent and adjuvant TMZ. Whether PCV can be replaced by TMZ in anaplastic oligodendroglioma with 1p/19q co-deletion is presently being investigated in the CODEL trial, which compares radiotherapy followed by PCV with radiotherapy plus concurrent and adjuvant TMZ (Jaeckle et al., 2016). Furthermore, whether radiotherapy can be deferred to prevent radiotherapy-induced neurotoxicity in those 1p/19q co-deleted chemosensitive tumours is being assessed in the POLCA trial, comparing upfront radiotherapy plus PCV versus upfront PCV plus deferred radiotherapy at progression (Assistance Publique, 2015).

#### 1.1.3.4 GBM (WHO IV)

GBM is the most common and the most aggressive brain tumour in adults, accounting for 45% of all malignant primary brain tumours and 15% of all primary brain tumours (Ostrom et al., 2015). Most GBM patients do not survive beyond a year, and only ~5% survive for more than 5 years (Ostrom et al., 2017). Management of GBM includes a combination of neurosurgery, radiotherapy, and chemotherapy. The preferred surgical treatment is a maximal safe resection, which is significantly associated with longer patient survival (Lacroix et al., 2001, Sanai et al., 2011). In 2005, Stupp et al. presented the results of a phase III clinical trial and established the current

standard of care for postoperative management of newly diagnosed GBM. The treatment in the trial consisted of radiotherapy to 60 Gy over 6 weeks with concurrent daily TMZ, followed by at least 6 cycles of adjuvant TMZ. This regimen resulted in a median OS of 14.6 months, compared with 12.1 months for patients treated with radiation alone (Stupp et al., 2005). Further, the benefits of adjuvant radiotherapy with TMZ lasted throughout 5 years of follow-up and MGMTp methylation status identified patients most likely to benefit from the addition of TMZ (Stupp et al., 2009).

In addition to the conventional treatment modalities mentioned above, a relatively new treatment option for GBM is tumour-treating fields (TTFields), which is an antimitotic treatment modality that interferes with cell division and organelle assembly by delivering low-intensity alternating electric fields to the tumour (Hottinger et al., 2016). The TTFields portable device has been approved by the US Food and Drug Administration (FDA) for treatment of newly diagnosed GBM after an interim analysis of a phase III clinical trial in 2015. The results suggested that the addition of TTFields to standard therapy significantly prolonged PFS and OS, with minimal additional toxicity (Stupp et al., 2015). In 2017, the final analysis of the trial reported that the use of TTFields with maintenance TMZ increased the median OS by nearly 5 months, from 16.0 to 20.9 months, and increased the PFS by about 3 months, from 4.0 to 6.7 months (Stupp et al., 2017). Importantly, all subgroups of GBM patients benefited from the TTFields, regardless of age, sex, KPS, MGMTp methylation status, geographic region, or extent of resection.

#### 1.1.3.5 Medulloblastoma (MB)

MB is the most prevalent type of malignant brain tumour in children, making up ~20% of all paediatric brain tumours (Ostrom et al., 2016b). The standard treatment for childhood MB includes a combination of maximal safe resection, radiation therapy (in patients aged >3 years), and chemotherapy. Complete surgical resection is the best initial treatment, which has consistently been correlated with improved survival, especially in patients with non-disseminated disease (Albright et al., 2000). Following surgery, patients are

conventionally stratified into average- or high-risk group based on the patient's age, the extent of surgical resection and metastatic status at the time of diagnosis (Packer et al., 2010). High-risk patients have one of the following features: age ≤ 3 years, residual tumour ≥ 1.5 $cm^2$, and presence of metastasis at the time of initial diagnosis. Whereas average-risk patients do not have any of the features listed under the high-risk group (Quinlan and Rizzolo, 2017). Once the stratification is finished, craniospinal irradiation (CSI) is the standard of care for children older than 3 years. The treatment dose of CSI is 23.4 Gy for average-risk patients and 36 Gy for high-risk patients. In addition, the tumour bed receives a boost dose to a total of 55.8 Gy due to the high risk of local recurrence (Packer et al., 2006, Gajjar et al., 2006). Children under 3 years of age often suffer severe long-term cognitive effects from radiation, therefore, they are generally spared this treatment and instead receive more intense chemotherapy (De Braganca and Packer, 2013). Various chemotherapy regimens are used concurrently with radiation and/or after radiation. Importantly, all drugs involved in these regimens must be able to penetrate the BBB. The common chemotherapeutic agents include vincristine, cisplatin, cyclophosphamide, lomustine, etoposide, methotrexate, TMZ, and carboplatin. With the current therapies, patient survival has improved significantly, the 5-year disease-free survival is more than 80% in average-risk group and ~60-65% for high-risk group (Rutkowski et al., 2010). However, 30-40% of patients will relapse within 2 years after primary therapy, and the prognosis after recurrence is extremely poor, with a median survival of less than 6 months and the 2-year survival rate is around 10-15% (Pfister et al., 2009, Rudin et al., 2009, Hill et al., 2017).

The international consensus, published in 2012, recognises four main subgroups of MB: WNT, SHH, group 3, and group 4 (Taylor et al., 2012). These subgroups demonstrate distinct clinicopathological features and the application of this subgrouping drives initial subgroup-directed therapies. To date, there are no standard targeted therapies, but a number of clinical trials have shown some interesting results with more trials ongoing. WNT subgroup

accounts for approximately 10% of all MBs and occurs most frequently among children older than 3 years. More than 95% of WNT MB patients survive more than 5 years, making this the subgroup with the most favourable prognosis (Kool et al., 2012). In light of this excellent prognosis, current clinical trials are focusing on de-escalation of radiation or chemotherapy in the hope of lessening long-term side effects (Udaka and Packer, 2018). A pilot study assessing the feasibility of a surgery and chemotherapy-only approach in children with WNT-positive MB is currently ongoing (Sidney Kimmel Comprehensive Cancer Center, 2016) (NCT02212574). Meanwhile, some other studies are trying to find suitable targeted therapies for this subgroup of patients. Although targeting WNT is a promising field of research, it has been extremely difficult to develop novel drugs that specifically target this pathway. Two potential drugs of interest, cantharidin and norcantharidin, have shown the ability to reduce the size of intracranial tumours in *in vivo* models (DeSouza et al., 2014). Other potential drugs that may effectively target WNT pathway are poly ADP ribose polymerase (PARP) inhibitors. It has been found that PARP inhibition results in the destruction of β-catenin and subsequent apoptotic cell death in MB mouse models (MacDonald et al., 2014). Unfortunately, advances in targeting this specific pathway are still needed before innovative and highly effective treatment will be available for this cohort of patients.

The SHH pathway is an essential embryonic signalling cascade that regulates stem cell and progenitor cell differentiation in multiple developmental processes (Ingham and Placzek, 2006). SHH MB comprises approximately 30% of all MBs and occurs most frequently in young children aged <5 years or in patients aged >16 years. The SHH patients have a 5-year survival rate of 75%, which is worse than WNT subgroup but more favourable than patients from group 3 (Liu et al., 2017). Current studies have tried to target all aspects of SHH signalling pathway in clinical trials. The smoothened (SMO) inhibitor vismodegib was the first drug approved for clinical use. However, while tumour response is immediate, tumour regrowth appears common upon

termination of drug treatment (Rudin, 2012). Moreover, a more recent clinical trial investigating vismodegib plus TMZ versus TMZ alone in patients with SHH MB was terminated in advance in 2017, due to insufficient numbers of successful cases at the end of the first stage of the trial (Centre Leon Berard, 2012) (NCT01601184). Therefore, new preclinical therapeutic avenues for the SHH patients shift onto the agents that act on downstream targets of the SHH pathway, such as bromodomain inhibitors, PI3K inhibitors, aurora kinase inhibitors, itraconazole, arsenic trioxide, and GLI antagonists (Ramaswamy and Taylor, 2017). However, the diverse tumour heterogeneity, multiple mutations, and resistance mechanisms make appropriate therapy selection difficult. Further studies on inhibiting the SHH pathway are needed.

Group 3 accounts for ~25% of all MBs and overall has the worst prognosis among the four subgroups, with a 5-year OS of around 50% (Glod et al., 2016). Group 3 tumours are most frequently found in infants and children, with very few in adults. Many of these group 3 patients (~17%) display MYC amplification, which is usually associated with poor prognosis. Preclinical studies have suggested that histone deacetylase (HDAC) inhibitors (e.g. panobinostat) and bromodomain inhibitors (e.g. JQ1) may be potential therapeutic agents for those with MYC amplification (Delmore et al., 2011, Pei et al., 2016). In addition, the mutations of EZH2 and KDM6A are also commonly found in group 3 and 4 tumours, making them potential future targets for these two subtypes. Although several EZH2 inhibitors have shown promising anti-tumour activity in pre-clinical studies (Robinson et al., 2015), additional clinical trials are urgently needed to specifically define the role of these drugs.

Group 4 MB is the most prevalent subgroup, making up more than 30% of all MBs and is diagnosed mainly in infants and children. The metastasis rate at the time of diagnosis is ~35-40%, which is similar to group 3. The group 4 MB is the least understood among the four subgroups, because the most common molecular aberrations are found in only a small fraction of cases, and the exact molecular pathology in this subgroup is unclear (Gajjar and Robinson,

2014). There are some similarities between group 3 and group 4, suggesting that drugs targeting group 3 MB might also represent candidate therapeutics for at least a subset of group 4 MB. Taken together, no real advances have been made in developing treatments to target this specific subgroup. Additional research is required to identify the main genetic drivers so as to facilitate drug development for group 4 tumours.

Although a lot of progress is being made regarding molecular characterisation of brain tumours, and their prognostic/predictive importance, there is little known, unlike other tumour types, regarding the role of redox proteins in brain tumour progression, therapy response and patient outcome. The following section will summarise the main antioxidant systems that regulate redox homeostasis and discuss their biological function and activity in cancers, and how targeting such proteins and systems may improve the radioresponse.

## 1.2 ROS, redox homeostasis, the thioredoxin system and cancer

Reactive oxygen species (ROS) are formed in biological systems as natural by-products of the cellular metabolism of oxygen. ROS encompasses a wide range of molecules with the three major ROS of physiological significance being the superoxide anion ($O_2^{\bullet-}$), the hydroxyl radical ($^{\bullet}OH$), and hydrogen peroxide ($H_2O_2$) (Bast, 1986). They are chemically reactive molecules containing oxygen with free radicals carrying one or more unpaired electrons in their outer shell (Halliwell, 1992). In mammalian cells, the mitochondrial respiratory chain constitutes the main intracellular source of ROS, accounting for about 90% of the total cellular ROS generation. During mitochondrial oxidative metabolism, ROS can be formed by losing or gaining an electron from a non-radical through three serial reactions shown as follows (Michaels and Hunt, 1978):

$$O^2 + e^- \rightarrow O_2^{\bullet-} \qquad \text{(Reaction 1)}$$

$$2O_2^{\bullet-} + 2H^+ \rightarrow H_2O_2 + O_2 \qquad \text{(Reaction 2)}$$

$$H_2O_2 + e^- \rightarrow {}^{\bullet}OH + OH^- \qquad \text{(Reaction 3)}$$

In addition to mitochondria, a number of other endogenous sources of ROS also exist in mammalian cells, including nicotinamide adenine dinucleotide phosphate (NADPH) oxidases (NOX) and dual oxidase (DUOX) in cell membranes (Babior, 1999), and a group of intracellular enzymes that catalyse ROS production during their enzymatic reactions, such as xanthine oxidase, cyclooxygenases, cytochrome p450 enzymes, and lipoxygenases (Di Meo et al., 2016). Certain organelles, such as peroxisomes and endoplasmic reticulum (ER), are also able to produce ROS (Antonenkov et al., 2010, Malhotra and Kaufman, 2007). Moreover, ROS can also be induced by exogenous factors such as ultraviolet light, pollutants, ionising radiation, and chemicals (e.g. quinones) (Sheu et al., 2006).

ROS are physiologically necessary but potentially harmful (Nita and Grzybowski, 2016). Low levels of ROS are required in the modulation of several cellular events, including immune response, mitogenic responses, signal transduction, proliferation, and gene expression (Carlson et al., 2012). However, at high levels, ROS can cause oxidative damage to key cellular components such as nucleic acids, proteins and lipids, potentially leading to subsequent apoptotic or necrotic cell death (Martindale and Holbrook, 2002). An imbalance favouring ROS production in amounts exceeding the cellular defence capacities is often referred to as 'oxidative stress' (Avery, 2011), and which is, as described later, one of the major ways by which conventional low-linear energy transfer (LET) radiotherapy exerts its cytotoxic effects on cells (Zhang and Martin, 2014). Intracellular ROS levels are under tight control by various antioxidant systems. Redox homeostasis is a balance between ROS generation and their clearance by the antioxidant systems. A delicately maintained redox homeostasis is vital to prevent the living organisms from getting damaged by oxidative stress (Mahmood et al., 2013).

### 1.2.1 Antioxidants and redox protein families

In order to detoxify ROS cells have evolved several antioxidant systems to regulate their levels and maintain redox homeostasis. The cellular antioxidant

systems can be categorised into two broad groups: non-enzymatic antioxidants and enzymatic antioxidant (i.e. redox proteins) (Misra et al., 2014). Although the non-enzymatic antioxidant molecules play an important role in the regulation of intracellular redox homeostasis, the main intracellular antioxidants are enzymatic in mammals. The functions and characteristics of each antioxidant are briefly discussed below.

#### 1.2.1.1 Non-enzymatic antioxidants

Non-enzymatic antioxidants can counteract free radicals and neutralize oxidants, thus protecting cells against ROS-induced damage and regulating redox-sensitive signalling pathways. Based on their solubility, non-enzymatic antioxidants can be further divided into water-soluble and lipid-soluble antioxidants (Pal et al., 2014). Water-soluble antioxidants comprise glutathione (GSH), ascorbic acid (vitamin C), flavonoids, and uric acid; whereas lipid-soluble antioxidants include α-tocopherol (vitamin E), carotenoids and vitamin A, α-lipoic acid/dihydrolipic acid, and ubiquinol/ubiquinone (coenzyme $Q_{10}$) (Table 1.1).

**Table 1.1 Summary of cellular antioxidants.**

| Non-enzymatic Antioxidants | Enzymatic Antioxidants (Redox proteins) |
|---|---|
| **Water-soluble antioxidants** | **ROS-dependent enzymes** |
| • Glutathione (GSH)<br>• Ascorbic acid (vitamin C)<br>• Flavonoids<br>• Uric acid | • Superoxide dismutase (SOD)<br>• Catalase<br>• Peroxiredoxin (Prx)<br>• Glutathione peroxidase (GPx) |
| **Lipid-soluble antioxidants**<br>• α-Tocophenol (vitamin E)<br>• Carotenoids and vitamin A<br>• α-Lipoic acid/Dihydrolipic acid<br>• Ubiquinol/Ubiquinone (coenzyme $Q_{10}$) | **Glutathione system**<br>• Glutathione reductase (GR)<br>**Thioredoxin system**<br>• Thioredoxin (Trx)<br>• Trx reductase (TrxR)<br>• Trx-interacting protein (TxNIP)<br>**Glutaredoxin system**<br>• Glutaredoxin (Grx) |

Table adapted from (Zhang and Martin, 2014). Copyright© 2014 by Elsevier with permission conveyed through Copyright Clearance Centre Inc.

### *Water-soluble antioxidants*

GSH and ascorbic acid are the most powerful water-soluble antioxidants and they act as potent scavengers of ROS primarily in the aqueous environment (Blokhina et al., 2003, Krishnamurthy and Wadhwani, 2012). The antioxidant function of GSH will be discussed later with the GSH system together as a whole. Ascorbic acid is an important chain-breaking antioxidant, with the ability to scavenge a wide spectrum of ROS, such as $O_2^{\bullet-}$, $H_2O_2$, $^{\bullet}OH$, hypochlorous acid (HOCl), aqueous peroxyl radicals, and singlet oxygen ($^1O_2$). It is also capable of quenching the free radicals cooperatively with vitamin E and regenerating reduced form of vitamin E in membranes and lipoproteins (Amir Aslani and Ghobadi, 2016). Flavonoids are a group of natural benzo-γ-pyran derivatives possessing strong antioxidant activities. The flavonoids complexed with the copper or iron can prevent the generation of the ROS (Angaji et al., 2012). Uric acid possesses high radical scavenging activity and it contributes for as much as two-thirds of all free radical scavenging activities in the plasma (Nimse and Pal, 2015).

### *Lipid-soluble antioxidants*

Lipid-soluble antioxidants are able to protect cell and organelle membranes against lipid peroxidation (Hatwalne, 2012). Specifically, vitamin A can directly bind peroxyl radicals before they propagate peroxidation to lipids. CoQ10 can neutralise the oxidative effect of lipid peroxyl radicals and regenerate vitamin E. Vitamin E is able to halt lipid peroxidation by donating its phenolic hydrogen to the peroxyl radicals forming tocopheroxyl radicals which, despite also being radicals, are unreactive and unable to continue the oxidative chain reaction (Mehta and Gowder, 2015). Both α-lipoic acid and its reduced form dihydrolipic acid can scavenge reactive molecules, meanwhile they can also regenerate other antioxidants, such as vitamin C, vitamin E, and GSH (Amir Aslani and Ghobadi, 2016).

#### 1.2.1.2 Redox proteins

In comparison to the non-enzymatic antioxidants, the antioxidant enzymes are more effective in protecting cells from massive oxidative stress (He et al., 2017). In mammalian cells, the enzymatic antioxidants consist of ROS-dependent enzymes and three thiol redox buffering systems. The major ROS-dependent enzymes comprise superoxide dismutase (SOD), catalase, peroxiredoxin (Prx) and GSH peroxidase (GPx), they can directly counteract ROS. While the enzymatic redox buffering systems include the reduced GSH/oxidised GSH (GSSG) system, the glutaredoxin (Grx) system, and the thioredoxin (Trx)/Trx reductase (TrxR) system (Table 1.1), they are able to reverse disulfide formation or to donate electrons to peroxidases, so as to support ROS scavenging and modulate cellular redox status (Giles, 2006, Tew and Townsend, 2011).

***ROS-dependent antioxidant enzymes***

SODs are a group of enzymes that catalyse the dismutation of two superoxide radicals into hydrogen peroxide and oxygen (Reaction 2). Hydrogen peroxide, in turn, is converted into water and oxygen by the catalases and peroxidases (i.e. Prx and GPx) (Reaction 4).

$$2H_2O_2 \rightarrow 2H_2O + O_2 \qquad \text{(Reaction 4)}$$

In this way, two toxic species, superoxide radical and hydrogen peroxide, are converted to the harmless product water (Figure 1.1).

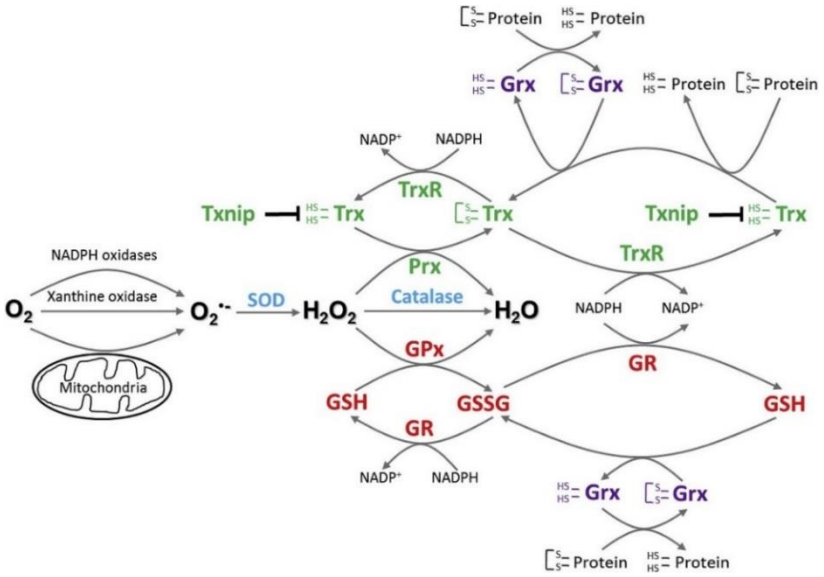



**Figure 1.1 Redox proteins and ROS regulation.** Abbreviations: Prx, peroxiredoxin; SOD, superoxide dismutase; GPx, glutathione peroxidase; GSH, reduced glutathione; GSSG, oxidised glutathione; GR, glutathione reductase; GRx, glutaredoxin; Trx, thioredoxin; TrxR, thioredoxin reductase; TxNIP, thioredoxin-interacting protein; NADPH, nicotinamide adenine dinucleotide phosphate. 'HS' represents the reduced form of the protein; 'S' denotes the oxidised form. Figure cited from (Zhang and Martin, 2014). Copyright© 2014 by Elsevier with permission conveyed through Copyright Clearance Centre Inc.

There are three SOD isoforms that localise to different sub-cellular sites: SOD1 (CuZn-SOD) is the major intracellular SOD found in the nucleus and cytoplasm; SOD2 (Mn-SOD) exists in mitochondria and SOD3 (extracellular SOD (EC-SOD)) is expressed in the extracellular matrix and fluids. All SODs are very efficient catalysts, and they work by similar mechanisms (Fattman et al., 2003). Catalases are common enzymes found in nearly all living organisms exposed to oxygen. They can catalyse the two-stage conversion of $H_2O_2$ to $H_2O$ and $O_2$, with an extremely high peroxide turnover rate: one molecule of catalase can convert millions of $H_2O_2$ molecules to $H_2O$ and $O_2$ per minute (Mehta and Gowder, 2015). Catalases functions mainly in sub-cellular organelles known as peroxisomes (Weydert and Cullen, 2010). Based on their enzymological properties, catalases can be classified into three types: monofunctional catalases, bifunctional catalase-peroxidases and manganese-containing catalases (Chelikani et al., 2004).

The Prxs are a ubiquitous family of proteins which can protect cells against oxidative stress through the detoxification of cellular peroxides such as $H_2O_2$ and different alkyl hydroperoxides (Amir Aslani and Ghobadi, 2016). The ROS

scavenging ability of Prxs is mainly achieved by using Trx as its electron donor (Reaction 5 and 6) (Figure 1.1).

$$Prx(red) + H_2O_2 \rightarrow Prx(ox) + 2H_2O \qquad \text{(Reaction 5)}$$

$$Prx(ox) + Trx(red) \rightarrow Prx(red) + Trx(ox) \qquad \text{(Reaction 6)}$$

Mammals possess six Prx isoforms with different cellular locations (Prx I-VI) and each isoform contains a conserved cysteine residue at the $NH_2$-terminal region, which is the main site of oxidation by $H_2O_2$ (Tavender et al., 2008). GPx, a selenium-containing enzyme, is also able to protect cells from the toxicity of hydroperoxides. GPx requires several secondary enzymes (e.g. GSH reductase and glucose-6-phosphate dehydrogenase) and cofactors (e.g. reduced GSH, NADPH, and glucose 6-phosphate) to function at high efficiency (Liu et al., 2004). There are eight GPx isoenzymes (GPx1-8) found in humans with GPx1 considered a major enzyme responsible for removing $H_2O_2$ (He et al., 2017).

### *The GSH and Grx systems*

The tripeptide GSH (γ-glutamyl-cysteinyl-glycine) is the most abundant small molecular thiol in millimolar concentrations in cells (Morgan et al., 2013). GSH has a critical role in cellular signalling and antioxidant defences either by directly reacting with ROS or by acting as an essential cofactor for GSH S-transferases and GPx. GSH together with its dependent enzymes, known as the GSH system, is a major thiol-dependent antioxidant system in mammalian cells, responsible for the maintenance and regulation of the thiol-redox status (Morris et al., 2014). Under physiological conditions, reduced GSH is the major form of GSH pool in cells. However, under pathological conditions, or in response to electrophilic agents, GSH can be oxidised into its disulfide form (GSSG) after reduction of target molecules (Reaction 7) (Wang and Hai, 2016). The oxidised GSSG can then be reduced back into the reduced form GSH, with the assistance of the dimeric flavoenzyme GSH reductase (GR) at the expense of NADPH (Reaction 8) (Lillig et al., 2008) (Figure 1.1).

$$2GSH + R\text{-}S\text{-}S\text{-}R \rightarrow 2R\text{-}SH + GSSG \qquad \text{(Reaction 7)}$$

$$GSSG + NADPH + H^+ \rightarrow 2GSH + NADP^+ \qquad \text{(Reaction 8)}$$

The ratio between GSH and GSSG is an important indicator of the redox status of a cell (Meister, 1994). Typically, in a resting cell, the GSH: GSSG ratio is >10:1 in the cytosol and mitochondria, but, under oxidative stress, this ratio decreases due to the increased formation of GSSG (Becker et al., 2007).

Grxs are small ubiquitous oxidoreductases with a Trx-fold structure, functioning in antioxidant defence, redox signalling and iron metabolism (Fernandes and Holmgren, 2004). Grxs can regulate disulfide reduction and deglutathionylation through the catalysis of monothiol and dithiol, with both GSH and Trx as electron donors (Figure 1.1). After the reduction of protein disulfides, the oxidised form of Grx isoenzymes could be reduced by GSH, ferredoxin or NADPH-dependent TrxR (Wang and Hai, 2016). Structurally, Grxs belong to the Trx fold family of protein. However, compared to Trxs, Grxs are more versatile with respect to the choice of substrate and reaction mechanisms (Lillig et al., 2008). To date, four Grxs have been discovered in mammals: cytosolic dithiol Grx1, mitochondrial Grx2, multidomain monothiol Grx3, and mitochondrial single-domain monothiol Grx5 (Johansson et al., 2004).

### *Thioredoxin (Trx) system*

The Trx system is another key antioxidant pathway in defence against oxidative stress through its disulfide reductase activity regulating protein dithiol/disulfide balance. The system comprises TrxR, its characteristic and ubiquitous substrate Trx and the endogenous inhibitor of this system - Trx-interacting protein (TxNIP). Oxidised Trx (Trx-$S_2$) is reduced to the active form (Trx-$(SH)_2$) by receiving electrons from NADPH in the presence of TrxR. Subsequently, the reduced Trx reduces oxidised cysteine groups on down-stream proteins thereby regulating their function (Nordberg and Arner, 2001, Arner and Holmgren, 2000, Powis et al., 2000) (Figure 1.1). The functions and mechanism of each member of Trx system are discussed in detail below.

*Trx*

Trx is a ubiquitous small molecular weight (12 kDa) enzyme with a -CGPC- motif within its active site. It was originally identified in Escherichia coli as a

hydrogen donor for ribonucleotide reductase, an enzyme required for DNA synthesis (Laurent et al., 1964, Holmgren, 1985). The structure of Trx, known as the Trx fold, contains five β-strands in the internal core, and four α-helices and a short stretch of helix surround the central β-sheets (Martin, 1995). Reduced Trxs are powerful reductases, with a relatively broad spectrum of substrates, that act via a disulfide (-S-S-) - dithiol (-SH, -SH) exchange mechanism to catalyse the conversion of disulfide bonds into thiols with high efficiency. Oxidised Trxs are then recycled back to a reduced state through the action of TrxRs and NADPH (Karlenius and Tonissen, 2010). In mammalian cells, there are three isoforms of Trx: cytosolic Trx (Trx1), mitochondrial Trx (Trx2), and a testis-specific isoform of Trx (Trx3).

Trx1 has two thiol moieties in redox-active cysteine residues Cys32 and Cys35, which are important for the activity and conformation of Trx. In addition to these two cysteine residues, Trx1 also contains three additional cysteine residues (i.e. Cys62, Cys69 and Cys73), which are crucial for post-translational modifications (Matsuzawa, 2017). Trx1 can be found in the nucleus, cytoplasm, and extracellular environment. Depending on its sub-cellular localisation, Trx1 exerts distinct roles (Arai et al., 2006). In the nucleus, Trx1 interacts with many transcription factors such as redox factor-1 (Ref-1), hypoxia-inducible factor-1α (HIF-1α), nuclear factor kappa-light-chain-enhancer of activated B cells (NF-κB), p53, activator protein-1 (AP-1), nuclear factor-like 2 (Nrf-2), glucocorticoid receptor, estrogen receptor (ER), and others (Mahmood et al., 2013), thereby regulating gene expression. In the cytoplasm, Trx1 modulates the cellular redox environment and also the activity of certain proteins, such as apoptosis signal-regulating kinase-1 (ASK-1), hence controlling apoptosis (Saitoh et al., 1998a, Lu and Holmgren, 2012). In the extracellular environment, Trx1 exhibits chemokine-like activity with multiple functions, including acting as a growth factor, initiating an inflammatory response, or supporting reduction of oxidised protein thiols in the extracellular environment (Nordberg and Arner, 2001, Masella and Mazza, 2009).

Trx-2 is a mitochondrial redox protein containing a conserved Trp-Cys-Gly-Pro-Cys redox active site. Trx-2 is required for embryonic development, since the Trx2 -/- homozygous murine embryos do not survive to birth and die after implantation at early stage, whereas Trx2 -/+ heterozygous mice appear normal (Nonn et al., 2003). Like Trx1, Trx2 can also regulate cell viability and apoptosis, as its knockdown in endothelial cells increases tumour necrosis factor (TNF)/ASK-1-induced cytochrome c release and cell death (Zhang et al., 2004). Additionally, overexpressed Trx2 confers resistance to oxidant-induced apoptosis in human osteosarcoma cells (Chen et al., 2002).

Trx3 has been exclusively found in the testis and is predominately localised to the Golgi apparatus of mammalian spermatocytes and spermatids. It is more abundant in morphologically abnormal human spermatozoa from infertile men. Trx3 has been identified as a novel sperm post obstruction autoantigen. Therefore, Trx3 can be used as a specific marker for diverse sperm and testis pathologies (Jimenez et al., 2004).

*TrxR*

Mammalian TrxRs are homodimeric selenium-containing flavoproteins with a molecular weight of ~115 kDa. They catalyse the NADPH-dependent reduction of Trx disulfide and numerous other oxidised cell constituents. TrxR is indispensable to several cellular events, such as cell proliferation, antioxidant defence, and redox signalling. There are three isoforms of TrxRs in mammals including the cytosolic TrxR1, the mitochondrial TrxR2, and the third isoform TrxR3 or Trx GSH reductase (TGR) which is mainly present in the testes (Lu and Holmgren, 2014). Mammalian TrxR1 and TrxR2 contain flavin adenine dinucleotide (FAD) and NADPH binding domains and an interface domain. But TGR is unusual among TrxRs in that it has an extra Grx domain in the N-terminus, therefore it can reduce GSH disulfide in addition to Trx (Prast-Nielsen et al., 2011).

Both TrxR1 and TrxR2 consist of homodimers with each subunit containing two active site regions. The first active site region of TrxR1 is positioned at the N-terminus from residues 59 to 64 containing the following motif -cys-val-asn-

gly-cys-. The second active region is located at the C-terminus of the protein and contains a selenocysteine -gly-cys-sec-gly-, which is critical for the reduction of Trx and other substrates (Sandalova et al., 2001, Zhong and Holmgren, 2000). The first active site receives electrons from NADPH via the FAD molecule, thereafter transfers electrons to the selenocysteine redox active site present in the other subunit. Thus the selenolate formed in the C-terminal active site can then act to reduce the required substrates (Zhong et al., 2000, Tonissen and Di Trapani, 2009). Notably, the C-terminal tail of TrxRs is flexible, and thereby they have a very broad range of substrates including proteins such as Trx, glutaredoxin, protein disulfide isomerase, and some small molecules such as selenite, vitamin C, lipoic acid, ubiquinone, and cytochrome c, or some cancer drugs (e.g. motexafin gadolinium and alloxan) (Mahmood et al., 2013).

*TxNIP*

TxNIP, also known as vitamin D3 up-regulated protein 1 (VDUP1) or Trx-binding protein 2 (TBP2), is a negative regulator of Trx function and expression. It can directly interact with the catalytic centre of Trx1, to block its reducing activity as well as disrupt the interaction between Trx1 and its downstream factors. To be specific, this interaction is mediated by the formation of a disulfide bond between the active centre Cys32 in Trx1 and Cys247 in TxNIP (Nishiyama et al., 1999, Junn et al., 2000). TxNIP expression is ubiquitous and is induced by a variety of stresses, such as ultraviolet light, γ-rays, heat shock, oxidative stress, and glucose. Overexpression of TxNIP renders cells more susceptible to oxidative stress so as to promote apoptosis (Saxena et al., 2010). Additionally, TxNIP is not only an inhibitor of Trx, but also a multifunctional molecule that regulates lipid and glucose metabolism, inflammation, cardiac function, and carcinogenesis (Matsuzawa, 2017).

### 1.2.2 Role of Trx system in cancer

Increased levels of Trx/TrxR have been found in numerous different tumour types compared to levels observed in corresponding healthy cells (Berggren et al., 1996, Lincoln et al., 2003b). The upregulated Trx system may have

different functions in the cancer cells depending on the stage of cancer development. At early stages, Trx may be beneficial for preventing cancer by scavenging carcinogen-triggered ROS. Once a cell has initiated a cancer phenotype then high levels of Trx may assist cancer development, via using its redox reactions to perform many biological functions, such as supplying reducing equivalents to Trx peroxidases and ribonucleotide reductases, regulation of transcription factor activity, inhibition of apoptosis, and stimulation of cell growth (Powis and Montfort, 2001). At later stages of cancer progression, the Trx system may be involved in angiogenesis and metastasis. The Trx system may also alter chemotherapy (e.g. cisplatin and docetaxel) and radiotherapy responses (Yamada et al., 1996, Kim et al., 2005). The following sections will discuss, in greater detail, the function and activity of the Trx system in cancer.

#### 1.2.2.1 Proliferation, apoptosis and cell cycle

The Trx system regulates cell growth, apoptosis and cell cycle through interactions with different signalling molecules, by regulating their redox status. Trx has been shown to regulate the apoptotic process in several ways. The reduced form of Trx1 protects cells against apoptosis through directly binding and inhibiting the kinase activity of ASK-1, a key regulator whose activation is essential for TNFα-induced apoptosis (Baker et al., 1997b). Meanwhile, Trx directly inhibits apoptosis by catalysing S-nitrosylation of procaspase 3 and caspase 3 (Mitchell and Marletta, 2005). In addition, Trx1 can regulate apoptosis-inducing factor (AIF)-dependent cell death through impeding AIF-mediated DNA damage (Shelar et al., 2015). More interestingly, some electrophilic inhibitors of TrxR have shown their direct capacity to promote apoptosis (Anestal and Arner, 2003).

Trx has been reported to selectively activate the DNA binding of certain transcription factors which, in turn, regulate the growth and apoptosis of cancer cells. Trx1 increases the DNA binding of NF-κB to assist its function in regulating the responses of cells to oxidative stress, apoptosis, and tumourigenesis (Powis et al., 2000). Trx also enhances p53-DNA binding

activity either in a direct way or through redox factor 1 (Ref-1) mediation (Mahmood et al., 2013, Ueno et al., 1999). Other transcription factors, such as AP-1, HIF-1aα, and HDAC can also be activated by the Trx system (Lu and Holmgren, 2014).

Due to its redox-modulating properties, Trx also controls the activity of several proteins that are essential for cell cycle progression. For instance, in cells that are stimulated to exit from quiescence (G0) to G1 phase, Trx activates the transcription factor AP-1 by reducing nuclear redox factor Ref-1/Hap-1 (Vogt et al., 2000). In the G1 phase, Trx positively regulates the cell cycle via cyclin D1 transcription and the ERK/AP-1 signalling pathways (Mochizuki et al., 2009). During S phase, Trx supplies a source of reducing equivalent for ribonucleotide reductase to synthesise deoxyribonucleotides (Vogt et al., 2000). Apart from the above, Trx-1 inhibition by the novel agent PX-12 (aka IV-2) inhibits the growth of A549 lung cancer cells via G2/M phase arrest and ROS-dependent apoptosis (You et al., 2014).

As an endogenous negative regulator of Trx, overexpression of TxNIP inhibits tumour cell proliferation and increases apoptosis by suppressing the activity of Trx (Junn et al., 2000). TxNIP also has tumour-suppressive functions independent of its role as a negative regulator of Trx. Han et al. revealed that the upregulation of TxNIP by TGF-β1 and 1,25-dihydroxy vitamin D3 inhibits tumour cell growth by blocking cell-cycle progression (Han et al., 2003b). TxNIP also negatively regulates hepatocarcinogenesis by suppressing TNF-α-induced NF-κB activation (Kwon et al., 2010).

#### 1.2.2.2 Migration, invasion and metastasis

Trx has an active functional role in stimulating cancer cell invasion and migration. Trx may reduce disulfides in extracellular matrix proteins (e.g. laminin) and stimulate both matrix metalloproteinase activity and tumour cell invasiveness (Farina et al., 2001, Farina et al., 2003). A low dose of the Trx1 inhibitor, PX-12, can decrease cell migration of colorectal cancer cells (Wang et al., 2015a). The inhibition of the Trx system through the addition of auranofin, an antirheumatic drug and inhibitor of TrxR, decreased the cell

migration capacity of breast cancer cells, whilst increasing ROS levels (Bhatia et al., 2016b). Moreover, knockdown of TrxR1 by siRNA inhibited the growth and metastasis of lung tumours in mice (Yoo et al., 2006). In addition, overexpression of TxNIP inhibited metastasis through induction of the KISS-1 metastasis suppressor gene in melanoma cells (Goldberg et al., 2003). Furthermore, the redox protein thioredoxin-like 2 (TXNL2) regulates the cancer cell growth and metastasis through a redox signalling mechanism. Knockdown of TXNL2 in human breast cancer cell lines can increase ROS levels and reduce NF-κB activity, thus inhibiting invasion and metastasis (Qu et al., 2011). The analysis of primary breast cancer patient samples has shown that elevated TXNL2 expression correlates with higher metastatic rates to the lung and brain, with decreased overall patient survival (Qu et al., 2011).

#### 1.2.2.3 Trx system in regulating radioresponse

Preclinical studies have suggested that up-regulation of Trx/TrxR is associated with radiation resistance. In contrast, inhibition of Trx/TrxR can sensitise cancer cells to ionising radiation, thus the Trx system can be considered as a potential modulator of radiosensitivity (Patwardhan et al., 2015). As a specific inhibitor of Trx1, IV-2 (1-methyl-1-propyl-2-imidazolyl disulfide) was shown to significantly increase the sensitivity of HeLa cervical cancer cells to ionising radiation (Smart et al., 2004). Another *in vitro* study found that malignantly transformed and immortalised human bronchial epithelial cells exhibited a significant decrease in sensitivity to ionising radiation accompanied by an increase in Trx1 and MnSOD as well as a decrease in GPx1 expression. Further, using the siRNA knockdown approach, this study identified that Trx1 was a main radiosensitivity modulator (Demizu et al., 2008). Moreover, as the only known enzyme to reduce Trx, TrxR is also involved in the modulation of radiosensitivity in cancer cells. Several studies have revealed that the TrxR inhibitor auranofin (commonly used, as mentioned, in treating rheumatoid arthritis) sensitised breast cancer stem cell populations to radiation *in vitro* (Rodman et al., 2016). The combination of auranofin, buthionine sulfoximine and radiation significantly increased the radioresponse and decreased survival

of breast cancer in *in vivo* models (Wang et al., 2017a, Rodman et al., 2016). Dimethoxycurcumin, a more stable analogue of curcumin, increased the radiation sensitivity of A549 lung cancer cells via inhibiting TrxR (Jayakumar et al., 2016). Another TrxR inhibitor motexafin gadolinium (MGd) has been shown to enhance the effects of ionising radiation in preclinical studies (Xu et al., 2001). Clinical evaluation of MGd has also been conducted to assess its radiosensitising effect. For example, a phase III clinical trial has shown that the combination of MGd and prompt whole brain radiotherapy (WBRT) significantly prolonged the interval to neurologic progression in non-small-cell lung cancer patients with brain metastases (Mehta et al., 2009). Finally, overexpression of TxNIP may also sensitise cancer cells to radiation. D-allose, one of the rare sugars, was shown to significantly upregulate the expression of TxNIP (Yamaguchi et al., 2008) so as to increase intracellular ROS level and the radiosensitivity of human head and neck cancer cells (Hoshikawa et al., 2011). Lately, a study from the same research group has found that D-allose could enhance the anti-tumour effects of chemoradiotherapy whilst sparing normal tissues in an *in vivo* model of head and neck cancer (Hoshikawa et al., 2018).

## 1.3 Radiotherapy of brain tumours

### 1.3.1 Basics of radiotherapy

#### 1.3.1.1 Ionising radiation

The absorption of energy from radiation in biologic material may lead to excitation or ionisation. The raising of an electron in an atom or molecule to a higher energy level without ejection is called excitation. Whereas, ionisation is the process by which one or more orbital electrons are ejected from the atom or molecule. If this has resulted from the radiation, that radiation is then called ionising radiation. For convenience, ionising radiations are usually classified as either electromagnetic or particulate (Hall and Giaccia, 2012).

### *Electromagnetic radiation*

X- and γ-rays are two forms of electromagnetic radiation, they do not differ in nature or in properties, but in the ways they are produced. γ-rays are produced by nuclear reactions, decay of subatomic particles, or radioactive decay within the nucleus. They have high energy with a prominent penetration power and can penetrate lead shield (Islam, 2017). Historically, x-rays were generated by radioactive decay of isotopes, such as cobalt-60 ($^{60}$Co) however in the modern era, x-rays are produced using a linear accelerator (LINAC) that accelerates electrons to high energy and then stops them in a target made of tungsten or gold. Generally, x-rays have lower energy than γ-rays (Ghia, 2018). X-rays may be considered from two different standpoints: waves of electrical and magnetic energy or streams of photons. The concept of x-rays being composed of photons is very important in radiobiology (Hall and Giaccia, 2012). By far, a high-energy photon beam is the most common form of radiation used for cancer treatment. An external photon beam (x-ray) radiation cabinet was used experimentally for the present study and is discussed in more detail later.

### *Particulate Radiation*

Other types of radiation include electrons, protons, α-particles, neutrons, negative π- mesons, and heavy charged ions. Some are also used in radiotherapy and diagnostic radiology. Electrons are small and negatively charged particles that can be accelerated to high energy to a speed of light by an electrical device. They are commonly used in everyday radiation therapy treatment and are particularly useful to treat tumours close to a body surface since they do not penetrate deeply into tissues. Protons are positively charged particles and are almost 2,000 times heavier than electrons. Although their production requires more complex and expensive equipment, they are increasingly used for paediatric brain tumour treatment in specialised centres because of their favourable dose distribution. α-particles are nuclei of helium atoms and consist of two protons and two neutrons. They are positively charged and highly ionised with low penetration power. The depth of

penetration is a few centimetres of air, with them being stopped by the skin. Neutrons are particles with a mass similar to that of protons, but they do not carry electrical charges. Heavy charged particles are nuclei of carbon, neon, argon, or even iron with positive charges. They must be accelerated to energies of thousands of millions of volts to be used in radiotherapy (Hall and Giaccia, 2012).

#### 1.3.1.2 Direct and indirect action of radiation

Radiation damage to the cells can be caused by the direct or indirect action of radiation on the DNA molecules. In the direct action, the radiation hits the DNA molecule directly, disrupting the molecular structure. Such structural change leads to cell damage or even cell death. Damaged cells that survive may later become cancerous or give rise to other abnormalities (Desouky et al., 2015). This direct action is the dominant process of high-LET radiations, such as neutrons or α-particles; but for low-LET radiation, such as x- and γ-rays, the indirect action is dominant. LET is a parameter that is used to describe energy transferred per unit length of the track in an absorber (Hall and Giaccia, 2012).

Indirect action is when the radiation interacts with other molecules in the cell to produce free radicals that are able to diffuse far enough to reach and damage the critical targets, such as nucleic acids, lipids and proteins. When radiation interacts with water which constitutes 80% of a cell, the water molecule may become ionised (water radiolysis) and form a variety of free radicals including the ion radical ($H_2O^+$) and the hydroxyl radical ($^\bullet OH$):

$$H_2O \longrightarrow H_2O^+ + e^-$$

$$H_2O^+ + H_2O \longrightarrow H_3O^+ + {}^\bullet OH$$

The hydroxyl radical is a comparatively long-lived and highly reactive free radical and can diffuse to, react with and damage DNA. It is estimated that about two-thirds of x-ray induced damage to DNA in mammalian cells is caused by the hydroxyl radical (Hall and Giaccia, 2012). The results of the

indirect action of radiation on DNA molecules is the impairment of function or death of the cell.

#### 1.3.1.3 Mechanisms of cell death after irradiation

Radiation can kill cancer cells by a variety of mechanisms, which can be broadly classified into two classes: those that occur relatively soon after irradiation and before cell division; and those that occur comparatively late or after division. Most cell death after radiation occurs late in response to mitotic catastrophe and not from the initial response to damage. Major cell death pathways after radiation include apoptosis, senescence, autophagy and necrosis (Joiner and Van der Kogel, 2016).

##### *Early cell death: pre-mitotic*

In a small minority of cell types, cell death occurs rapidly, within several hours after irradiation (Endlich et al., 2000). This type of cell death is limited primarily to thymocytes, lymphocytes, spermatogonia, and other cells in rapidly proliferating tissues such as hair follicles, small intestine and developing embryos. Early cell death is also observed in some types of cancer that arise from these cell types, such as lymphoma, but it is rarely observed in solid tumours. The possible mechanisms underlying the rapid cell death include the activation of DNA damage response (DDR) within minutes, which leads to the induction of cell-cycle checkpoints and DNA repair. In certain rare cell types mentioned above, this response also activates p53, upregulates pro-apoptotic proteins and then induces apoptosis or other forms of cell death. Other than DNA damage, early activation of cell death pathways can also occur in cells as a result of damage caused to cellular structures. For example, relatively high radiation doses (>15Gy) can induce apoptosis via damaging cellular membrane and activating the enzyme ceramide synthase (Garcia-Barros et al., 2003).

##### *Late cell death: post-mitotic*

The vast majority of proliferating normal and tumour cells die at a relatively long time after irradiation, usually after attempting to divide one or more

times. Time-lapse video microscopy has shown that following a transient delay (owing to activation of checkpoints) most cells resume proliferation and progress through cell cycle one or more times before eventually ceasing proliferation (Forrester et al., 1999). This has given rise to the initial characterisation of radiation-induced cell death as reproductive or mitotic cell death. In cells that die late after irradiation the DDR activates both cell-cycle checkpoints and DNA repair systems that aid in the cell survival and remove much of the initial damage caused by irradiation. However, DNA damage may not be fully repaired after irradiation, or may be improperly repaired, causing mitotic catastrophe, subsequently leading to a secondary form of programmed cell death, including apoptosis, autophagy, necrosis and senescence (Joiner and Van der Kogel, 2016).

#### *"Bystander" death*

A much less understood type of cell death that has been described in response to irradiation is known as bystander-induced death (Mothersill and Seymour, 2004). The bystander effect describes a phenomenon in which cell death can occur in cells from irradiation of neighbouring cells. Studies have shown that irradiation of a select group of cells leads to increased cell death in the unirradiated cells. The precise mechanism or importance of this effect has not yet been determined. One possible reason could be the sharing of long-lived ROS between irradiated and unirradiated cells (Baskar, 2010).

### 1.3.2 Radiotherapy options in brain tumours

As discussed above, radiotherapy is a very important treatment modality in the management of brain tumours. Radiotherapy has been incorporated into the upfront treatment of many brain tumours either as adjuvant therapy for resected tumours or as palliative treatment for unresectable malignancies. Radiation therapy has been found to improve several clinical endpoints in brain tumours, such as OS in GBM, PFS in LGGs, and local tumour control in MB. However, the long-term side effects of radiation therapy remain a major obstacle for survivors of brain tumours, especially for children. Over the last few decades, a number of crucial technological advances have been made to

improve the therapeutic efficacy and at the same time reduce the risks of toxicities. The following sections describe the current radiotherapy strategies and recent technological advances in radiotherapy for some of the most common brain tumours, such as HGGs and LGGs and MB.

#### 1.3.2.1 Tumour-specific management by radiation

##### *HGGs*

Radiotherapy has long been the standard adjuvant approach for GBM, and it remains the primary treatment modality in unresectable GBM. In 2005, a randomised phase III trial reported improved PFS and OS for patients with GBM with the addition of concomitant and adjuvant TMZ to radiotherapy following maximal safe resection. Since then, the standard postsurgical treatment for newly diagnosed GBM has become concurrent TMZ therapy with fractionated radiotherapy (60 Gy in 30 fractions), followed by 6 monthly cycles of TMZ (Stupp et al., 2005, Stupp et al., 2009). However, this recommendation was limited to patients with good performance status and patients 18 to 70 years of age. The safe radiation regimens for the elderly or frail remain controversial. Recently, a hypofractionated radiotherapy schedule may be preferentially considered for elderly patients or those with poor performance status as hypofractionation utilises higher than standard doses per fraction and commonly shortens the radiation treatment course, without affecting treatment efficacy (Perry et al., 2017). For anaplastic gliomas, there is no accepted standard of treatment. Typically, patients with anaplastic gliomas are treated with maximal safe resection, followed by radiotherapy, and adjuvant TMZ (Scoccianti et al., 2012). While clinical trials (EORTC 26081-22086, NCT00887146 and CATNON study) are being conducted, radiotherapy for anaplastic gliomas varies by institution. Generally, patients are treated with a total dose of 50-60 Gy, 1.8-2 Gy per fraction (Ghia, 2018). In order to offer highly conformal high-dose distribution of the target while minimising dose to nearby critical structures, intensity-modulated radiation therapy (IMRT) is the technique commonly employed to treat HGGs (Hermanto et al., 2007).

### *LGGs*

The OS rate of LGGs is rather good, the main concern is treatment-related late toxicity. The use of adjuvant radiotherapy for LGG patients is thus controversial. Although the optimal timing of radiotherapy remains unclear, mounting evidence supports delaying radiotherapy until the time of progression. In adult patients with grade I/II supratentorial astrocytomas and oligodendrogliomas, a phase III randomised trial found no difference in OS (but improved PFS) between early radiotherapy and no or late radiotherapy, moreover, radiotherapy could be avoided altogether in 35% of patients (van den Bent et al., 2005). Additionally, another study indicates that patients treated with radiotherapy for LGGs (*vs.* those who were not treated with radiotherapy) have a higher rate of significant neurocognitive side effects (53% *vs.* 27%) (Douw et al., 2009). Furthermore, a recent phase III trial (EORTC 22033-26033) found no significant difference in PFS in patients with LGG when treated with either radiotherapy alone or TMZ chemotherapy alone. Further results for OS analyses are pending (Baumert et al., 2016). Due to the above reasons, many clinicians delay radiotherapy until tumour progression and failure of systemic chemotherapy. Currently, the dose of radiotherapy for LGGs remains 45-50.4Gy, given the lack of evidence for improved outcomes with higher doses (Kiebert et al., 1998, Shaw et al., 2002). Proton therapy may be utilised in some cancer centres and offers the advantage of minimising the volume of the brain receiving lower radiation doses.

### *MB*

Radiotherapy remains the main modality in the curative treatment of patients with MB. There is a general agreement that radiotherapy should start no later than 4-6 weeks postoperatively. Given the propensity of MB to disseminate via the cerebrospinal fluid (CSF), current standard practice involves the use of CSI with a boost to the posterior fossa/primary tumour bed (Bartlett et al., 2013). After surgery, the mainstay for average-risk patients older than 3-5 years is “reduced-dose” CSI with a total dose of 23.4 Gy plus a boost with conformal therapy restricted to the tumour bed up to 54-55.8 Gy. The

"reduced-dose" CSI is usually combined with weekly concurrent single-drug (vincristine) and followed by a multidrug chemotherapy (Taylor et al., 2003, Packer et al., 2006). For high-risk patients (>3-5 years), the current standard of care includes maximum safe resection, concurrent chemoradiotherapy of 36-39.6 Gy CSI and vincristine, with a boost up to 60 Gy to the primary site, followed by cisplatin-cyclophosphamide-based chemotherapy (Esbenshade et al., 2017, von Bueren et al., 2016, Tarbell et al., 2013). Children under the age of 3-5 years are usually treated with surgery followed by intensive chemotherapy alone to delay radiation therapy, because of devastating long-term sequelae of radiation to the developing brain. In terms of radiation techniques, 3D-conformal therapy, IMRT and proton therapy are all acceptable radiotherapy modalities for MB patients.

#### 1.3.2.2 Technological advances in radiotherapy for brain tumours

In the past few decades, radiotherapy has seen technical advances in all aspects of treatment, including improvement in patient immobilisation, imaging, treatment planning and delivery. Radiation techniques have evolved from 3D conformal radiotherapy (3D-CRT) to IMRT, volumetric-modulated arc therapy (VMAT), and stereotactic technique, including stereotactic radiosurgery (SRS) and fractionated stereotactic radiotherapy (FSRT). All of these techniques allow the delivery of higher radiation doses to the target volume, at the same time reducing the toxicity to normal tissues as compared with conventional radiotherapy. Proton therapy may represent a treatment alternative to photon irradiation, due to the more favourable dose distribution to the target volume. The following sections summarise current developments in radiation therapy and their clinical impact on the management of patients with brain tumours.

##### *IMRT and VMAT*

IMRT represents the main evolution of 3D-CRT, it provides a highly conformal dose distribution to a tumour with good sparing of normal tissues. Unlike conventional radiotherapy the radiation beams in IMRT are delivered as a sequence of many small beams modulated by a dynamic multi-leaf collimator

(MLC). Tomotherapy, the next generation IMRT, is a rotational form of IMRT in which dose conformity to the tumour is achieved by modulating the intensity of a rotating fan beam using MLCs. It offers improved target conformity and sensitive structure sparing compared with conventional static field IMRT plans (Rong and Welsh, 2011). A further evolution of the IMRT technique is VMAT, in which the precisely-sculptured 3D dose distribution is delivered as the gantry of the LINAC rotates 360-degrees around the patient through single or multiple arcs. Compared to conventional IMRT, VMAT improves dose conformity while shortening treatment times (up to 8 times faster) (Teoh et al., 2011). The increased conformity with IMRT and VMAT allows escalated tumour dose or hypofractionated radiation without increasing toxicity to normal tissue, and thus may improve local tumour control and survival. Because of these advantages, IMRT and VMAT are increasingly used for hippocampal sparing during brain irradiation, with the aim of avoiding long-term neurocognitive decline (Kazda et al., 2014). When used for either LGGs or HGGs, IMRT and VMAT allow for improved tumour conformity and normal tissue sparing, this might result in reduced late toxicities associated with radiotherapy. In patients with MB, treatment with IMRT can achieve a lower risk of ototoxicity and long-term neurocognitive decline as compared with 3D-CRT (Polkinghorn et al., 2011, Blomstrand et al., 2012, Pichandi et al., 2015). Although all these studies have shown the dosimetric superiority of IMRT and VMAT over 3D-CRT for different types of brain tumours, randomised trials are needed to assess the actual clinical benefit and risk of late toxicities for these techniques (Wagner et al., 2009, Chen et al., 2013).

### *Stereotactic radiotherapy*

Stereotactic radiotherapy is a high-precision radiation technique that delivers radiation with the use of either a frame-based or a frameless mask stereotactic system, depending on the treatment machine (e.g. Cyberknife®, Novalis®, Gamma Knife®, etc.). High doses of stereotactic radiation can be delivered as single-fraction/multi-fraction SRS (2-5 fractions), or as FSRT when

conventional fractions of 1.8-2.0 Gy per fraction are used. Due to the ability to provide highly precise tumour irradiation whilst sparing surrounding normal tissues, stereotactic radiotherapy is frequently used to ablate small, well-defined primary and metastatic tumours anywhere in the body (Baskar et al., 2012). It has shown excellent results in the treatment of various tumour types including brain tumours. For example, in patients with benign brain tumours (including meningiomas, pituitary adenomas, craniopharyngiomas, and acoustic neuromas), local control rates after either SRS or FSRT is in the range of 80-95% at 5-10 years, with a low incidence of long-term toxicity (Kondziolka et al., 2008, Minniti et al., 2009, Li et al., 2017, Murphy and Suh, 2011). The use of SRS in the management of patients with brain metastases is also increasingly recognised, and SRS is emerging as an acceptable alternative to whole-brain radiotherapy to treat patients with up to 10 brain metastases due to its preservation of neurocognitive function (Pham et al., 2017). Besides, re-irradiation with SRS/FSRT alone or in combination with chemotherapy may improve clinical outcomes for patients with recurrent or progressive malignant gliomas, with a reported median survival of 6-12 months (Ryu et al., 2014, Nieder et al., 2016).

### *Proton therapy*

Proton beam radiotherapy is a form of positively charged particle therapy. It can offer better dose distribution due to its unique absorption profile in tissues, known as Bragg's peak, allowing highest energy deposition at the tumour site while minimising the damage to healthy tissues along their path (Baskar et al., 2012). This property makes proton therapy an excellent choice for the treatment of paediatric malignancies and for tumours located next to critical structures such as spinal cord, eyes, and brain, where maximal normal tissue sparing is crucial (Levin et al., 2005). Proton therapy is increasingly used in the treatment of paediatric brain tumours with the aim of reducing long-term side effects of radiation on the developing brain. As compared with photon technique, proton therapy has been shown to significantly reduce normal tissue doses and acute treatment-related toxicity for MB patients

treated with CSI (Yuh et al., 2004, Yoon et al., 2011, Barney et al., 2014). Additionally, in another comparison of proton and photon radiotherapy for a range of paediatric brain tumours (e.g. LGG, ependymoma, craniopharyngioma, and MB), proton therapy has shown consistent advantages in reducing the low and intermediate dose areas and preserving critical normal organs, such as cochlea and hypothalamus (Merchant et al., 2008). Although a number of studies have shown that proton therapy offers excellent tumour control with low long-term radiation-induced toxicity in brain tumours, the therapeutic effect is equivalent to stereotactic photon irradiation (Bishop et al., 2014, Ronson et al., 2006, Halasz et al., 2011). Therefore, randomised clinical trials are required for full evaluation of the superiority of proton therapy to photon irradiation for brain tumours (Mizumoto et al., 2017).

Additional advances to our knowledge continue with recent data suggesting that delivery of photon radiotherapy at exceptionally high dose rates, so called 'flash' radiotherapy, can maintain high levels of tumour cell kill but with no associated normal tissue toxicities. Such effects have been shown in lung and in brain cancers (Durante et al., 2018). With the poor prognoses associated with many brain tumour types, and associated toxicities with current treatments there is a real need to identify new treatment options, such as flash radiotherapy, that will improve efficacy whilst minimising toxicities. The current project seeks to identify such a novel approach, targeting redox homeostasis in brain cancers, using a new agent, IQ10.

## 1.4 Hypotheses and aims

### 1.4.1 Hypotheses

1. Trx system proteins are expressed in brain tumours to variable levels across different types with expression being of prognostic significance.
2. Targeting TrxR with IQ10 will be cytotoxic and combining the drug with radiation will increase radiosensitivity.
3. Bioreduction of IQ10 will lead to ROS generation, that will lead to increased

DNA damage with the drug being more effective under 3D, hypoxia containing conditions, than 2D normoxic conditions.

4. In addition to the above cytotoxic mechanisms, TrxR inhibitor IQ10 will exhibit potential anti-invasive and anti-metastatic abilities shown by inhibition of epithelial-mesenchymal transition (EMT) characteristics.

### 1.4.2 Aims and objectives

#### 1.4.2.1 Aims

1. Explore the potentially prognostic role of Trx, TrxR and TxNIP expression in different types of brain tumours.
2. Investigate the chemotherapeutic and radiosensitising effects of novel TrxR inhibitor IQ10 on a range of brain cancer cells and the mechanisms underlying its action.

#### 1.4.2.2 Objectives

1. Assess whether expression of Trx, TrxR and TxNIP proteins in a variety of brain tumour patient specimens associates with clinicopathological variables and prognosis.
2. Investigate the effect of the novel TrxR inhibitor IQ10 as a single agent (in comparison to controls), and in combination with radiation, in brain cancer cell lines using a variety of endpoint assays in normoxic and hypoxic conditions (2D *vs.* 3D models).
3. Examine potential mechanisms of action of IQ10 and validate TrxR as the main target for IQ10, and to explore if any potential additional targets are involved in drug action.
4. Investigate potential anti-migratory/metastatic abilities of IQ10 by quantifying the expression of EMT-related genes.

# Chapter 2 Clinical importance of thioredoxin system protein expression in brain tumours

## 2.1 Introduction

### 2.1.1 Challenging issues in brain tumours

Primary brain tumours represent a diverse collection of diseases with varying prognoses, clinical courses, and treatment strategies. These tumours occur in both adult and paediatric populations often with genomic drivers that differ between age groups (Ramkissoon et al., 2018). Gliomas are considered the most frequent type of primary brain tumours in both adult and children, with GBM being the most malignant and most common type of brain tumours in adults (Ostrom et al., 2017). The WHO classification system classifies gliomas into four different grades on the basis of their histological and morphologic characteristics; grade I and II gliomas are classified as low-grade exhibiting non-malignant features and low proliferation rates; whilst grade III and IV are grouped as high-grade, exhibiting high proliferation rates, aggressive behaviour and high rates of recurrence and mortality (Louis et al., 2016). Despite advances in diagnosis and treatments, survival times have not significantly improved for malignant gliomas, especially GBM patients, whose median survival time is only around 15 months from diagnosis and a 5-year survival rate of 6% (Stupp et al., 2005).

MB is the most frequent primary malignant brain tumour in children (Ramaswamy and Taylor, 2017). Treatment generally consists of maximum safe surgical resection followed by radiotherapy and chemotherapy; however 15-20% of average-risk and 30-40% of high-risk patients develop recurrences resulting in poor survival outcome (Othman et al., 2014). The median survival after relapse is around 10 months (Koschmann et al., 2016) and 5-year survival after relapse is 6% (Sabel et al., 2016). Long term survivors usually suffer from treatment associated complications that lead to a decline in quality of life (Ribi et al., 2005, von Hoff et al., 2009).

Both malignant gliomas and metastatic MBs are highly invasive, recurrence after treatment is almost inevitable, resulting in extremely poor prognosis. Meanwhile, the side effects of chemo/radiotherapy on patients are usually

severe, especially for children under 3-5 years. Therefore, there is a pressing need to identify reliable and robust prognostic biomarkers to better stratify patients in order to improve patient survival.

### 2.1.2 Trx system and its association with clinical outcome in brain tumours

Redox homeostasis is often disrupted in cancer cells due to increased oxidative stress caused by the accelerated proliferation, high metabolic rate and persistent growth promoting signalling pathways of tumours (Woolston et al., 2013). To maintain the redox balance, antioxidant systems such as the Trx system are often deregulated/overexpressed in aggressive tumours to counteract the increased oxidative stress (Woolston et al., 2012). The Trx system, which has been illustrated in detail in Chapter 1, is one of the major enzyme families that regulates the homeostasis of the cellular redox state (Zhang and Martin, 2014) and includes Trx, TrxR and TxNIP (Powis et al., 2000). The Trx system participates in multiple cellular processes, such as maintenance of a reducing cellular environment, DNA synthesis, transcriptional regulation (e.g. NF-kB, P53, HIF-1α), promotion of cell growth, and apoptosis (reviewed in (Powis and Montfort, 2001, Biaglow and Miller, 2005, Gromer et al., 2004, Nguyen et al., 2006)). Furthermore, upregulation of the Trx system has been associated with resistance to chemotherapy and radiotherapy (Yokomizo et al., 1995, Penney and Roy, 2013, Selenius et al., 2012). Accordingly, inhibition of the Trx system is known to inhibit cell proliferation and to improve drug and radiation sensitivity (Holmgren and Lu, 2010, Urig and Becker, 2006). Studies performed in a variety of primary tumours have shown that the members of the Trx system are often over/underexpressed in tumoural tissues compared with corresponding normal tissues. More importantly, their expression levels often correlate with tumour grade, metastasis and prognosis (Miyazaki et al., 1998, Lichtenfels et al., 2003, Soini et al., 2001, Lincoln et al., 2003a, Raffel et al., 2003). The associations between the expression of Trx, TrxR and TxNIP and clinical outcomes in cancer patients are individually discussed below.

Trx expression has been reported to be elevated in a variety of cancer types including lung, colorectal, cervical, hepatic, and pancreatic cancers (Choi et al., 2002, Lincoln et al., 2003b, Powis et al., 1998, Welsh et al., 2002a, Kakolyris et al., 2001, Raffel et al., 2003, Kim et al., 2003b, Han et al., 2002, Hedley et al., 2004). Additionally, overexpression of Trx has been correlated with aggressive tumour growth, poorer prognosis and decreased patient survival in human lung and colorectal cancers (Kakolyris et al., 2001, Raffel et al., 2003). High Trx levels were also associated with poor patient prognosis in breast cancer (Bhatia et al., 2016c). Besides, the expression level of Trx positively correlated with increasing tumour grade according to a tissue proteome study in gliomas of different grades (Gollapalli et al., 2017). In a study of 85 oligodendroglial tumours, the immunoreactivity for Trx was observed in 29% and TrxR in 76% of cases. Increased Trx expression was found to be correlated with higher tumour grade, cell proliferation and apoptosis. Trx was also shown to be associated with poor prognosis in both univariate survival and Cox multivariate analysis, indicating that Trx expression has a correlation with patient outcome for oligodendrogliomas (Jarvela et al., 2006).

TrxR expression has been shown to be overexpressed in many primary human tumours including breast cancer, thyroid cancer, prostate cancer, hepatocellular cancer and melanoma as well as a number of human cancer cell lines, such as Jurkat and A549 cells (Choi et al., 2002, Lincoln et al., 2003a, Nguyen et al., 2006). It has been suggested that the level of TrxR in tumour cells is 10-fold or greater than in corresponding normal tissues (Mustacich and Powis, 2000). In a cohort of 433 astrocytomas, expression of TrxR was observed in 66% and Trx in 46% of the cases, and both were significantly associated with increased grade, but only patients with increased Trx had a poorer prognosis (Haapasalo et al., 2003). The findings from another study with a relatively small sample size (40 patients) were consistent with this study, showing that the TrxR expression significantly increased with astrocytoma grade (Esen et al., 2015). The level of TrxR in GBM patients was

significantly higher than in normal brain tissue, indicating that TrxR may be related to the progression of GBM (Kemerdere et al., 2013).

TxNIP has been identified as a major redox regulator and a tumour suppressor in various solid tumours and haematological malignancies (Zhou et al., 2011b, Zhou and Chng, 2013, Yoshihara et al., 2014). Loss of TxNIP expression was reported to be associated with the development of some solid tumours (Kim et al., 2007) and TxNIP is down-regulated in a number of cancers (Han et al., 2003a, Butler et al., 2002). Additionally, TxNIP was found to be an independent prognostic factor for distant metastasis-free survival and OS in locally advanced primary breast cancer (Woolston et al., 2012). A recent study has demonstrated that low TxNIP expression in glioma was associated with higher histological grade and shorter patient survival. Furthermore, knockdown of TxNIP in the U251 GBM cell line promoted cell proliferation, invasion, and migration (Zhang et al., 2017b).

Taken together, with a poor prognosis and high recurrence rate there is a clear need to identify novel prognostic markers to improve patient outcome for brain tumours. The clinical studies mentioned above suggest that expression of Trx system proteins has prognostic or predictive power in various type of tumours. Although the protein expression of Trx system in gliomas has, as mentioned above been previously investigated, few studies have assessed the prognostic or predictive value of Trx system proteins as a whole and the clinical importance of the Trx system remains understudied in brain tumours. Furthermore, there have been no studies conducted in paediatric patients (i.e. paediatric LGG, HGG or MB), and none of the studies assessed expression of Trx, TrxR and TxNIP all together, simultaneously, across a variety of brain tumour types. To our knowledge, this is the first study to assess the expression of all three members of the Trx system in different brain tumour types. As subcellular localisation of Trx system proteins may be important for their function (Woolston et al., 2010), this study assessed both cytoplasmic and nuclear localisation of TrxR and Trx.

### 2.1.3 Hypotheses and aims

#### 2.1.3.1 Hypotheses

1. Trx system proteins, namely TrxR, Trx and TxNIP, are expressed in brain tumours to variable levels across different types.
2. The expression of Trx system proteins will have prognostic or predictive power in brain tumour patients.
3. There are significant differences in the Trx system protein expression between different brain tumour regions or between different tumour types/grades.

#### 2.1.3.2 Aims

1. Investigate the expression levels of Trx system proteins (i.e. TrxR, Trx and TxNIP) in adult GBM, paediatric LGG, paediatric HGG and MB patients using immunohistochemical approaches.
2. Determine the clinical importance of Trx system proteins in terms of associations with clinicopathological variables and clinical outcome in four different brain tumour cohorts.
3. Compare the expression levels of Trx system proteins between different tumour regions or between different tumour types/grades.

## 2.2 Materials and methods

### 2.2.1 Cell lines and culture conditions

The adult GBM cell line SNB19, paediatric GBM cell lines SF188 and KNS42, and MB cell lines DAOY and UW228-3 were used in the current study. Breast cancer cell lines MDA-MB-231 and MCF-7 were used as positive controls for assessing antibody specificity. Normal cell types, MRC5 lung fibroblast and foetal neural stem cell FB83, were used for comparing drug cytotoxicity. SNB19 was supplied locally by Dr. Anna Grabowska; SF188 and KNS42 were kindly provided by Mr. Stuart Smith; DAOY, UW228-3 and FB83 were a kind gift from Dr. Beth Coyle. MRC5 was originally obtained from the European Collection of Authenticated Cell Cultures (ECACC). MDA-MB-231 and MCF-7

were originally obtained from the American Type Culture Collection (ATCC). Cells were routinely cultured in T75 flasks in a humidified incubator at 37˚C with 20% $O_2$ and 5% $CO_2$. Other sizes of tissue culture flasks or plates were used according to the requirement of specific experiments. When conducting experiments under hypoxic conditions, cells were placed into a gas-controlled INVIVO$_2$400 humidified hypoxia workstation (Baker Ruskinn, Sanford) at 37˚C with 5% $CO_2$ and 1% $O_2$ for indicated time intervals. Cells in logarithmic growth phase were used for experiments. All cell lines were used within a 12 passage window. Different cell lines were cultured in specific medium listed in Appendix A-Table A1. Iron supplemented donor bovine serum (Gibco, Life Technologies) was heat-inactivated by incubating for 30 min in a 56°C water bath before use. Cells were authenticated by multiplex short tandem repeat (STR) system (Powerplex 16, Promega) approximately every 4-6 months and regularly tested, by technicians every 1-2 months, for mycoplasma using a MycoProbe® Mycoplasma Detection Kit (R&D Systems).

### 2.2.2 Subculture

Tissue culture was performed in a class II biological safety hood, which was disinfected with 70% ethanol before and after use. Cells were cultured in T75 tissue culture flasks with routine culture media until reaching 70-80% confluence. To subculture cells, the spent medium was removed and cell layer gently washed with Dulbecco's phosphate buffered saline (PBS) (without $Ca^{2+}$ and $Mg^{2+}$) (Sigma). 0.5 mg/ml trypsin-EDTA (Sigma) was added to completely cover the cells (2ml was added to T25 flask, 5ml to T75 flask and 7ml to T175 flask) and left for 15-30 seconds. Then the trypsin-EDTA was aspirated and the flask was incubated at 37˚C for 1-3 minutes (the incubation time used was dependent on the cell type). Cells were observed using a microscope to ensure detachment. Complete medium was added to deactivate trypsin-EDTA (volume of medium was equal to that of trypsin-EDTA) prior to harvesting the cells. A certain volume (according to the specific cell type) of cell suspension was transferred into a new tissue culture flask and fresh medium was added to give an appropriate total volume (5ml in T25 flask, 15ml in T75 flask and

25ml in T175 flask). The new tissue culture flask was then placed back into the incubator at 37˚C with 5% $CO_2$. Routinely, SF188, DAOY, UW228-3 and MRC5 cells were passaged using a 1:10 splitting ratio, SNB19 and KNS42 cells were split at a ratio of 1:5.

### 2.2.3 Cryopreservation and cell recovery

In order to ensure the cells used in the experiments were at early passages, cells were initially expanded then stored in liquid nitrogen to keep them at low passage number. Viable cells at 70-80% confluence were brought into suspension using trypsin-EDTA and the total number of cells was counted by a Countess® Automated Cell Counter (Life Technologies). The cell suspension was then centrifuged at 1,000 rpm for 5 min. The supernatant was discarded and the cell pellet was resuspended in an appropriate volume of freezing medium (10% dimethyl sulfoxide (DMSO) in complete culture medium) to achieve a final concentration of ~$1x10^6$ cells/ml. The cells were preserved in cryovials and frozen at -80°C overnight in a cell freezing container before placing into liquid nitrogen (~-180˚C) for long-term storage.

To thaw cryopreserved cells, cryovials containing the frozen cells were taken out from liquid nitrogen storage and placed immediately into a 37˚C water bath. The thawed cells were transferred dropwise into a centrifuge tube containing 9 ml of pre-warmed complete growth medium, followed by centrifugation at 1,000 rpm for 5 min. The supernatant was discarded and the cell pellet gently resuspended in fresh medium, transferred into a T25$cm^2$ tissue culture flask, and placed into the incubator. Culture medium was refreshed the next day to remove residual DMSO, and the cells were then cultured following routine procedures.

### 2.2.4 Cell lysis and protein extraction

Cells were harvested and pelleted by centrifugation at 1,000 rpm for 5 min. The cell pellets were washed once with PBS and pelleted again by centrifugation as before. Pellets were then lysed at 5 x $10^6$ - 1 x $10^7$ cells per ml in RIPA buffer (Sigma), supplemented with 1 X Halt™ Protease Inhibitor

Cocktail (ThermoFisher Scientific) containing protease inhibitors, phosphatase inhibitors and EDTA on ice for 15 min. The resulting whole cell lysates were aliquoted and frozen at -20°C or -80°C for long-term storage and thawed before use. Upon thawing, the lysates were clarified by centrifugation at 13,000 rpm for 10 min at 4°C and the supernatants collected in fresh tubes as whole-cell protein. Thawed lysates were kept on ice prior to use and repeated freeze-thaw cycles avoided.

### 2.2.5 Western blotting

Buffers needed for Western blotting were prepared as described in Appendix A-Table A2. The cell lysates were mixed with 1x NuPAGE™ LDS Sample Buffer (Invitrogen) and 1x NuPAGE™ Reducing Agent (Invitrogen). The mixture was boiled at 100°C for 5 min using a heat block then cooled on ice. 20 µl of protein mixture was loaded into each well of a Bolt™ 4-12% Bis-Tris Plus Gel (ThermoFisher Scientific), after which proteins were separated by gel electrophoresis at 125V for 90 min. Following separation by SDS-PAGE, the proteins were transferred from the gel onto a nitrocellulose membrane (GE Healthcare) by electrophoresis at 25V for 90 min.

The blot was then incubated with blocking buffer at room temperature for 1 h and then probed with a primary antibody diluted in the blocking buffer at 4°C overnight. The antibodies used in the present study, their dilution ratios and host species are listed in Table 2.1

**Table 2.1 List of antibodies used in Western Blotting.**

| Antibodies | Source | Catalogue number | Host species | Dilution | Size (kDa) |
|---|---|---|---|---|---|
| **Anti-TrxR** | Abcam | ab16847 | Mouse | 1:1000 | 55 |
| **Anti-Trx** | Abcam | ab133524 | Rabbit | 1:5000 | 12 |
| **Anti-TxNIP** | Abcam | ab188865 | Rabbit | 1:1000 | 44/50 |
| **Anti-CA9** | 2BScientific | ab00414-1.1 | Mouse | 1:1000 | 49 |
| **Anti-P450** | Abcam | ab180597 | Rabbit | 1:2000 | 77 |
| **Anti-NQO1** | Cell signalling | 3187 | Mouse | 1:500 | 29 |
| **Anti-NQO2** | Abcam | ab137612 | Rabbit | 1:250 | 26 |
| **Anti-β-actin** | Abcam | ab8226 | Mouse | 1:2000 | 42 |
| **Anti-β-actin** | Abcam | ab8227 | Rabbit | 1:1000 | 42 |
| **Rabbit anti-mouse HRP** | Dako | P0260 | Rabbit | 1:1000 | - |
| **Goat anti-rabbit HRP** | Dako | P0448 | Goat | 1:2000 | - |
| **Donkey anti-mouse** | Li-COR IRDye® | 926-68072 | Donkey | 1:10000 | - |
| **Donkey anti-rabbit** | Li-COR IRDye® | 926-32213 | Donkey | 1:10000 | - |

After 3 x 5 min washes with 0.1% PBS/Tween, the membrane was incubated with secondary antibody solution according to the host species of the primary antibody, at room temperature for 1 h**.** After another wash as before, the protein bands were visualised with 1:1 mixture of Amersham enhanced chemiluminescence reagents (GE Healthcare) and developed using Amersham hyperfilm (GE healthcare) or scanned using an Odyssey® FC Imager (LI-COR Biosciences). If two colour infrared Western blotting was performed, the infrared intensity of the bands was quantified using Image Studio Version 4.1 (LI-COR Biosciences) and normalised against the signals of β-actin, which was used as an internal control to ensure equal loading of the samples in the gel. If the membrane needed to be re-probed, it was incubated in stripping buffer (Abcam) at room temperature for 5-10 min, washed and blocked again as described above, followed by re-probing with appropriate primary and secondary antibodies. Then the membrane was visualised again as described above.

### 2.2.6 Clinical samples

This study is reported in accordance with REMARK (reporting recommendations for tumour marker prognostic studies) criteria (McShane et

al., 2005). Ethical approval was granted by Local Regional Ethics Committee in Nottingham (11/EM/0076; R&I 14CS005), under the title 'Comparative molecular analysis of childhood brain tumours'. Formalin-fixed, paraffin-embedded tissue microarray (TMA) sections (4 μm) from four independent cohorts (i.e. adult GBM, paediatric LGG, paediatric HGG and MB) were provided by Prof. Richard Grundy and Mr. Stuart Smith from the Children's Brain Tumour Research Centre (CBTRC), at the University of Nottingham, UK. A total of 405 brain tumour samples were collected from various hospitals across England (mainly Nottingham and Birmingham) between 1958 and 2015. Exclusion of referral, miscoded, and recurrent cases resulted in 312 primary brain tumour cases with available clinical information. Clinical data of patients were retrieved from the original medical documents and pathological characteristics were re-evaluated by a multi-disciplinary team of experts including a paediatric neuro-oncologist and a neuropathologist at CBTRC, Nottingham University Hospitals NHS Trust, according to WHO 2007 criteria (Louis et al., 2007). Any differences were resolved by careful discussion. Patient follow-up data were also updated regularly by researchers at CBTRC. OS was calculated as the time interval (in months) from the date of the original diagnosis to the time of death, or from the time of diagnosis to the last date known to be alive for those patients censored. The median follow-up period, in all cohorts, was 160 months (ranging from 0 to 552 months).

Eighteen adult GBM patients were treated at Queen's Medical Centre (QMC), University of Nottingham, in the period between 2013 and 2015. There were 10 females and 8 males and the median age of the patients was 59 years, ranging from 26 to 73 years. The median follow-up time was 15 months (ranging 1-42). The 12-month survival rate was 65%. In this cohort, only one patient had a tumour with the R132H mutation in the IDH1 gene and the vast majority of cases (17/18) had wild-type IDH1 gene. 50% of patients (9/18) had hypomethylated MGMT promoter, 1 patient had hypermethylated MGMT promoter and the status of MGMT promoter was not available for the remaining 8 patients. 77.8% (14/18) of patients received complete resection

while the remaining 22.2% (4/18) of patients had partial resection. After surgery, 16 patients completed 60 Gy (2 Gy per fraction over 6 weeks) radiotherapy and adjuvant TMZ treatment whilst the remaining 2 patients were treated with radiotherapy alone. Half of the patients (9/18) received Gliadel wafers, which are biodegradable copolymers impregnated with the alkylating agent carmustine (Ashby et al., 2016). Detailed clinicopathological data was recorded at the time of surgery and is shown in Table 2.2.

**Table 2.2 Clinicopathological variables of the adult GBM cohort.**

| Variable | Number of Patients | Percentage (%) |
|---|---|---|
| Age (years) | | |
| ≤59 | 10 | 55.6 |
| >59 | 8 | 44.4 |
| Gender | | |
| Male | 8 | 44.4 |
| Female | 10 | 55.6 |
| Tumour Site | | |
| Parietal | 8 | 44.4 |
| Temporal | 5 | 27.8 |
| Occipital | 1 | 5.6 |
| Frontal | 4 | 22.2 |
| Resection status | | |
| Complete | 14 | 77.8 |
| Partial | 4 | 22.2 |
| Radiotherapy | | |
| 60 Gy | 17 | 94.4 |
| < 60 Gy | 1 | 5.6 |
| Temozolomide | | |
| Yes | 16 | 88.9 |
| No | 2 | 11.1 |
| Gliadel wafer | | |
| Yes | 9 | 50.0 |
| No | 9 | 50.0 |
| IDH-1 | | |
| Wild-type | 17 | 94.4 |
| Mutant | 1 | 5.6 |
| MGMT status | | |
| Hypomethylated | 9 | 90.0 |
| Hypermethylated | 1 | 10.0 |
| N/A | 8 | |
| Survival status | | |
| Living | 4 | 28.6 |
| Deceased | 14 | 77.8 |

Abbreviations: GBM, glioblastoma; IDH1, isocitrate dehydrogenase 1; MGMT, O-6-methylguanine DNA methyltransferase; N/A, not available.

136 paediatric patients with LGG were treated at various hospitals in England between 1958 and 2003. The median age of the patients was 6 years, ranging from 3 months to 16 years, 48.7% of patients were boys (56/115), 33.6% of patients had supratentorial disease (38/113), 82.3% of patients had grade I disease (102/124) and 42.5% of patients developed recurrence (48/113); where patient number did not total 136 information was not available for the remaining patients. The median follow-up time was 167 months (ranging 0-560). Unfortunately, surgical and adjuvant treatment data were not available. The clinicopathological criteria of the cohort are shown in Table 2.3.

The paediatric HGG cohort included 137 patients who were diagnosed at various hospitals in England between 1982 and 2007. The median follow-up time was 12 months (ranging 0-206). The median age of patients was 8 years, ranging from 5 days to 21 years. In this cohort 63.0% of patients (80/127) were boys, 71.8% of patients had supratentorial disease (84/117), 26.7% of patients had grade III tumours (35/131) and 73.3% of patients had grade IV tumours (96/131). 15.8% of patients had complete tumour resection (16/101), 43.6% of patients had partial resection (44/101), and 40.6% of patients had biopsies (41/101). 88.9% of patients developed recurrence (96/108) and 11.1 % of patients were recurrence-free (12/108) at the time of follow-up. Where patient number does not total 137 information was not available for the remaining patients. The clinicopathological criteria of the cohort are shown in Table 2.3. The treatment strategies for this cohort were, unfortunately, also not recorded in the original databases and data retrieval was extremely difficult. This is primarily due to the fact that electronic health record systems were not introduced into the UK until 2002 and the cases in the cohort were collected as early as 1950s from multiple hospitals across England.

**Table 2.3 Clinicopathological variables of the paediatric LGG and HGG cohorts.**

| Variable | pLGG N (%) | pHGG N (%) |
|---|---|---|
| Age (years) | | |
| ≤3 | 27 (23.5) | 23 (20.2) |
| >3 | 88 (76.5) | 91 (79.8) |
| ND | 21 | 23 |
| Gender | | |
| Male | 59 (51.3) | 80 (63.0) |
| Female | 56 (48.7) | 47 (37.0) |
| ND | 21 | 10 |
| Tumour site | | |
| Supratentorial | 38 (33.6) | 84 (71.8) |
| Infratentorial | 75 (66.4) | 33 (28.2) |
| ND | 23 | 20 |
| Tumour grade | | |
| I | 102 (82.3) | 0 (0.0) |
| II | 22 (17.7) | 0 (0.0) |
| III | 0 (0.0) | 35 (26.7) |
| IV | 0 (0.0) | 96 (73.3) |
| ND | 12 | 6 |
| Resection status | | |
| Complete | NA | 16 (15.8) |
| Partial | NA | 44 (43.6) |
| Biopsy | NA | 41 (40.6) |
| ND | 136 | 36 |
| Recurrent status | | |
| Yes | 48 (42.5) | 96 (88.9) |
| No | 65 (57.5) | 12 (11.1) |
| ND | 23 | 29 |
| Survival status | | |
| Living | 79 (69.9) | 19 (17.3) |
| Deceased | 34 (30.1) | 91 (82.7) |
| ND | 23 | 27 |

Abbreviations: pLGG, paediatric low-grade glioma; pHGG, paediatric high-grade glioma; ND, not determined.

In the MB cohort, 114 patients were diagnosed and treated at Birmingham and Nottingham University Hospitals between 1985 and 2012. The median follow-up time was 53 months (ranging 1-249). The median age of the

patients was 6.8 years (ranging from 9.1 months to 19 years), and 72.2% (78/108) of patients were boys. According to conventional histological classification, 61.3% of patients were classified as classic MB (57/93), 16.1% as desmoplastic MB (15/93), 17.2% as large cell/anaplastic MB (16/93), 1.1% as MB with extensive nodularity (1/93) and 4.3% as MB with myogenic differentiation (4/93). The metastatic stage of MBs was determined according to the Modified Chang Staging System (Chang et al., 1969), where the extent of metastasis is subdivided into M0 (no metastasis), M1 (presence of tumours in the cerebrospinal fluid), M2 (gross nodular seeding present intracranially beyond the primary tumour site), M3 (metastasis in spinal subarachnoid space), and M4 (metastases outside the cerebrospinal axis). Among the 92 patients with available metastatic information, 60.9% of patients were M0 stage (56/92), 6.5% of patients were M1 stage (6/92), 10.9% of patients were M2 stage (10/92), 18.5% of patients were M3 stage (17/92), and 3.3% of patients were M4 stage (3/92). As with the paediatric LGG and HGG cohorts, the treatment details were also not available for this cohort. The clinicopathological variables of the cohort are listed in Table 2.4.

**Table 2.4 Clinicopathological variables of the MB patient cohort.**

| Variable | Number of Patients | Percentage (%) |
|---|---|---|
| Age (years) | | |
| ≤3 | 20 | 18.7 |
| >3 | 87 | 81.3 |
| ND | 7 | |
| Gender | | |
| Male | 78 | 72.2 |
| Female | 30 | 27.8 |
| ND | 6 | |
| Histological Classification | | |
| Classical | 57 | 61.3 |
| Desmoplastic | 15 | 16.1 |
| Large cell/anaplastic | 16 | 17.2 |
| Extensive nodularity | 1 | 1.1 |
| myogenic | 4 | 4.3 |
| ND | 21 | |
| Resection status | | |
| Complete | 52 | 61.2 |
| Partial | 33 | 38.8 |
| ND | 29 | |
| Recurrent status | | |
| Yes | 42 | 44.7 |
| No | 52 | 55.3 |
| ND | 20 | |
| Metastatic stage | | |
| M0 | 56 | 60.9 |
| M1 | 6 | 6.5 |
| M2 | 10 | 10.9 |
| M3 | 17 | 18.5 |
| M4 | 3 | 3.3 |
| ND | 22 | |
| Survival status | | |
| Living | 44 | 45.4 |
| Deceased | 53 | 54.6 |
| ND | 17 | |

Abbreviations: MB, medulloblastoma; ND, not determined.

### 2.2.7 Antibody optimisation

Prior to immunohistochemical staining of patients' specimens, the specificity of the primary antibodies (i.e. mouse anti-TrxR antibody (ab16847, Abcam), rabbit anti-Trx antibody (ab133524, Abcam), and rabbit anti-TxNIP antibody (ab188865, Abcam)) was determined by Western blotting described in Section 2.2.5, using a range of brain and breast cancer cell lysates prepared following procedures described in Section 2.2.4. The specificity of these antibodies was confirmed previously in pancreatic cancer cell lines by Khaled Alhadyan, a previous PhD student in our group. Antibodies yielding expected single bands without non-specific bands were applicable for immunohistochemistry (IHC) staining. The antibody concentrations applied in IHC was further optimised using whole mount paraffin-embedded tissue sections from 2 adult GBM cases, following the procedures described in Section 2.2.8. The whole tissue sections were also used to evaluate the heterogeneity and the pattern of protein expression across the tumours. Optimisation of antibody concentration was performed using an immunohistochemical staining kit - Novolink polymer detection kit (Leica). Three different concentrations of each antibody were initially tried, including one as recommended by the manufacturer in the datasheet, one higher and one lower. Breast tumour composite sections, which consisted of six stage I breast carcinoma specimens (grade I to III), were used as positive and negative controls for optimisation; negative controls omitted primary antibody (Woolston et al., 2012).

### 2.2.8 TMAs and Immunohistochemistry

Expression of Trx system proteins was assessed in brain tumour TMAs by using IHC in a single staining run. The TMAs were constructed and maintained within the CBTRC at the University of Nottingham. In total, 31 TMAs were kindly provided to the current author by Prof. Richard Grundy and Mr. Stuart Smith. For paediatric LGG, HGG and MB TMAs, two/three 0.6 mm cores were used for each patient with the cores being taken from a representative tumour area as assessed by neuropathologists. Adult GBM TMAs were constructed as described previously (Smith et al., 2017). In short, triplicate

cores were collected from each of three regions (inner tumour core, rim and invasive margin) per tumour specimen. The invasive margin was defined by the region with 5-aminolevulinic acid (GliolanTM) fluorescence at surgery beyond the T1 enhancing region on magnetic resonance imaging (MRI) (Smith et al., 2017). Several cores from other tissues were also included in each TMA block to act as potential positive controls and to aid orientation. Freshly cut 4 µm thick TMA sections were mounted onto Superfrost$^{+}$ microscope slides (Menzel-Glaser) then quickly dried at 37°C overnight (by Lisa Storer, CBTRC, University of Nottingham). Sections were then stored, sealed from air at 4°C and stained using the procedures described below within 1 week of section cutting and mounting.

Immunohistochemistry (IHC) was performed as previously described using a Novolink Polymer Detection Kit (Leica) according to the manufacturers' instructions (Zhang et al., 2019b). Briefly, slides were deparaffinised with two xylene baths (5 min each), sequentially rehydrated in a decreasing series of industrial methylated spirit (IMS) baths (2x in 100% IMS for 2 min and 1x in 70% IMS for 2 min), followed by a 5 min wash in running tap water. Antigen retrieval was performed in 0.01 M sodium citrate buffer (pH 6.0) in a microwave for 20 min, with 10 min at 750W and 10 min at 450W. Following microwaving, slides were washed immediately under running tap water to stop the retrieval process. The slides were then loaded onto sequenza slide racks (ThermoFisher Scientific). 100 µl Peroxidase Block solution was added to tissues for 5 min at room temperature to neutralise the endogenous peroxidase activity and the slides were then washed 2 x 5 min with Tris-buffered saline (TBS) (50 mM Tris-Cl, 150 mM NaCl, pH 7.6). 100 µl of Protein Block solution was then added for another 5 min, to minimise the non-specific interactions of the subsequent detection reagents, and washing was carried out as above before incubating the slides with 100 µl of primary antibody solution overnight at 4°C. The primary antibodies were diluted in bond primary antibody diluent (Leica) and the dilution of each antibody solution was optimised as described in Section 2.2.7, which was: anti-Trx antibody

1:2000, anti-TrxR antibody 1: 150, and anti-TxNIP antibody 1:1000. Following antibody incubation, the slides were washed 2 x 5 min with TBS prior to the application of 100 µl Post Primary solution (a polymer penetration enhancer) for 30 min at room temperature, slides were subsequently washed and incubated with 100 µl of NovoLink Polymer (anti-mouse/rabbit IgG-Poly-horseradish peroxidase (HRP)) for another 30 min followed by a 2 x 5 min TBS wash. Immunohistochemical reactions were visualised using 3, 3'-diaminobenzidine (DAB) solution (1:20 DAB chromogen in DAB substrate buffer) as the chromogenic substrate and slides were counterstained with haematoxylin for 6 min, removed from the sequenza trays, and placed in the Leica autostainer for dehydration and fixation: 5 min wash with running tap water followed by 3 x 2 min IMS baths (1x in 70% IMS and 2x in 100% IMS), and then 2 x 5 min 100% xylene baths. Slides were mounted with DPX mounting medium (Sigma) and left to dry overnight. Breast tumour composite sections comprised of grade 1 and 2 early stage invasive tumours were included as positive and negative controls with each run; negative controls omitted primary antibody.

### 2.2.9 Immunohistochemical scoring

Training, use and review of scoring methods was provided by a consultant neuropathologist, Dr. Simon Paine. Slides were scanned at high-resolution using a Nanozoomer Digital Pathology Scanner (Hamamatsu Photonics) with 200x magnification. Cytoplasmic staining was assessed semi-quantitatively using an immunohistochemical H-score, where staining intensity was divided into four grades: none (0), weak (1), medium (2), and strong (3). H-scores were then calculated by multiplying the percentage of staining area by the intensity grade, giving a range between 0 and 300 (i.e. 0 x negatively stained tumour % + 1 x weakly stained tumour % + 2 x moderately stained tumour % + 3 x strongly stained tumour %). Nuclear staining was assessed as the percentage of nuclei with any intensity of staining. TrxR and Trx showed both cytoplasmic and nuclear staining whilst TxNIP only showed cytoplasmic staining when assessed. An average score was generated by taking the mean

score of two or three cores as appropriate and it was used as the final score for each case.

Greater than 30% of the cases were initially scored by two independent assessors blinded to the clinical outcome of patients and each other's scores (Dr. Sarah Storr scored the TrxR expression; Khaled Alhadyan scored the Trx and TxNIP expression). The single measure intra-class correlation coefficient (ICC) analysis was conducted to determine the level of concordance between scorers and, if sufficiently robust, the current author then scored the remaining cores. The single measure ICCs were above 0.7 for all markers assessed across all brain tumour cohorts, indicating excellent concordance between scorers (Table 2.5). Cores that were lost/damaged during sectioning or had less than 10% tumour tissue were not scored.

**Table 2.5 Intra-class correlation coefficient (ICC) analysis of Trx, TrxR and TxNIP scoring across different brain tumour cohorts.**

| Markers | Tumour types | | | |
|---|---|---|---|---|
| | Adult GBM | Paediatric LGG | Paediatric HGG | MB |
| Cytoplasmic TrxR | 0.701 | 0.724 | 0.702 | 0.712 |
| Nuclear TrxR | 0.796 | 0.741 | 0.836 | 0.900 |
| Cytoplasmic Trx | 0.835 | 0.734 | 0.874 | 0.897 |
| Nuclear Trx | 0.790 | 0.700 | 0.925 | 0.892 |
| Cytoplasmic TxNIP | 0.808 | 0.740 | 0.873 | 0.956 |

Abbreviations: GBM, glioblastoma; LGG, low-grade glioma; HGG, high-grade glioma; MB, medulloblastoma.

Optimal cut-offs for each protein were obtained based on OS using X-tile bioinformatics software, version 3.6.1. X-tile is a graphical method that provides an unbiased cut-point by describing the presence of substantial tumour subpopulations and showing the robustness of the relationship between tumour biomarker expression and patient outcomes (Camp et al., 2004). The cut off points for individual markers are listed in Table 2.6 and these cut-offs were used to stratify the tumours into low- *vs.* high-expression for each protein.

**Table 2.6 X-tile cut points for stratification of TrxR, Trx and TxNIP expression in all four brain tumour cohorts.**

| Markers | Adult GBM | | | Paediatric LGG | Paediatric HGG | MB |
|---|---|---|---|---|---|---|
| | Core | Rim | Invasive | | | |
| Cytoplasmic TrxR | 78 | 100 | 86 | 163 | 160 | 180 |
| Nuclear TrxR (%) | 63 | 80 | 85 | 60 | 58 | 58 |
| Cytoplasmic Trx | 143 | 150 | 105 | 37 | 160 | 172 |
| Nuclear Trx (%) | 38 | 23 | 60 | 12 | 57 | 60 |
| TxNIP | 175 | 173 | 175 | 40 | 195 | 125 |

Abbreviations: GBM, glioblastoma; LGG, low-grade glioma; HGG, high-grade glioma; MB, medulloblastoma; TrxR, thioredoxin reductase; Trx, thioredoxin; TxNIP, thioredoxin-interacting protein.

Mean and median values of both cytoplasmic and nuclear scores were also determined and shown in Appendix A-Table A3 and Table A4.

### 2.2.10 Statistical analysis

Data analysis was performed using IBM SPSS Statistics (version 24). The relationships between categorised protein expression and clinicopathological variables were examined using Pearson's chi-square ($\chi^2$) test of association or Fisher's exact test if a cell count was less than 5 in a 2 × 2 table. To assess the relationship between protein expression and survival outcomes, survival curves were plotted using the Kaplan-Meier method with statistical significance determined using the Log-rank test. Cox proportional hazards regression model was used to test the statistical independence and significance of the predictors on OS. The differences in protein expression between different tumour types/grades or tumour regions were determined using one-way ANOVA or non-parametric Kruskal-Wallis test when the homogeneity of variance was violated. Multiple comparisons between two groups were conducted using a pairwise post-hoc t-test or Mann-Whitney U test when the data were not normally distributed. A *P* value of <0.05 was considered statistically significant.

## 2.3 Results

### 2.3.1 Antibody specificity and IHC optimisation

As mention in Section 2.2.7, before conducting the immunohistochemical staining of patients' specimens, the specificity of TrxR, Trx and TxNIP

antibodies were assessed by Western blotting using various brain and breast cancer cell lysates. Breast cancer cell lines (MDA-MB-231 and MCF-7) were included as a positive control (previously confirmed as expressing these proteins in the study of a previous PhD student, Yimin Zhang, in Prof. Stewart Martin's group) (Zhang, 2014). The TrxR, Trx and TxNIP antibodies detected single bands of the expected size at 55 KDa, 12 KDa and 50 KDa (or 44 kDa), respectively over multiple human cell lines (Figure 2.1).

No non-specific bands were detected by any of the antibodies across any of the cell lines. Results suggested that TrxR, Trx and TxNIP antibodies tested were specific and detected the correct protein bands. They were therefore deemed suitable for use in immunohistochemical staining of brain tumour patients' specimens, with the appropriate concentration of each antibody to be used in IHC optimised as shown in Appendix A-Figure A1-Figure A3. The concentration of each antibody applied in IHC was optimised in adult GBM composite tissue sections prior to immunohistochemical staining on brain tumour TMAs.

The appropriate staining concentrations for each antibody were confirmed by discussion and consultation with the local neuropathologist, Dr. Simon Paine. A dilution of 1:150 for anti-TrxR antibody, 1:2000 for anti-Trx antibody, and 1:1000 for anti-TxNIP antibody was determined to give the optimal staining on the GBM tissue sections.

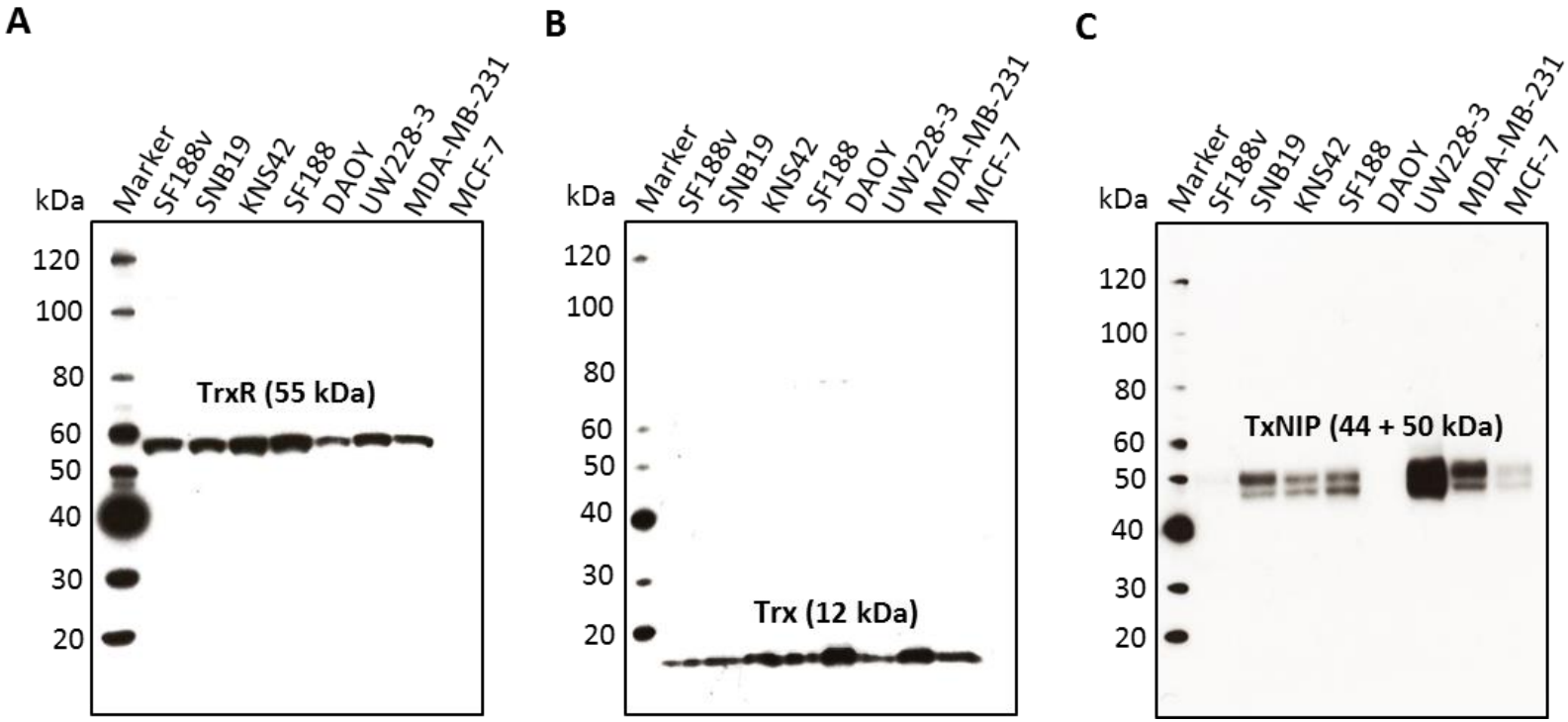



**Figure 2.1 The specificity of anti-TrxR, anti-Trx and anti-TxNIP antibodies was determined in Western blotting by using various cell lines**. Lysates from human brain cancer SF188v, SNB19, KNS42, SF188, DAOY and UW228-3 cells and breast cancer MDA-MB-231 and MCF-7 cells were subjected to Western blotting to assess the specificity of (A) TrxR, (B) Trx and (C) TxNIP primary antibodies. Figures present the representative blots of 2 independent experiments with lysates from cells with different passage numbers.

### 2.3.2 Staining pattern and frequency of Trx system expression in brain tumours

Following confirmation of antibody specificity and optimisation of antibody concentration, expression of TrxR, Trx, and TxNIP protein was assessed by using IHC in the adult GBM, paediatric LGG, paediatric HGG, and MB cohorts. All three markers - TrxR, Trx and TxNIP - displayed a mixture of diffuse and granular cytoplasmic staining in all types of brain tumour cells. Some diffuse nuclear staining was observed for TrxR and Trx but not for TxNIP. Heterogeneous staining was shown between, as well as within, certain tumour cores for all markers, varying from weak to strong staining. Occasional stromal and endothelial cell staining was also observed, however, this was not scored as part of this study. In certain tumour cases, there was also heterogeneous staining between the triplicate cores. In line with this, heterogeneous distribution pattern of these markers was observed in the whole mount sections in adult GBM cases, but triplicate cores allow for this potential heterogeneity to be presented. Representative photomicrographs of staining patterns in adult GBM are shown in Figure 2.2, paediatric LGG in Figure 2.3, paediatric HGG in Figure 2.4, and MB in Figure 2.5.

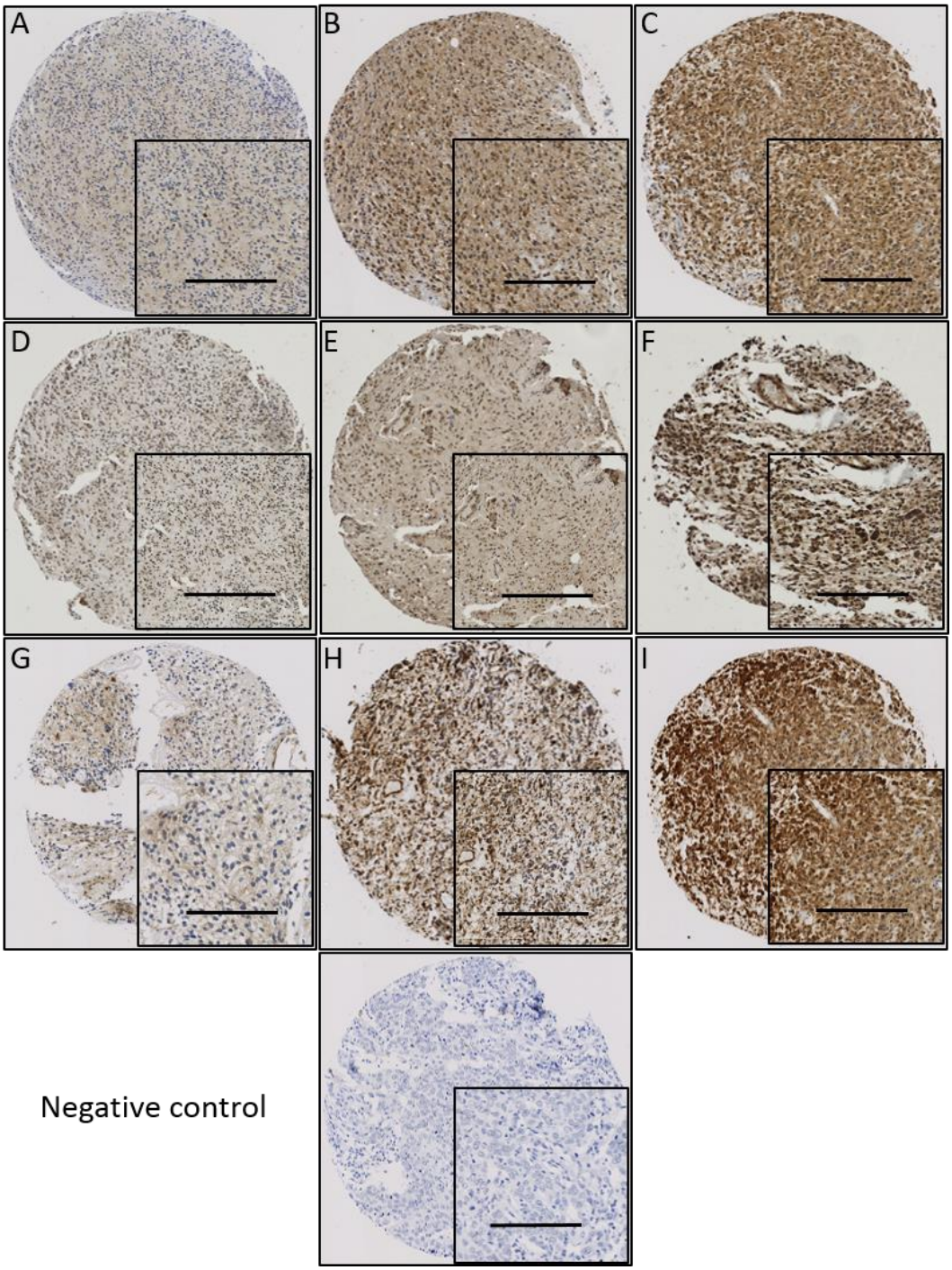



**Figure 2.2 Representative photomicrographs of Trx, TrxR and TxNIP expression in adult GBM.** Expression levels, including low (left), moderate (middle) and high (right) staining, of Trx (A-C), TrxR (D-F) and TxNIP (G-I) at 10X magnification with 20X magnification inset panel. Scale bar represents 100 µm.

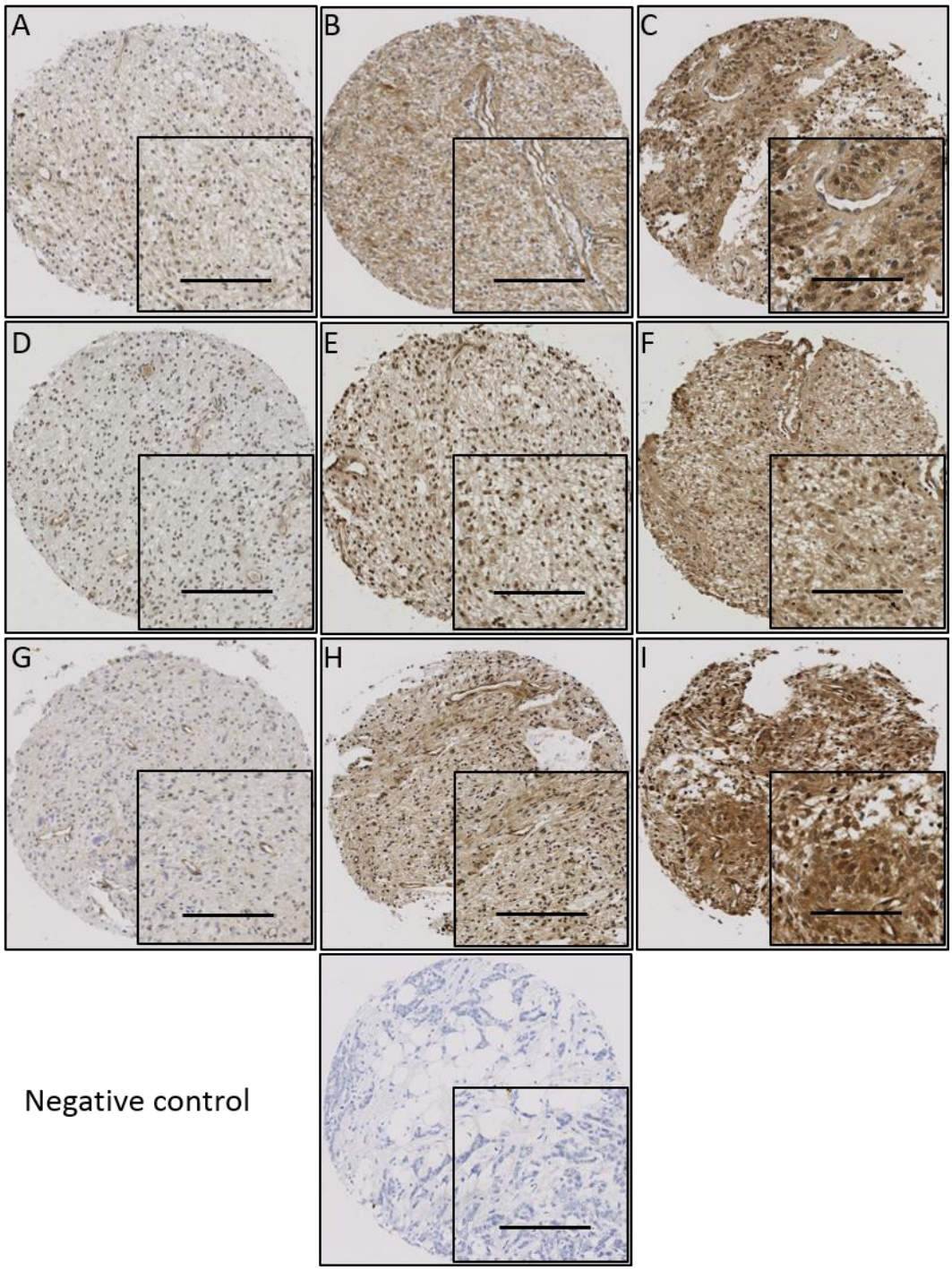



**Figure 2.3 Representative photomicrographs of Trx, TrxR and TxNIP expression in paediatric LGG.** Expression levels, including low (left), moderate (middle) and high (right) staining, of Trx (A-C), TrxR (D-F) and TxNIP (G-I) at 10X magnification with 20X magnification inset panel. Scale bar represents 100 µm.

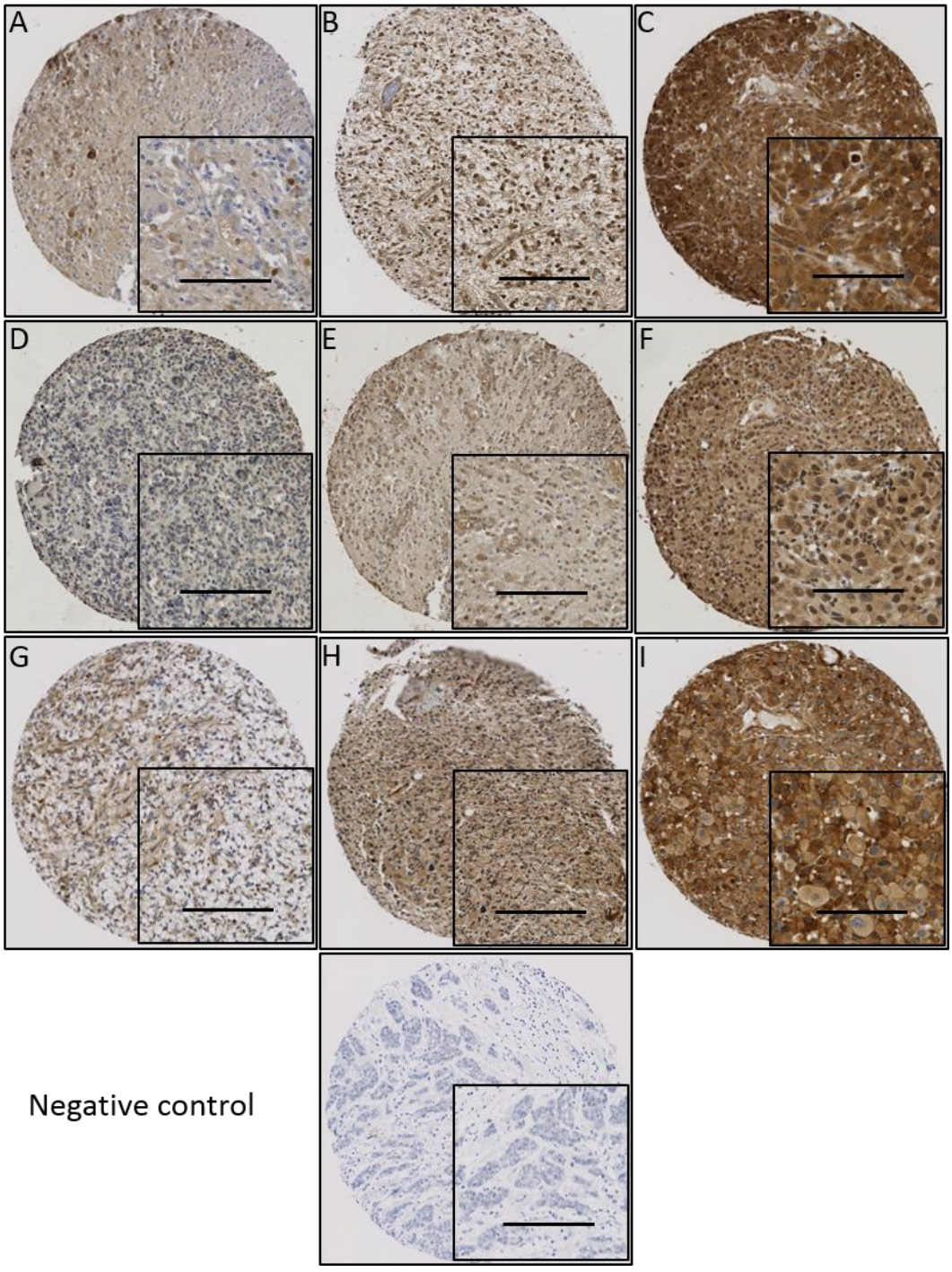



**Figure 2.4 Representative photomicrographs of Trx, TrxR and TxNIP expression in paediatric HGG.** Expression levels, including low (left), moderate (middle) and high (right) staining, of Trx (A-C), TrxR (D-F) and TxNIP (G-I) at 10X magnification with 20X magnification inset panel. Scale bar represents 100 µm.

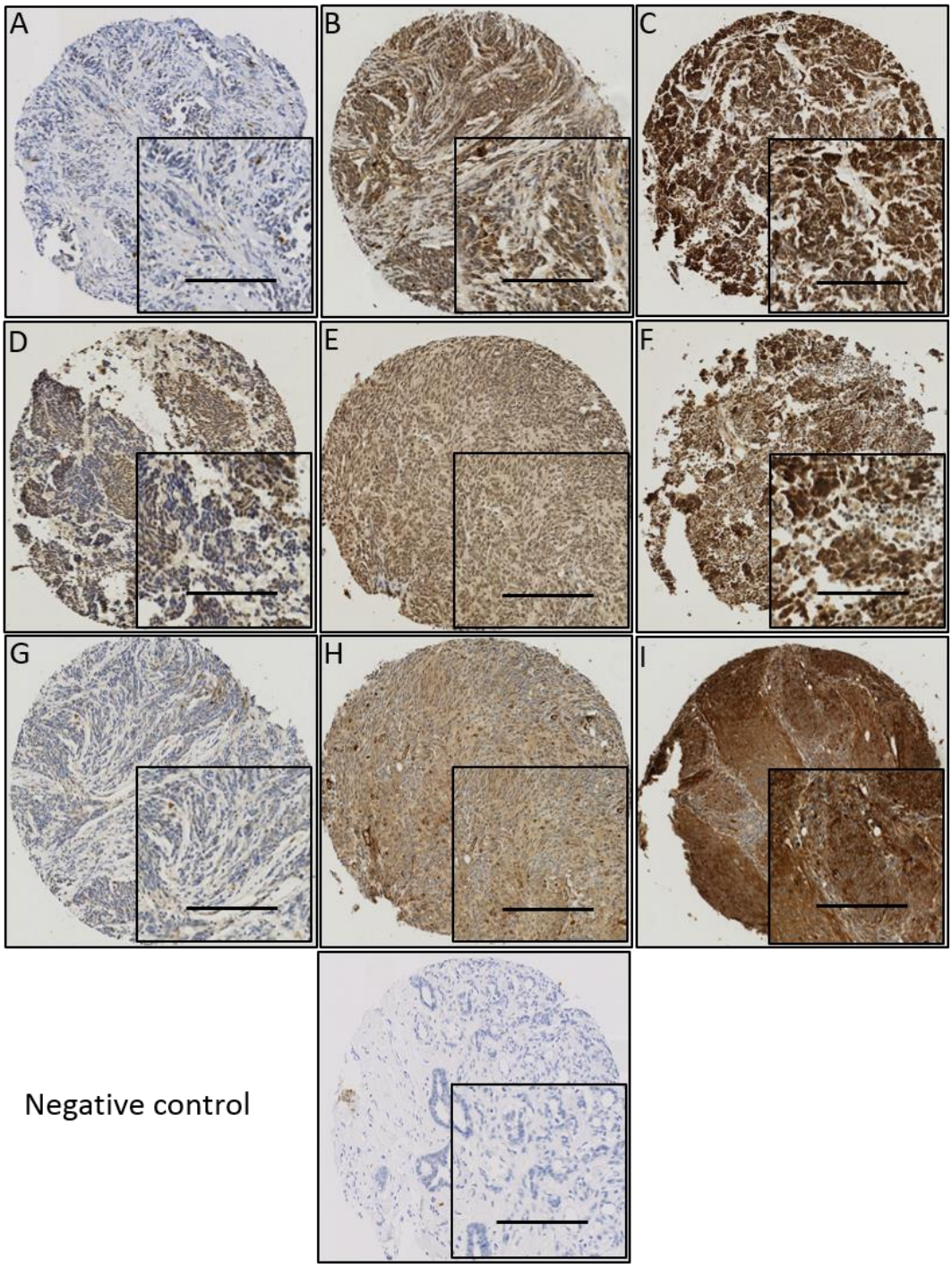



**Figure 2.5 Representative photomicrographs of Trx, TrxR and TxNIP expression in MB.** Expression levels, including low (left), moderate (middle) and high (right) staining, of Trx (A-C), TrxR (D-F) and TxNIP (G-I) at 10X magnification with 20X magnification inset panel. Scale bar represents 100 µm.

Cytoplasmic staining of all three markers and nuclear staining of TrxR and Trx were scored over the four brain tumour cohorts. The median scores and ranges of TrxR, Trx and TxNIP expression for each tumour cohort are shown in

Table 2.7. The statistics of both H-score and nuclear score of each protein expression are described in detail in Appendix A-Table A3 and Table A4.

**Table 2.7 The median scores and ranges of TrxR, Trx and TxNIP expression in brain tumour cohorts.**

| Markers | Adult GBM | | | Paediatric LGG | Paediatric HGG | MB |
|---|---|---|---|---|---|---|
| | Core | Rim | Invasive | | | |
| Cytoplasmic TrxR | 78 (30-187) | 100 (77-190) | 86 (50-105) | 120 (5-235) | 67 (0-217) | 130 (0-270) |
| Nuclear TrxR (%) | 47 (7-95) | 72 (15-100) | 79 (45-98) | 55 (0-95) | 36 (0-100) | 64 (0-100) |
| Cytoplasmic Trx | 122 (5-185) | 105 (0-198) | 105 (90-140) | 97 (0-273) | 110 (0-283) | 137 (0-280) |
| Nuclear Trx (%) | 35 (0-90) | 34 (0-90) | 52 (10-85) | 19 (0-88) | 30 (0-98) | 38 (0-99) |
| Cytoplasmic TxNIP | 168 (30-228) | 140 (30-222) | 170 (115-195) | 173 (0-280) | 192 (10-280) | 150 (12-2) |

Abbreviations: GBM, glioblastoma; LGG, low-grade glioma; HGG, high-grade glioma; MB, medulloblastoma.

Bioinformatics software X-tile was used to generate an optimal cut point for each protein based on OS, which stratified the scores of tumour samples into low- *vs.* high- score. The cut-off points of TrxR, Trx and TxNIP expression for all four brain tumour cohorts are listed in Table 2.6. In the adult GBM cohort (rim), the X-tile cut point for cytoplasmic TrxR was 100, nuclear TrxR was 80, cytoplasmic Trx was 150, nuclear Trx was 23, and TxNIP was 173; with 60.0% (9/15), 53.3% (8/15), 26.7% (4/15), 53.3% (8/15), and 53.3% (8/15) respectively having high protein expression. In the paediatric LGG cohort, the X-tile cut point for cytoplasmic TrxR was 163, nuclear TrxR was 60, cytoplasmic Trx was 37, nuclear Trx was 12, and TxNIP was 40; with 17.4% (15/86), 49.4%% (43/87), 89.7% (78/87), 47.1% (40/85), and 89.9% (80/89) respectively having high protein expression. In the paediatric HGG cohort, the X-tile cut point for cytoplasmic TrxR was 160, nuclear TrxR was 58, cytoplasmic Trx was 160, nuclear Trx was 57, and TxNIP was 195; with 12.5% (13/104), 23.1% (24/104), 27.1% (29/107), 17.6% (19/108), and 47.4% (45/95) respectively having high protein expression. In the MB cohort, the X-tile cut point for cytoplasmic TrxR was 180, nuclear TrxR was 58, cytoplasmic Trx was 172, nuclear Trx was 60, and TxNIP was 125; with 17.1% (14/82), 66.3%

(53/80), 30.0% (24/80), 21.3% (17/80), and 65.8% (52/79) respectively having high protein expression. A proportion of cores within the TMAs could not be assessed due to insufficient tumour cells or the cores being missing.

### 2.3.3 Relationship of Trx system expression with clinicopathological variables and clinical outcome in the adult GBM cohort.

The relationships between Trx system expression and clinicopathological variables and patient survival were independently assessed in each brain tumour cohort and within the adult GBM cohort the analysis was separately conducted by tumour region (core, rim, and invasive margin). In adult GBM core samples, high nuclear TrxR expression was associated with tumours located at temporal lobe ($\chi^2$=9.370, df=3, *P*=0.008); in samples taken from the invasive margin, low cytoplasmic TrxR expression was linked with female patients ($\chi^2$=8.571, df=1, *P*=0.015) (Appendix A-Table A5 and Table A6). No significant associations were observed between Trx or TxNIP expression and clinicopathological variables in any tumour region (data not shown).

High cytoplasmic TrxR expression was significantly associated with adverse OS (*P*=0.027) in rim samples (Figure 2.6A), whereas nuclear TrxR expression was not (*P*=0.462) (Figure 2.6B). The expression of cytoplasmic Trx, nuclear Trx and TxNIP was also not associated with OS in rim samples (*P*=0.147, 0.752 and 0.977, respectively) (Figure 2.6C-E). No associations were observed between TrxR, Trx and TxNIP expression and OS in either core or invasive samples (Appendix A-Figure A4 and Figure A5). The association between protein expression and patient survival in the rim samples was explored further. All traditional prognostic variables were individually tested for their association with survival in the rim samples using the Kaplan-Meier with significance determined using the log-rank test. The results showed that none of the traditional prognostic variables was associated with patient survival including patient age, tumour site, resection status and IDH-1 status (with individual Kaplan-Meier statistics of *P*=0.396, *P*=0.484, *P*=0.855, and *P*=0.643 respectively). Therefore, multivariate analysis was not performed to

determine whether cytoplasmic TrxR had independent prognostic value in rim samples.

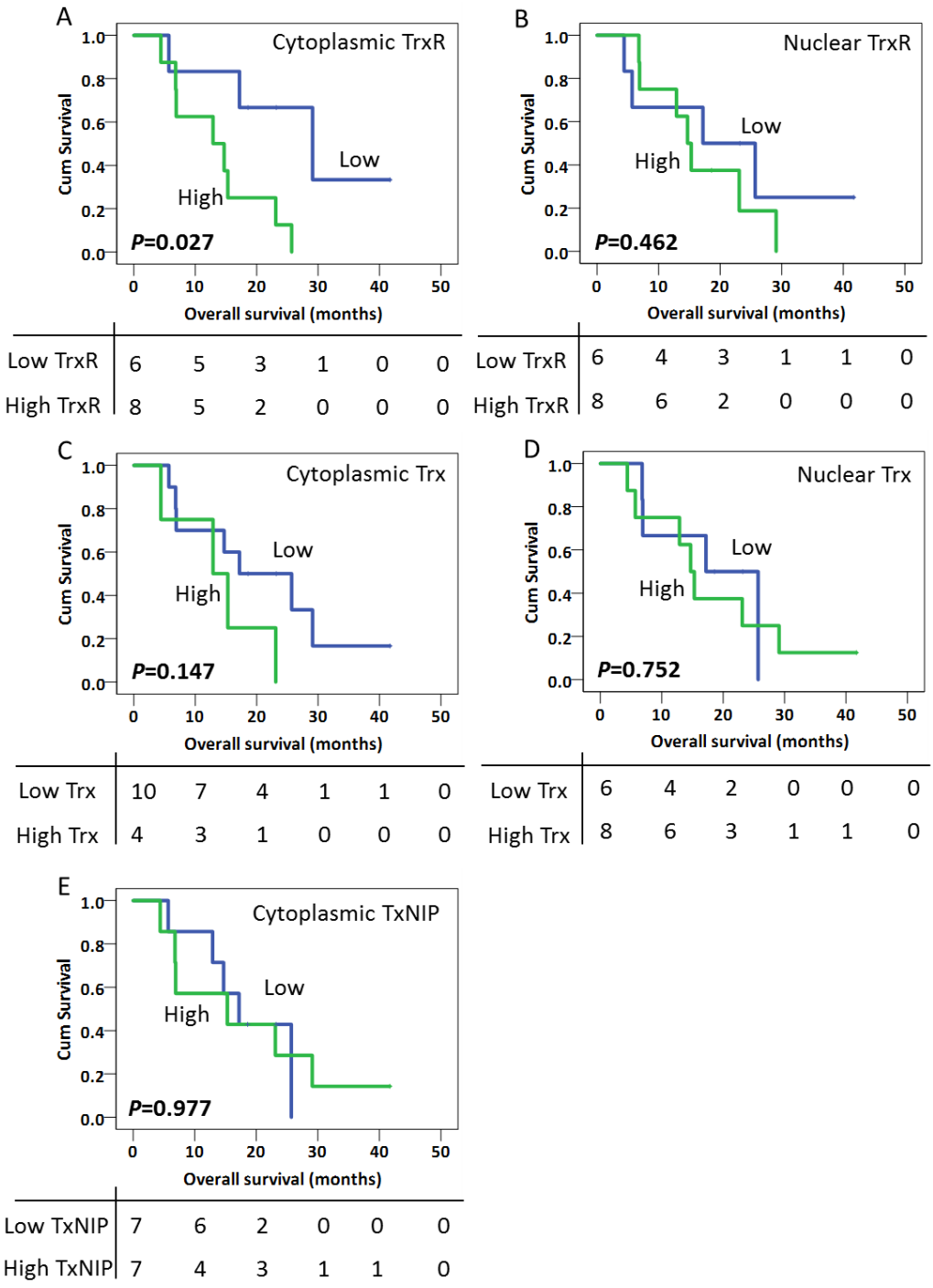



**Figure 2.6 Kaplan-Meier survival curves of TrxR, Trx and TxNIP expression and OS in the adult GBM cohort (rim).** High expression of cytoplasmic TrxR (A) is associated with poor overall survival (*P*=0.027). No significant associations are detected between nuclear TrxR (B), cytoplasmic/nuclear Trx (C/D) and TxNIP (E) expression and overall survival (all *P* values >0.05). Curves show low (blue line) and high protein expression (green line) with significance determined using the log-rank test. The numbers below the Kaplan-Meier curve are the number of patients at risk at the specified month.

### 2.3.4 Relationship of Trx system expression with clinicopathological variables and clinical outcome in the paediatric LGG cohort.

In the paediatric LGG cohort, high cytoplasmic TrxR was associated with supratentorial tumours ($\chi^2$=10.568, df=1, *P*=0.003) and the presence of tumour recurrence ($\chi^2$=9.736, df=1, *P*=0.006), whereas high nuclear TrxR expression was associated with the absence of tumour recurrence ($\chi^2$=4.762, df=1, *P*=0.029). Low TxNIP expression was associated with infratentorial tumours ($\chi^2$=4.189, df=1, *P*=0.041) (Appendix A-Table A7).

Kaplan-Meier survival analysis showed that high expression of cytoplasmic TrxR was significantly associated with poor OS (*P*=0.001) (Figure 2.7A) whereas high TrxR expression in the nucleus was significantly associated with better OS (*P*=0.034) (Figure 2.7B). High expression of Trx within both cytoplasm and nucleus was significantly associated with better OS (*P*=0.002 and *P*=0.048, respectively) (Figure 2.7C and D). In addition, high TxNIP expression was also associated with improved OS (*P*=0.003) (Figure 2.7E). The multivariate analysis was not performed in this cohort as none of the potential confounding factors were significantly associated with patient survival including tumour grade, tumour site, patient age, and gender (with individual Kaplan-Meier statistics of *P*=0.110, *P*=0.270, *P*=0.403, and *P*=0.724 respectively).

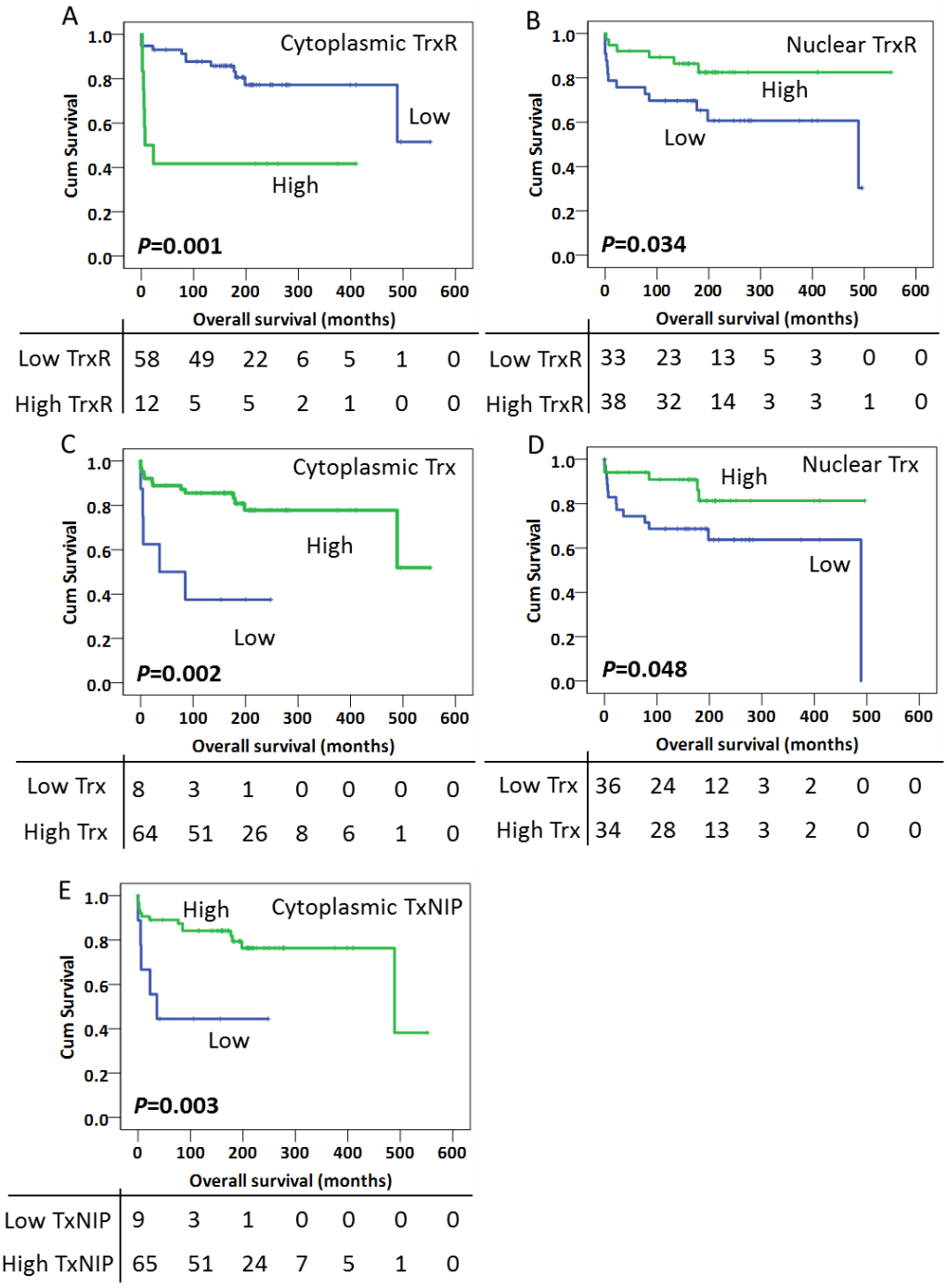
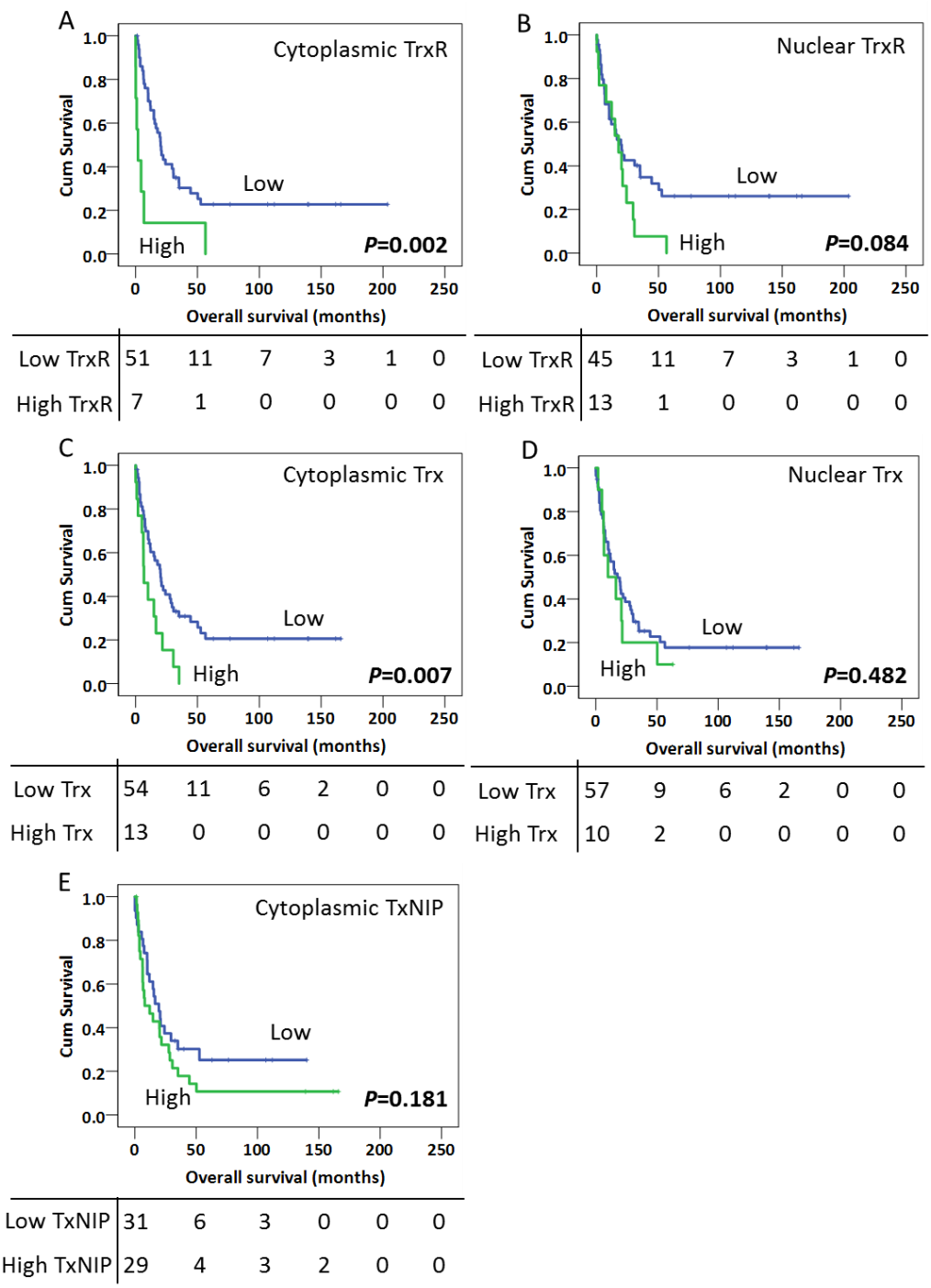



**Figure 2.7 Kaplan-Meier survival curves of TrxR, Trx and TxNIP expression and OS in the paediatric LGG cohort.** High expression of cytoplasmic TrxR (A) is associated with adverse overall survival (*P*=0.001) whilst high expression of nuclear TrxR (B) is correlated with better overall survival (*P*=0.034). High expression of Trx within the cytoplasm (C) or the nucleus (D) is associated with improved overall survival (*P*=0.002 and *P*=0.048 respectively). High expression of TxNIP (E) is also associated with better overall survival (*P*=0.003). Curves show low (blue line) and high protein expression (green line) with significance determined using the log-rank test. The numbers below the Kaplan-Meier curve are the number of patients at risk at the specified month.

### 2.3.5 Relationship of Trx system expression with clinicopathological variables and clinical outcome in the paediatric HGG cohort.

In the paediatric HGG cohort, anaplastic oligodendroglioma was significantly associated with high cytoplasmic Trx expression whilst GBM with low cytoplasmic Trx expression ($\chi^2$=9.785, df=2, *P*=0.008). High cytoplasmic TxNIP expression was linked with GBM ($\chi^2$=9.362, df=2, *P*=0.009), supratentorial tumours ($\chi^2$=5.314, df=2, *P*=0.021) and higher tumour grade ($\chi^2$=7.923, df=1, *P*=0.005) (Appendix A-Table A8 and Table A9). No associations between both cytoplasmic and nuclear TrxR expression and clinicopathological variables were observed (data not shown).

Univariate survival analysis showed that high expression of both cytoplasmic TrxR and Trx was significantly associated with adverse OS (*P*=0.002 and *P*=0.007, respectively) (Figure 2.8A and C). However, expression of both TrxR and Trx in the nucleus was not significantly associated with OS (*P*=0.084 and *P*=0.482 respectively) (Figure 2.8B and D). No association was detected between TxNIP expression and OS (*P*=0.181) (Figure 2.8E). Multivariate analysis could not be conducted as none of the potential confounding factors, namely age at diagnosis, gender, histological subtypes, tumour grade, tumour site and extent of surgery, were found to be significantly associated with survival in univariate analysis (with individual Kaplan–Meier statistics of *P*=0.224, *P*=0.949, *P*=0.211, *P*=0.085, *P*=0.688, and *P*=0.494 respectively). Therefore, the independent prognostic value of TrxR and Trx was unable to be determined at this point.




| | | | | | | |
|---|---|---|---|---|---|---|
| Low TrxR | 51 | 11 | 7 | 3 | 1 | 0 |
| High TrxR | 7 | 1 | 0 | 0 | 0 | 0 |

| | | | | | | |
|---|---|---|---|---|---|---|
| Low TrxR | 45 | 11 | 7 | 3 | 1 | 0 |
| High TrxR | 13 | 1 | 0 | 0 | 0 | 0 |

| | | | | | | |
|---|---|---|---|---|---|---|
| Low Trx | 54 | 11 | 6 | 2 | 0 | 0 |
| High Trx | 13 | 0 | 0 | 0 | 0 | 0 |

| | | | | | | |
|---|---|---|---|---|---|---|
| Low Trx | 57 | 9 | 6 | 2 | 0 | 0 |
| High Trx | 10 | 2 | 0 | 0 | 0 | 0 |

| | | | | | | |
|---|---|---|---|---|---|---|
| Low TxNIP | 31 | 6 | 3 | 0 | 0 | 0 |
| High TxNIP | 29 | 4 | 3 | 2 | 0 | 0 |

**Figure 2.8 Kaplan-Meier survival curves of TrxR, Trx and TxNIP expression and OS in the paediatric HGG cohort.** High expression of cytoplasmic TrxR (A) and Trx (C) is associated with adverse OS (*P*=0.002 and *P*=0.007 respectively). No significant associations are found between the expression of nuclear TrxR (B), nuclear Trx (D), and TxNIP (E) and OS (*P* = 0.084, 0.482 and 0.181, respectively). Curves show low (blue line) and high protein expression (green line) with significance determined using the log-rank test. The numbers below the Kaplan-Meier curves are the number of patients at risk at the specified month.

### 2.3.6 Relationship of Trx system expression with clinicopathological variables and clinical outcome in the paediatric MB cohort.

In the MB cohort, high expression of both cytoplasmic and nuclear Trx was associated with the presence of tumour recurrence ($\chi^2$=4.655, df=1, *P*=0.031 and $\chi^2$=5.851, df=1, *P*=0.016 respectively). High nuclear Trx expression was also linked with extensive nodularity subtype of medulloblastoma whilst low expression with classic subtype ($\chi^2$=9.941, df=4, *P*=0.041) (Appendix A-Table A10). No other significant associations were found between protein expression and clinicopathological variables (data not shown).

In univariate analysis, patients with high TrxR expression in the cytoplasm had a significantly shorter OS compared with low expression (*P*=0.013) (Figure 2.9A). High Trx expression within cytoplasm and nucleus were both associated with adverse OS (*P*=0.033 and *P*=0.007 respectively) (Figure 2.9C and D). No significance was observed between nuclear TrxR or TxNIP expression and OS (*P*= 0.230 and *P*= 0.287 respectively) (Figure 2.9B and E). In multivariate Cox regression model, cytoplasmic TrxR and nuclear Trx expression remained significantly associated (*P*=0.009 and 0.013 respectively) with OS when including the potential confounding factors of age, extent of surgery and metastatic status (with individual Kaplan–Meier statistics of *P*=0.001, *P*=0.038, and *P*<0.001 respectively), whereas cytoplasmic Trx expression was not independently associated with survival when potential confounding factors were included in the analysis (*P*=0.206) (Table 2.8).

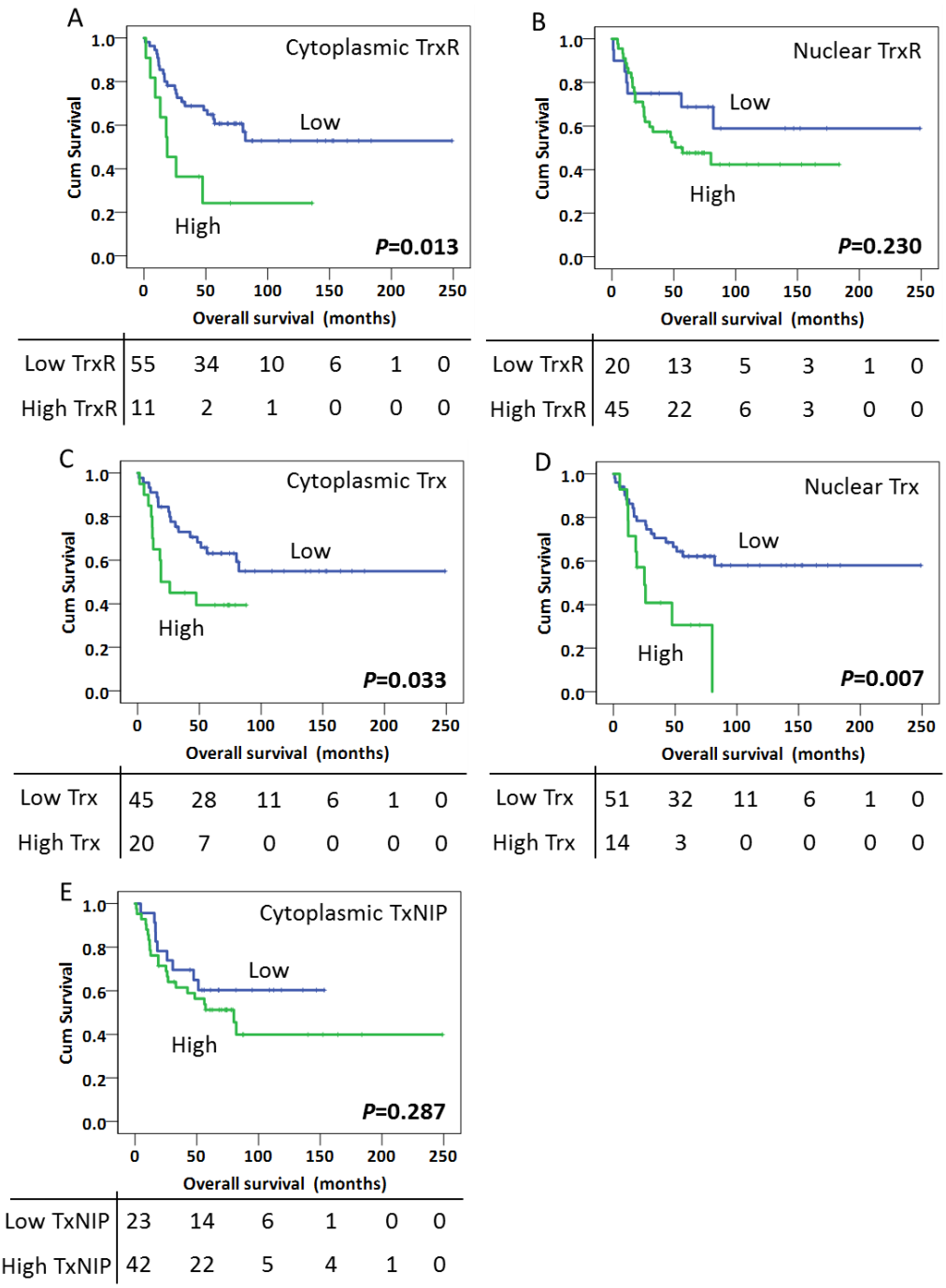



**Figure 2.9 Kaplan-Meier survival curve of TrxR, Trx and TxNIP expression and OS in the MB cohort.** High expression of cytoplasmic TrxR (A), cytoplasmic Trx (C) and nuclear Trx (D) are associated with adverse OS (*P*=0.013, *P*=0.033 and *P*=0.007 respectively). No significance was observed between nuclear TrxR or TxNIP expression and OS (*P*= 0.230 and *P*= 0.287 respectively). Curves show low (blue line) and high protein expression (green line) with significance determined using the log-rank test. The numbers below the Kaplan-Meier curve are the number of patients at risk at the specified month.

**Table 2.8 Multivariate Cox proportional hazards analysis for predictors of overall survival in medulloblastoma patients.**

| Variables | *P* value | Exp (B) | 95% CI for Exp(B) | |
|---|---|---|---|---|
| | | | Lower | Upper |
| Cytoplasmic TrxR expression | **0.009** | 4.850 | 1.487 | 15.822 |
| Age (3 years) | **0.004** | 0.190 | 0.062 | 0.585 |
| Extent of surgery | 0.397 | 0.643 | 0.232 | 1.785 |
| Metastatic status | **0.000** | 6.354 | 2.266 | 17.816 |
| Cytoplasmic Trx expression | 0.206 | 1.895 | 0.703 | 5.107 |
| Age (3 years) | **0.007** | 0.221 | 0.074 | 0.662 |
| Extent of surgery | 0.549 | 0.716 | 0.240 | 2.132 |
| Metastatic status | **0.003** | 5.640 | 1.812 | 17.555 |
| Nuclear Trx expression | **0.013** | 5.386 | 1.418 | 20.451 |
| Age (3 years) | **0.003** | 0.188 | 0.062 | 0.572 |
| Extent of surgery | 0.097 | 0.311 | 0.079 | 1.233 |
| Metastatic status | **0.011** | 4.033 | 1.375 | 11.827 |

Significant *P* values are indicated by bold type. Exp(B) is used to denote hazard ratio and 95% CI is used to denote 95% confidence interval.

### 2.3.7 Comparison of protein expression between different regions in adult GBM patients

As shown in Figure 2.10A, the levels of cytoplasmic TrxR expression significantly differed between the core, rim and invasive regions of adult GBM tumours when comparing the data from each group using the non-parametric Kruskal-Wallis test (*P*=0.043). Core samples had a median H-score of 78 (range 60-187), rim samples a median of 108 (range 80-190), and invasive samples a median of 86 (range 50-105). On a post-hoc t-test, there was a higher median of cytoplasmic TrxR expression in the rim region than the invasive region (*P*=0.036), but there were no significant differences between core and rim (*P*=0.713) or core and invasive regions (*P*=0.190).

The median nuclear expression of TrxR was 49% for core samples (range 7%-95%), 80% for rim samples (range 15%-100%), and 85% for invasive samples (range 45%-98%). Using the one-way ANOVA test, a significant difference was observed in nuclear TrxR expression between these three intra-tumour regions (*P*=0.003). On post-hoc *t*-test, there was a significant difference between core and rim samples (*P*=0.019), and between core and invasive

samples (*P*=0.004), but not between rim and invasive samples (*P*=0.724) (Figure 2.10B). The expression levels of cytoplasmic Trx, nuclear Trx and TxNIP were also compared between different tumour areas, but no statistically significant variations between areas were detected (*P*=0.987, 0.442 and 0.944, respectively) (Figure 2.10C, D, and E respectively).

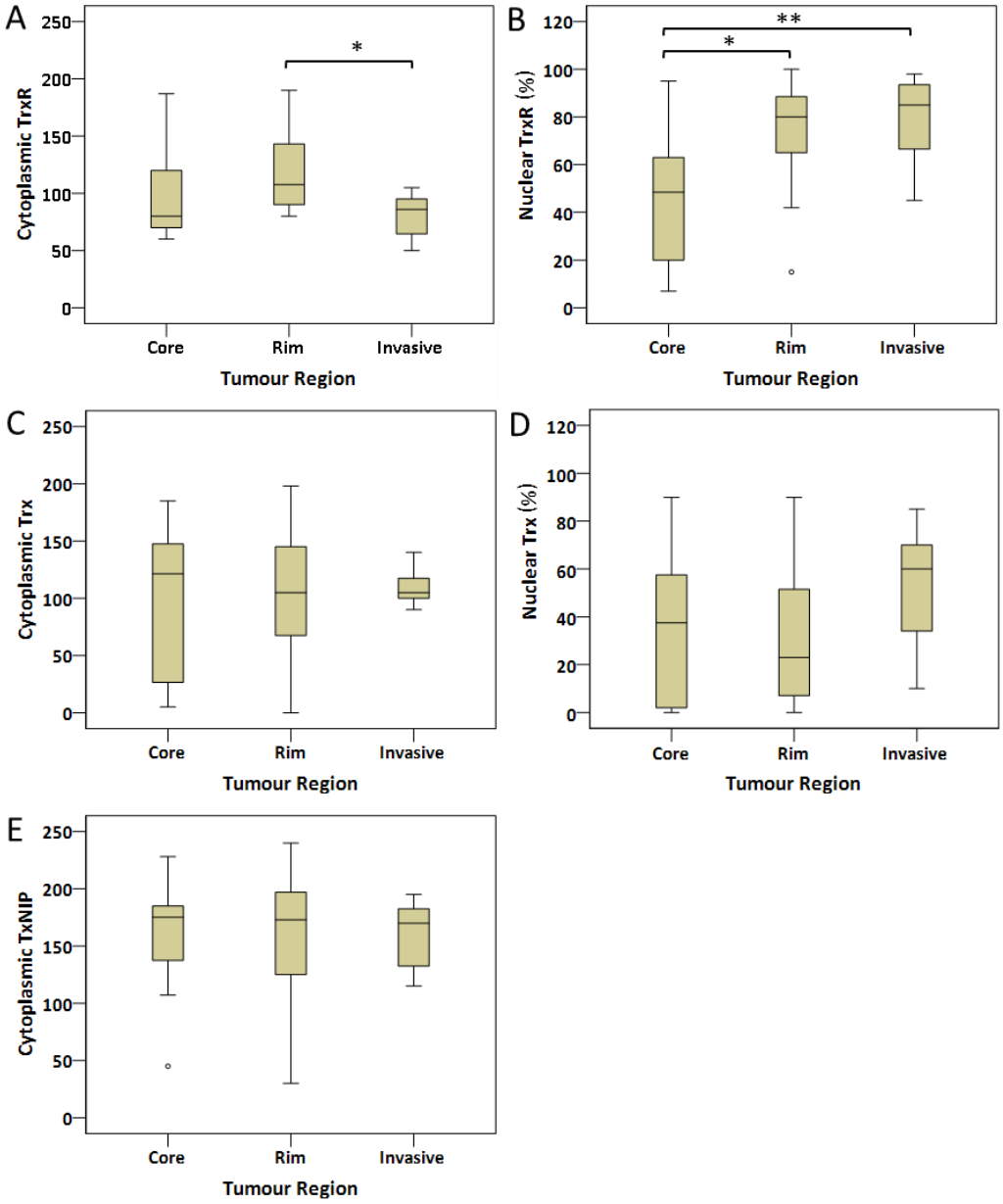



**Figure 2.10 Box plots demonstrating the differences in expression of TrxR, Trx and TxNIP between core, rim and invasive regions of adult GBM tumours.**
A significantly higher expression of cytoplasmic TrxR (A) is noted in the rim samples compared to the invasive samples (*P*=0.036 on post-hoc *t*-test). Significant differences in nuclear TrxR expression (B) were observed between core and rim regions (*P*=0.019) and between core and invasive regions (*P*=0.004) but not between rim and invasive regions (*P*=0.724). No statistically significant variations between areas are detected for Trx (C and D) and TxNIP expression (E).

### 2.3.8 Comparison of protein expression between different tumour types

The median H-score of cytoplasmic TrxR was 78 (range 30-187) for the adult GBM cohort, 120 (range 5-235) for the paediatric LGG cohort, 80 (range 0-213) for the paediatric HGG cohort, and 130 (range 0-270) for the MB cohort (Figure 2.11A). Using the non-parametric Kruskal-Wallis test, there was a significant difference in cytoplasmic TrxR expression between these four brain tumour cohorts ($P$<0.001). From the post-hoc t-test, there were significant differences between paediatric LGG and paediatric HGG ($P$<0.001), and between paediatric HGG and MB ($P$<0.001). No significant differences were detected between adult GBM and any of the other three tumour types.

The adult GBM cohort had a median of 49% nuclear TrxR expression (range 7%-95%), paediatric LGG a median of 57% (range 0%-95%), paediatric HGG a median of 28% (range 0%-100%), and MB a median of 73% (range 0%-100%) (Figure 2.11B). There were statistically significant variations of nuclear TrxR expression between different tumour types ($P$<0.001 one-way ANOVA), with significant differences detected between paediatric LGG and HGG cohorts ($P$<0.001) and between paediatric HGG and MB cohorts ($P$<0.001) on Mann-Whitney U test.

The median H-score of cytoplasmic Trx was 122 (range 5-185) for the adult GBM cohort, 97 (range 0-273) for the paediatric LGG cohort, 110 (range 0-285) for the paediatric HGG cohort, and 136 (range 0-280) for the MB cohort (Figure 2.11C). There was a significant difference in cytoplasmic Trx expression between different types of brain tumours ($P$=0.003, Kruskal-Wallis test). On pairwise comparison tests, the difference between paediatric LGG and MB was the only pair that achieved statistical significance ($P$=0.004 post-hoc t-test).

Significant differences were also found between brain tumour types for nuclear Trx expression ($P$<0.001 Kruskal-Wallis). The median nuclear Trx expression was 38% (range 0%-90%) for adult GBM, 12% (range 0%-88%) for paediatric LGG, 20% (range 0%-98%) for paediatric HGG, and 34% (range 0%-99%) for MB (Figure 2.11D). On the Mann-Whitney U test, MB had

significantly higher levels of nuclear Trx expression, relative to both the paediatric LGG ($P$=0.011) and paediatric HGG tumours ($P$<0.001). Paediatric HGG tumours also showed significantly greater nuclear Trx expression, compared with the paediatric LGG tumours ($P$= 0.027). Among all four brain tumour types adult GBM had the highest expression of nuclear Trx, although no statistical significance was achieved on pairwise comparison tests.

The levels of TxNIP expression significantly differed between different tumour types from one-way ANOVA ($P$=0.017). Median TxNIP expression was highest for the paediatric HGG (188, range 10-280), followed by adult GBM (175, range 45-228), paediatric LGG (173, range 0-280), and lowest for MB (150, range 12-270) (Figure 2.11E). There were significant differences, from Mann-Whitney U tests, between paediatric LGG and HGG tumours ($P$=0.022), and between paediatric HGG and MB tumours ($P$=0.004).

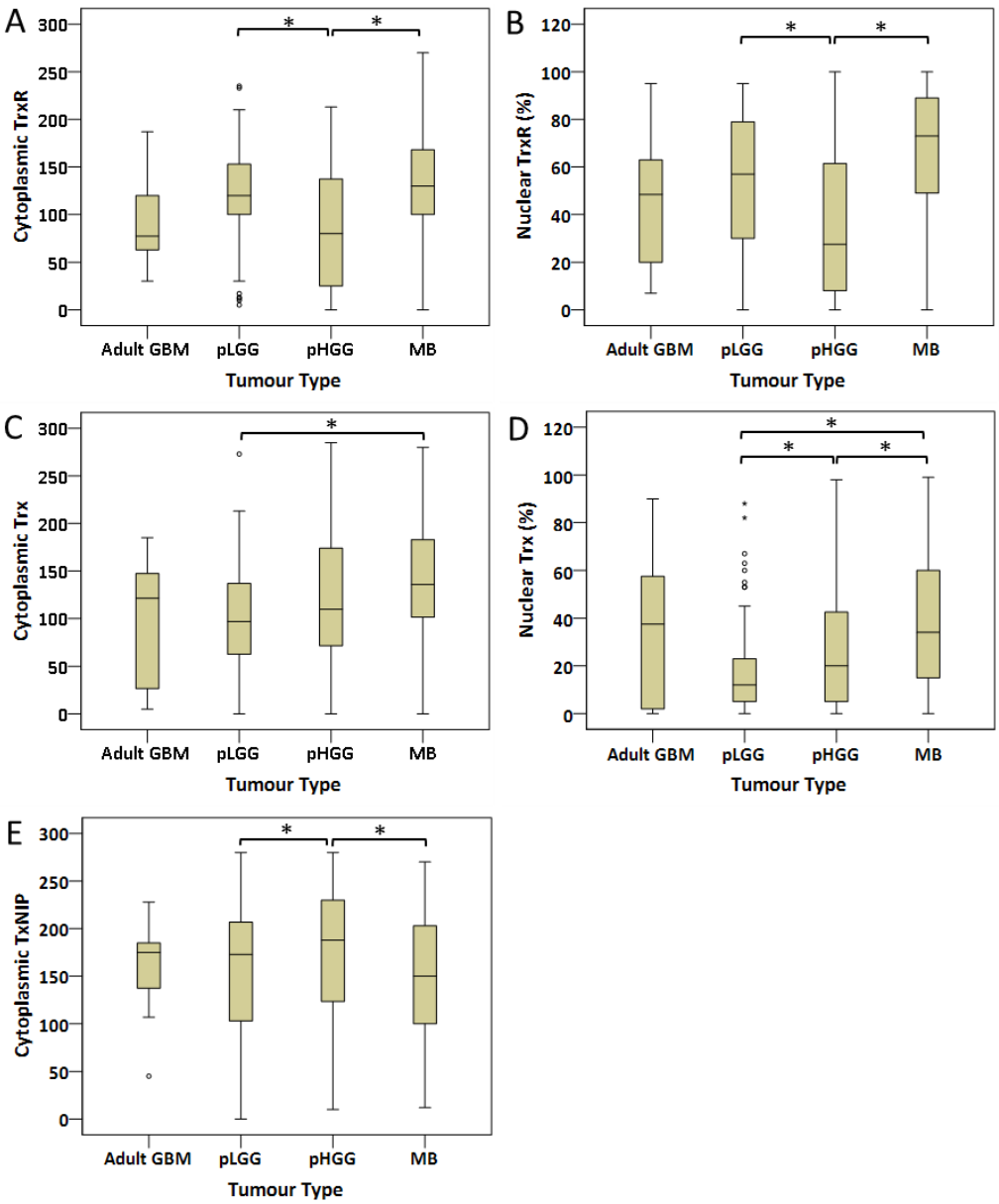



**Figure 2.11 Box plots of TrxR, Trx and TxNIP in different brain tumour types.** The expression of both cytoplasmic (A) and nuclear (B) TrxR is significantly lower in pHGG than pLGG and MB. Cytoplasmic Trx (C) expression is significantly higher in MB compared to pLGG, and nuclear Trx (D) expression significantly differs between pLGG, pHGG and MB, with pLGG having the lowest level and MB having the highest level. A significantly higher expression of TxNIP (E) is noted in pHGG compared to pLGG and MB. Abbreviations: GBM, glioblastoma; pLGG, paediatric low-grade glioma; pHGG, paediatric high-grade glioma; MB, medulloblastoma.

### 2.3.9 Comparison of protein expression between different tumour grades in paediatric gliomas

The levels of TrxR, Trx and TxNIP expression were also compared between different tumour grades in paediatric gliomas. In total, there were 159 valid cases of paediatric gliomas including 82 grade I gliomas, 25 grade III gliomas,

and 52 grade IV gliomas. Unfortunately, the grade II gliomas were not included in this analysis, as scoring was not able to be conducted due to missing cores or insufficient tumour tissues. As shown in Figure 2.12A, the expression of cytoplasmic TrxR was significantly higher in grade I gliomas than both grade III (*P*=0.010) and grade IV gliomas (*P*=0.001). The grade I gliomas showed the highest median H-score of 120 (range 5-235), followed by grade IV gliomas with a median score of 80 (range 3-217), and then grade III gliomas with a median score of 60 (range 0-200). Like cytoplasmic TrxR expression, grade I gliomas showed the highest level of nuclear TrxR expression whilst the grade III gliomas had the lowest level. The median positive fraction was 57% (range 0%-95%) for grade I gliomas, 25% (range 0%-95%) for grade III, and 28% (range 0%-100%) for grade IV (Figure 2.12B). A significant difference in nuclear TrxR expression was observed between grade I and grade IV gliomas (*P*=0.001), but not between grade I and III (*P*=0.085) or between grade III and IV gliomas (*P*=0.974).

The expression levels of cytoplasmic Trx were almost equal between grade I, grade III, and grade IV gliomas with median values of H-score ranging from 92 to 101 (*P*=0.876) (Figure 2.12C). Nuclear Trx expression appeared to be showing elevated levels of expression in both the grade III and grade IV gliomas compare with reduced levels in grade I gliomas but this did not achieve statistical significance (*P*=0.448) (Figure 2.12C and D). As shown in Figure 2.12E, the median H-score of TxNIP expression was 164 (range 0-280) for grade I gliomas, 173 (range 50-258) for grade III gliomas, and 204 (range 53-280) for grade IV gliomas. The expression of TxNIP was elevated as the pathological grades escalated, and the expression was significantly higher in grade IV than in grade I gliomas (*P*=0.001), but no difference in TxNIP expression was noted between grade I and III gliomas (*P*=0.556) or between grade III and IV gliomas (*P*=0.052).

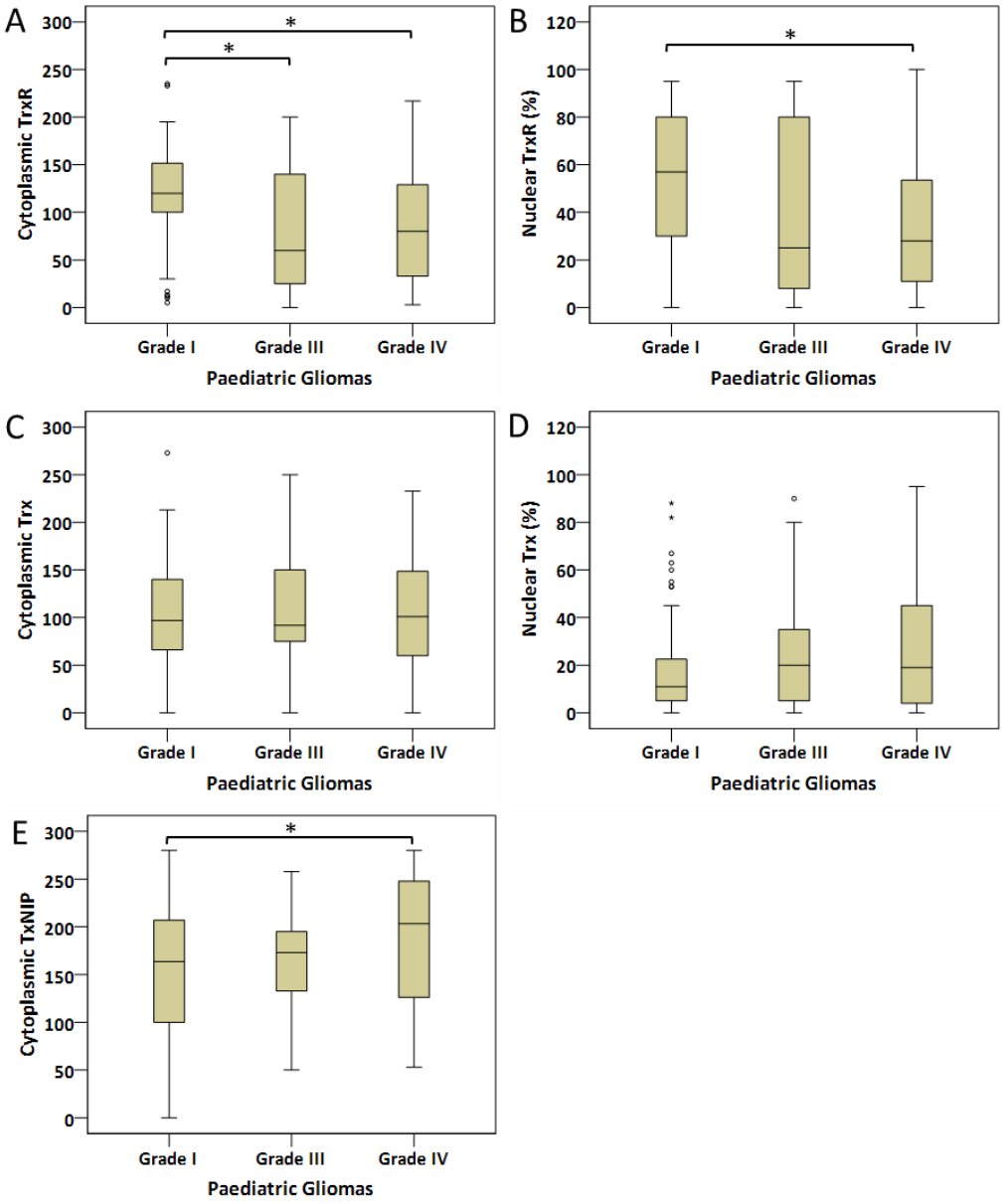



**Figure 2.12 Box plots demonstrating the differences in expression of TrxR, Trx and TxNIP between different WHO grades of paediatric gliomas.** The expression of cytoplasmic TrxR (A) is significantly higher in grade I gliomas than both grade III (*P*=0.010) and grade IV gliomas (*P*=0.001). The expression of nuclear TrxR (B) is also significantly greater in grade I gliomas than grade IV gliomas (P=0.001), but not grade III gliomas (*P*=0.085). No significant difference of both cytoplasmic Trx (*P*=0.876) and nuclear Trx (*P*=0.448) expression is detected between tumour grades. A significantly higher expression of TxNIP (E) is noted in grade IV gliomas compared to grade I gliomas (*P*=0.001).

## 2.4 Discussion

The current study examined the expression of TrxR, Trx and TxNIP in four independent brain tumour cohorts and determined whether any associations existed between their expression and patient survival or clinicopathological variables. It also investigated and compared the levels of Trx system protein expression between different brain tumours types/grades and between different tumour regions. This is the first study to report upon the expression of all three members of Trx system proteins together in such a broad variety of brain tumours. Overall, some significant associations between protein expression of the Trx system and clinicopathological/survival criteria were found. Interesting variations in protein expression between different tumour types/grades/regions were also observed.

In the adult GBM cohort, as the samples were separately collected from core, rim, and invasive regions, the statistical analysis was performed independently for the individual region. A significant association was observed between high nuclear TrxR expression and tumour located at temporal lobe in core samples, and between high cytoplasmic TrxR expression and male patients in invasive samples. High cytoplasmic TrxR expression was significantly associated with adverse OS in rim samples ($P$=0.027), but this could not be demonstrated in multivariate analysis. Other studies have also investigated the expression of Trx system in GBMs, including a study of 27 GBM patients, which showed significantly increased TrxR levels in serum and tumoural tissues of GBM patients compared to healthy controls, but this study did not assess associations with patient survival (Kemerdere et al., 2013). A study investigating 40 GBM patients showed significantly higher TrxR and Ki-67 expression in primary GBMs and TrxR expression was found to be highly correlated with the Ki-67 index, but the study also did not assess for associations with patient survival (Erdi et al., 2018). Furthermore, TrxR has been assessed in 20 GBM patients to show higher TrxR expression in GBMs containing intratumoural haemorrhage, indicating a role of TrxR expression in the promotion of tumoural angiogenesis and growth, but again the

associations with patient survival were not described (Kaya et al., 2016). To our knowledge, there is no information in GBMs regarding the relationship between the protein expression of Trx system and clinical outcome/clinicopathological features prior to the present study with this being first study to describe the expression of all three members of Trx system together in adult GBM patient tumour samples and to evaluate their prognostic significance.

The number of adult GBM patients included in the current study (n=18) could be regarded as being rather small however the low incidence of this tumour type should be borne in mind. The standardised incidence of GBM in England is only ~5 per 100,000 persons per year (Philips et al., 2018). The patient number in this study compares well against others that have sought to examine Trx system in GBM i.e. the studies from Kaya et al. (2016) (n=20) and Kemerdere et al. (2013) (n=27).

One of the most important hallmarks of GBM is molecular and cellular heterogeneity which hinders effective treatment (Friedmann-Morvinski, 2014). Molecular studies have shown that the heterogeneity exists not only across but also within GBMs (Aum et al., 2014). Indeed, different regions of GBM tumours have different profiles of molecular abnormalities and differing expression profiles for known tumour markers (Smith et al., 2017). The current study assessed and compared the diversity of expression of Trx system proteins across distinct adult GBM intra-tumour regions with results revealing that the rim region had the highest cytoplasmic TrxR expression as compared to the other two regions. The higher expression of nuclear TrxR was observed at the rim and invasive margin relative to the core region, indicating that TrxR overexpression in periphery tumour regions may be linked to GBM invasiveness and migration. However, it should be noted that this cohort is a relatively small (n=18) and homogeneous population, and the results were obtained through the TMA technique. The main criticism of TMA is that the amount of tissue evaluated is limited and may be not representative of the whole tissue section, especially for antigens with heterogeneous staining

patterns in tumours (Su et al., 2006, Khouja et al., 2010). Thus, further studies with larger population are required to evaluate the validity and reliability of using TMA to assess the TrxR expression in adult GBMs, by analysing the concordance between data obtained from TMAs and whole mount sections.

The Trx system in LGG is relatively understudied and poorly understood, only very few studies assessing its clinical importance, however none of them included paediatric patients. One study investigating the prognostic significance of Trx system in grade I pilocytic astrocytomas (n=42) found no associations between TrxR or Trx expression and clinicopathological or survival criteria (Haapasalo et al., 2003). On the contrary, significant associations were seen in the current study, which showed that high cytoplasmic TrxR expression was significantly associated with tumour recurrence and adverse overall survival (*P*=0.001); whereas high nuclear TrxR expression was associated with lower risk of recurrence and improved overall survival (*P*=0.034). Such findings were similar to the results obtained in a previous breast cancer study by our group (Woolston et al., 2011), i.e. a high nuclear expression of TrxR was associated with a better overall survival. The different results between cytoplasmic and nuclear TrxR may be due to the subcellular localisation of TrxR that can influence its function within the cell and therefore its involvement in the carcinogenic process and/or prediction of clinical outcome. Another study investigating 85 oligodendrogliomas showed that high Trx expression was associated with poor prognosis in univariate analysis (*P*=0.0343) and remained significant in multivariate analysis (*P*=0.009) (Jarvela et al., 2006). This is in disagreement with the current study which demonstrated that Trx was a good prognostic factor in paediatric LGG. Differences with the results presented here may be due to a number of factors including study populations. The LGG cohort in the current study mainly consisted of grade I pilocytic astrocytomas from paediatric patients, while the study from Jarvela et al. included both grade II and III oligodendrogliomas. Besides, the different forms of Trx may also contribute to the disagreement, as the immunohistochemical technique and the antibodies

that are currently available cannot discriminate the oxidized and reduced forms of the protein in archival material (Woolston et al., 2010). Apart from Trx, high TxNIP expression was also a prognostic factor for better overall survival in this cohort, which is in consistent with a study conducted in breast cancer patients (Woolston et al., 2012).

In the paediatric HGG cohort, high cytoplasmic expression of both TrxR and Trx was significantly correlated with worse OS (*P*= 0.002 and *P*= 0.007, respectively). However, the independent prognostic value of these two markers could not be determined as none of the potential confounding factors were found significantly associated with survival from univariate analysis. Cytoplasmic Trx expression significantly correlated with histological subtypes. In addition, TxNIP expression was significantly associated with histological subtypes, tumour site and tumour grade, but not patient survival. As with LGG, limited studies have investigated the protein expression of the Trx system in the HGGs with no known reports previously conducted in paediatric tumours. Haapasalo et al. (2003) demonstrated that Trx expression was associated with a worse prognosis in diffuse astrocytomas (n=391), which is in agreement with our findings. In addition, Trx was found to be of independent prognostic value in addition to histology and proliferation, but this was not observed in the current study. In a study of 54 glioma patients (29 LGGs and 25 HGGs), high TxNIP expression was shown to be associated with extended patient survival (Zhang et al., 2017b), however, no association was observed between TxNIP and survival of HGG patients in the current study.

In the MB cohort, high expression of cytoplasmic TrxR (*P*=0.01), cytoplasmic Trx (*P*=0.033), and nuclear Trx (*P*=0.007) was found to be associated with an adverse OS. The associations of cytoplasmic TrxR and nuclear Trx expression remained significant in multivariate analysis (*P*=0.009 and *P*=0.013, respectively). Additionally, high cytoplasmic and nuclear expression of Trx was associated with the risk of tumour recurrence, and high nuclear Trx expression was also linked with histological subtype. These findings strongly suggest the

importance of the Trx system in the progression of MB and suggest the potential of using Trx system protein expression to predict clinical outcome. To our knowledge, no known clinical or laboratory studies have previously examined the protein expression of the Trx system in MB. Additional clinical studies with larger patient numbers are required to further validate this promising result.

Although MB is historically considered as a single disease, it is now widely accepted that it comprises 4 distinct subgroups (i.e. WNT, SHH, group 3, and group 4) that have prognostic significance, based on their DNA methylation profiling. Unfortunately, such methylation information is not included in this study as advances in molecular testing, to allow sub-grouping, was not available at the time of presentation. In addition, the relatively small sample size (n=114) might be problematic if subgrouping was conducted. Based upon the interesting data shown above, further studies are warranted, with larger numbers of patients (and hopefully more contemporary), to allow subgroup analysis to be conducted. The subgroup analysis can direct the selection of appropriate MB cell lines used for *in vitro* studies in the future.

Apart from the exploration of the relationship between protein expression and clinicopathological or survival criteria, the protein levels of Trx system in different types of brain tumours were also examined in the current study. Among the adult GBM, paediatric LGG, paediatric HGG and MB tumours, paediatric HGG had a significantly lower expression of both cytoplasmic and nuclear TrxR when compared to paediatric LGG and MB; but the situation is reversed for TxNIP expression, which a higher level of TXNIP was observed in paediatric HGG. In addition, cytoplasmic Trx expression was significantly higher in MB compared to paediatric LGG, and nuclear Trx expression was also higher in MB compared to paediatric LGG and HGG. These results indicate that there are some protein expression differences between different types of brain tumours. MB tumours are significantly more likely to display increased expression of TrxR and Trx, and decreased expression of TxNIP, which may confer a more aggressive behaviour to the disease. Although the adult GBM

tumours showed some increased/decreased protein expression compared to the paediatric tumours, no significance was achieved and this is probably due to the small sample size of the adult GBM cohort (n=18). Further investigations are required to detect the variation in protein expression between adult and paediatric tumours.

When comparison analysis was narrowed down to paediatric gliomas alone, the protein expression of the Trx system could be compared across different tumour grades. Unfortunately, the scores for grade II gliomas were unavailable for the current study due to missing cores or insufficient tumour tissues in the TMAs. A significantly higher expression of both cytoplasmic and nuclear TrxR was observed in grade I gliomas, and the grade IV gliomas had the highest TxNIP expression. No significant variation in Trx expression was noted between different tumour grades. These results are, perhaps, unexpected as previous data in gliomas have indicated that high levels of TrxR/Trx were associated with increased tumour grade and TxNIP expression was inversely associated with tumour grade. Haapasalo et al. (Haapasalo et al., 2003) reported that TrxR and Trx immunoreactivities were increased in most of the astrocytoma cases evaluated and diffuse astrocytomas showed more intense immunostaining when compared with pilocytic astrocytomas. Recently, Esen et al. (2015) found that grade I-IV astrocytomas showed significantly higher TrxR expression when compared with their normal tissues counterparts and TrxR was overexpressed in astrocytomas according to their ascending tumour grade. In addition, in glioma downregulation of the negative Trx regulator TxNIP has been shown to be associated with higher histopathological glioma grade and shorter overall patient survival (Zhang et al., 2017b). In line with this, Trx expression was also increased with glioma grade (Gollapalli et al., 2017). It is apparent that the results from the current study are in disagreement with some of previous studies. The discordant results could be due to a number of factors including study populations, antibodies used, sample sizes, methodological problems, and other potential confounding factors. It should be noted that the samples in the current study

were all from paediatric patients, and the others mainly focused on adult samples. Histologically, adult and childhood brain tumours are usually similar, but they differ dramatically in their genetic and epigenetic profiles.

This current study used four independent brain tumour cohorts including both adult and paediatric patients to demonstrate associations between the expression of the Trx system and clinicopathological or survival criteria. Although some mixed results were observed between different cohorts, there was a consistent finding that high levels of cytoplasmic TrxR equated with a worse prognosis across all cohorts, supporting the prognostic value for determination of TrxR expression in different brain tumour types. The Trx system is a key, but relatively understudied, antioxidant system responsible for regulating cellular redox homeostasis in brain tumours. The majority of the studies to date have assessed only one or maximum two members of the Trx system in focused brain tumour population. However, the current study took a further step to examine a panel of all three members of the Trx system in a wide range of brain tumour types. In addition, the current study also demonstrated differential protein expression of Trx system between brain tumour types, between tumour grades, and between intra-tumour regions, which perhaps indicates the complex and heterogeneous features of brain tumours and the high levels of inter-tumour and intra-tumour heterogeneity may hinder accurate diagnosis and effective treatment.

Although the current study offers several strengths, there are some limitations to it as well. Firstly, this study did not compare protein levels of Trx system in brain tumours with that found in corresponding normal tissues. It would be useful to include the normal tissue as a comparator and to investigate whether the Trx system is dysregulated in brain tumours as seen in various other types of cancer. Secondly, quite an amount of important clinical data was missing from the database and a proportion of cores within the TMAs could not be assessed, which reduced the numbers of cases that could be used for generating robust statistical analyses. Unfortunately, the missing clinical data could not easily be retrieved within the current study from the

paper-based medical records archived decades ago. Thirdly, as the IHC technique and antibodies currently available cannot distinguish between active and inactive forms of proteins, it is, perhaps, not surprising that some conflicting results were presented by different studies. Lastly, the sample sizes in the current study are relatively small, but with the interesting results obtained, further investigation of these observations in larger cohorts are warranted.

## 2.5 Conclusions

In summary and conclusion it appears that, from the current data, TrxR, Trx, and TxNIP proteins are expressed to variable levels across a variety of brain tumour types including adult GBM, paediatric LGG, paediatric HGG and MB tumours. High cytoplasmic TrxR expression was associated with adverse OS in adult GBM and paediatric LGG patients. In contrast, high expression of nuclear TrxR, cytoplasmic and nuclear Trx, and TxNIP was associated with improved OS in paediatric LGGs. For patients with HGG, both high cytoplasmic TrxR and Trx expression were associated with poor OS. Similarly, high expression of cytoplasmic TrxR and Trx, and nuclear Trx was also associated with worse prognosis in MB; the associations remained significant in multivariate analysis for cytoplasmic TrxR and nuclear Trx. In all tumour types, high cytoplasmic TrxR consistently equates to a worse prognosis suggesting that it is potentially a very important therapeutic target in brain cancers generally. Significant variation in protein expression of the Trx system was detected between different tumour regions and between different tumour types/grades. Collectively, these results suggest that determining the expression of the Trx system may be of clinical relevance in patients with GBM, LGG, HGG, and MB. The Trx system may have prognostic potential and may have utility as therapeutic targets; these findings warrant further investigations in larger cohorts with increased number of patients.

Data suggest that TrxR is an important therapeutic target – subsequent chapters will investigate the use of a novel TrxR inhibitor in *in vitro* brain cancer efficacy studies.

# Chapter 3 *In vitro* drug sensitivity of the TrxR inhibitor IQ10 in brain cancer cells

## 3.1 Introduction

### 3.1.1 TrxR inhibitors in cancer therapy

The expression levels of Trx/TrxR are increased in a variety of human primary tumours compared with corresponding normal tissues and linked to tumour growth, progression, metastasis, chemo-resistance, and poor prognosis (Mahmood et al., 2013, Selenius et al., 2010). Inhibiting the Trx system results in the modulation of intracellular redox state, which can make cells more sensitive to certain chemotherapeutic agents and to radiation, as a result of the alteration of certain apoptosis signalling pathways and ROS accumulation (Powis et al., 2000, Baker et al., 1997a). Trx/TrxR have, therefore, emerged as promising biomarkers and drug targets for cancer therapy. A number of Trx system inhibitors have, in recent years, been developed as potential anti-cancer agents or as adjuncts to existing therapy (Gandin and Fernandes, 2015). It is beyond the scope of the current section to cover all however details have been reviewed elsewhere (Cheng and Qi, 2017, Zhang et al., 2017a, Gandin and Fernandes, 2015, Cai et al., 2012b, Tonissen and Di Trapani, 2009, Bindoli et al., 2009, Zhang et al., 2019a). The current section discusses several of the most promising and well-defined TrxR inhibitors. The agents can be roughly divided into three classes: metal-containing compounds, naturally occurring products and their derivatives, and other newly emerged inhibitors.

#### 3.1.1.1 Metal-containing inhibitors

MGd, is a member of a class of porphyrin-like molecules called texaphyrins, that are, in complex with the gadolinium (III) cation, utilised in the treatment of different cancers (Magda and Miller, 2006). MGd has a strong affinity for electrons in the presence of oxygen, accepting electrons from various intracellular reducing metabolites and forming superoxide and other ROS by redox cycling (Magda and Miller, 2006, Magda et al., 2001a). MGd enhances the cytotoxicity of ionising radiation and various chemotherapy reagents both *in vitro* and *in vivo*, and may be directly cytotoxic to cancer cells under certain conditions (Magda et al., 2001a). It has been shown to cross the disrupted

blood-brain barrier associated with brain tumours, but it is not detectable in normal brains (Qiu et al., 2016). One of the molecular targets for MGd appears to be TrxR which, when inhibited, results in cellular redox stress, cytotoxicity and an increase in tumour responsiveness to a variety of treatments (Hashemy et al., 2006). In a phase III trial, combining MGd with prompt whole brain radiotherapy significantly prolonged time to neurologic progression in lung cancer patients with brain metastases (Mehta et al., 2009). A recent phase I/II trial demonstrated that the combination of standard radiotherapy with TMZ and MGd did not achieve a significant survival advantage compared to historical controls in patients with newly diagnosed GBM (Brachman et al., 2015b). MGd is currently being evaluated in many clinical trials as monotherapy or in combination with radiation and/or chemotherapy for the treatment of different types of cancer (Raviraj et al., 2014).

Auranofin (AF) is a gold (I) compound widely used in the treatment of rheumatoid arthritis. It has been shown to inhibit TrxR activity at nanomolar concentrations in human ovarian cancer cells, with no effect on glutathione reductase activity (Marzano et al., 2007). Furthermore, AF was shown to overcome cisplatin resistance and induce apoptosis in both cisplatin-sensitive and -resistant ovarian cancer cells (Marzano et al., 2007). Pessetto et al. (2013) and Fiskus et al. (2014) also demonstrated the *in vitro* apoptotic activity of AF against gastrointestinal stromal tumour and chronic lymphocytic leukaemia (CLL) cells. It has been suggested that AF exerts cytotoxic effects by causing direct mitochondrial damage through selective modification of the selenol active site in TrxR (Rigobello et al., 2004), resulting in the release of cytochrome-c into the cytoplasm and subsequent apoptotic cell death (Cox et al., 2008). AF is currently in phase I/II clinical trials for the treatment of lung cancer (NCT01737502) and recurrent GBM (NCT02770378).

Platinum compounds, such as cisplatin, belong to a group of metal complexes with demonstrated ability to cause cell death in a variety of human malignancies (Urig and Becker, 2006), and have been widely used in cancer

therapy for the past 40 years. Cisplatin is generally recognised as DNA-damaging compound due to its binding to DNA, forming irreversible DNA-platinum adducts (Wang and Lippard, 2005). Several studies have shown that cisplatin-induced cytotoxicity is closely related to increased ROS generation (Choi et al., 2015). Cisplatin is also a potent inhibitor of TrxR with the inhibition of TrxR correlating with cytotoxicity (Urig and Becker, 2006, Arner et al., 2001, Sasada et al., 1999). In the Hela cell line, cisplatin inhibited TrxR activity in a dose- and time-dependent manner with a corresponding decrease in cell viability (Sasada et al., 1999). The inhibition of TrxR by cisplatin appears to be an important trigger for apoptosis (Tonissen and Di Trapani, 2009). Further studies demonstrated that TrxR inhibition by cisplatin was irreversible and highly specific as the activity of glutathione reductase was unaffected (Arner et al., 2001). The highly reactive selenocysteine residue at the C-terminal domain of TrxR was suggested to be the target of cisplatin (Witte et al., 2005).

#### 3.1.1.2 Natural products

Polyphenols such as curcumin and some flavonoids have been identified as potential anticancer reagents with a mechanism of action that may be mediated by effects on the Trx system. TrxR can be irreversibly inhibited upon interaction of the C-terminal redox active site with curcumin with the modified enzyme converted into a pro-oxidant that stimulates ROS production via an acquired NADPH oxidase activity (Fang et al., 2005). Curcumin can also drastically down-regulate Trx1 protein level as well as its enzyme activity in HeLa cells, in turn elevating intracellular ROS production, and subsequently inducing oxidative DNA damage (Cai et al., 2012a). Furthermore, curcumin has been reported to act as a radiosensitiser on prostate cancer cells (Chendil et al., 2004) and as a radioprotective agent on human lymphocytes (Srinivasan et al., 2006). Although curcumin has been shown in numerous clinical trials to be effective against different types of cancer (Reviewed in (Kunnumakkara et al., 2017)), its application as a therapeutic agent is obstructed to a certain degree owing to its colour, lack of water solubility, and poor bioavailability (Anand et

al., 2007); hence extensive preclinical and clinical studies are currently being conducted to overcome these limitations.

Arsenic trioxide (ATO) is an effective therapeutic drug used in the treatment of acute promyelocytic leukaemia (APL) and potentially used in a wide range of solid tumours (Hoonjan et al., 2018). Multiple mechanisms of action have been suggested to explain its activity, including induction of elevated oxidative stress and apoptosis, inhibition of cell proliferation, and anti-angiogenic effects (Falchi et al., 2016). In addition, ATO can irreversibly inhibit mammalian TrxR - both the N-terminal redox-active dithiol and the C-terminal selenothiol-active sites of TrxR interact with ATO (Lu et al., 2007). It has also been shown that growth inhibition of human breast cancer cells MCF-7 by ATO was correlated with irreversible inactivation of TrxR and subsequent Trx oxidation (Lu et al., 2007). ATO was approved as frontline drug therapy for the treatment of APL and relapsed APL by the FDA, since 2000 and 2002 respectively (Falchi et al., 2016). ATO in combination with chemotherapy has shown encouraging results in hepatocellular carcinoma, osteosarcoma, and Ewing sarcoma (Wang et al., 2015b, Chen et al., 2011, Emadi and Gore, 2010). There are a large number of completed and ongoing clinical trials investigating ATO alone or in combination with other agents for the treatment of haematologic malignancies and solid tumours.

#### 3.1.1.3 Other compounds - Quinones

Quinones are a widespread group of oxygen-substituted, often biologically active, aromatic compounds (Cenas et al., 2004). They are found as naturally occurring products, as synthetic drugs for clinical use, or as components of environmental pollutants. The anti-tumour activity of quinones is mainly believed to stem from effects due to redox cycling of their free radical or hydroquinone states, derived from reduction by flavoenzymes, or from covalent modifications of DNA and cellular nucleophiles (Hargreaves et al., 2000, O'brien, 1991, Cenas et al., 2004). Since quinones are highly redox-active compounds, some are substrates and/or inhibitors of TrxR (Cenas et al., 2006). Chew et al. (2008) and Mukherjee et al. (2005) studied the ability of

anti-tumour quinols to inhibit TrxR, these quinols showed irreversible inhibition of TrxR in a concentration-, time-, and NADPH-dependent manner with IC50 values in the low micromolar range and the inhibition was mediated through a direct quinol attack on the C-terminal selenocysteine residues of TrxR. Xu and Arnér (2012) found that pyrroloquinoline quinone (PQQ) had substantial effects on TrxR and it efficiently inhibited the activity of TrxR in reducing its native substrate Trx. In addition, they demonstrated that PQQ was a weak substrate of TrxR.

Compounds containing the indolequinone (IQ) core structure often possess powerful biological activity (Inman et al., 2014). Examples include the well-known natural product mitomycin C (MMC) used clinically for the treatment of solid tumours (Ragonese et al., 2016) and the synthetic MMC analogue EO9 (apaziquone, EOquin) currently being trialled as a treatment for bladder cancer (Karsh et al., 2018) (Figure 3.1).

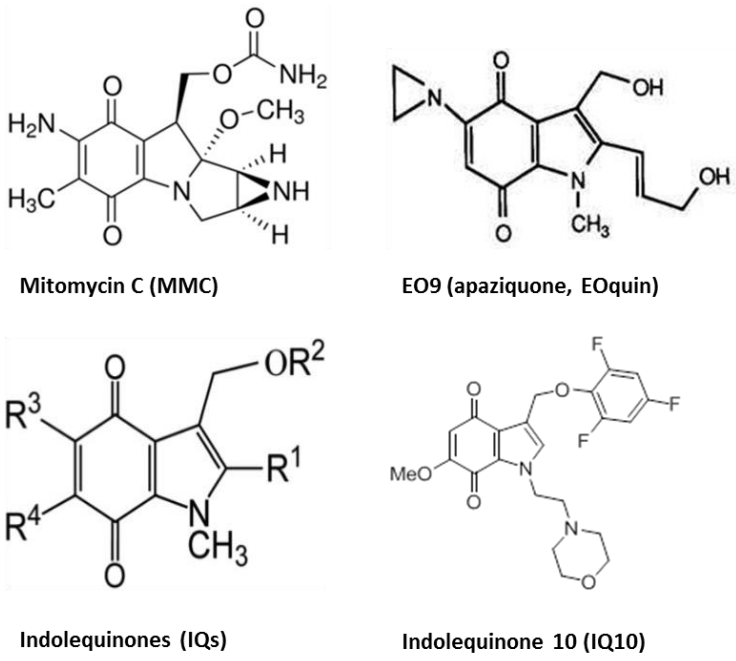



**Figure 3.1 Chemical structures of Indolequinones**.

IQs have attracted considerable interest in the anticancer area not only as cytotoxins, but also as bioreductively activated prodrugs (Tanabe et al., 2005, Huang et al., 2009, Huang et al., 2010). Prof. Chris Moody's group (School of Chemistry, University of Nottingham) and their collaborators have developed

and examined a series of novel IQ compounds that exhibited potent anti-tumour activity against human pancreatic cancer both *in vitro* and *in vivo* (Yan et al., 2009a). These IQs were found to induce time- and concentration-dependent apoptosis and to be potent inhibitors of TrxR in pancreatic cancer cell lines at nanomolar concentrations (Yan et al., 2009a). These compounds share an IQ backbone but vary in the substitution pattern on both the quinone ring and the indole ring (Figure 3.1). The proposed mechanism of action involves quinone reduction, followed by loss of a leaving group, and generation of an electrophile resulting in alkylation of the selenocysteine residue in the active site of TrxR (Yan et al., 2009a) (Figure 3.2). A subsequent study on IQ3 and MAPK signalling revealed that inhibition of TrxR led to Trx oxidation, dissociation of free ASK1, phosphorylation of JNK/p38, and subsequent apoptosis (Yan et al., 2012).

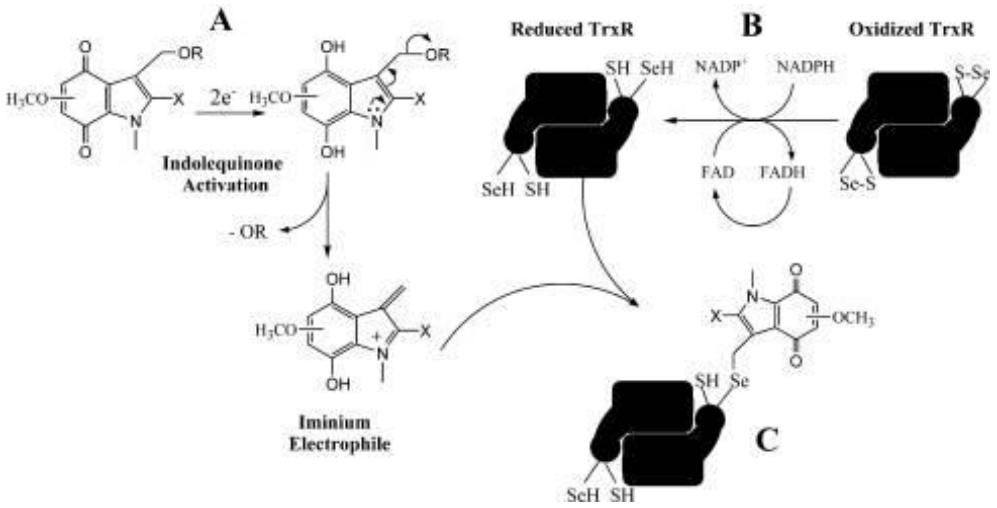



**Figure 3.2 A proposed mechanism for the inhibition of TrxR by indolequinones.** Reduction of indolequinones leading to loss of a leaving group and formation of an iminium electrophilic capable of inactivating the enzyme TrxR. Reproduced from (Yan et al., 2009a) with copyright© permission from American Society for Pharmacology and Experimental Therapeutics.

IQs, as introduced above, showed potent anti-tumour activity as single agents against pancreatic cancer models, however, the *in vitro* efficacy of IQs against other cancer types such as brain cancer has never been examined. Hence, IQ10, one of the most potent IQs (2-unsubstituted class) was examined as a single agent or in combination with radiation in different types of brain cancers in the current study. IQ10 was kindly synthesised and provided by

Prof. Chris Moody's research group and the chemical structure is shown in Figure 3.1.

### 3.1.2 Trx system and hypoxia

Hypoxia is a state of low oxygen tension below $pO_2$ 7 mmHg. Normal tissues have an oxygen level of $pO_2$ 9 mmHg - $pO_2$ 100 mmHg (1.2-13% $O_2$) (Vaupel, 2004). Hypoxia is frequent in most solid tumours due to uncontrolled cell proliferation, altered metabolism, and abnormal tumour vascularisation resulting in reduced transport of oxygen and nutrients (Muz et al., 2015). Hypoxia is one of the fundamental physiological differences between normal and tumour tissues (Harris, 2002b), associated with chemoradiotherapy resistance and poor survival (da Motta et al., 2017). Additionally, it promotes resistance to apoptosis, encourages hypermutation by inhibiting DNA repair, enhances local invasiveness, drives metastatic spread, and provides a sanctuary for cancer stem cells (Carames Masana and de Reijke, 2017). Hypoxia constitutes a major concern for brain tumour patients, particularly high-grade brain tumours, and has been shown to be a poor prognostic marker associated with progression and worse survival in patients with GBM (Rong et al., 2006). Spence et al. (2008) have shown that survival in GBM patients whose tumour contained hypoxic volume ratios greater than the median survived only about 4 months as compared to more than 12 months for those with less than median hypoxic burden ($P$<0.001); multivariate analyses showed that only hypoxic volume was the independent prognostic factor for survival.

Hypoxia is a strong stimulus for tumour angiogenesis (Krock et al., 2011). Under conditions of low oxygen, the activity of the important transcription factor, HIF-1, is increased (Spence et al., 2008). HIF-1 is a heterodimer composed of the hypoxic response factor HIF-1α and the HIF-1β subunits. As oxygen concentration decreases, HIF-1 binds to hypoxia response elements, thereby activating the expression of numerous hypoxia-response genes, such as the pro-angiogenic growth factor vascular endothelial growth factor (VEGF), glycolytic enzymes, glucose transporters, and carbonic anhydrase 9 (CA9) etc.

(Harris, 2002a, Denko et al., 2003, Said et al., 2007). This, in turn, triggers more aggressive tumour growth, survival, invasion and metastasis, and increases the stem cell component of tumours (McIntyre and Harris, 2015). Thus, hypoxia via multiple downstream effects imposes a significant barrier to successful therapy for many cancers.

As introduced in Chapter 1, Trx/TrxR are small redox proteins often overexpressed in a number of human primary tumours. The Trx system has been implicated in many cellular functions, such as cell growth, antioxidant defence, chemotherapy resistance, regulation of transcription factors (e.g. NF-κβ, specificity protein 1 (SP-1), AP-1 and HIF1-α), inhibition of apoptosis, and stimulation of VEGF-induced angiogenesis (Naranjo-Suarez et al., 2013). In hypoxic environments, Trx is usually upregulated due to oxidative stress. Exposure of colon cancer cells to hypoxia resulted in a 14-fold increase in Trx mRNA expression, and a transient 4-fold increase in TrxR mRNA (Berggren et al., 1996). Expression of Trx has been described to increase not only HIF-1α DNA binding and transcriptional activity, but also HIF-1α stability, in various cell lines (Welsh et al., 2002b, Zhou et al., 2007). Trx overexpression also causes a significant increase in VEGF production in a number of different cell lines (Welsh et al., 2002b). *In vivo* studies using Trx transfected cells showed significantly increased tumour VEGF levels and angiogenesis (Welsh et al., 2002b). Trx has been shown to stimulate VEGF-induced angiogenesis in tumours through increasing SP-1 and AP-1 transcription factor activity under normoxia (Bloomfield et al., 2003) and HIF-1 activity under hypoxia (Welsh et al., 2002b). It has been reported that Trx can directly enhance SP-1 and AP-1 DNA binding activity for VEGF promoter (Hirota et al., 1997, Powis and Kirkpatrick, 2007) and results in the initiation and activation of VEGF gene transcription (Jośko and Mazurek, 2004). Taken together, it suggests that Trx system proteins are often upregulated by hypoxia, and this increased Trx expression is associated with increased HIF-1α activity and HIF transactivation in cancer cells together with increased VEGF production and enhanced tumour angiogenesis.

Given the negative impact of hypoxia on tumour biology and therapy resistance, it is a key area of research for improving anti-cancer therapy. Different classes of bioreactive prodrugs to act in hypoxia have been developed. These prodrugs are usually reduced and activated by intracellular oxidoreductases in an oxygen-sensitive manner to form cytotoxins (Carames Masana and de Reijke, 2017). EO9 (apaziquone) is one such prodrug that requires activation by cellular reductase enzymes to become cytotoxic (Walton et al., 1991). Several oxidoreductases are capable of reducing EO9 but the major ones are the two-electron reductase NQO1 (NADPH: quinone oxidoreductase, also known as DT-diaphorase) and a series of one-electron reductases including cytochrome P450 (Phillips et al., 2013). Reduction of EO9 by one- and/or two-electron reductases leads to DNA damage by free radical generation and alkylation (Bailey et al., 2001, Walton et al., 1991). In addition to the presence of oxidoreductases, the oxygenation state of cells has a significant impact on the drug response. Under normoxic conditions, EO9 is reduced mainly by the two-electron reductase NQO1 and several studies have shown that IC50 values are generally inversely proportional to NQO1 activity (Choudry et al., 2001, Plumb et al., 1994, Robertson et al., 1994). Under hypoxic conditions, however, marked hypoxic sensitisation to EO9 is only seen in the cells that lack NQO1 activity (Robertson et al., 1994, Plumb and Workman, 1994). In cells that are devoid of NQO1 activity, reduction of EO9 is oxygen sensitive with the semiquinone rapidly cycling back to the parent compound resulting in the production of ROS. When oxygen is low or absent, the half-life of the semiquinone increases, providing more time to either directly damage DNA or be reduced further to produce the hydroquinone (Workman, 1994). Hence, the cytotoxicity of EO9 is suggested to be determined by a number of parameters including NQO1 activity, one-electron reductase activity (e.g. cytochrome P450), oxygen level, acidic extracellular pH, and DNA damage repair (Phillips et al., 2017).

As IQ10 is structurally related to EO9 (both IQ-based drugs), we hypothesise that IQ10 might share a similar mechanism of action with EO9 and that it

might potentially exhibit enhanced hypoxic toxicity in brain cancer cells with low/no NQO1 activity. In addition, as Trx and TrxR have been reported to be upregulated under hypoxia (Berggren et al., 1996), the potential TrxR inhibitor IQ10 might be more effective under hypoxic conditions. Taken together, it was thought worthwhile to determine the efficacy of IQ10 under hypoxic conditions, with a view to then conducting drug-radiation combination assessments under hypoxic conditions.

### 3.1.3 Three-dimensional (3D) spheroid culture

Development of more effective treatments for malignant brain tumours requires simple yet realistic tumour models that enable proper evaluation of their therapeutic efficacy prior to their clinical use (Mirab et al., 2019). For several decades, drug efficacy evaluations have been conducted using cells cultured as two-dimensional (2D) monolayers on flat tissue culture plastics. Despite the ease of use, these 2D systems often fail to predict the *in vivo* tissue response to candidate drugs as they do not account for cell-cell interactions, physiological gradients of the hypoxic microenvironment, tumour stromal heterogeneity, and extracellular matrix (ECM) components (Ferreira et al., 2018). In contrast, animal models provide a powerful tool and allow a greater understanding of the events involved in tumourigenesis, and also aid in the translation of basic cellular research into clinical application. However, design complexity and the high cost of animal models restrict the studies needed to identify the specific biochemical and cell biological pathways involved in tumour formation and progression. Therefore, to address the limitations imposed by *in vitro* and *in vivo* experiments, *in vitro* cell-based 3D model systems, which provides cells with an *in vivo*-like microenvironment and a 3D organisation, have been developed, and are being increasingly utilised, as powerful cell-based models to bridge the gaps between epithelial monolayer cultures and animal models.

Multicellular tumour spheroids have emerged as one of the promising *in vitro* 3D models that can inexpensively resemble many functional and structural properties of solid tumours *in vivo* (Li and Kumacheva, 2018). Spheroid

cultures are of intermediate complexity containing many elements found in tumours including chemical gradients (e.g. oxygen, nutrients, metabolite/catabolite, and pH), regions of chronic hypoxia, ECM, cell-cell and cell-matrix interactions, and necrosis (Hirschhaeuser et al., 2010). Moreover, their ease of assembly, reproducibility, and the capability to provide high-throughput drug screening have rendered them as one of the most popular models for preclinical evaluation of novel therapeutic agents (Ferreira et al., 2018, Li and Kumacheva, 2018).

Certain studies have shown that cells cultured in spheroids display differences in morphology (Mayer et al., 2001), growth kinetics, and metabolic rates compared to 2D cultures (Ivascu and Kubbies, 2006). They also showed altered gene expression and chemotherapy and/or radiotherapy resistance in various cancer cells (Imamura et al., 2015b, Lee et al., 2013, Ivascu and Kubbies, 2006). Generally, cancer cells cultured in 3D systems become more refractory to various treatments, although the opposite has also been observed (reviewed in (Lovitt et al., 2014, Cox et al., 2015)). Consequently, many studies have focused on the difference in drug cytotoxicity in various cancer models (Stock et al., 2016, Imamura et al., 2015b, Shelper et al., 2016, Huber et al., 2016, Breslin and O'Driscoll, 2016).

Taken together, the studies mentioned above illustrated the power of 3D spheroid model as a novel approach to mimic the biological activities of cancer genes and pathways that are active *in vivo*. One objective of this study was to prepare uniform and highly viable brain tumour spheroids to evaluate and compare the efficacy of TrxR inhibitor IQ10 in 2D monolayer *vs.* 3D spheroid cultures.

### 3.1.4 Hypotheses and Aims

#### 3.1.4.1 Hypotheses

1. Trx system proteins are differently expressed in a variety of brain cancer cell lines and their activity/expression levels are altered upon IQ10 treatment.

2. Inhibiting TrxR with IQ10 causes potent cytotoxicity against a variety of brain cancer cells under 2D normoxic conditions with IQ10 being more effective under 3D culture, hypoxia containing, conditions than 2D normoxic conditions due to enhanced hypoxic bioreduction.
3. TrxR is an important target for IQ10 and the cytotoxic effect of IQ10 in brain cancer cells is due, in part, to functional inhibition of TrxR.

#### 3.1.4.2 Aims

1. Investigate the *in vitro* efficacy of novel TrxR inhibitor IQ10 as a single agent against brain cancer cell lines using a variety of endpoint and *in vitro* assays (i.e. insulin reduction, Western blotting, cell growth curve, clonogenic survival and resazurin reduction assays) under normoxic and hypoxic conditions (2D vs. 3D models). Experiments include control drugs, such as temozolomide (TMZ), to help optimise experiments and to compare the efficacy of IQ10.
2. Examine potential mechanisms of action of IQ10 and validate TrxR as the main target for IQ10 in brain cancer cells by using a siRNA approach.

## 3.2 Materials and methods

### 3.2.1 Cell lines and culture conditions

All cell lines and tissue culture methodologies were described in Section 2.2.1, 2.2.2, and 2.2.3.

### 3.2.2 Drug preparation and treatments

IQ10 was synthesised by Dr. Martyn Inman from Prof. Chris Moody's group at the School of Chemistry, University of Nottingham, UK. IQ10 was initially dissolved in DMSO as a stock solution at 10 mM. TMZ (Sigma), auranofin (Sigma) and doxorubicin (Sigma) were chosen as control drugs to optimise experiments and compare results against. Both TMZ and auranofin were dissolved in DMSO to reach 100 mM and 10 mM, respectively. Doxorubicin was also prepared in DMSO at a stock concentration of 50 mM. All stock solutions were aliquoted, protected from light, stored at -20°C, and used

within 6 months. On the day that drugs were to be added to cells, the stock solutions were sub-diluted in complete growth medium to achieve the final concentrations for individual treatments. DMSO was added to the negative control groups at the same amount equivalent to that in the drug treatment group (the final percentage of DMSO was < 0.1% v/v, except that indicated in the individual experiment).

### 3.2.3 Cell growth curves

Before starting any experiments, growth curves were initially conducted over a period of 96 h to determine characteristics. $2\times10^5$ cells were plated into each well of a 6-well plate and cell numbers were measured in triplicate using a Countess® Automated Cell Counter. At every 24 h, spent culture media was removed and cells were washed once with 1 ml of PBS. 500 µl of trypsin-EDTA was subsequently added to detach cells from the well surface by incubating for 1-2 min in an incubator. Once all cells detached, the cells were resuspended in a further 500 µl of medium. 10 µl of cell suspension was then mixed with 10 µl of 0.4% trypan blue and loaded into a chamber slide and cell counts and viability measures were performed using the Countess® cell counter. Duplicate measurements were made for each well to account for pipetting errors. The cell growth curve was generated by plotting cell number versus time. The population doubling time is the time interval required for cells to double in number during the exponential phase of growth.

Apart from being used to determine growth characteristics, and that cells were growing as expected according to the literature, cell growth curves were also performed to evaluate effects of TMZ and IQ10 on cell proliferation across the range of brain cancer cell lines. Briefly, $2\times10^5$ cells were seeded into each well of a 6-well plate and incubated overnight to allow adherence. Cells were then treated, in triplicate, with different concentrations of TMZ (0, 250, 500, 750, and 1000 µM) or IQ10 (0, 0.25, 0.5, 0.75 and 1 µM) for up to 72 h. DMSO was added to the negative control groups at the same volume equivalent to that in the treatment groups. For hypoxic experiments, cells were seeded as described above and pre-incubated in 1% $O_2$ for 24 h prior to

drug treatment. Cells were then treated with different concentrations of IQ10 in hypoxia for up to 72 h. Normoxic control experiments were always conducted in parallel with hypoxic experiments. Every 24 h after initiating drug treatment, cells were trypsinised and counted using the Countess® system. Cell counts were recorded, analysed and plotted over the 72 h period. Growth inhibition was expressed as the percentage of total cells in drug treatment cultures compared with untreated controls.

At each time point, the cells from both normoxic and hypoxic conditions were harvested after cell counting and cell suspensions were diluted to appropriate numbers in appropriate diluents, for use in additional assays, such as the clonogenic survival assay (Section 3.2.4) and Western blotting (Section 2.2.5).

### 3.2.4 Clonogenic survival assay

Cells for use in clonogenic survival assays were collected from cell growth assays mentioned above (Section 3.2.3). The cells from different treatment conditions were serially diluted in complete growth medium to appropriate concentrations and plated into T25cm$^2$ tissue culture flasks. Cells were then incubated for 12 days (21 days for KNS42) at 37°C, 5% $CO_2$ to allow colony formation (30-100 colonies per flask were required). Flasks for clonogenic assays were incubated in an exclusive incubator separated from routine tissue culture, without disturbance. At the end of the incubation period, colonies were rinsed once with PBS, fixed with 50% methanol in PBS for 15 min, and then fixed with 100% methanol for another 15 min, followed by staining with 0.5% crystal violet. Colonies were counted by eye and confirmation by microscope carried out as necessary. Any cluster of cells greater than 50 in number was counted as a surviving colony. Plating efficiency (PE) for each cell line was initially assessed before being applied in further experiments. The PE was calculated from the untreated controls using the following equation:

$$PE = \frac{\text{number of colonies formed}}{\text{number of cells seeded}} \times 100\%$$

The surviving fraction (SF) of cells following treatment was calculated as:

$$SF = \frac{\text{number of colonies formed after treatment}}{\text{number of cells seeded X PE}}$$

For chemosensitivity analysis, SFs were plotted on a linear scale and the dose at which 50% cell death was achieved was calculated as IC50 (Woolston and Martin, 2011a). Data represent the mean SF ± SD of three independent experiments, with each experiment containing six parallel sets.

### 3.2.5 Protein concentration determination and insulin reduction assay (TrxR activity)

Sub-confluent cells were treated with various concentrations of IQ10 or with 1 µM of auranofin (a well characterised TrxR inhibitor, used as a positive control and comparator) for 4 and 48 h. Cells were trypsinised, counted, and lysed in M-PER protein extraction reagent (ThermoFisher) for 20 min. Lysates were analysed immediately or stored for future use at -80°C. The protein concentration in lysates was determined by the Bio-Rad DC protein assay following the manufacturer's instructions. Briefly, seven dilutions of bovine serum albumin (BSA) (Sigma) (range 0-2 mg/ml) were prepared before measurement. 25 µl of solution A, prepared by adding 20 µl of Reagent S to 1 ml of Reagent A, was added to each well of a 96-well plate. To this, 5 µl of protein sample or a known standard was added in triplicate. Finally, 200 µl of Reagent B was added to each well and the plate was incubated at room temperature for 15-30 min. Absorbance at 620 nm in each well was measured using a microplate reader (BMG FLUOstar OPTIMA). A protein standard curve was generated by plotting the known protein concentrations versus their absorbance value. Absorbance values of unknown samples were then interpolated onto the plot or formula of the standard curve to determine their concentrations.

TrxR activity was measured in 96-well plates using the endpoint insulin reduction assay as described previously (Holmgren and Bjornstedt, 1995, Mukherjee et al., 2007) with appropriate modifications. The assay mixture contained the following in a final volume of 100 µl HE buffer (100 mM HEPES, pH 7.2; 5 mM EDTA): 80 µg of protein from each cell extract, 2 µM *Escherichia*

*coli* Trx, 1 mg/ml bovine insulin, and 1 mM NADPH. All ingredients were freshly reconstituted for each experiment. Duplicate samples were used, either with or without exogenous Trx enzyme. A cell-free enzyme assay was simultaneously conducted, using 10 µl of different concentrations of TrxR (0, 0.025, 0.05, 0.1, 0.25, 0.5, 0.75, and 1 µM), to generate a standard curve. The reaction was incubated at 37°C for 1 h before addition of 150 µl stop buffer containing 10 mM DTNB, 6 M guanidine hydrochloride, and 50 mM Tris (pH 8.0). The absorbance was measured at 405 nm using a microplate reader. The absorbance of the sample lacking exogenous Trx was subtracted from that of the corresponding sample containing exogenous Trx. The difference in absorbance indicates TrxR function. The amount of functional TrxR was calculated from the standard curve, generated simultaneously, with pure enzymes. The TrxR activity was expressed as the percentage of DMSO-treated control. The results shown are representative of three independent experiments, each conducted in duplicate and values are expressed as mean ± SD.

### 3.2.6 Western blotting

The effect of IQ10 on regulating protein expression (i.e. Trx, TrxR, TxNIP, NQO1, NQO2, P450 and CA9) was assessed under both normoxic and hypoxic conditions by Western blotting. The knockdown efficiency of TrxR siRNA in DAOY and SF188 cells was also assessed using Western blotting. The antibody details were shown in Table 2.1. The methodology for Western blotting followed the same steps as described in Section 2.2.5.

### 3.2.7 TrxR siRNA experiments

#### 3.2.7.1 Optimisation of cell seeding density

Gene silencing of TrxR was performed using a siRNA knockdown system. Prior to conducting transfection, the cell seeding density of DAOY and SF188 was initially optimised to maximise transfection efficiency. A density that will promote cell division to obtain 30-50% confluency for transfection on the following day was recommended from instructions. Cells were seeded at

various concentrations, ranging from 2 x $10^4$ to 8 x $10^4$ cells/well in 500 µl growth medium in a 24-well plate and the cell confluency was examined under a microscope by next day. A cell seeding density of 2 x $10^4$ cells/well for DAOY cells and 5 x $10^4$ cells/well for SF188 cells provided the 30-50% confluency at 24 h post-plating. Therefore, these cell seeding densities were used for all transfection experiments later on.

#### 3.2.7.2 Optimisation of the volume of transfection reagent

In order to achieve a higher transfection efficiency with minimal toxicity, the volume of HiPerFect Transfection Reagent (Qiagen) was optimised in DAOY and SF188 cells using trypan blue exclusion test. Following 24 h incubation cells were treated with 1.5, 3 or 4.5 µl/well HiPerFect for 48 h in a 24-well plate. Cell viability was determined using trypan blue solution and the results demonstrated that all three concentrations of HiPerFect showed 95% cell viability as compared with the untreated control for both cell lines. Therefore, a HiPerFect dose of 4.5 µl/well was chosen for the subsequent siRNA transfection experiments.

#### 3.2.7.3 Optimisation of siRNA concentration and post-transfection incubation time

SiRNA experiments were carried out with a pre-designed siRNA directed against human TrxR-1 (SI00050876, Qiagen) or with a non-silencing siRNA control (Allstars negative control, Qiagen). The targeted and control siRNAs were delivered using HiPerFect transfection reagent. In order to achieve a higher transfection efficiency, two concentrations of siRNA (10nM and 20nM final concentration) were initially optimised in both DAOY and SF188 cells. Briefly, 2 x $10^4$ (DAOY) or 5 x $10^4$ (SF188) cells in 500 µl medium were seeded in triplicate in 24-well plates and incubated overnight to allow for attachment. The cell medium in each well was replaced with 400 µl of fresh medium. Then 2.5 or 5 µl of 2 µM TrxR siRNA (this will give a final siRNA concentration of 10 nM or 20 nM) was added into a mixture of 4.5 µl HiPerFect transfection reagent and 93 or 90.5 µl medium (serum and antibiotic free), and incubated at room temperature for 10 min to allow complex formation. 100 µl of the

mixture was added dropwise to the corresponding wells. The cells were then incubated for a period of 7 days at 37°C in 5% $CO_2$. For the untreated control group, 500 µl medium was added instead of the transfection medium. In the HiPerFect alone control group, no siRNA was added. The negative group was received 10/20 nM mock siRNA instead of the TrxR siRNA. After transfection, cells were harvested for protein extraction every other day and the transfection efficiency was determined by comparison with protein levels from the transfected cells, scrambled control, HiPerFect control and wild-types, by Western blotting. The TrxR siRNA concentration providing higher transfection efficiency was selected and the day with the best knockdown effects was chosen as the optimal time for drug treatment.

#### 3.2.7.4 Evaluation of the sensitivity of IQ10 in transfected cells

The sensitivity of IQ10 was examined in TrxR silenced DAOY and SF188 cells using the procedure shown in Table 3.1. In brief, DAOY ($2 \times 10^4$) or SF188 ($5 \times 10^4$) cells were seeded in 24-well plates. Following 24 h incubation, cells in each well were transfected with the control or TrxR siRNA (10 nM) using HiPerFect as described above. Two days later, non-transfected/transfected cells were re-plated in 6-well plates at a density of $1 \times 10^5$ cells/well and incubated for 24 h to allow attachment. Cells were then treated with various concentrations of IQ10 for an additional 48 h. Growth curve and clonogenic survival assays were used as the endpoint to assess the drug effects. TrxR expression level was assessed by Western blotting to confirm that the TrxR expression was efficiently suppressed by siRNA for the duration of the experiment, with β-actin being used as a loading control.

**Table 3.1 The procedure of siRNA transfection experiments.**

| Time | Procedure |
|---|---|
| Day0 | 2 x $10^4$ DAOY cells or 5 x $10^4$ SF188 cells were seeded in 24-well plates. |
| Day1 | 30-50% confluent cells were transfected with control or 10nM TrxR siRNA for 48 h. |
| Day3 | Transfected and non-transfected cells were re-plated in triplicate in 6-well plates at a density of 1 x $10^5$ cells/well. |
| Day4 | Transfected and control cells were treated with varying concentrations of IQ10 for 48 h.<br>Cell number was counted and transfected and non-transfected cells were lysed for Western blotting. |
| Day6 | Growth curve was used as the endpoint to assess the drug effects and following counting cells were re-plated for clonogenic survival assay.<br>Cell lysates from transfected and non-transfected cells were collected for Western blotting. |

### 3.2.8 3D spheroids experiments

#### 3.2.8.1 3D spheroids formation and imaging

Subconfluent cells were trypsinised, counted and seeded in ultra-low attachment (ULA) round-bottomed 96-well plates (Corning) at different densities (1000, 3000, 5000, 10,000 and 15,000 cells/well) in 100 µl of culture medium. The plates were centrifuged lightly at 2,000 rpm for 10 min after seeding to aggregate the cells, minimise cell death and encourage the formation of a single spheroid (Ivanov et al., 2014b). 100 µl of fresh medium was added to each well after 24 h of culture and then the culture medium was carefully changed every other day, taking care not to disturb the spheroids, and spheroids were cultured for 7 days. To monitor spheroid growth overtime, 6 replicate spheroids for each cell seeding concentration were imaged daily using an inverted microscope with a 10 x objective and an attached camera (Leica EC4). The scale of images was determined using a haemocytometer counting chamber. Images were analysed using ImageJ software (Fiji package). The measured area (S) of the 2D projection of the spheroids was used to calculate the diameter ($D = 2\sqrt{S/\pi}$).

#### 3.2.8.2 Spheroids dissociation and PE

Spheroids from six wells representing the same conditions were pooled in a microcentrifuge tube and centrifuged at 1000 rpm for 5 min. The medium was discarded and the spheroids washed twice with PBS, followed by 10 min incubation with trypsin/EDTA at 37°C. Mechanical dissociation with a pipette was carried out to form a single cell suspension and complete medium was then added to inactivate the trypsin. Cell counts were performed using the haemocytometer and cells were plated in the conventional 2D clonogenic assay to assess the PE as described in Section 3.2.4. In order to compare the PE between 2D and 3D culture, the PE was also tested, in parallel, in 2D culture conditions.

#### 3.2.8.3 Visualisation of drug penetration in spheroids

Before conducting drug exposure experiments in the spheroid model, it was important to determine whether the drug could penetrate different types of brain tumour spheroids. Doxorubicin was used as a representative drug to evaluate the drug-penetrating ability in spheroids due to its intrinsic red fluorescence. Intact 4-day-old DAOY and UW228-3 spheroids were exposed to doxorubicin for 4 or 24 h at a concentration of 10 µM. For each group, 30 spheroids were harvested in microcentrifuge tubes, washed twice with PBS and fixed in PBS containing 4% paraformaldehyde at room temperature for 10 min. After another two PBS washes, fixation was stopped by 2 x volume of 100 mM glycine in PBS for 10 min. Spheroids were then resuspended in ice-cold methanol and pipetted onto slides, allowed to air dry and mounted in ProLong™ antifade mounting medium (Invitrogen). The distribution of doxorubicin within the spheroids was determined by a laser scanning confocal microscope (Leica TCS SPE) (λ excitation=468 nm; λ emission=550 nm). A stack of confocal images was captured using the 10 x objective through the spheroids with a step size of 15 µm between adjacent optical planes, starting from one pole of the spheroids. This allowed determination of the cellular distribution of the drugs and the degree to which they had penetrated the

spheroids. Negative controls, in which doxorubicin was substituted with DMSO, did not give rise to any detectable signals.

#### 3.2.8.4 Resazurin reduction and clonogenic survival assays using spheroid models.

Spheroids were formed as described in Section 3.2.8.1 and were allowed to grow for 4 days under standard culture conditions to become mature. In order to compare the effects of IQ10 between 3D and 2D cultures, cells were simultaneously seeded on flat-bottom 96-well plates at a density of 6 x $10^3$ cells/well and cultured for 24 h. All samples were subsequently treated with different concentrations of IQ10 (0-1 μM) for 48 h. Afterwards, the cell viability was determined using Resazurin reduction assay (CellTiter-Blue®, Promega) following the manufacturer's protocol. Briefly, medium in each well was replaced with a mixture of 100 μl fresh medium and 20 μl dye and the plates were placed back in the incubator for 4 h. Fluorescence was measured with an excitation wavelength of 560 nm and emission 590 nm on a plate reader (BMG FLUOstar OPTIMA). Negative control cells were cultured with 0.01% DMSO and used to determine 100% viability. Six replicates per condition were assessed in each experiment.

The cytotoxicity of IQ10 was assessed, as mentioned, using the conventional 2D clonogenic survival assay as described in Section 3.2.4 but was also assessed from spheroid exposure. 12 replicate spheroids per condition were produced and left to grow for 4 days before being treated with IQ10 as described above. 2D controls were plated the day before drug exposure and were treated at the same time with those in 3D culture. Afterwards, spheroids from the same treatment conditions were pooled, washed with PBS, and dissociated with trypsin/EDTA (Section 3.2.8.2). Trypsinisation was quenched with appropriate cell culture medium and cells were counted and plated in conventional 2D clonogenics. Cells from 2D controls were trypsinised and subjected to clonogenic assay in parallel.

### 3.2.9 Statistical analysis

Statistical analysis was carried out using SPSS 24.0 or GraphPad Prism 7 software. Data were represented as mean ± SD of two or more, as indicated, independent experiments with each performed in duplicate or triplicate. For comparing two variables, the Student's *t*-test was used and the one-way ANOVA test was used to compare three or more groups. *P* values < 0.05 were considered as statistically significant. For combining errors from individual experiments when pooling data, the following formula was used:

$$\text{SD combined} = \sqrt{\frac{\{(n_1 - 1) \times SD_1^2 + (n_2 - 1) \times SD_2^2\}}{(n_1 + n_2 - y)}}$$

Where $SD_{combined}$ is the combined standard deviation from y (number of experiments, here 2) experiments where SD1, SD2 are standard deviations in individual experiments and n1 and n2 are number of replicates in each experiment (Mukherjee et al., 2007).

## 3.3 Results

### 3.3.1 Basic characteristics of brain cancer cell lines

Prior to conducting any experiments, the cell growth curves (Figure 3.3) of a range of cell lines were determined by cell counting. Based on the growth curves, the average doubling time for SNB19, SF188, KNS42, DAOY, UW228-3 and MRC5 were calculated as 31, 24, 28, 26, 20 and 18 h, respectively. Such results are comparable to published data (Tseng et al., 1999, Bax et al., 2009, Kominsky et al., 1998, Macaulay et al., 1999), except for KNS42 cell line whose doubling time was shorter than has been previously reported (i.e. 28 h *vs.* 40-48 h) (Takeshita et al., 1987).

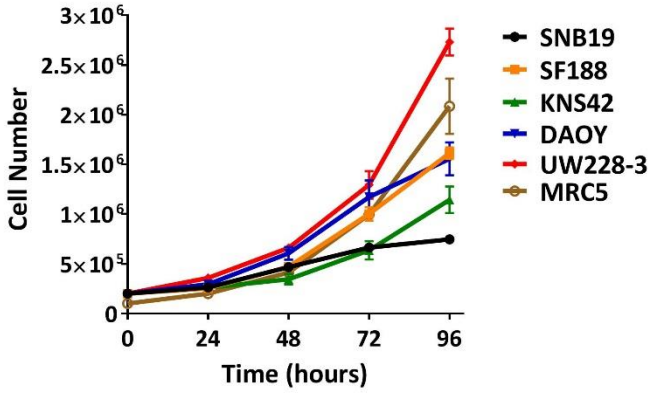



**Figure 3.3 Growth curves of SNB19, SF188, KNS42, DAOY, UW228-3 and MRC5 cell lines.** Data represent the mean cell number/well ± SD of two independent experiments, with each experiment conducted in triplicate.

PE, an inherent characteristic of cell lines, was assessed across the range of cell lines, in normoxia and hypoxia, using the clonogenic survival assay. Sub-confluent cells without drug treatment were initially plated for clonogenics at a series of cell densities (i.e. 100, 200, 400, and 800 cells/T25 flask) and incubated for different time periods (usually 10-21 days) without disturbance. The cell density and the incubation time that generated the highest PE with appropriate colony size was applied in subsequent experiments. As shown in Table 3.2, the PEs of SNB19, SF188, KNS42, DAOY, UW228-3, and MRC5 were 58 ± 9%, 50 ± 9%, 50 ± 6%, 55 ± 10%, 92 ± 4%, and 83 ± 8%, respectively, which were high enough to produce representative results. Following 72 h incubation under hypoxia, the colony-forming ability of DAOY and UW228-3 cells were unaffected with PEs of 61 ± 11% and 81 ± 12%, respectively. The optimal incubation time for colony formation was 14 days for SNB19 cells, 12 days for SF188, 21 days for KNS42, and 10 days for DAOY, UW228-3 and MRC5 cells. As 30-100 colonies are generally required per T25 flask, 100/200 cells were determined as optimal cell seeding number for all lines, except UW228-3 and MRC5 cells, in which 50/100 cells were enough to form appropriate numbers of colonies. The foetal neural stem cell FB83 demonstrated extremely low proliferation rate and did not form colonies at all, so it was not used in any further experiments.

**Table 3.2 Plating efficiencies of different cell lines.**

| Cell lines | Optimal incubation time | PE (%) Normoxia | PE (%) Hypoxia | Optimal cell seeding numbers in T25cm$^2$ flask |
|---|---|---|---|---|
| SNB19 | 14 days | 58 ± 9 | N/A | 100 and 200 |
| SF188 | 12 days | 50 ± 9 | N/A | 100 and 200 |
| KNS42 | 21 days | 50 ± 6 | N/A | 100 and 200 |
| DAOY | 10 days | 55 ± 10 | 61 ± 11 | 100 and 200 |
| UW228-3 | 10 days | 92 ± 4 | 81 ± 12 | 50 and 100 |
| MRC5 | 10 days | 83 ± 8 | N/A | 50 and 100 |

Abbreviations: PE, plating efficiency; N/A, not applied/performed.

### 3.3.2 Role of IQ10 in regulating protein activity and expression

#### 3.3.2.1 TrxR activity

Endpoint insulin reduction assay was employed to measure the TrxR activity in three different brain cancer cell lines: SF188, DAOY and UW228-3. Cells were treated with 1 µM of auranofin or increasing concentrations of IQ10 (0.25, 0.5, 0.75 and 1 µM) for 4 or 48 h. Auranofin, the most active inhibitor of TrxR characterised to date (Urig and Becker, 2006), was used as a positive control and comparator in this assay. The endogenous level of TrxR activity was compared between the untreated control cells. Among the three cell lines, SF188 cells had the highest level of active TrxR (291.84 ± 22.17 nM), followed by UW228-3 (173.86 ± 21.81 nM), and DAOY cells presented the lowest TrxR activity (122.70 ± 20.12 nM).

As illustrated in Figure 3.4A, in comparison to controls, the treatment of the three cell lines with IQ10 for 4 h resulted in a significant decrease in TrxR activity in a dose-dependent pattern. A 50% inhibition of TrxR activity by IQ10 was observed at a dose of ~0.34 µM, 0.58 µM and 0.44 µM in SF188, DAOY, and UW228-3 cells, respectively. The maximal inhibition effects of TrxR activity was ~87%, which was observed at a concentration of 1 µM IQ10 treatment in SF188 cells.

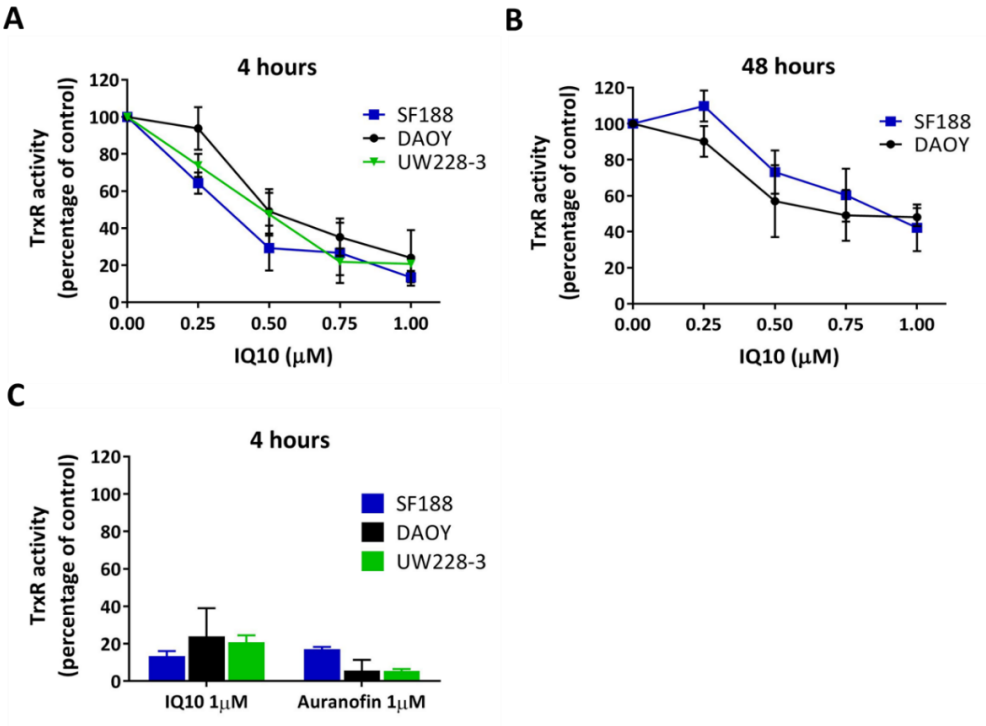



**Figure 3.4 Inhibition of TrxR activity across different brain cancer cells.** SF188, DAOY and UW228-3 cells were treated with various concentrations of IQ10 for 4 and 48 h or 1 μM auranofin for 4 h. (A) Inhibition of TrxR activity in SF188, DAOY and UW228-3 cells by IQ10 after 4 h treatment. (B) Inhibition of TrxR activity in SF188 and DAOY cells by IQ10 after 48 h of treatment. (C) Inhibition of TrxR activity in SF188, DAOY and UW228-3 cells by 1 μM of IQ10 and auranofin after 4 h treatment. Data were expressed as percent of DMSO-treated control. Data represent the mean ± SD of three independent experiments, with each conducted in duplicate.

The TrxR activity was also assessed in a 48-h time point and the results showed that IQ10 also inhibited TrxR activity in a dose-dependent manner in both SF188 and DAOY cells, with IC50 values of ~0.88 μM and 0.79 μM, respectively (Figure 3.4B). The maximal inhibition effects of TrxR activity were ~58% and ~52% for SF188 and DAOY cells, respectively. In comparison to 4-h treatment, the inhibitory effect of IQ10 on TrxR activity was less potent at 48 h, therefore, 4 h was chosen as the treatment time for subsequent drug-radiation combination experiments that will be described in Chapter 4. At a concentration of 1 μM, the positive control drug auranofin caused an average of ~83-95% inhibition of TrxR activity across the three cell lines at 4 h following drug treatment. The same IQ10 dose inhibited ~76-87% of the TrxR activity (Figure 3.4C), indicating that IQ10 exhibited almost equal potency to auranofin as a TrxR inhibitor. Although higher endogenous TrxR activity was

seen in SF188, there were no significant differences with respect to the inhibitory ability of IQ10 between SF188, DAOY, and UW228-3 cell lines as indicated by the IC50 values.

### 3.3.2.2 Protein expression under normoxia

Before assessing the effect of IQ10 on regulating protein expression, the endogenous expression levels of TrxR, Trx, and TxNIP were initially quantified using Western blotting across the five brain cancer cell lines. The representative blots and the quantification analysis are shown in Figure 3.5.

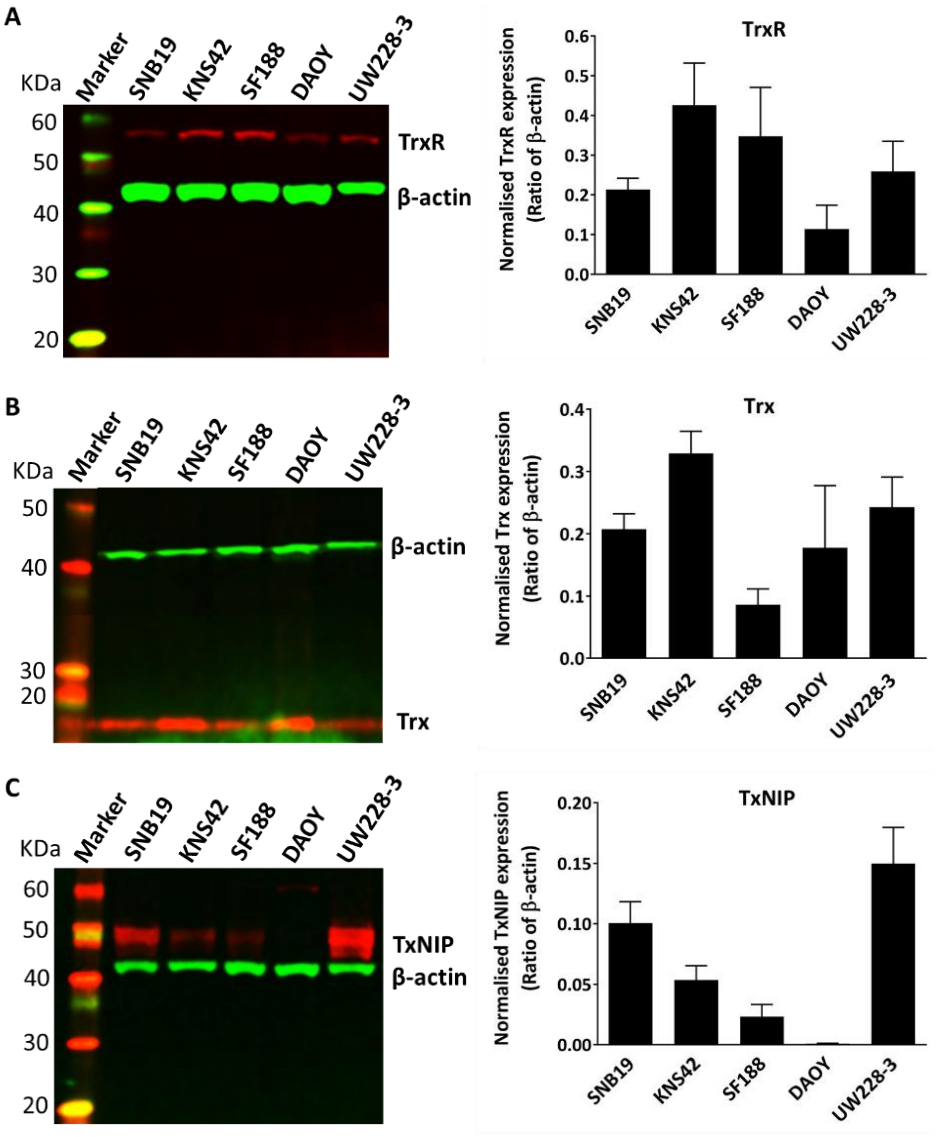



**Figure 3.5 Quantification of Trx system protein expression across different brain cancer cells.** The representative blots are shown above. Red bands indicate TrxR (A), Trx (B) and TxNIP (C) expression and green bands represent β-actin (left panels). Data in the bar charts (right panels) represent the mean of normalised protein expression to β-actin ± SD of three independent experiments, with separate cell lysates from different passage numbers

of cells.

As can be seen, the expression level of TrxR was relatively higher in KNS42, SF188 and UW228-3 cells, while lower but detectable amounts were observed in SNB19 and DAOY cells, with the latter one exhibiting the lowest expression (Figure 3.5A). The sequence of endogenous TrxR expression level, from high to low, was KNS42 > SF188 > UW228-3 > SNB19 > DAOY. The expression of Trx was highest in KNS42 cell line and lowest in SF188 cell line, while the remaining three cell lines showed comparable Trx expression (Figure 3.5B). The sequence of endogenous Trx expression level, from high to low, was KNS42 > UW228-3 > SNB19 > DAOY > SF188. UW228-3 cells expressed the highest level of TxNIP, while the expression level in DAOY cells was very low, with protein bands hardly detectable (Figure 3.5C). The sequence of endogenous TxNIP expression level, from high to low, was UW228-3 > SNB19 > KNS42 > SF188 > DAOY.

The effect of IQ10 on protein expression of TrxR, Trx and TxNIP was subsequently examined by Western blotting in DAOY and UW228-3 cells as the role of Trx system has never been assessed in these two MB cell lines. As shown in Figure 3.6, the expression of all three members of the Trx system was detected in both DAOY and UW228-3 cells at the expected size; however, according to the quantification analysis, no obvious alterations in the expression of any of the Trx system proteins were observed in either of the cell lines after varying concentrations of IQ10 treatment for 48 h. Taken together, data suggest that IQ10 potently inhibits TrxR activity with the IC50 values in the submicromolar range in brain cancer cells without affecting Trx system protein expression.

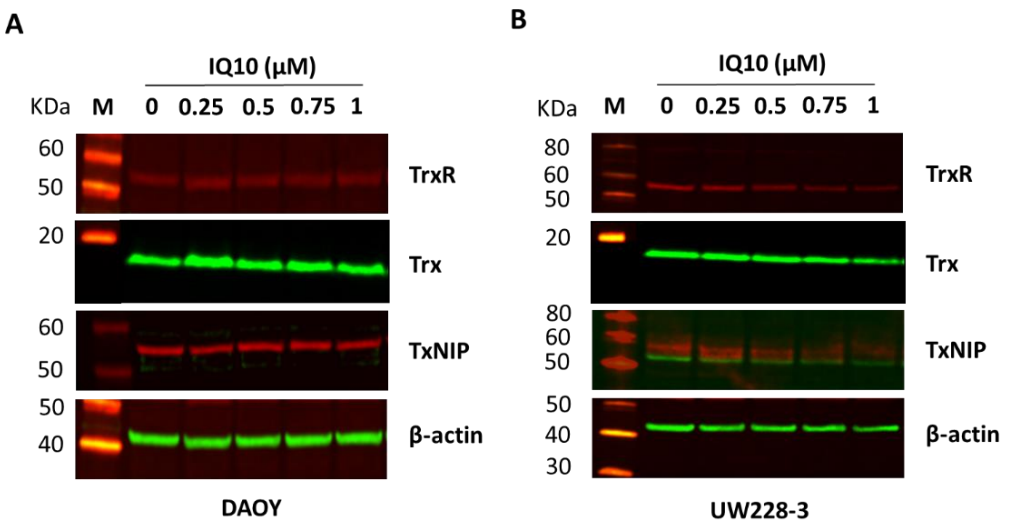



**Figure 3.6 Effect of IQ10 on the expression of Trx system proteins in brain cancer cells.** Cells were treated with increasing concentrations of IQ10 for 48 h. Cells were then collected and subjected to Western blotting to assess the expression of TrxR, Trx and TxNIP with β-actin as internal control. Experiments were conducted twice, with separate lysates of different passage number of cells. The representative blots are shown above.

### 3.3.2.3 Protein expression under hypoxic conditions

The effect of IQ10 on protein expression under hypoxic conditions was further assessed by Western blotting. Cells were pre-incubated under hypoxic conditions for 24 h before exposure to IQ10 (IC50 dose obtained from growth assay in Section 3.3.3.1) for an additional 48 h in hypoxia. Cells cultured under normoxic conditions were used as the control. The effect of IQ10 on the expression of the hypoxic marker CA9, used as a confirmatory indicator of the hypoxic condition, was initially assessed in DAOY and UW228-3 cells. As shown in Figure 3.7, CA9, a molecule known to be substantially upregulated by hypoxic stress in other cancer cell lines (Wykoff et al., 2000), was markedly increased in both cell lines exposed to hypoxic conditions compared with those maintained under control normoxic conditions ($P$<0.01). CA9 expression was almost below the detectable levels in the normoxic controls cells. Furthermore, IQ10 treatment reduced the expression levels of CA9 under hypoxia in both DAOY and UW228-3 cells, but only the reduction in DAOY cells reached statistical significance ($P$<0.01).

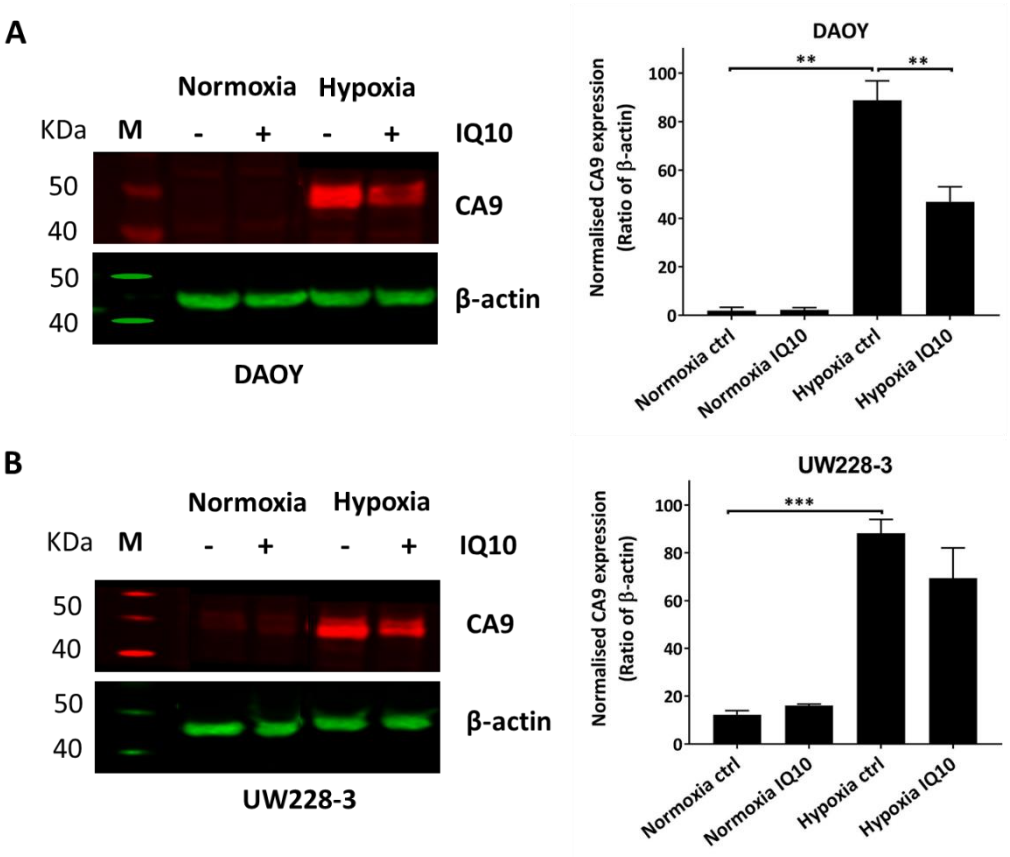



**Figure 3.7 Effect of IQ10 on CA9 expression in brain cancer cells under normoxic and hypoxic conditions.** Cells were treated with IQ10 (IC50 dose) for 48 h in normoxia or hypoxia. Cells were then collected and subjected to Western blotting to assess the expression of CA9 with β-actin as internal control. The representative blots are shown above (left panel). Data represent the mean ± SD of three independent experiments, with separate lysates of different passage number of cells. ** $P$<0.01 and *** $P$<0.001 *vs.* control (student's *t*-test). Abbreviations: M, marker; ctrl, control.

Western blotting was also conducted to analyse the alterations of TrxR, Trx and TxNIP expression in DAOY and UW228-3 cells treated with IQ10 for 48 h under both normoxia and hypoxia. When comparing the protein expression of untreated controls between normoxic and hypoxic conditions, the expression levels of TrxR, Trx and TxNIP were unaffected by hypoxic incubation in both cell lines (Figure 3.8). Further, in line with the results from normoxia (Section 3.3.2.2), there was no significant alteration in the TrxR, Trx or TxNIP protein levels in either cell line following drug treatment under hypoxia (Figure 3.8).

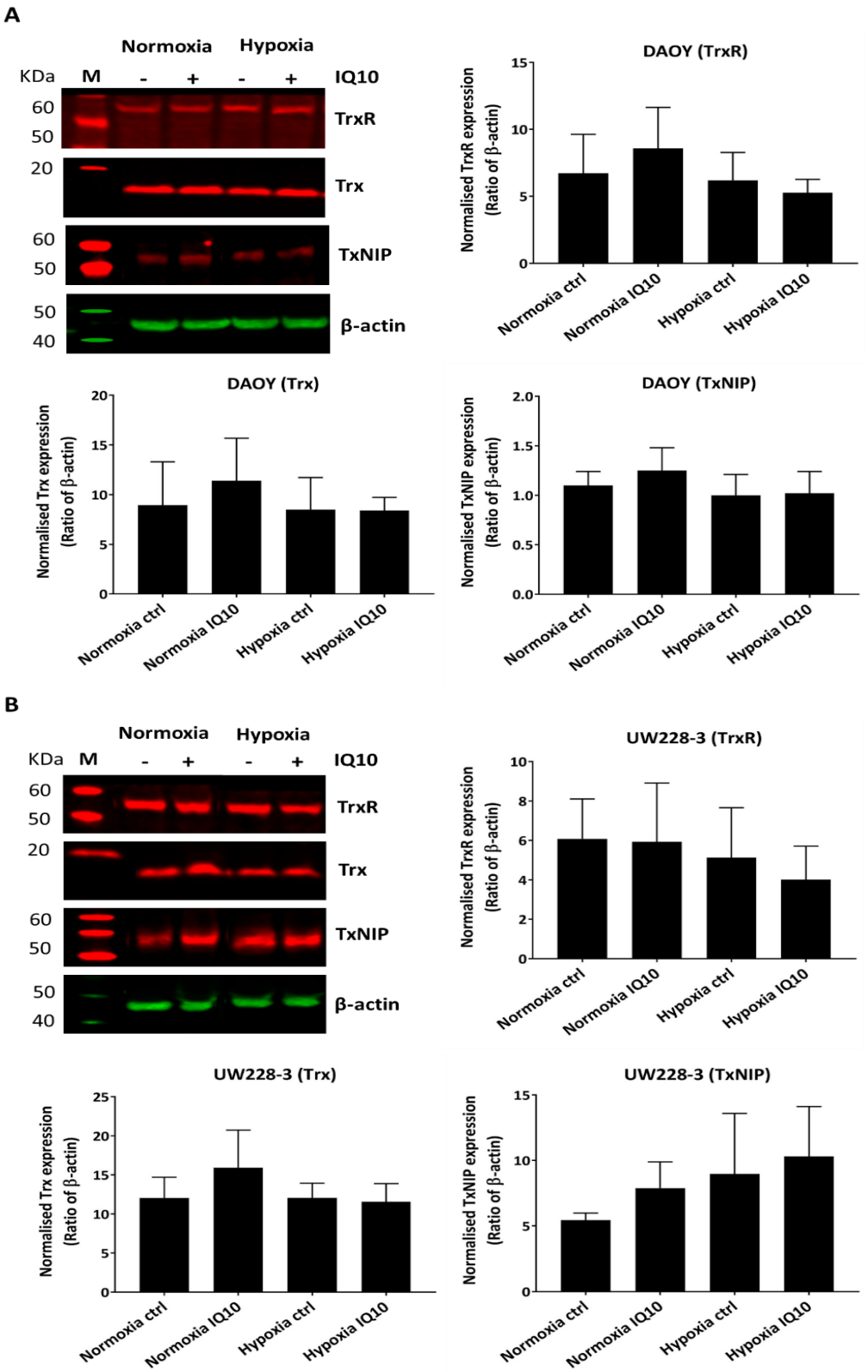



**Figure 3.8 Effect of IQ10 on TrxR, Trx and TxNIP expression in brain cancer cells under normoxic and hypoxic conditions.** (A) DAOY and (B) UW228-3 were treated with IQ10 (IC50 dose) for 48 h in normoxia or hypoxia. Cells were then harvested and subjected to Western blotting to assess the expression of Trx system proteins with β-actin as internal control. The representative blots are shown above. Data represent the mean ± SD of three independent experiments, with separate lysates of different passage number of cells. Abbreviations: M, marker.

In order to investigate the potential mechanism(s) of drug activation, the expression levels of three reductases (i.e. cytochrome P450, NQO1 and NQO2) were assessed by Western blotting in DAOY and UW228-3 cells treated with IQ10 in normoxic or hypoxic conditions. As shown in Figure 3.9, the endogenous expression level of NQO1 was significantly lower ($P$<0.001), and the NQO2 expression was higher ($P$<0.001), in DAOY than in UW228-3, while the P450 expression was the same in the two cell lines. In both cell lines, hypoxia did not affect expression levels of P450, NQO1 or NQO2. Following drug treatment, no significant alterations in P450 or NQO1 expression were observed in either cell line under either normoxia or hypoxia. However, the Western blotting quantification analysis showed a 1.7-fold decrease in NQO2 expression in DAOY cells under hypoxic but not normoxic conditions ($P$<0.01). Interestingly, the expression levels of NQO2 in UW228-3 were very low in both IQ10-treated and control cells in both normoxic and hypoxic conditions, with protein bands hardly detectable.

Although P450 and NQO1 expression were unaffected by hypoxia or IQ10 treatment, the alterations of their activity were not measured in the present study due to time limitations, therefore, further investigations are required to clearly determine the enzyme activity of the reductases after drug treatment under both hypoxic and normoxic conditions. Current data suggest that the two MB cell lines (DAOY and UW228-3) have different endogenous NQO1 and NQO2 protein levels, and NQO2 may contribute to the activation of IQ10 in DAOY cells under hypoxic conditions.

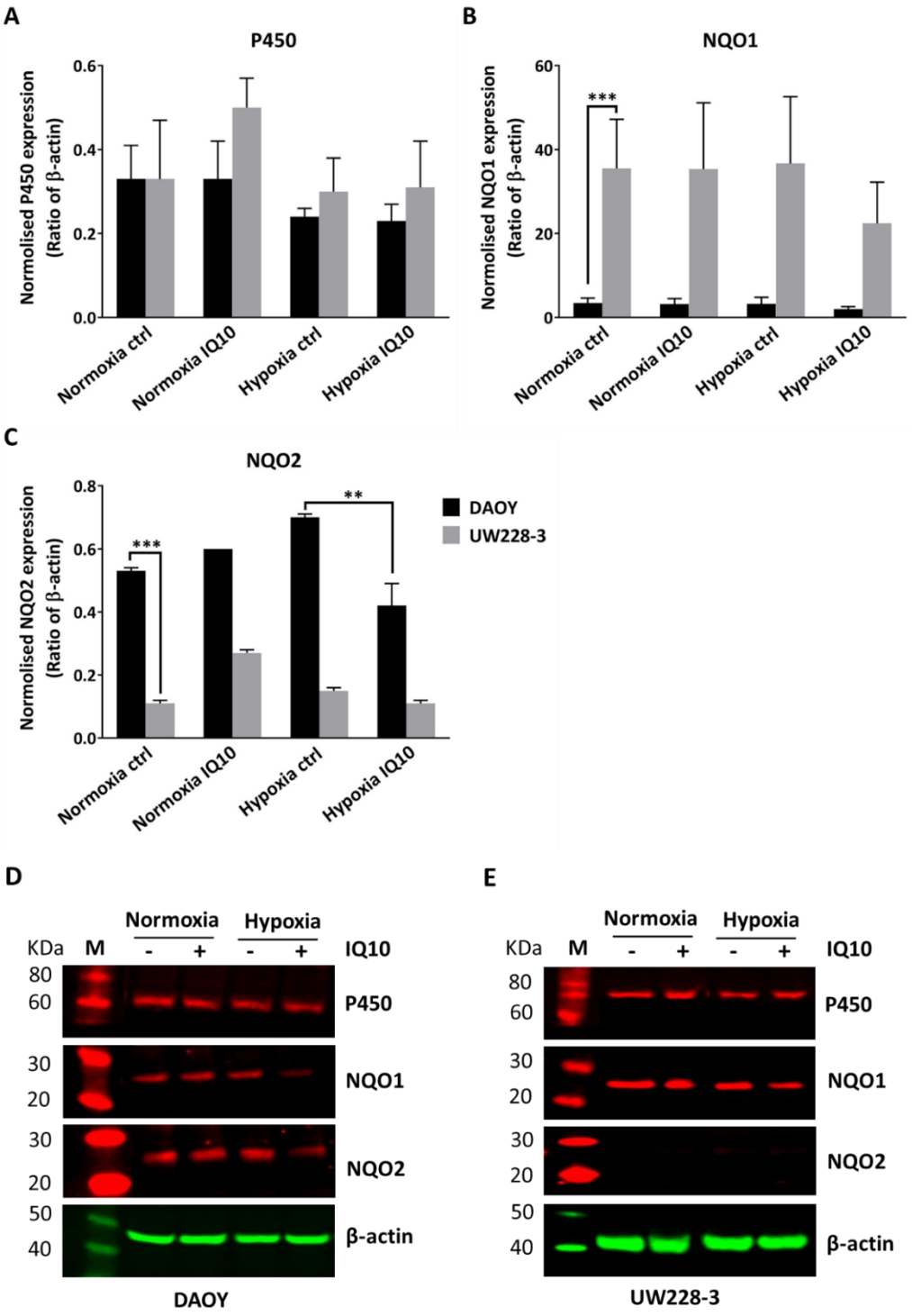



**Figure 3.9 Effect of IQ10 on P450, NQO1 and NQO2 expression in brain cancer cells under normoxic and hypoxic conditions.** Cells were treated with IQ10 (IC50 dose) for 48 hours in normoxia or hypoxia. Cells were then harvested and subjected to Western blotting to assess the expression of (A) P450, (B) NQO1, and (C) NQO2 with β-actin as internal control. Data represent the mean ± SD of three independent experiments, with separate lysates of different passage number of cells. ** $P<0.01$ and *** $P<0.001$ (student's *t*-test). The representative blots of DAOY (D) and UW228-3 (E) are shown above. Abbreviations: M, marker.

### 3.3.3 Cytotoxicity of IQ10 on brain cancer cells cultured in 2D

#### 3.3.3.1 Proliferation

*Normoxic conditions*

The antiproliferative effects of IQ10 and TMZ were examined on five brain cancer cell lines (i.e. SNB19, KNS42, SF188, DAOY, and UW228-3) and MRC5 fibroblasts. TMZ, a well-known chemotherapy agent that is widely used in clinical treatment of brain tumour, was used as a comparator and positive control. The effects of TMZ on cell proliferation was examined by treating cells with various concentrations of TMZ (0-1000 µM) for 24, 48 and 72 h, and the corresponding growth curves plotted. As shown in Figure 3.10, TMZ inhibited cell proliferation in a dose- and time-dependent manner for all brain cancer cell lines. The maximum anti-proliferative effect was evident after 72 h drug incubation. The estimated IC50 values (50% growth inhibitory concentration) of all cell lines lie between 148.4 ± 14.7 µM and 980.1 ± 280.8 µM after 72 h of treatment (Table 3.3).

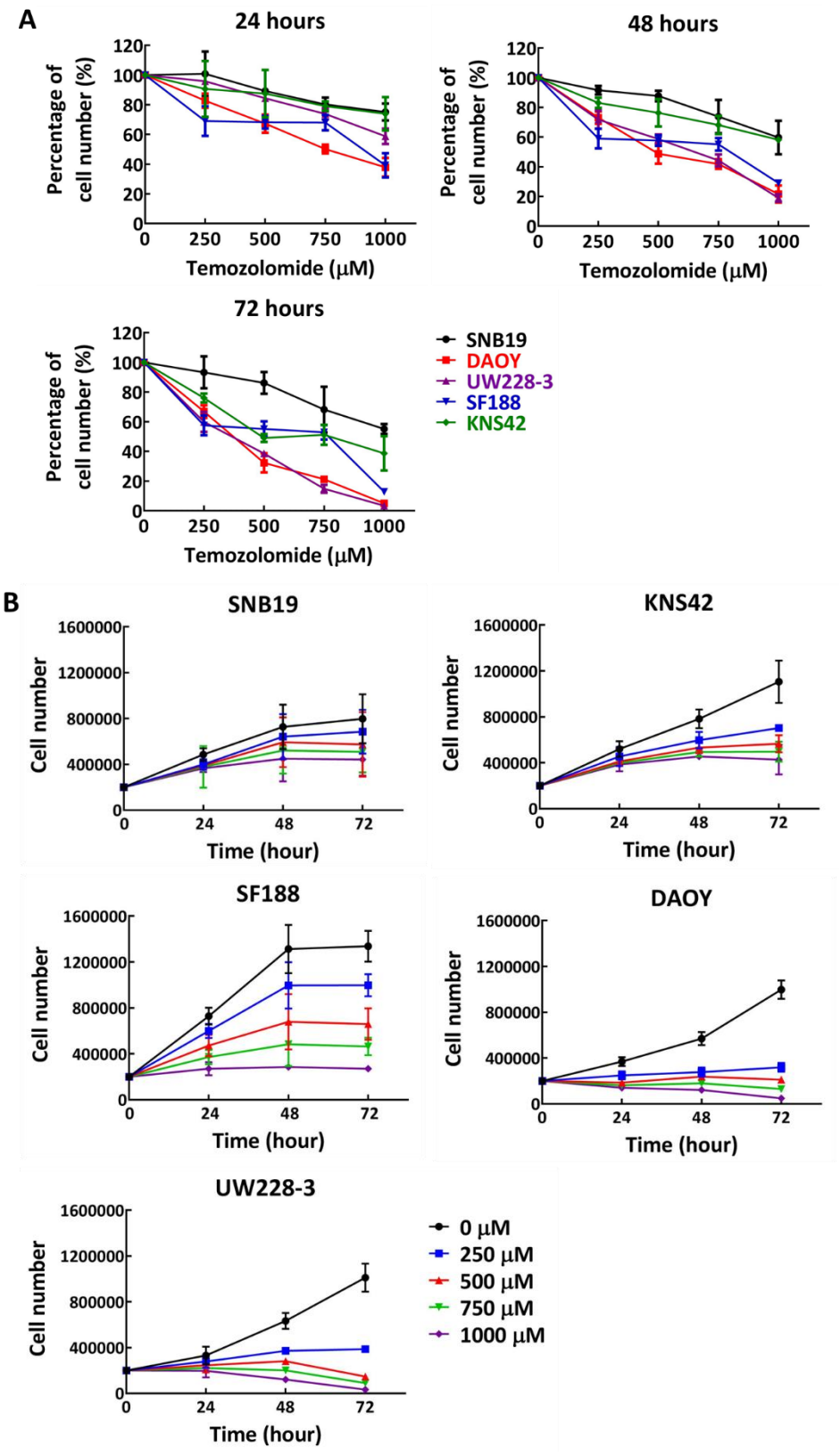



**Figure 3.10 Effect of TMZ on cell proliferation of brain cancer cells and the corresponding growth curves.** Cells were treated with various concentrations of TMZ for 24, 48, and 72 h. (A) Cell counting of different cell lines after various concentrations of TMZ treatment was plotted as a percentage of control for each time point. (B) Cell number of each treatment group were counted at each time point and plotted. Data represent the mean ± SD of two independent experiments, with each experiment performed in triplicate.

**Table 3.3 Summary of the proliferation assay IC50 values of the brain cancer and fibroblast cells treated with IQ10 and TMZ.**

| Cell lines | TMZ (μM) | | | IQ10 (μM) | | |
|---|---|---|---|---|---|---|
| | 24 h | 48 h | 72 h | 24 h | 48 h | 72 h |
| SNB19 | >1000 | >1000 | 980.1±280.8 | 3.8±0.5 | 2.2±0.3 | 2.0±0.3 |
| DAOY | 546.9±11.6 | 248.3±49.8 | 162.5±14.3 | 1.0±0.2 | 0.5±0.1 | 0.4±0.1 |
| UW228-3 | >1000 | 313.6±17.8 | 148.4±14.7 | 0.3±0.1 | 0.2±0.0 | 0.2±0.0 |
| SF188 | >1000 | 320.7±86.8 | 188.0±24.1 | 0.7±0.1 | 0.2±0.0 | 0.2±0.0 |
| KNS42 | >1000 | >1000 | 731.2±24.3 | >1 | >1 | 1.0±0.1 |
| MRC5 | NA | NA | NA | >1 | 0.9±0.2 | 0.8±0.2 |

The IC50 values were calculated by log-probit analysis in SPSS. Abbreviations: TMZ, temozolomide; NA, not applicable/not performed.

The antiproliferative effects of IQ10 were also assessed by plotting cell growth curves following treatment of the cells with different concentrations of IQ10 for 24, 48 and 72 h. Results showed that IQ10 potently inhibited the cell proliferation of various brain cancer cells at sub-micromolar or low micromolar concentrations and in a dose- and time-dependent manner (Figure 3.11). Among the five brain cancer cell lines, SF188 and UW228-3 were relatively more sensitive to IQ10, followed by DAOY, and then SNB19 and KNS42 were the most resistant. The IC50 values lie between 0.2 ± 0.0 μM and 2.0 ± 0.3 μM after 72 h of treatment (Table 3.3) for all brain cancer cell lines. In comparison to the IC50 values of TMZ, IQ10 was ~450-1000 fold more potent in terms of inhibiting cell proliferation.

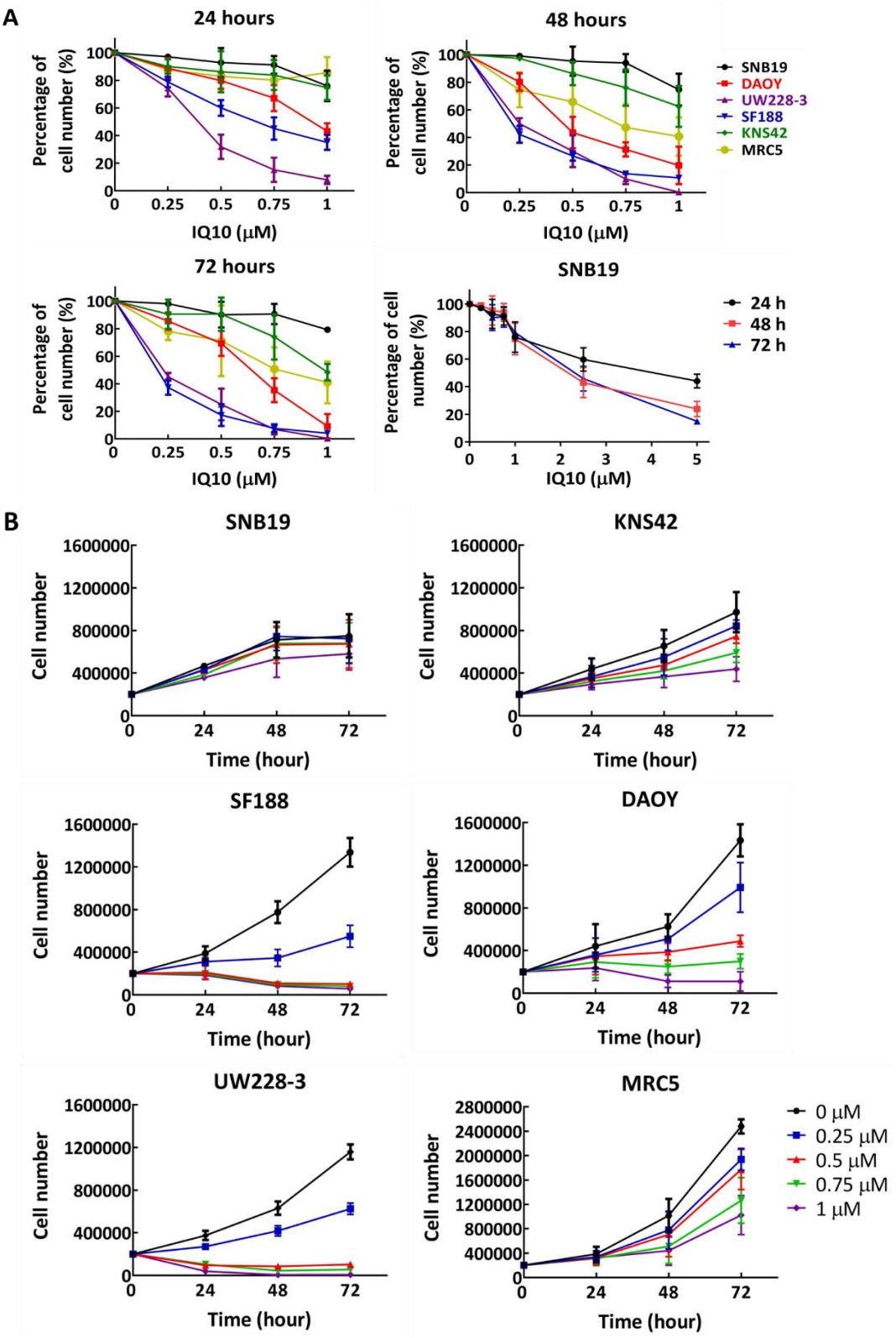



**Figure 3.11 Effect of IQ10 on cell proliferation of brain cancer cells and the corresponding growth curves.** Cells were treated with various concentrations of IQ10 for 24, 48, and 72 h. (A) Cell counting of different cell lines after various concentrations of IQ10 treatment was plotted as a percentage of control for each time point. SNB19 was treated with higher doses (up to 5 μM) of IQ10 to reach 50% growth inhibition. (B) Cell number of each treatment group were counted at each time point and plotted. Data represent the mean ± SD of two independent experiments, with each experiment performed in triplicate.

As it was impossible to use the foetal neural stem cell FB83 in current endpoints, to further investigate if IQ10 has selective cytotoxicity toward brain cancer cells, human normal lung fibroblast MRC5 cells were used to examine the anti-proliferative effects. As shown in Figure 3.11A, a dose-dependent inhibition of cell proliferation was observed in MRC5 and the most evident inhibition was seen after 72 h of treatment. When comparing the anti-proliferative effect of IQ10 between MRC5 and the brain cancer cells, MRC5 was relatively resistant to IQ10 after 24 h of treatment, with an IC50 of > 1 µM. But when the treatment time prolonged to 48 and 72 h, MRC5 became more sensitive to IQ10 than SNB19 and KNS42, with IC50 values of 0.9 ± 0.2 µM and 0.8 ± 0.2 µM, respectively (Table 3.3). As shown in Figure 3.11B, with the range of doses used all brain cancer cell lines showed a cytotoxic response to IQ10, especially at the higher doses, but MRC5 was apparently much more resistant with only antiproliferative rather than an obvious cytotoxic effect evident. Such results might be due to the high proliferation rate of MRC5, but clonogenic results were needed to more fully understand the cytotoxic effects of IQ10 (data below).

### *Hypoxic conditions*

Certain quinone based agents (e.g. MMC and apaziquone) show enhanced cytotoxic action under hypoxic conditions, due to elevated reductases expression (e.g. NQO1), increased reductase activation, prolonged half-life of highly active intermediates or increased DNA cross-links (Phillips et al., 2017, Ahn et al., 2013), so the effect of hypoxia on the cytotoxicity of IQ10 was examined. Cells were pre-incubated in 1% $O_2$ for 24 h, then treated with increasing concentrations of IQ10 for up to an additional 72 h under hypoxia. Meanwhile, a control set of cells were treated with IQ10 for the same period of time under normoxia. In normoxia, population doubling times were ~26 and ~20h for untreated DAOY and UW228-3, respectively. While, under hypoxic conditions, both cell lines showed a slower rate of cell growth requiring ~40 and ~31h respectively. Growth curves for DAOY and UW228-3 cells treated with IQ10 showed a time- and dose-dependent inhibition of cell

proliferation in both cell lines under both normoxic and hypoxic conditions (Figure 3.12).

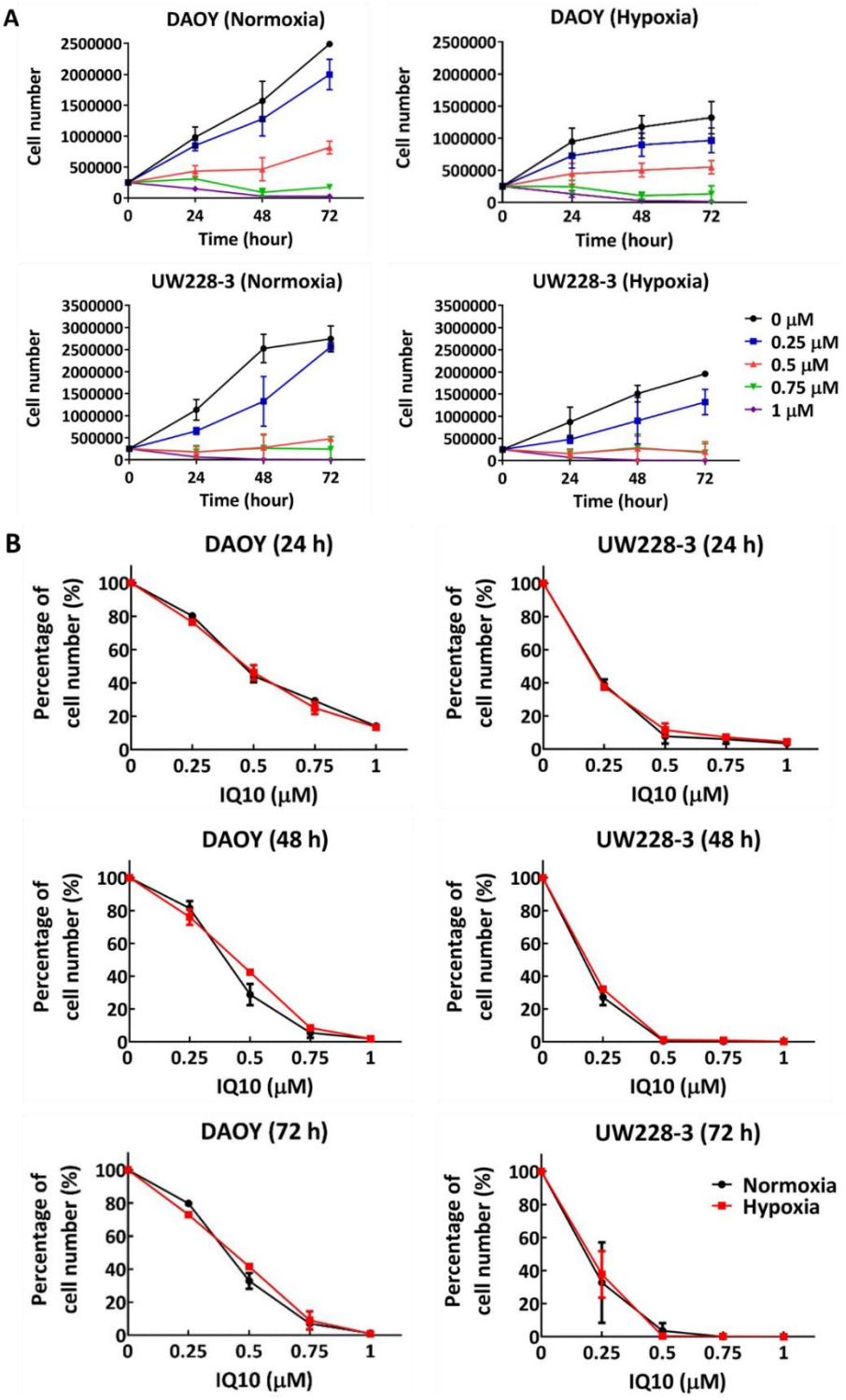



**Figure 3.12 Effect of IQ10 on cell proliferation of brain cancer cells under normoxia and hypoxia.** Cells were treated with various concentrations of IQ10 for 24, 48, and 72 h under both normoxia and hypoxia. (A) Cell number of each treatment group were counted at each time point and plotted. (B) Cell counting of normoxia and hypoxia was plotted as a percentage of control for each time point. Data represent the mean ± SD of two independent experiments, with each experiment performed in triplicate.

The IC50 values of IQ10 in normoxia and hypoxia are listed in Table 3.4 for both cell lines.

**Table 3.4 Comparison of proliferation assay IC50 values (μM) of IQ10 between normoxia and hypoxia in DAOY and UW228-3 cells.**

| Cell lines | Normoxia | | | Hypoxia | | |
|---|---|---|---|---|---|---|
| | 24 h | 48 h | 72 h | 24 h | 48 h | 72 h |
| DAOY | 0.47±0.01 | 0.38±0.02 | 0.38±0.01 | 0.45±0.06 | 0.39±0.03 | 0.38±0.02 |
| UW228-3 | 0.28±0.02 | 0.22±0.01 | 0.21±0.06 | 0.22±0.06 | 0.21±0.01 | 0.22±0.06 |

The IC50 values were calculated by log-probit analysis in SPSS.

When comparing the IC50s between the two culture conditions, the hypoxic cells appeared equally as sensitive as their normoxic equivalents to the drug at all time points tested, indicating that there was no significant increased hypoxia-induced drug sensitisation and that the slower rate of proliferation in hypoxia did not markedly affect the drug sensitivity. Collectively, these results indicated that IQ10 potently inhibited the proliferation of DAOY and UW228-3 cells in a dose- and time-dependent manner, under both normoxia and hypoxia, with no induced hypoxic sensitivity observed. It is interesting to additionally note that although hypoxia has been shown, with certain agents (e.g. cisplatin, doxorubicin and etoposide etc.) (Doktorova et al., 2015) to induce chemoresistance no such induced resistance was evident in the current experiments with IQ10 being equally effective under both normoxia and hypoxia.

Following cell counting for the growth assays, cells were collected and subjected to Western Blotting for assessing the effects of hypoxia (± IQ10) on expression levels of CA9, Trx, TrxR, TxNIP, P450, NQO1, and NQO2. The expression of the hypoxic marker CA9 was significantly increased following 48, 72, or 96 h of hypoxic incubation in both DAOY and UW228-3 cells (Figure 3.13), verifying that cells were in the hypoxic state during the whole period of drug treatment. The effect of IQ10 in regulating protein expression under hypoxia was presented in Section 3.3.2.3.

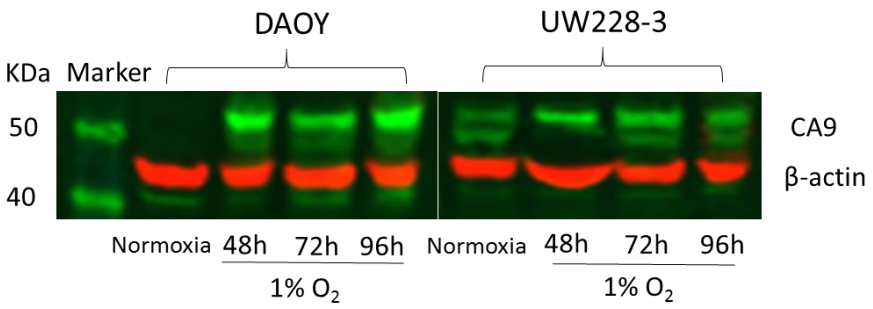



**Figure 3.13 CA9 expression in DAOY and UW228-3 cells following hypoxic incubation.** Cells were incubated under hypoxia for 48, 72, and 96 h. Cell lysates were collected and subjected to Western blotting to assess the expression of CA9 with β-actin as internal control. Cell lysates from normoxic conditions were loaded as a negative control. Experiments were repeated twice, with separate lysates of different passage number of cells and the representative blots are shown above.

### 3.3.3.2 Clonogenic survival

#### *Normoxic conditions*

The effect of the control drug TMZ on the survival of the range of brain cancer cell lines was assessed by clonogenic assay. As shown in Figure 3.14A, TMZ decreased cell survival of all five brain cancer cell lines in a dose-dependent manner post 48 h drug exposure.

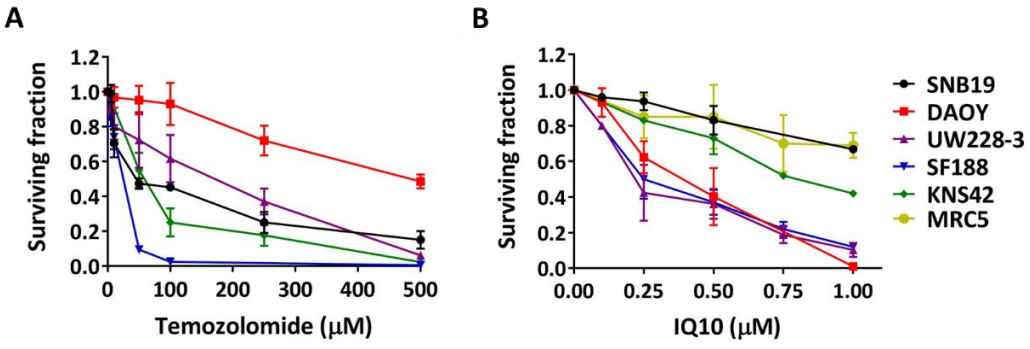



**Figure 3.14 Effect of TMZ and IQ10 on cell survival under normoxic conditions.** Cells were treated with various concentrations of (A) TMZ or (B) IQ10 for 48 h (cells without drug treatment as control) under normoxia. Data represent the mean ± SD of three independent experiments, with each experiment containing six parallel data sets. PEs of individual cell lines under normoxia were as follows: SNB19 - 58 ± 9%; DAOY, 55 ± 10%; UW228-3 92 ± 4%; SF188 - 50 ± 9%; KNS42 - 50 ± 6%; MRC5 - 83 ± 8%.

The clonogenic IC50 value of TMZ for each cell line is listed in Table 3.5. In comparison to the corresponding IC50s from growth assays (Table 3.3), the IC50s obtained from clonogenic survival were approximately 3-20 fold lower

in all cell lines, except DAOY, in which the clonogenic IC50 was about 2 fold higher.

**Table 3.5 The clonogenic assay IC50 values (μM) of TMZ and IQ10 in various cell lines post 48 h drug exposure.**

| Cell lines | TMZ | IQ10 |
|---|---|---|
| SNB19 | 63.7±10.0 | >1 |
| DAOY | 463.5±20.1 | 0.4±0.1 |
| UW228-3 | 93.1±30.0 | 0.3±0.0 |
| SF188 | 15.2±0.9 | 0.3±0.1 |
| KNS42 | 49.5±11.4 | 1.0±0.2 |
| MRC5 | NA | >1 |

The IC50 values were calculated by log-probit analysis in SPSS. All data are expressed as mean ± SD of three independent experiments, with each experiment containing six parallel data sets. Abbreviations: TMZ, temozolomide; NA, not applicable/not performed.

The cytotoxicity of IQ10 in the brain cancer and MRC5 cells was also assessed by clonogenic survival assay. As shown in Figure 3.14B, IQ10 inhibited clonogenic survival of all cell lines in a dose-dependent manner post 48 h drug exposure. The clonogenic IC50 value of IQ10 for each cell line is listed in Table 3.5. These IC50 values were approximately consistent with their corresponding values determined by the cell growth assay (Table 3.3) but with MRC5's being one of the most resistant cell types, alongside SNB19's. In comparison to TMZ, the clonogenic IC50s of IQ10 was ~30-1000 fold lower, suggesting that IQ10 was far more potent than TMZ in terms of cell killing.

When comparing the effect of IQ10 on clonogenicity of different cell lines, SNB19, KNS42 and MRC5 were relatively more resistant, with estimated IC50 values of greater than or equal to 1 μM; while DAOY, UW228-3 and SF188 cells were more sensitive, having IC50 values of between 0.3-0.4 μM (Table 3.5). It appeared that the majority of the brain cancer cell lines were more sensitive to IQ10 than the normal fibroblast MRC5 in the clonogenic assay, indicating that the drug may have the potential to preferentially kill brain cancer cells, however, the drug response in normal brain cells should be examined in the future experiments.

### *Hypoxic conditions*

The effect of IQ10 on the cell survival was also assessed under hypoxic conditions in two MB cell lines, DAOY and UW228-3, which were previously used to assess the effect of IQ10 on protein activity/expression in Section 3.3.2. Colony formation was unaffected by hypoxia as PEs of both DAOY and UW228-3 cells under hypoxic conditions were similar to the results from normoxia (Table 3.2). After 48 h of drug exposure, there was a decrease in the surviving fraction in a dose-dependent manner under both normoxia and hypoxia in DAOY and UW228-3 (Figure 3.15).

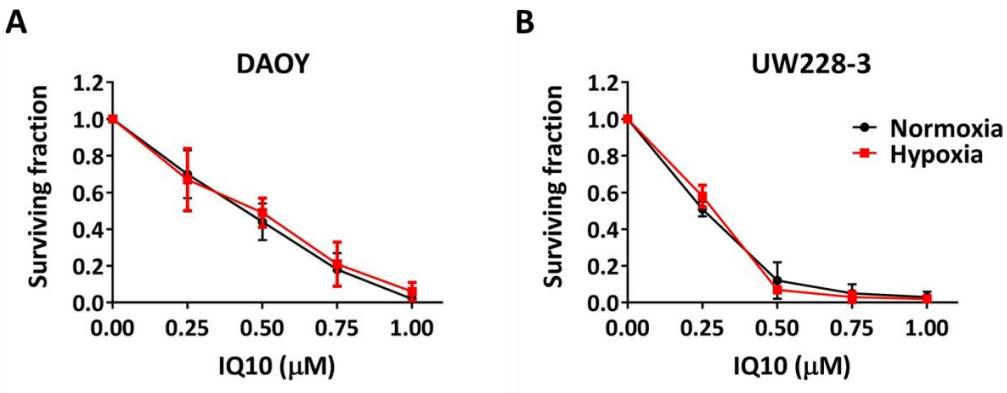



**Figure 3.15 Effect of IQ10 on clonogenic survival of brain cancer cells under both normoxic and hypoxic conditions.** (A) DAOY and (B) UW228-3 cells were treated with various concentrations of IQ10 for 48 h (cells without IQ10 treatment as control) under normoxia or hypoxia. Data represent the mean ± SD of three independent experiments, PEs for normoxia and hypoxia were 55 ± 10% and 61 ± 11% for DAOY, and 92 ± 4% and 81 ± 12% for UW228-3, respectively.

The IC50 values for both conditions were similar and in the sub-micromolar range (Table 3.6), indicating that the potency of IQ10 was preserved in hypoxia. However, there was no increased hypoxic cytotoxicity observed at any of the doses of IQ10 in either DAOY or UW228-3 cells. When comparing the effect of IQ10 on survival between DAOY and UW228-3 cells, UW228-3 cells were slightly more sensitive under both normoxic and hypoxic conditions, with IC50 values of ~0.25 μM and ~0.26 μM, respectively as opposed to ~0.40 μM and ~0.41 μM for DAOY's.

**Table 3.6 Comparison of clonogenic assay IC50 values (μM) of IQ10 between normoxia and hypoxia in DAOY and UW228-3 cells post 48 h drug exposure.**

| Cell lines | IQ10 | |
|---|---|---|
| | Normoxia | Hypoxia |
| DAOY | 0.40±0.09 | 0.41±0.13 |
| UW228-3 | 0.25±0.00 | 0.26±0.04 |

The IC50 values were calculated by log-probit analysis in SPSS. All data are expressed as mean ± SD of three independent experiments, with each experiment containing six parallel data sets.

### 3.3.4 Cytotoxicity of IQ10 on brain cancer spheroids

#### 3.3.4.1 Spheroid morphology and growth

To monitor the growth characteristics of spheroids, the morphology and growth of DAOY and UW228-3 spheroids were observed using an inverted microscope and images were captured daily for 7 days. The average diameters of spheroids were analysed and plotted against time for each seeding density. Figure 3.16A shows representative optical images of DAOY and UW228-3 spheroids with different cell seeding numbers per well (i.e. 1000/3000/5000/10,000 and 15,000 cells). Both DAOY and UW228-3 cells gradually formed tight well-defined rounded spheroids that centrally positioned in each well of the 96-well plates over a period of 7 days. The average size of DAOY and UW228-3 spheroids over time in the five seeding density groups is shown in Figure 3.16B. The spheroid diameter of all groups increased sequentially after an initial slight decrease in the first two days. Tumour spheroids have several unique features, i.e. they possess chemical gradients (oxygen, nutrients or catabolites) at diameters starting from 200 μm and develop a central secondary necrotic area from a diameter of 500 μm onwards (Zanoni et al., 2016). As shown in Figure 3.16B, DAOY cells at a seeding density of 15,000 cells/well generated spheroids with a diameter of >500 μm within 4 days. For UW228-3, both 10,000 and 15,000 cells/well produced spheroids with a diameter of >500 μm within 4 days. Therefore, a cell seeding density of 15,000 cells/well for DAOY and 10,000 cells/well for UW228-3 was chosen for all subsequent experiments.

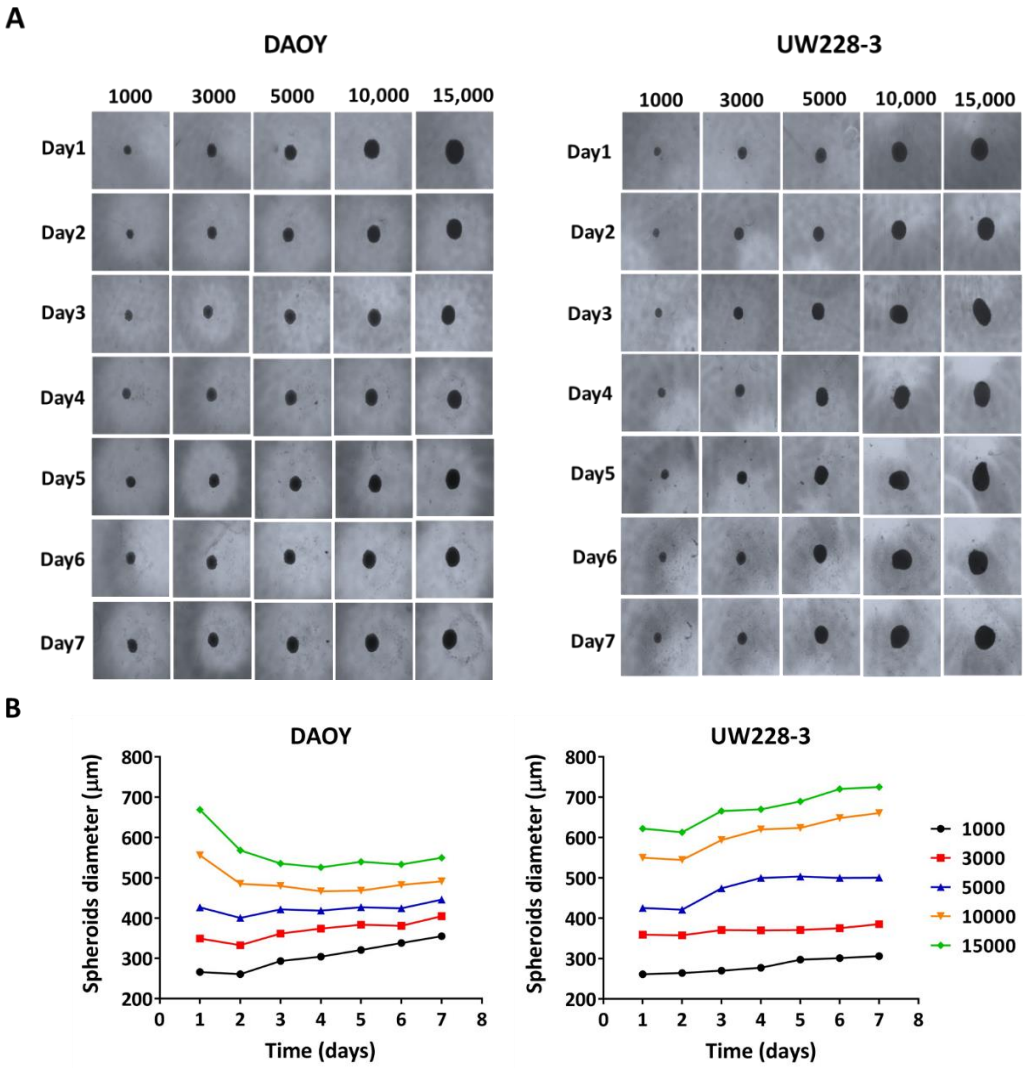



**Figure 3.16 Spheroids growth assay.** Spheroids of DAOY and UW228-3 cells were initiated with 1000, 3000, 5000, 10,000 and 15,000 cells/well in ULA 96-well plates. (A) Representative phase contrast micrographs of DAOY and UW228-3 spheroids from Day 1 to 7. (B) Diameters of DAOY and UW228-3 spheroids with various cell seeding numbers over a 7-day culture. Each point represents the average diameter calculated from measurements of 6 spheroids of two experiments.

### 3.3.4.2 PEs of cells from spheroids

Before conducting any additional spheroid experiments, the 2D PEs of DAOY and UW228-3 cells from spheroids were initially assessed. 4-day-old untreated spheroids were disaggregated into single cell suspension by trypsin/EDTA and plated in the conventional 2D clonogenic assay to assess their colony formation ability. Meanwhile, the PEs of cells in 2D culture were examined in parallel to compare against the spheroid results. PEs for both cell lines were slightly lower from spheroids than from conventional 2D culture, i.e. 62.1% and 41.0% (± 10.2% and 8.6%) for DAOY and UW228-3 spheroids, in

comparison to 72.0± 8.1% and 88.7± 4.7% for 2D culture (Figure 3.17). The differences in the PEs between 2D and 3D spheroid cultures were significant for both cell lines ($P$<0.05 for DAOY and $P$<0.001 for UW228-3).

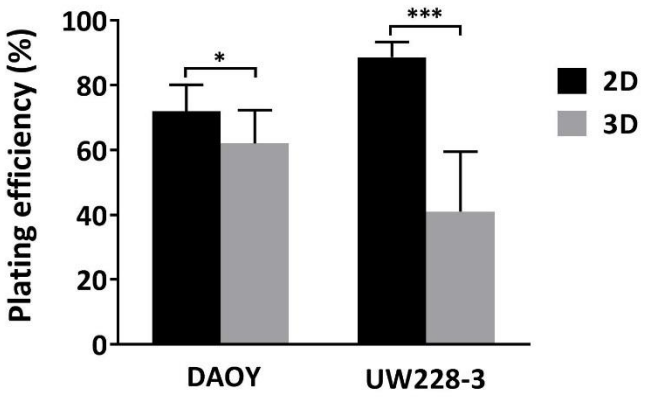



**Figure 3.17 PEs of DAOY and UW228-3 cells in 3D spheroids *vs.* 2D culture.** Data represent the mean ± SD of three independent experiments, with each experiment containing six parallel data sets. *$P$<0.05 and ***$P$<0.001 (student's $t$-test).

### 3.3.4.3 Drug penetration in spheroids

Before assessing the cytotoxicity of IQ10 in the spheroid models, it was important to determine drug penetration depth, as it is one of the major factors that affect the effectiveness of chemotherapy in solid tumours (Minchinton and Tannock, 2006). With an intrinsic red fluorescence, doxorubicin was chosen as a positive control drug to evaluate the drug-penetrating ability in brain cancer spheroids. As the molecular weight of IQ10 is comparatively lower (450.41 *vs.* 543.52 g/mol) and its lipophilicity is higher (ClogP value 2.26 *vs.* 0.32) than doxorubicin, the assumption is that if doxorubicin would penetrate into the spheroids, IQ10 would also have the similar ability.

The distribution of doxorubicin within the spheroids was qualitatively determined by a laser scanning confocal microscope. As shown in Figure 3.18A, fluorescent Z-stack imaging of spheroid cross-sections revealed that doxorubicin could easily penetrate through both DAOY and UW228-3 spheroids at 24 h post-treatment. As the drug-radiation combination experiments in Chapter 4 were conducted at 4 h after drug treatment, the penetrating ability of doxorubicin was also examined at 4 h. Figure 3.18B

shows that even with a shorter drug exposure time, doxorubicin could also penetrate through both spheroids.

In terms of spheroids size, UW228-3 formed larger spheroids with an average diameter of ~500 µM, whereas DAOY's formed smaller and tighter appearing spheroids, and for this reason it is interesting to investigate whether the size and morphology potentially influence drug ability to penetrate into the spheroids. But from current results, it appears that whether they are small and tight or large and looser, the drug can equally penetrate into both types of spheroids. Drug penetration should not, therefore, be a factor that might influence IQ10's cytotoxic effect in spheroids.

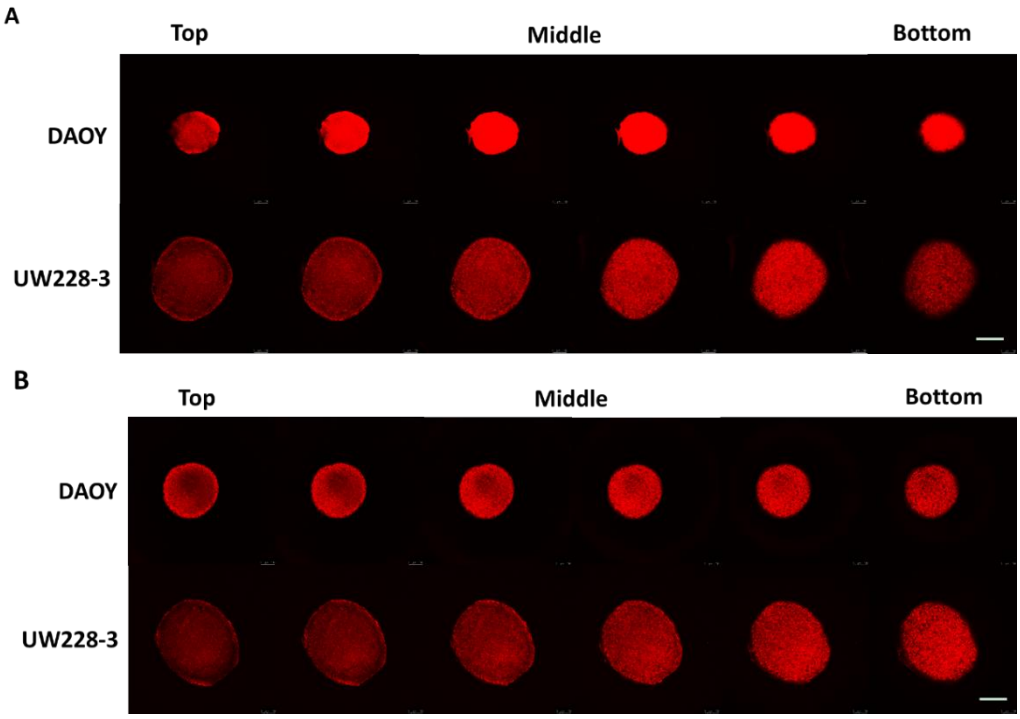



**Figure 3.18 Penetration of doxorubicin in DAOY and UW228-3 spheroids.** Spheroids were incubated with 10 µM doxorubicin for (A) 24 h or (B) 4 h. Confocal microscope representative images of spheroid cross-sections (10X magnification, step size 15 µm) are shown above. Experiments were repeated twice, with each containing 30 spheroids. Scale bar represents 200 µm.

#### 3.3.4.4 Cytotoxicity of IQ10 in spheroids

In order to compare the drug sensitivity in 2D *vs.* 3D, two cancer cell lines, DAOY and UW228-3 were assessed. Resazurin cell viability assays were performed in 2D and 3D for these two cell lines treated with IQ10 for 48 h. The IC50 values observed from 3D spheroids were compared against those

obtained from 2D experiments. Figure 3.19 shows that IQ10 inhibited cell viability in a dose-dependent manner in both 2D and 3D spheroids. 3D IC50 values of cells treated with IQ10 were 0.64 ± 0.10 µM for DAOY and >1 µM for UW228-3, in comparison to 0.29 ± 0.08 µM and 0.16 ± 0.04 µM for 2D values. The data suggest that although DAOY and UW228-3 cells still susceptible to IQ10 they are less sensitive in 3D compared to 2D in terms of cell viability.

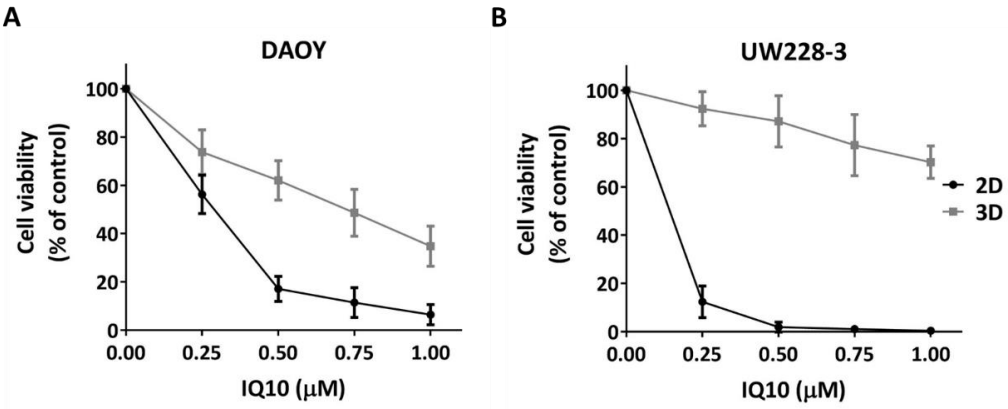



**Figure 3.19 Effect of IQ10 on cell viability of brain cancer cells whilst growing in 2D or 3D spheroid culture.** (A) DAOY and (B) UW228-3 cells in 2D or 3D spheroid cultures were treated with various concentrations (0-1 µM) of IQ10 for 48 h. Cell viability was determined by Resazurin reduction assay. Shown is percentage of cell viability normalised to DMSO-treated control. Data represent the mean ± SD of three independent experiments, with each experiment performed in 6 replicate wells.

The difference in sensitivity to IQ10 between 2D culture and 3D spheroids was further assessed by clonogenic assays in DAOY and UW228-3 treated with IQ10 for 48 h. As with proliferation results showed increased resistance to IQ10 in 3D spheroids compared to 2D cultures in both cell lines (Figure 3.20). The 3D clonogenic IC50 values of IQ10 in DAOY and UW228-3 spheroids were 0.56 ± 0.07 µM and 0.83 ± 0.09 µM, in comparison to 0.37 ± 0.03 µM and 0.30 ± 0.04 µM for 2D values. Although both cell lines, particularly UW228-3, became more resistant to IQ10 when cultured in spheroids, the IC50 values were still less than 1 µM, indicating that IQ10 maintained its cytotoxic effect in 3D culture.

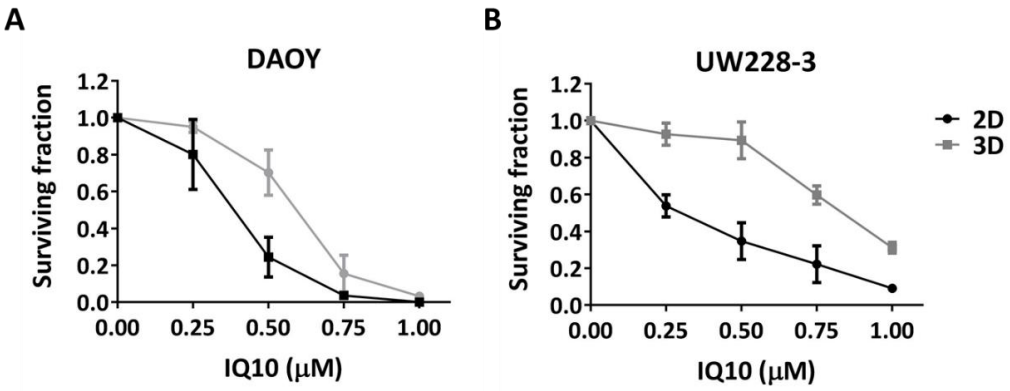



**Figure 3.20 Effect of IQ10 on clonogenic survival of brain cancer cells whilst growing in 2D culture and 3D spheroids.** (A) DAOY and (B) UW228-3 cells cultured in 2D or spheroids were treated with various concentrations of IQ10 (0-1 μM) for 48 h (cells treated with DMSO as control). Data represent the mean ± SD of three independent experiments, with each experiment containing six parallel data sets. The average PEs for DAOY and UW228-3 cells in 2D were 72 ± 8% and 89 ± 5%; and PEs for spheroids were 62 ± 10% and 41 ± 8%, respectively.

### 3.3.5 Knockdown of TrxR using siRNA

#### 3.3.5.1 Optimisation of siRNA concentration and post-transfection incubation time

Transient siRNA mediated knockdown of TrxR was carried out on DAOY and SF188 as they are medulloblastoma and paediatric GBM cell lines respectively, and they represent the cell lines with comparatively low and high endogenous TrxR levels (Section 3.3.2). Two concentrations of siRNA (10 nM and 20 nM) were initially optimised and the transfection efficacy determined by Western blotting over a period of 7 days post-transfection. As shown in Figure 3.21, both concentrations of TrxR siRNA resulted in a reduction of TrxR protein expression in DAOY and SF188 cells during 7 days post-transfection. Cells transfected with 10 nM of siRNA had a maximal suppression of TrxR protein expression after 3 days of transfection. The decrease was about 67% for DAOY and 80% for SF188 cells, compared with untreated controls. When cells were transfected with 20 nM TrxR siRNA, a maximal inhibition of TrxR expression was also obtained at 3 days post-transfection, and an maximal inhibition of ~64% and ~69% was observed for DAOY and SF188 cells, respectively. From day 3 onwards, the expression of TrxR protein gradually increased to ~60% and ~73% of untreated controls at day 7 in DAOY and SF188 cells, respectively.

Collectively, data suggest that the optimal concentration of siRNA for efficient silencing of TrxR in DAOY and SF188 cells is 10 nM and the maximal inhibition is observed at 3 days post-transfection. Therefore, these optimal conditions were used for subsequent transfection experiments.

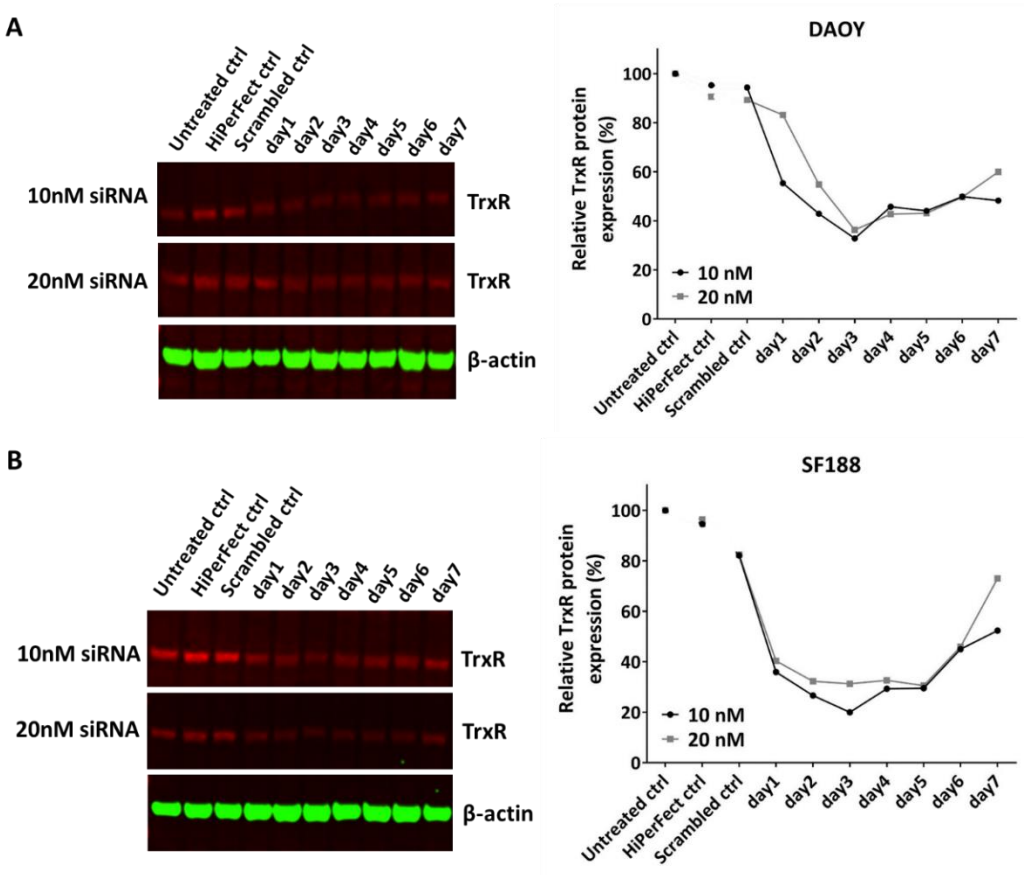



**Figure 3.21 Transient siRNA-mediated knockdown of TrxR in DAOY and SF188 cells.** (A) DAOY and (B) SF188 cells were transfected with 10 or 20 nM of TrxR siRNA and protein levels were measured with Western blotting over a period of 7 days post-transfection. The line charts (right panel) show relative expression level of the TrxR protein with β-actin as internal control. Experiments were conducted twice, with separate cell lysates from different passage numbers of cells. The representative blots are shown above (left panel). Abbreviations: ctrl, control.

### 3.3.5.2 The cytotoxicity of IQ10 on TrxR knockdown cells

To determine whether TrxR is an important, if not main, target of IQ10 a siRNA approach was used to knockdown TrxR expression in DAOY and SF188 cells. Three days post siRNA transfection, cells were treated with increasing concentrations of IQ10 for 48 h, and cytotoxicity determined by proliferation and clonogenic assays. Western blotting was used to monitor the TrxR knockdown efficiency during IQ10 treatment. As shown in Figure 3.22A, TrxR

siRNA effectively reduced ~52-65% and ~64-77% of endogenous TrxR protein expression at 3-5 days post-transfection in DAOY and SF188 cells, respectively, as compared with cells transfected with control siRNA. Such results verified that TrxR expression was inhibited by siRNA and allowed subsequent assessment of drug sensitivity on TrxR silenced cells.

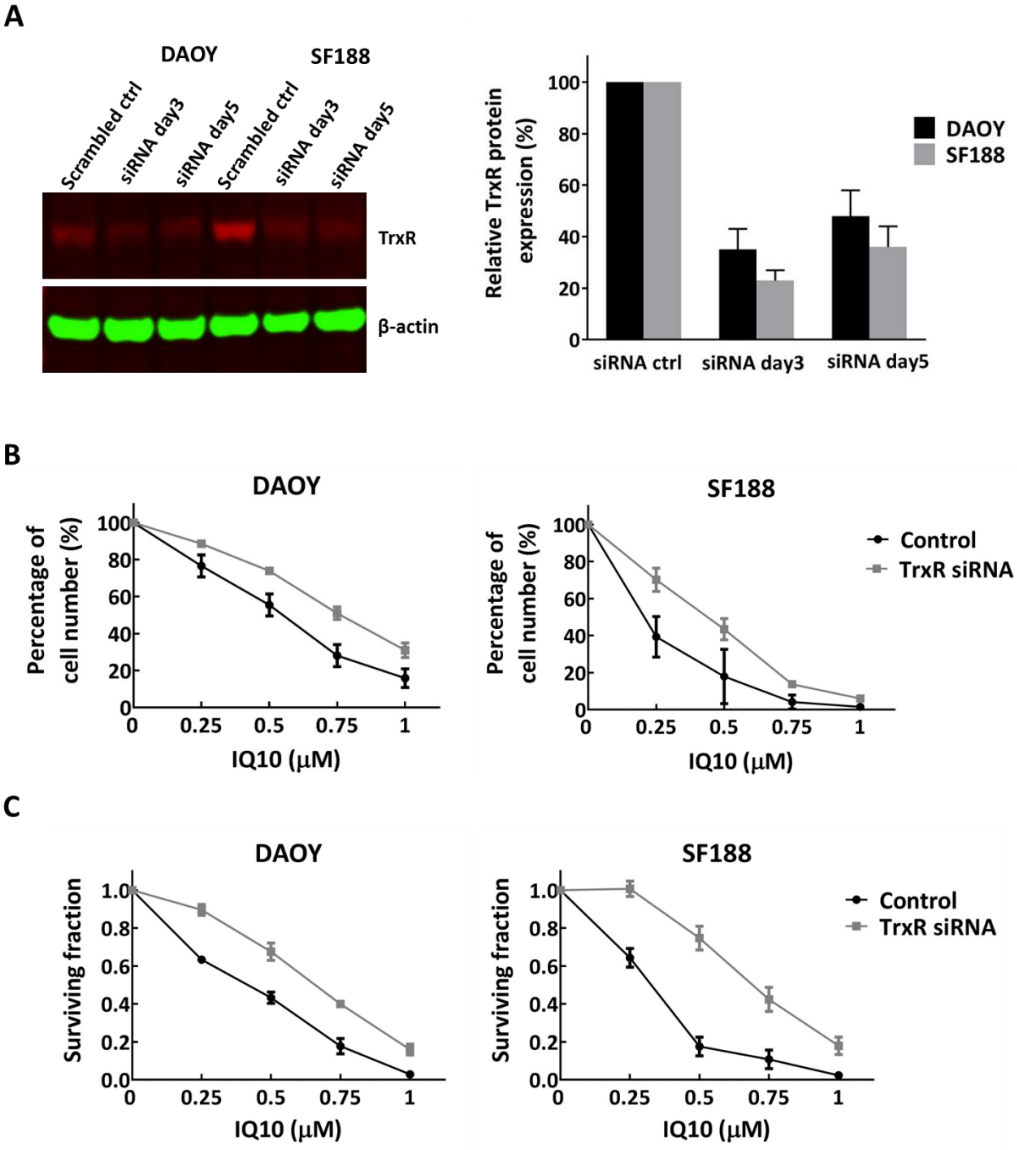



**Figure 3.22 The cytotoxicity of IQ10 on TrxR silenced DAOY and SF188 cells.** Cells were transiently transfected with TrxR siRNA or control scrambled siRNA (siRNA ctrl). (A) Cells were collected at 3 or 5 days post-transfection and subjected to Western blotting to assess the TrxR expression with β-actin as internal control. Data are expressed as percent of scrambled siRNA-treated control in the bar chart. Experiments were conducted twice, with separate cell lysates from different passage numbers of cells. The representative blots are shown above. (B) Cell proliferation and (C) clonogenic survival assays were conducted to assess the cytotoxicity of IQ10 in transfected cells treated with IQ10 for 48 h. Data represent the mean ± SD of three independent experiments, with each performed in triplicate. The PEs of cells were as follows: control DAOY-70±8%; siRNA DAOY-70±13%; control SF188-40±10%;

siRNA SF188-45±8%.

The cell proliferation and survival results (Figure 3.22B and C) show that TrxR silenced DAOY and SF188 cells were still sensitive to IQ10 but that there was a reduction of IQ10 cytotoxicity accompanied with a significant increase in IC50 values indicating the importance of TrxR as a drug target. The proliferation IC50 values of IQ10 on the TrxR silenced DAOY and SF188 cells were 0.75 ± 0.08 µM and 0.38 ± 0.04 µM, as compared with the IC50s of 0.49 ± 0.07 µM and 0.22 ± 0.04 µM for the parental cells. The clonogenic IC50s of IQ10 on the TrxR silenced DAOY and SF188 cells were 0.61 ± 0.06 µM and 0.68 ± 0.08 µM, as compared with the IC50s of 0.36 ± 0.02 µM and 0.31 ± 0.03 µM for the parental cells. As mentioned above, the increased IC50s in TrxR silenced cells indicate the importance of TrxR to IQ10 activity.

## 3.4 Discussions

Many anti-tumour agents, including MGd, auranofin, 1,3-bis-(2-chloro-ethyl)-1-nitrosourea (BCNU), cisplatin, curcumin, cyclophosphamide, and ATO, are TrxR inhibitors and have been previously assessed in brain cancers (Brachman et al., 2015a, Klein et al., 2017, Sordillo et al., 2015, Wang et al., 2017b, Ferrer-Font et al., 2017, Ghaffari et al., 2016, Kast, 2010). Specific inhibitors of the TrxR have also been developed, such as PX916 (Powis et al., 2006) and AW464 (Chew et al., 2008). More recently, Prof. Chris Moody's research group developed a class of small-molecule TrxR inhibitors IQs that have been shown to exhibit potent anti-tumour activity against several human cancer types, especially pancreatic cancers (Inman et al., 2014). However, no studies have been conducted to examine the anti-cancer activity of these novel IQs in brain cancer cells. Therefore, this chapter set out to examine the *in vitro* activity of one of the most potent IQs, IQ10, in various types of brain cancer cell line models and also investigate the potential mechanisms of action underlying its efficacy.

In order to test whether IQ10 could inhibit TrxR activity in brain cancer cells, the alterations of TrxR activity was first assessed in SF188, DAOY and UW228-3 cells after 4- and 48-h drug treatment using the insulin reduction assay. In a

previous study from Prof. Chris Moody's group, and their collaborators, IQs were found to be potent inhibitors of TrxR activity in pancreatic cancer cells. A dose-dependent inhibition of TrxR activity was observed for both IQ3 and IQ9 after 4-h drug treatment and the I50 values for TrxR inhibition were 0.15 and 0.08 μM for IQ3 and 9, respectively (Yan et al., 2009a). Similar with this study, current results showed that IQ10 significantly inhibited TrxR activity in a dose-dependent manner at both 4- and 48-h post-treatment in brain cancer cells and the TrxR activity was almost abolished by 1 μM of IQ10 treatment for 4 h in SF188 cells (~87% of TrxR inhibition). When comparing the results between 4 and 48 h, IQ10 tends to display a stronger TrxR inhibiting ability with a shorter incubation time of 4 h. This decreased inhibition of TrxR activity at the later time point might be explained by an increased compensation in cancer cells attempting to overcome the loss of TrxR function. In addition, the gradual degradation of IQ10 in the media during the prolonged incubation time might be another factor that contributes to the decreased potency. Therefore, treatment with 1 μM IQ10 for 4 h was set as the experimental condition for the subsequent drug-radiation combination experiments in Chapter 4. Auranofin, a well-known TrxR inhibitor, was used to compare the TrxR inhibition potency of IQ10. As expected, IQ10 exhibited almost equal potency to auranofin as inhibitors of TrxR in brain cancer cells. Moreover, IQ10 seemed to show similar inhibition potency across different brain cancer cells although varying endogenous TrxR activity was observed between them.

The expression patterns of Trx system proteins across a panel of five different brain cancer cell lines were initially screened before assessing the effect of IQ10 on protein expression. Semi-quantitative Western blotting results showed that TrxR, Trx and TxNIP were differentially expressed across five brain cancer cell lines. Paediatric GBM lines KNS42 and SF188 expressed a relatively higher level of TrxR, followed by UW228-3 and SNB19, and DAOY had the lowest level of TrxR. It is noteworthy that among SF188, DAOY and UW228-3 cells, the endogenous expression level of TrxR protein was consistent with the corresponding activity data, suggesting a positive

correlation between TrxR protein expression and activity. Trx expression was highest in KNS42 and lowest in SF188, and was similar across SNB19, DAOY and UW228-3. TxNIP expression also varied significantly between cells; UW228-3 had the highest level, while DAOY had an extremely low level, with protein bands hardly detectable. These observations suggest that the endogenous levels of Trx system proteins seem to be relevant to the characteristics of individual cell lines rather than cell types. Although the expression of individual members of Trx system has been previously examined in different brain cancer cells (Haas et al., 2018a, Zhang et al., 2017b, Ahmad et al., 2015), no studies have thus far assessed and compared the endogenous expression of all three members of Trx system proteins in such a wide range of brain cancer cells.

Previous studies have suggested that high levels of Trx/TrxR in cancer cells are associated with resistance to chemo and radiation therapy, while overexpression of TxNIP sensitises cancer cells to treatments (Haas et al., 2018b, Kahlos et al., 2001, Patwardhan et al., 2015). Thus the brain cancer cells with different endogenous levels of Trx system proteins might display different responses to drug and/or radiation treatments. For instance, KNS42 might be more resistant to the treatments than the other four brain cancer lines as it has the highest expression levels of TrxR and Trx and relatively low level of TxNIP, however, the effects of Trx system on anticancer drug resistance or radiation are complex and may depend on the tissue type (Haas et al., 2018a). The relationship between the efficacy of IQ10/radiation and endogenous levels of Trx system will be discussed in detail later.

The role of IQ10 in regulating expression of Trx system proteins was assessed in DAOY and UW228-3 cells. After 48 hours' treatment with varying concentrations of IQ10, there were no significant alterations of TrxR, Trx and TxNIP expression in either line. This is consistent with results from Yan et al. (2009a), which showed that there was no alteration in total TrxR protein levels following IQ3 treatment in pancreatic cancer cells. However, a dose-dependent decrease in the amount of free selenocysteine TrxR was observed

and treatment with either IQ1 or IQ2 induced a dose-dependent increase in oxidised Trx expression accompanied by a decrease in the reduced form (Yan et al., 2012). In cervical cancer cells, a TrxR inhibitor B5 (curcumin analogue) was shown to alter the expression levels of Trx and TrxR with concomitant accumulation of oxidised Trx. It has been suggested that the elevation of Trx/TrxR protein expression in cells may be an adaptive response for cells to cope with the increased cellular ROS produced during the process of drug treatment (Shao et al., 2015). Although current data show no alterations in the expression of Trx system proteins in brain cancer cells, further experiments might wish to assess the expression of free selenocysteine TrxR and oxidised/reduced Trx after IQ10 treatment. Taken together, results from the current study suggest that the TrxR inhibitor IQ10 did not alter TrxR expression, but significantly inhibited its functional activity in brain cancer cells. The decreased TrxR activity in cells may be attributed to the direct inhibition of the enzyme activity by IQ10 rather the indirect alteration of protein expression.

In order to investigate the *in vitro* cytotoxic effects of IQ10 on various brain cancer cells, cell growth and clonogenic assays were conducted by treating cells with varying concentrations of IQ10 for different time periods. TMZ, a standard chemotherapeutic treatment for brain tumours, was used to compare the activities and potencies of IQ10. TMZ showed a time- and dose-dependent anti-proliferative effect across all brain cancer cells with IC50s ranging between ~148-980 µM after 72 h treatment. In the previous studies, a similar range of IC50 values have been reported for TMZ, ranging from 194 to 1000 µM for SNB19, DAOY, KNS42 and SF188 cells (Ahmed et al., 2018, Zhou et al., 2011a, Gaspar et al., 2010), but the IC50 values of TMZ were not available in the literature for the MB cell line UW228-3.

TMZ resistance has frequently been related to the expression of MGMT. MGMT promoter status is responsible for the regulation of MGMT expression and its methylation has been associated with improved survival in GBM patients receiving TMZ treatment (Hegi et al., 2005). A number of *in vitro*

studies have reported that TMZ is more effective in MGMT promoter methylated cells, but MGMT is not the only molecular mechanism that accounts for the TMZ resistance as other repair mechanisms such as the mismatch repair system may also be implicated (Perazzoli et al., 2015). SNB19 and KNS42 cells contain a methylated MGMT promoter, whereas SF188, DAOY and UW228-3 cells harbour an unmethylated promoter (Gaspar et al., 2010, Festuccia et al., 2018, von Bueren et al., 2012, Faoro et al., 2011). The proliferation results showed that SF188, DAOY and UW228-3 cells were relatively sensitive to TMZ, with IC50 values between 140-190 µM after 72 h treatment. The remaining two cell lines (SNB19 and KNS42) were resistant to TMZ treatment, with IC50 values of >700 µM. There seems to be a reverse correlation between MGMT methylation and TMZ sensitivity, suggesting alternative mechanisms of resistance. Consistent with this finding, Gaspar et al. (2010) also identified that the paediatric GBM cell line KNS42 was resistant to TMZ despite an absence of MGMT expression.

TMZ is a DNA alkylating agent that is widely used for high-grade glioma treatment and has been shown to significantly improve patient survival. However, the increase in median survival for treatment with TMZ plus radiotherapy is only 2.5 months compared with radiotherapy alone in patients with newly diagnosed GBM (Stupp et al., 2005). TMZ is administered at high dose, and a prolonged treatment results in a series of side-effects, TMZ resistance and poor responsiveness to subsequent treatment, thus leading to recurrence in 60-75% of patients (Lee, 2017, Beier et al., 2011, Chamberlain, 2010). Additionally, repeated administration of TMZ is required due to its short half-life (1.8 h) in plasma and low solubility in physiological media (Newlands et al., 1992). Therefore, despite the survival benefit of TMZ, its therapeutic limitations highlight the need for novel chemotherapy/targeted therapy drugs that are more effective and safe.

In comparison to TMZ, IQ10 significantly suppressed the brain cancer cell growth with much lower IC50 values at the 72 h time point, ranging between ~0.2-2 µM. Apparently, IQ10 is much more potent than TMZ with respect to

inhibiting proliferation of brain cancer cells. The anti-proliferative effect of IQs has also been examined in pancreatic cancer cells by Yan et al. (2012), showing that IQs exhibited marked growth inhibitory activity with IC50 values in the low nanomolar range. In addition, selected IQs were also screened against the NCI-60 (National Cancer Institute-60) cancer cell line panel and were found to be particularly effective against colon, renal, and melanoma cancer cells. The similar findings from others and the current study suggest that IQs may have the ability to potently inhibit cell proliferation against a wide range of cancer types.

The comparison of estimated IC50 values showed that the five brain cancer cell lines had different sensitivities against IQ10. DAOY, UW228-3 and SF188 cells were comparatively more sensitive to IQ10 than SNB19 and KNS42 in respect to cell growth and clonogenic assays. The reason for such differential sensitivity of IQ10 is unclear. As mentioned above, the protein levels of TrxR varied significantly between cell lines: KNS42, SF188 and UW228-3 cells expressed a relatively higher level of TrxR, whilst SNB19 and DAOY had a lower level. The correlation between the expression level of TrxR and IQ10 IC50 in these 5 brain cancer cell lines were analysed using Spearman Rank Correlation. No association was found between the endogenous TrxR expression and IQ10 IC50 ($r^2$<0.001, *P*=0.995), suggesting that the sensitivity of brain cancer cells to the TrxR inhibitor IQ10, may not be directly related to the endogenous TrxR levels, however, the drug response may be cell type dependent. Consistent with our findings, a previous study indicates that high expression of TrxR has a complex impact that not necessarily linked to Trx function that nonetheless modulates drug-specific cytotoxic responses (Eriksson et al., 2009).

Given that IQ10 demonstrated potent anti-proliferative effects in brain cancer cells, it was decided to further assess the effect of IQ10 on clonogenic survival. As colony forming ability is an essential requirement for the clonogenic assay, a wide range of cell lines representing adult GBM (i.e. SNB19), paediatric GBM (i.e. SF188 and KNS42), MB (i.e. DAOY and UW228-3), and normal healthy

tissues (i.e. MRC5) were initially assessed for their PEs. PEs for SNB19, SF188, KNS42, DAOY, UW228-3, and MRC5 cells were 12%, 40%, 29%, 28%, 20-30%, and 31% in previous studies (Rutka et al., 1987, Chautard et al., 2010, Takeshita et al., 1987, Janss et al., 1998, Bobola et al., 2005, Mukherjee et al., 2005). PEs for these cell lines in the present study, i.e. 58 ± 9%, 50 ± 9%, 58 ± 6%, 55 ± 10%, 92 ± 4%, and 83 ± 8%, respectively, were all higher than those reported in the literature. The reasons for the increased PEs in the current study may be due to the optimised culture conditions including low cell passage number, optimised recipes of cell culture medium and source of serum, appropriate tissue culture flasks and colony formation time. In general, a higher PE would give more confidence that data would be representative of the behaviour and characteristics of the majority population of the cell line.

Following the measurement of PEs, clonogenic assays were performed to assess if IQ10 treatment had any effect on the ability of brain cancer and MRC5 cells to form colonies. The results showed a decrease in clonogenic survival across all cell lines indicating a cytotoxic rather than cytostatic mechanism of action. As with the growth assay, IQ10 was again much more potent than TMZ in terms of cell killing. When comparing the IC50 values between growth and clonogenic assays following a 48 h drug exposure, no significant difference in IC50 values obtained by the two methods was observed for IQ10 treatment, but a difference was revealed for TMZ. The IC50 values of TMZ in the clonogenic assay were ~3-20 fold lower than that obtained from growth assay; which is consistent with previous studies showing that IC50 values of TMZ for the survival inhibition were lower than that for the proliferation inhibition in GBM cell lines (Kohsaka et al., 2012, Sarowar, 2016). These findings indicate that the proliferation assays potentially underestimates the level of killing achieved by TMZ. Hence, the short term proliferation assays cannot replace the clonogenic assay in determining the IC values of a cytotoxic compound (Yadav et al., 2016). In certain cell types, such as leukaemias, lymphomas, and some solid tumours, apoptosis is the primary mode of cell death and cells rapidly undergo

apoptosis after toxic insult. While in other solid tumours, particularly carcinomas, cells do not immediately die after treatment, and apoptosis may not be the main mediator of cell killing. Therefore, short-term assays (e.g. trypan blue/propidium iodide exclusion and annexin V staining) measuring early functional changes would provide little information on the overall toxicity of treatment. It is important to conduct multiple assays that measure the viability/survival in both the short- and long-term (Woolston and Martin, 2011b).

It has been reported that certain TrxR inhibitors can selectively kill cancer cells but spare normal cells. For example, EF24, a molecule having structural similarity to curcumin, was able to selectively kill human gastric cancer cells but not normal cells. By inactivating TrxR activity and increasing intracellular ROS levels, EF24 induced lethal ER stress in gastric cancer cells (Zou et al., 2016). In order to investigate whether IQ10 could preferentially kill brain cancer cells, the cytotoxic effect of IQ10 on MRC5 fibroblasts was assessed using growth and clonogenic assays. The results demonstrated that IQ10 seemed to exhibit less toxicity in the fibroblasts than the majority of brain cancer cell lines tested, however, due to time limitations, the present study did not include a normal brain cell line (e.g. normal human astrocytes) to directly compare the drug sensitivity against the brain cancer cells. Future investigations are required to examine the cytotoxic effect of IQ10 in at least one healthy brain cell line.

Hypoxia is a distinct feature of malignant brain tumours and strongly linked to tumour progression, treatment resistance and poor outcomes (Cavazos and Brenner, 2016). Although numerous drugs that can target hypoxic cells have been developed and assessed in preclinical/clinical studies over the past 40 years, no hypoxia-selective bioreductive drugs have been approved for use in humans (Ahmadi et al., 2014). Therefore, the development of more effective hypoxia-selective drugs is urgently needed. As TrxR has been reported to be upregulated during hypoxia (Berggren et al., 1996) and IQ10 shares some structural similarity to a widely known hypoxia-selective drug EO9, it was

reasonable to assume that IQ10 might be more effective under hypoxic conditions. The results from growth and clonogenic assays demonstrated that IQ10 was equally effective in both normoxic and hypoxic cells, indicating that there is no increased hypoxia-induced drug sensitivity in brain cancer cells. The reasons for such results are unclear; it may be partially due to the levels of the enzymes that are involved in the reduction and activation of the IQ10. Therefore, the expression levels of Trx system proteins and several oxidoreductases were measured under both normoxic and hypoxic conditions with results discussed below. It is interesting to note, however, that although no increased hypoxic sensitisation was seen, equally no hypoxic resistance was observed – hypoxia has been shown to make a variety of chemotherapy agents, and radiotherapy, less effective i.e. hypoxia can induce resistance to cytotoxic therapies in cancer cells (Graham and Unger, 2018).

CA9 is a transmembrane protein that regulates pH in tumour cells under low oxygen conditions and contributes to cell proliferation and transformation (Logsdon et al., 2016). CA9 expression is primarily driven by HIF-1 activity, and it has been established as a promising therapeutic cancer target because it is not detected in most normal tissues, and its expression in tumour tissues often indicates hypoxic regions and correlates with advanced disease and poor treatment response (Oosterwijk, 2014, McDonald et al., 2012, Logsdon et al., 2018). CA9 inhibitors are either entering or are in clinical trials (e.g. clinical trial NCT02215850 and NCT03450018). In this study, inhibition of TrxR by IQ10 led to a significant decrease in CA9 expression in DAOY cells following exposure to hypoxia. This finding is of great interest as it indicates that Trx system may regulate hypoxia signalling through the HIF-CA9 axis. Future studies could therefore focus on HIF-1α signalling and the regulation of the downstream molecule CA9 through Trx system in brain cancer cells.

As shown in Section 3.3.2.2, IQ10 did not alter TrxR, Trx or TxNIP protein levels in DAOY or UW228-3 cells under normoxic conditions. Consistent with this result, no alterations of Trx system protein levels were observed under hypoxic conditions, suggesting that although IQ10 is a potent inhibitor of TrxR

enzyme activity, it does not alter TrxR protein levels under either normoxic or hypoxic conditions. Also, hypoxia alone did not affect the expression levels of Trx system proteins, but some alterations of Trx/TrxR expression under hypoxia have been reported in previous studies, in other cancer cell line models. Trx protein levels were increased in human lung cancer A549 cells during growth in 0.05% oxygen (Kim et al., 2003a) and also in human endothelial progenitor cells and umbilical vein endothelial cells cultured in 1% oxygen (Park et al., 2010). Naranjo-Suarez et al. (2012) showed that hypoxia (1% $O_2$) downregulated TrxR mRNA and protein levels in both EMT6 (mouse breast carcinoma) and DT (mouse embryo) cell lines. In contrast, TrxR was reported to be increased in human endothelial progenitor cells but not in umbilical vein endothelial cells under hypoxia (Park et al., 2010). Such conflicting data suggest that the expression of the Trx system under hypoxia may depend on the specific cell line, oxygen levels or how samples are processed.

The mechanism of action of the IQs has been proposed to involve metabolic reduction by cellular reductases, loss of a leaving group to generate a reactive electrophile resulting in alkylation of the selenocysteine residue in the active site of TrxR (Yan et al., 2009a). However, which reductases are involved to catalyse the initial reduction step of IQs are unclear and still remain to be elucidated. Dehn et al. (2006) have previously reported the development of an IQ, ES936 (IQ1), which exhibited its antitumour activity via inhibiting two-electron reductase NQO1 in pancreatic cancer cell lines. In addition, NQO2 was shown to be able to activate IQs in cell-free systems to inhibit TrxR activity (Yan et al., 2012). Several oxidoreductases such as NQO1 and cytochrome P450 are capable of reducing the indolequinone-based compound EO9 (Phillips et al., 2013). These findings suggest that the two electron reductases NQO1 and NQO2 and the one-electron reductase P450 may be involved in the reduction step of IQ10. Therefore, in order to better understand the mechanism of action of IQ10 against brain cancer cells, the expression levels of these three reductases were measured by Western blotting in DAOY and UW228-3 cells under both normoxic and hypoxic

conditions. The endogenous expression level of NQO1 was significantly lower, and the NQO2 expression was higher, in DAOY than in UW228-3, while the P450 expression was the same in the two cell lines. According to the clonogenic survival data, it is apparently that the sensitivity of DAOY cells to IQ10 is lower than that of UW228-3 cells, with ~1.6-fold difference in the IC50 values (0.40 ± 0.09 μM and 0.25 ± 0.00 μM respectively). These findings might support the possible correlation between cellular NQO1/NQO2 levels and responsiveness of brain cancer cells to IQ10 treatment; but more cell lines are required to further explore this correlation in the future experiments. The relationship between the activities of these reductases and sensitivity to certain chemotherapeutic drugs has been widely examined in a variety of cancer cell lines. Siegel et al. (2012) found a positive correlation between NQO1 catalytic activity/expression and quinones (e.g. MMC, β-lapachone and 17AAG) sensitivity in several different cancer cell lines. There also existed a strong correlation between cellular NQO2 activity and the responsiveness of the breast cancer cells to the chemotherapeutic drug CB1954 (5-(-aziridin-1-yl)-2,4-dinitrobenzamide) (Nolan et al., 2012). The cytotoxicity of tirapazamine was found to correlate strongly with P450 reductase activity, and the drug being most toxic in the breast cancer cell lines with the highest P450 activity (Patterson et al., 1995).

In both DAOY and UW228-3 cell lines, hypoxia alone did not affect the expression levels of the three reductases, which contradicts the report from Ahn et al. (2013), showing that hypoxia increased NQO1 expression in human colon and lung cancer cells. Following IQ10 treatment no changes in expression levels of the three reductases were observed, except that IQ10 decreased the NQO2 expression in DAOY cells in hypoxia but not in normoxia. At present, it is difficult to explain why only NQO2 was downregulated by IQ10 in DAOY cells. Future experiments should assess the changes in enzyme activities rather expression levels of these reductases and search for other possible molecular targets to better understand the mechanism of action of IQ10 (upstream activators and downstream signalling pathways).

3D culture systems provide cells with a suitable 'architecture' to grow and to develop into tissue-like structures that better mimic the microenvironment *in vivo* compared to the traditional 2D monolayer (Edmondson et al., 2014). A number of studies have found that cells cultured in 3D models are more resistant to anticancer drugs than 2D cultures (Loessner et al., 2010, Karlsson et al., 2012). Therefore, a 3D spheroid culture model was introduced in the present study to compare the efficacy of IQ10 between 2D and 3D cultures using two MB cell lines DAOY and UW228-3. Both lines successfully formed spheroids in the ULA 96-well plates and the morphologies of each cell line were similar to those reported by previous studies (Tenga et al., 2016, Ivanov et al., 2014a, Ivanov et al., 2015, Cockle et al., 2015), i.e. both cell lines formed round-type spheroids with well-defined outlines, but unexpectedly, an exponential growth pattern of spheroids did not occur, perhaps due to lack of growth factors and/or nutrients. The spheroid formation protocol used in this study may not be ideal and this could alter the findings. Further optimisation and updated methods to produce actively growing spheroids would be useful for future experiments.

The major differences noticed in the current study was that the UW228-3 cells formed larger and relatively loose spheroids whilst DAOY formed smaller and dense appearing spheroids. Although DAOY and UW228-3 are both MB cell lines, they presented different 3D morphology that might have affected treatment responses. A study using a panel of 25 breast cancer cell lines showed that cell lines from the same phenotype did not necessarily share the same 3D colony morphology (Kenny et al., 2007). The morphological appearance of 3D spheroids is primarily cell line dependent, however, the type of 3D model utilised may also affect cellular morphology (Edmondson et al., 2014).

To further study the influence of cancer cell microenvironment on drug response, the sensitivity of IQ10 between 2D and 3D spheroid cell culture models were compared using DAOY and UW228-3 cells. Before assessing the cytotoxicity of IQ10 in spheroids, the 2D colony formation ability of both cell

lines after disaggregation from spheroids were initially measured. The PEs of both cells lines extracted from spheroids were slightly lower than those obtained from the conventional 2D culture. Consistent with current work, a decreased PE from 3D culture as compared to 2D monolayer was also observed with MCF10A cells (Lin et al., 2009). The results from both Resazurin reduction and clonogenic assays demonstrated that IQ10 was less potent against both DAOY and UW228-3 cells grown as 3D spheroids in comparison to cells cultured in 2D conditions. Such altered drug sensitivities in 3D culture models have also been observed in a number of previous studies (Lovitt et al., 2015, Nirmalanandhan et al., 2010, Brajša et al., 2016, Horning et al., 2008). The differential drug sensitivity between the two models is likely to be driven by various factors, including proliferation, hypoxic microenvironment, the cell-matrix adhesions, cell-cell junctions and communication (Håkanson et al., 2010, Imamura et al., 2015a). It is possible that specific signals are initiated only in the 3D cell culture systems, which encompass the complexities of the *in vivo* tissue architecture. In addition, a differential drug up-take rate may exist between different culture models which might be another factor that affects drug sensitivity.

Using spheroids analysis in drug screening is an important step forward in investigating the impact of hypoxia on drug sensitivity and also hypoxic tumour biology. However, utilising spheroids can be a complicated approach to analyse effects on the hypoxic fraction of cells, as it is difficult to differentiate between the effects on the normoxic and hypoxic fractions. For example, effects on cell proliferation or survival in the hypoxic fraction of spheroids can be masked by the proliferation of the normoxic cells (Leek et al., 2016). Therefore, based on current technologies, it is clear that corresponding work is generally required in 2D culture with cells grown in both normoxia and hypoxia, to help validate results from 3D culture (Leek et al., 2016). This is one of the important reasons why the cytotoxicity of IQ10 on brain cancer cells was additionally examined in 2D hypoxic conditions in the current study. The 2D hypoxia data suggest that hypoxia does not affect the efficacy of IQ10, but

its potency decreased in 3D spheroids, indicating that hypoxia may be not a major factor that contributes to the decreased drug sensitivity in 3D spheroids in our case.

Numerous aspects of the microenvironment in 3D models have been widely studied, but very little is known for other systems, such as redox regulation. One study has reported that auranofin treatment did not cause any significant change in expression of either Trx or TrxR in MDA-MB-231 cells cultured in 2D, however, expression of the Trx was decreased while TrxR expression was increased when cells cultured in 3D spheroids, indicating that the cancer cell environment influences the expression of the Trx system upon auranofin treatment (Bhatia et al., 2016a). These changes in Trx system expression may have consequences for the development of drug resistance. Therefore, future experiments might wish to focus upon redox system regulation in 3D and how this affects the effectiveness of TrxR inhibitor IQ10 by measuring the gene/protein expression of Trx system upon IQ10 treatment of cells cultured in 3D spheroids, using real-time RT-PCR, Western blotting and immunocytochemistry.

To determine whether TrxR is the target for IQ10, cell growth and clonogenic assays were performed on TrxR knockdown cells. DAOY and SF188 cells were transiently transfected using TrxR siRNA; and the knockdown of TrxR confirmed by Western blotting. The current results showed that siRNA transfection reduced up to ~65%-77% of TrxR expression and the TrxR silenced cells became less sensitive to IQ10 treatment. The IC50 values of IQ10 in TrxR silenced cells were higher, by approximately 1.5-1.7 fold, than untransfected and siRNA scrambled cells. Such results suggest that the effect of IQ10 in brain cancer cells is due, at least in part, to functional inhibition of TrxR and that TrxR is an important target for IQ10. However, other potential targets and mechanisms may also be involved in IQ10's anticancer activity. In the current study, TrxR was not completely and permanently inhibited by siRNA, therefore it is unclear how residual TrxR activity might affect the cytotoxic effect of IQ10 in transfected cells. More robust models, perhaps

using shRNA or CRISPR systems, are required to further validate the siRNA results. In addition, it would be interesting to identify or predict other potential drug targets to further delineate the mechanism of action of IQ10 in the future by using some computational approaches (e.g. different kinds of public -omics data and drug property data) (Dai and Zhao, 2015).

## 3.5 Conclusions

1. Trx system proteins are differentially expressed across a variety of brain cancer cells. IQ10 treatment significantly inhibits TrxR activity but does not affect expression levels of Trx system proteins in brain cancer cells.
2. IQ10 is a very potent drug exhibiting single agent anti-proliferative and cytotoxic effects against a variety of brain cancer cells under both normoxic and hypoxic conditions in 2D *vs.* 3D systems. It is approximately 30-1000 fold more potent than TMZ, a common agent currently used to treat brain cancers.
3. The effect of IQ10 in brain cancer cells is due, in part, to functional inhibition of TrxR with TrxR being an important target for this compound.

# Chapter 4 Effects of the novel TrxR inhibitor IQ10 on the radioresponse of brain cancer cells

## 4.1 Introduction

### 4.1.1 Radiosensitisers in brain tumours

The finding that most GBMs and SHH MBs relapse either near or within the primary site after radiation therapy has attracted great interest in the development of radiosensitisers to prevent local recurrence (Bindra et al., 2017, Zapotocky et al., 2018), however decades of preclinical and clinical studies testing a wide range of novel therapeutics have failed to yield any novel and clinically applicable radiosensitisers (Chang et al., 2007). Research continues to develop radiosensitising agents for the treatment of patients with brain tumours with DNA repair inhibitors recently entering clinical trials, and represent potential potent agents for brain tumour radiosensitisation. The following sections will present recent progress in the use of small molecule DNA damage response inhibitors as brain tumour radiosensitisers, recent progress in targeting hypoxia and use of targeted agents for brain tumour radiosensitisation.

#### 4.1.1.1 DNA repair inhibitors

A primary mechanism through which radiotherapy kills tumour cells is by induction of single- and double-strand DNA breaks, which, if not repaired, induce cell death (Kelley et al., 2016). To combat DNA damage, cells have evolved a sophisticated network of DNA damage response systems (Goldstein and Kastan, 2015). DNA damage induced by radiation can be repaired through different DNA repair pathways such as base excision repair (BER), nucleotide excision repair (NER), homologous recombination (HR) and non-homologous end-joining (NHEJ) (Helleday et al., 2008, Curtin, 2012). HR and NHEJ are the two major repair pathways that deal with DNA double-strand breaks (DSBs). HR repair uses a sister chromatid to effect high-fidelity repair in S and G2 phases of the cell cycle; whereas NHEJ results in error-prone rejoining of chromosomes throughout the cell cycle but is most important during G1 phase (Jackson et al., 2019). Despite many attempts to find specific inhibitors of HR, there are very few in pre-clinical development, with most inhibiting

Rad51 (Lv et al., 2016, Chernikova et al., 2012). Recent studies have suggested that the Rad51 inhibitors, for example RI-1, may sensitise to alkylating agents (Berte et al., 2016) and radiotherapy (Balbous et al., 2016) specifically in malignant gliomas. NHEJ has been implicated as the main DSB repair pathway for radiation-induced damage as NHEJ mutants appear to be much more sensitive than HR mutants to killing by radiation (Chernikova et al., 2012). NHEJ has therefore emerged as a potentially viable target for tumour cell radiosensitisation. Goglia et al. (2015) identified a novel inhibitor of this pathway, mibefradil dihydrochloride, which was previously approved by the FDA for the treatment of hypertension. This drug has been repurposed in a phase I trial as a radiosensitiser in recurrent GBM (NCT02202993) and preliminary results suggest that mibefradil and radiotherapy can be safely co-administered with the potential to improve disease response (Lester-Coll et al., 2018).

Several key targets within the DNA damage response pathways have been the focus of activity for the development of radiosensitisers (Jackson et al., 2019). As a master regulator of DNA damage signalling, ataxia-telangiectasia mutated (ATM) kinase regulates a multitude of cell cycle checkpoint processes and plays a vital part in facilitating DNA repair (Tichy et al., 2010). Consistent with this, ATM pharmacological inhibition or genetic ablation renders tumour cells hypersensitive to irradiation (Bindra et al., 2017, Durant et al., 2018). For example, inhibition of ATM kinase by KU-55933 produced potent radiosensitisation of GBM cancer stem cells (CSCs) and effectively abrogated the enhanced DSB repair proficiency at 24 h post-irradiation (Carruthers et al., 2015a). Another ATM inhibitor AZ1390 was also reported to radiosensitise glioma cell lines *in vitro*, with p53 mutant cells generally being more radiosensitive than wild type. In *in vivo* patient-derived glioma models, AZ1390 in combination with radiation significantly induced tumour regressions and increased survival compared to irradiation alone. AZ1390 is now in early clinical development for use as a radiosensitiser in patients with

GBM and brain metastases from solid tumours (NCT03423628) (Durant et al., 2018).

Chemical inhibitors of ataxia telangiectasia and Rad 3 kinase (ATR) are less potent radiosensitisers than ATM targeting agents (Vendetti et al., 2017), but they have also shown exciting radiosensitising activity in a variety of preclinical models, including pancreatic cancer (Fokas et al., 2012) and GBM (Ahmed et al., 2015). A phase I clinical trial (UK PATRIOT) is currently evaluating the safety of the ATR inhibitor AZD6738, alone or in combination with palliative radiotherapy in patients with solid tumours (NCT02223923), but clinical studies in GBM are not currently in development (Dillon et al., 2017).

Checkpoint kinase (Chk) 1 and 2 are two major checkpoint protein kinases that are activated down-stream of ATM and ATR (Pabla et al., 2008). Chk1 kinase inhibitors amplify the cytotoxic effect of ionising radiation by primarily inhibiting S and G2 phase checkpoints while Chk2 kinase inhibitors mainly inhibit G1 arrest (Ree et al., 2004, Ashwell and Zabludoff, 2008). Multiple Chk1/2 inhibitors are in pre-clinical and early clinical development in a variety of tumours (Mohindra et al., 2012, Babiker et al., 2017). Non-cytotoxic concentrations of Chk1 inhibitor AZD7762 was shown to enhance the radiosensitivity of GBM cell lines in clonogenic assays and this effect was greater in p53 deficient cells (Mitchell et al., 2010). In xenograft models, AZD7762 significantly sensitised lung cancer brain metastases to radiotherapy (Rundle et al., 2017, Yang et al., 2011).

Wee1, like Chk1/2, is also a cell-cycle checkpoint kinase and a key regulator of DNA damage surveillance pathways (Tabayashi et al., 2016). In response to extrinsically induced DNA damage, cell division is halted by Wee1 to allow time for effective DNA repair (Do et al., 2013). Use of Wee1 inhibitors such as MK-1775 has been shown to radiosensitise GBM and diffuse intrinsic pontine glioma (DIPG) cells (Caretti et al., 2013, Sarcar et al., 2011). MK-1775 is currently the only Wee1 inhibitor that enters phase I/II clinical trials in

combination with chemotherapy and radiotherapy for the treatment of patients with GBM and DIPG (NCT01849146 and NCT01922076).

As a critical component in the BER pathway, the enzyme PARP is involved in the repair of DNA single strand breaks (SSBs), part of the sublethal damage produced in cells by ionising irradiation (Rouleau et al., 2010, Kelley et al., 2016). PARP inhibitors have recently emerged as potential radiosensitising agents (Corso and Bindra, 2016, Lesueur et al., 2018) and there is a significant body of pre-clinical data supporting the use of PARP inhibitors in combination with both radiotherapy and TMZ to increase treatment responses (Chalmers, 2010). PARP inhibitors including ABT-888 (veliparib) and AZD-2281 (olaparib) have been shown to cause *in vitro* and *in vivo* radiosensitisation of glioma (Kelley et al., 2016) and are currently being investigated in clinical phase I/II trials to assess their toxicity and efficacy in malignant gliomas (veliparib NCT03581292 and olaparib NCT03212742).

#### 4.1.1.2 Hypoxic radiosensitisers

Hypoxic tumour cells are usually 2-3 times more resistant to radiation than those with normal levels of oxygen (Brown and Wilson, 2004) thereby resulting in decreased efficacy of radiotherapy. The hypoxia-induced radioresistance has been demonstrated in most solid tumours including primary brain tumours and brain metastases (Mohindra et al., 2012). Hypoxic cells prevalent in the solid tumours can be selectively targeted by hypoxia-activated prodrugs (HAP) whose activation are limited to hypoxic tumour regions thus minimising the systemic side effects (Xu et al., 2017). The most extensively studied hypoxic radiation sensitisers in brain tumours were the HAP family of nitroimidazoles (Bindra et al., 2017). However, a relatively large number of trials evaluated nitroimidazole-derived compounds in gliomas without clinical benefit (Overgaard, 2007). This is mainly due to the long half-lives of these compounds in humans that result in greater toxicities, preventing the high doses necessary to cause sufficient tumour drug concentration for radiosensitisation (Mistry et al., 2017).

Quinones and their derivatives are the earliest developed HAPs (Zeng et al., 2018). EO9, an indolequinone bioreductive prodrug, has been used to selectively target hypoxic cells over normoxic cells in malignant gliomas. In a murine model of human GBM, a combined treatment of EO9 and radiation increased tumour doubling time by 8.5 days, more than twice the effect of EO9 or radiation alone (Burd et al., 2005, Mistry et al., 2017). The addition of EO9 to radiotherapy did not increase the normal tissue toxicity (Burd et al., 2005), suggesting that EO9 is a promising radiosensitiser that should be explored further. However, EO9 exhibits poor systemic pharmacokinetics, hindering evaluation in tumour types in which local-regional administration is not possible (Workman et al., 1992, Phillips et al., 2013).

N-oxides are promising HAPs as they can be selectively reduced to effective therapeutic agents in hypoxic tumour regions. The most common and clinically advanced N-oxide analogue prodrug is the tertiary amine-oxides banoxantrone (AQ4N), whose reductive compound AQ4 can compete with topoisomerase II for binding to double strand DNA subsequently leading to apoptosis and tumour cell death (Zeng et al., 2018). AQ4N has been shown to enhance the antitumour response to radiation, cisplatin, and other chemotherapeutics in tumour models *in vivo* (Williams et al., 2009a). A phase I clinical trial demonstrated that AQ4N effectively crossed the BBB and was activated selectively in hypoxic regions of solid tumours in patients with GBM (Albertella et al., 2008). Unfortunately, the development of this promising therapeutic has not progressed further than phase II trials. A phase II trial investigating the efficacy and safety of AQ4N in combination with radiotherapy and TMZ for GBM patients was started in 2006, but no results have been published (NCT00394628).

Hyperbaric oxygen ($HBO_2$) therapy is a treatment modality in which a patient breathes pure $O_2$ while exposed to increased atmospheric pressure (Thom, 2011). Previous experimental and clinical studies have indicated that $HBO_2$ therapy could enhance the therapeutic effect of radiotherapy due to the increased oxygen supply to hypoxic tumour cells (Yahara et al., 2017). Several

phase II trials in patients with HGG have demonstrated that conventional radiotherapy delivered immediately after $HBO_2$ with chemotherapy was safe and effective, although the combined therapy was complex and time-consuming (Beppu et al., 2003, Ogawa et al., 2012). In addition, $HBO_2$ therapy shows promising potential for the treatment and/or prevention of delayed radiation injury of the brain (Kohshi et al., 2013). The above observations suggest that $HBO_2$ may be an attractive approach that warrants further investigation.

#### 4.1.1.3 Targeted agents as radiosensitisers

Many molecularly targeted therapeutics have shown great promise as radiosensitisers through a variety of pathways (Linam and Yang, 2015). Bevacizumab, a recombinant antibody against the angiogenesis stimulator VEGF, has shown great promise as a radiosensitising agent in trials of patients with locally advanced cervical cancer (Schefter et al., 2014) and head and neck cancer (Fury et al., 2012). Although the mechanism of radiosensitisation is incompletely understood, it has been suggested that bevacizumab leads to a normalisation of the abnormal tumour vasculature, allowing for increased blood flow and improved oxygen delivery, which in turn enhances the effectiveness of radiotherapy (Winkler et al., 2004). However, in two randomised clinical trials, bevacizumab did not improve OS in patients with newly diagnosed GBM. PFS was prolonged but did not reach the prespecified improvement target (Chinot et al., 2014, Gilbert et al., 2014).

Recently EGFR has emerged as a highly attractive therapeutic target in GBM based on its high frequency of gene amplification (40-50%) and mutation (Pang et al., 2017, Reardon et al., 2014). Multiple preclinical models have demonstrated that inhibition of EGFR can increase radiosensitivity of malignant gliomas (Lammering et al., 2001, Krishnan et al., 2003), however, no evidence of improved survival was observed in early clinical trials of the EGFR/tyrosine kinase inhibitor gefitinib/erlotinib in patients with recurrent or newly diagnosed GBM (Lieberman et al., 2004, Uhm et al., 2004, Chakravarti et al., 2006). In a phase II trial, a combined treatment of bevacizumab,

erlotinib, TMZ, and radiotherapy appeared to be well tolerated and effective in improving PFS but the primary endpoint of improved OS was not achieved (Clarke et al., 2014).

### 4.1.2 Redox homeostasis modulators in radiotherapy

One of the major mechanisms of radiation-induced cell death is based on ROS-mediated oxidative DNA damage. A large number of studies have indicated that compounds regulating redox homeostasis can increase the radiosensitivity of cancer cells and may be used as an effective strategy to enhance tumour radioresponse.

#### 4.1.2.1 Oxidative stress modifiers

Cancer cells are frequently under higher oxidative stress compared with normal cells. Targeting oxidative stress may represent a unique approach to selectively enhance cancer cell killing while simultaneously reducing normal tissue cytotoxicity (Xu et al., 2013). With its unique mechanism of action, generating ROS through futile redox cycling, MGd has been shown to enhance radiation responses in both animal models and clinical trials (Mehta et al., 2002, Mehta et al., 2003, Miller et al., 1999). MGd appears to selectively concentrate in tumours to a greater extent than normal tissue, showing promise in phase I clinical trial for patients with GBM (Ford et al., 2007), however, in a later phase I/II trial, MGd in combination with radiotherapy and TMZ did not result in a significant survival benefit compared to historical control (Brachman et al., 2015a). Over the past 20 years, a class of redox-active manganese (Mn) porphyrins (MnPs) has been developed as mimics of SOD enzymes. They are potent anti-inflammatory agents that catalytically inactivate a range of ROS and interact with transcription factors (Gad et al., 2016). MnPs have shown the unique function of protecting normal tissues against late radiation damage while also radiosensitising tumours in preclinical GBM and head and neck cancer models (Ashcraft et al., 2015, Weitzel et al., 2015). Based on these promising results, the lead MnPs compound, MnBuOE has entered into a phase I/II trial in patients with newly diagnosed HGG (NCT02655601) (Bindra et al., 2017).

#### 4.1.2.2 Metabolism related redox homeostasis modulators

Malignant tumours are strongly dependent on glycolysis as a source of cellular metabolic energy (Seyfried et al., 2011). Enhanced glycolysis generally observed in cancer cells may be responsible for the radioresistance, partly by enhancing the repair of DNA damage (Bhatt et al., 2015). Among the chemotherapy drugs, 2-deoxy-D-glucose (2-DG) is an effective inhibitor of glycolysis, glucose metabolism and the production of ATP (Oladghaffari et al., 2017). It has been found that the glucose-deprivation induced by nontoxic doses of 2-DG led to concentration-dependent inhibition of cell proliferation and radiosensitisation in malignant glioma cells (Kalia et al., 2009). A combined treatment of 2-DG and 6-aminonicotinamide induced downregulation of γ-glutamylcysteine synthetase, GR and GPx, resulting in abrogation of GSH-mediated defence, in turn, led to an accumulation of ROS and increased radiosensitisation of both head and neck carcinoma and glioma cells (Sharma and Varshney, 2012). In addition, several investigations have suggested that 2-DG also enhances radiation-induced DNA, chromosomal, and cellular damage and acts as a radiosensitiser in other types of cancer cells, including lung carcinoma, breast cancer and oral squamous carcinoma (Pirayesh Islamian et al., 2017, Kawata et al., 2017, Oladghaffari et al., 2017, Bhardwaj et al., 2012). 2-DG and radiotherapy was safely used in clinical trials against GBM, and trial results from over 100 patients revealed a modest survival advantage with improvement in patient quality of life (Shah et al., 2019).

#### 4.1.2.3 Neutraceuticals

A number of mild pro-oxidant compounds derived from natural herbal medicines might increase the radiosensitivity by modulating the redox state of cancer cells to high pro-oxidant levels (Xu et al., 2013). Curcumin, a natural plant polyphenol derived from the dietary spice turmeric, possesses diverse pharmacologic effects including anti-inflammatory, antioxidant, antiproliferative and antiangiogenic activities (Anand et al., 2007). When combining with radiotherapy, curcumin has been shown to increase the

radiosensitivity of head and neck squamous cell carcinoma (HNSCC) cells via inhibiting TrxR activity (Tuttle et al., 2012). Additionally, a study in human gliomas has demonstrated that tetrahydrocurcumin (a major metabolite of curcumin) also exhibited promising radiosensitising potential both *in vitro* and *in vivo* (Zhang et al., 2018). Indeed, a large volume of evidence demonstrates that curcumin is a potent radiosensitiser of multiple malignancies as well as a radioprotector of normal tissues (reviewed in (Goel and Aggarwal, 2010, Verma, 2016)). So far, however, no clinical evidence of radiosensitisation was observed and further research is urgently needed to strength curcumin's major weakness of poor oral bioavailability (Verma, 2016).

Parthenolide is a naturally occurring sesquiterpene lactone, which can easily be extracted from herbal plant feverfew (*Tanacetum parthenium*), that exhibits excellent anti-inflammatory and anti-tumour effects, making it an attractive candidate for further studies and drug development (Mathema et al., 2012). Parthenolide was able to selectively enhance radiosensitivity of prostate cancer cells without injury to normal prostate epithelial cells *in vitro* by increasing ROS generation and decreasing antioxidant defence capacity through activation of NADPH oxidase (Sun et al., 2010). The radiosensitising and protective effects of parthenolide was further confirmed in mouse xenograft tumours (Xu et al., 2013, Morel et al., 2017).

Pharmacological ascorbate (vitamin C) has been proposed as a potential anti-cancer agent when combined with radiation and chemotherapy (Schoenfeld et al., 2017). At pharmacologically relevant doses (> 1 mM), ascorbate acts as a pro-oxidant, generating extracellular ascorbyl radicals that drive $H_2O_2$-mediated oxidative stress leading to intracellular free radical production and damage to macromolecules. Pharmacological ascorbate radiosensitised GBM primary cells to a much greater extent than astrocytes (Herst et al., 2012). In GBM xenografts, ascorbate combined with radio-chemotherapy significantly increased OS, as compared to radio-chemotherapy alone. A phase I clinical trial demonstrated that pharmacological ascorbate was safe, tolerable, and potentially efficacious in combination with radio-chemotherapy in GBM (NCT

01752491) (Schoenfeld et al., 2017). A variety of other neutraceuticals are also reported to enhance the radiosensitivity of tumour cells by modulating redox homeostasis, including ferulic acid, isoliquiritigenin, tinospora cordifolia, resveratrol and piperine (Zhang and Martin, 2014).

### 4.1.3 Radioresponse of cells in 3D culture

The cellular responses to ionising radiation have predominantly been measured in 2D monolayer cultures. Although convenient for biochemical analysis, it is not always reflective of the *in vivo* cellular environment and such studies may not represent the true nature of radiation-induced responses (Sowa et al., 2010). In many studies, an enhanced cancer cell resistance to radiotherapy is sometimes observed in 3D cultured cells (Lin et al., 2009). 3D culture of human HNSCC and lung carcinoma cells has been shown to promote radioresistance compared with 2D culture, accompanied with reduced numbers of DNA DSBs and lethal chromosome aberrations (Storch et al., 2010b). Long-term culture of human mammary epithelial cells (MEC) in 3D was shown to offer a protective effect on cell survival after irradiation and the likely mechanism underlying the differential radiosensitivity observed in 3D structures versus 2D monolayers was the decreased amount of radiation-induced apoptosis (Sowa et al., 2010). In contrast, Lin et al. (2009) found no significant differences in the radioresponses of human MEC MCF10A cells in 2D or 3D cultures. Only very few studies have reported alterations of radioresponse between 2D and 3D cultures in brain cancer cells. One study with 3 patient-derived GBM lines demonstrated no difference in radiation sensitivity between 2D and 3D cultures, as measured by clonogenic survival assay (Gomez-Roman et al., 2017). Recently, a study conducted in 3 human bladder cancer cell lines reported that the difference in radiosensitivity between 2D and 3D culture systems was highly dependent on the cell line (Bodgi et al., 2019).

### 4.1.4 Hypotheses and Aims

#### 4.1.4.1 Hypotheses

1. The intrinsic radiosensitivity of brain cancer cells varies between different lines.
2. Brain cancer cells cultured in hypoxic or 3D conditions are more resistant to radiation, as compared to cells grown in 2D normoxic conditions.
3. The TrxR inhibitor IQ10 radiosensitises brain cancer cells with the drug being more effective under 3D and hypoxic conditions.
4. Increased ROS generation and subsequent oxidative DNA damage are mechanisms associated with IQ10-induced radiosensitisation.

#### 4.1.4.2 Aims

1. Assess the intrinsic radioresponse of different brain cancer cell lines.
2. Assess and compare the radiation responses of brain cancer cells in normoxic *vs.* hypoxic conditions and also in 3D *vs.* 2D cultures.
3. Investigate the *in vitro* radiosensitising effects of the novel TrxR inhibitor IQ10 on brain tumour cells in normoxic *vs.* hypoxic conditions and also in 3D *vs.* 2D cultures.
4. Investigate the potential mechanisms underlying the radiosensitising effect of IQ10 by measuring the intracellular ROS levels and quantifying DNA damage.

## 4.2 Methods

### 4.2.1 Cell irradiation

Subconfluent cells or 4-day old spheroids were irradiated using an Xstrahl RS225 cabinet at room temperature with 195 kV and 10 mA x-rays at a dose rate of 0.87 Gy/min. The cabinet was fitted with a 0.5 mm copper filter and used at a 48.4 cm focus-to-skin distance. X-ray irradiation was carried out at a single dose of 2, 4, 6 or 8 Gy. Sham irradiated cells were used as controls. Dosimetry was routinely checked by Radiotherapy physicist in the Department of Radiotherapy Physics, Nottingham University Hospitals NHS trust, City

Hospital campus. Following irradiation cells or spheroids were immediately trypsinised and plated for clonogenic survival assay as described in Section 3.2.4 and 3.2.8.

When investigating the effect of hypoxia on radioresponse, cells were seeded into T25cm$^2$ tissue culture flasks with plug-seal caps and allowed to attach overnight. Cells were then transferred into a hypoxic incubator (37°C, 1% $O_2$, 5% $CO_2$) and incubated under hypoxia for 48 h with the caps unsealed. A longer period of incubation time was applied here to ensure that adequate levels of intracellular hypoxia were reached prior to irradiation. Afterwards, the flasks were immediately sealed once the hypoxic incubator was opened, and cells immediately irradiated then plated for clonogenic survival as discussed above. The caps of flasks were kept sealed during the irradiation procedure in order to avoid reoxygenation which might influence results. Control flasks were sham irradiated.

### 4.2.2 Drug-radiation combination

The effect of IQ10 on radiosensitivity of brain cancer cells was assessed by clonogenic survival assay under both normoxic and hypoxic conditions and in both 2D and 3D spheroid cultures.

#### 4.2.2.1 Drug-radiation combination in 2D culture

Cells were seeded at a density of 1x10$^5$ cells/ml in T25cm$^2$ tissue culture flasks for 24 h to attach. The cells were pretreated with 1 µM of IQ10 (maximal inhibition effects of TrxR activity was observed at this concentration (Section 3.3.2.1)) or relative DMSO control for 4 h followed by mock or 2-8 Gy irradiation in a single fraction. Directly after irradiation, cells were trypsinised and plated for clonogenic survival as described in Section 3.2.4. When investigating the effect of hypoxia in these conditions, cells were treated with clonogenic IC50 dose of IQ10 under hypoxia (1% $O_2$) for 48 h prior to irradiation and plated for clonogenic survivals as discussed above.

#### 4.2.2.2 Drug-radiation combination in 3D spheroid culture

To observe the effect of IQ10 on radiosensitivity of cells in 3D spheroid culture model, cells were seeded in ULA 96-well plates and left in the incubator for 4 days to form mature spheroids (spheroid formation method and cell seeding number are described in Section 3.2.8.1 and 3.3.4.1, respectively). For each condition, at least 12 spheroids were prepared. 4-day-old spheroids were pretreated with 1 μM of IQ10 or relative DMSO for 4 h (a 4-h drug exposure time was able to allow drug penetration through spheroids, as revealed in Section 3.3.4.3) and irradiated with a single dose of 2, 4, 6, or 8 Gy (cells with sham irradiation were set as 0 Gy). Following irradiation, cells were disaggregated from spheroids immediately and plated for assessment of clonogenicity using the conventional clonogenic survival assay as described in Section 3.2.8. 2D controls were plated one day before drug treatment and subjected to 1 μM IQ10 or DMSO treatment for 4 h followed by irradiation at the same time as those in 3D spheroids. Following irradiation, 2D control cells were immediately trypsinised and plated for clonogenic assay.

### 4.2.3 TrxR knockdown and irradiation

DAOY and SF188 cells were transfected with 10 nM siRNA, to transiently knockdown expression of TrxR, using the protocol described in Section 3.2.7. After 48 h of transfection, cells were plated in T25cm$^2$ flasks at a density of 1 x $10^5$ cells/ml and cultured overnight to allow adherence. Cells were then irradiated with single doses of 2, 4, 6, or 8 Gy (cells with sham irradiation were set as 0 Gy) and subjected to clonogenic assay as described in Section 3.2.4. Cells with mock transfection and mock irradiations were set as control.

### 4.2.4 Measurement of intracellular ROS levels

The cell-permeable dye 2',7'-dichlorodihydrofluorescein diacetate ($H_2$DCFDA) (Invitrogen) was used to detect intracellular ROS levels in DAOY and UW228-3 cells. $H_2$DCFDA is an oxidation-sensitive fluorescent probe which passively diffuses into cells and is retained in the cells after cleavage by esterases. Upon oxidation by ROS, the nonfluorescent $H_2$DCFDA is converted to the highly

fluorescent 2', 7'-dichlorofluorescein (Vaughn and Deshmukh, 2008). Subconfluent cells were treated with various concentrations of IQ10 or auranofin (a positive control and comparator) for 4 h either alone or with subsequent 1 mM $H_2O_2$ exposure (ROS positive control) for 1 h. Cells treated with DMSO, at the same dilution ratio as IQ10 in complete cell culture medium, were set as negative controls. After treatment, cells were washed in PBS and stained with 1 µM $H_2$DCF-DA in fresh medium at 37°C for 30 min. Cells were then harvested and resuspended in PBS at a concentration of 1 x $10^6$ cells/ml. The ROS-dependent fluorescence intensity was immediately measured by a MACSquant flow cytometer (Miltenyi Biotec). A gate was set to include only healthy living cells in the analysis and gate out the dead cells. Data were analysed using FlowJo7.6.1 software (TreeStar) to obtain the median fluorescence intensity (MFI) of each group representing the amount of intracellular ROS generation.

### 4.2.5 Immunofluorescence

To assess DNA DSB damage following treatment, immunofluorescent staining of γH2AX foci was used. Briefly, cells were plated on Biocoat™ coverslips (Corning), allowed to attach overnight and exposed to 1 µM IQ10, or an equivalent concentration of DMSO as in the drug treatment group, for 4 h and irradiated with 2 Gy or sham irradiated. 30 min after irradiation, cells were fixed in 4% paraformaldehyde/PBS for 30 min then permeabilised and blocked in 0.3% Triton X-100 with 3% bovine serum albumin (BSA) in PBS for another 30 min at room temperature. Afterwards, cells were stained with primary anti-γ$H_2$AX antibody (1:500 dilution, Millipore) overnight at 4˚C followed by incubation with Alexa 647-conjugated goat anti-mouse secondary antibody (1:200 dilution, Abcam). Nuclei were counterstained with Vectashield containing DAPI (Vector). Imaging was performed at 63 x magnification on a confocal microscope (Leica TCS SPE). The number of γ$H_2$AX foci was counted using ImageJ with at least 100 nuclei analysed for each condition. Nuclei which exhibited confluent staining for γH2AX were assumed to be in S phase and were excluded from analysis (Carruthers et al., 2015b).

### 4.2.6 Statistical analysis

Statistical analysis was performed using SPSS 24.0 software. All experiments were repeated three times unless otherwise stated. Data points were expressed as the mean ± SD and analysed using the Student's *t*-test (for comparing 2 groups) and one-way ANOVA test (when comparing > 2 groups). For radiation survival analysis, the SF of radiation alone was calculated as number of colonies / (number of cells plated × PE); the SF of radiation plus IQ10 was corrected for independent cytotoxic effects of IQ10 and calculated as number of colonies / (number of cells plated × PE x SF of IQ10 alone). Survival curves were fitted to the L-Q model using the open source survival calculation programme CS-CAL developed by the German Cancer Research Centre (http://angiogenesis.dkfz.de/oncoexpress/software/cs-cal/). The mean values of parameters α, β, α/β, and SF2 (surviving fraction at 2 Gy) were calculated from the fitted curves. Sensitizer enhancement ratio (SER) was calculated as the radiation dose needed for radiation alone divided by the dose needed for IQ10 plus radiation to yield a SF of 1%. The oxygen enhancement ratio (OER) refers to the enhancement of a therapeutic or detrimental effect of ionising radiation due to the presence of oxygen, and was quantitatively defined as the ratio of doses required to achieve a SF of 10% for hypoxic and normoxic cells (Pasciak et al., 2016). P values < 0.05 were considered statistically significant.

## 4.3 Results

### 4.3.1 Intrinsic radiosensitivity of brain cancer cell lines

#### 4.3.1.1 2D normoxia and hypoxia

To evaluate the intrinsic radiosensitivity, clonogenic survival assays were performed on a panel of five brain cancer cell lines cultured in 2D monolayers under normoxic conditions. The radiation survival curves fitted by the L-Q model for each cell line are plotted in

Figure 4.1 and the radiobiologic parameters are listed in Table 4.1.

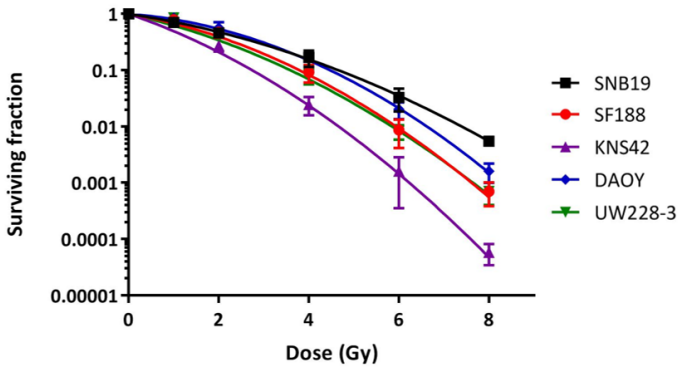



**Figure 4.1 Survival curves of brain cancer cells after single dose irradiation.** Brain cancer cells SNB19, SF188, KNS42, DAOY and UW228-3 were irradiated with single doses of 1, 2, 4, 6 or 8 Gy and sham irradiated cells (0 Gy) were set as controls. Data represent the mean SF ± SD of at least three independent experiments, with each experiment containing six parallel data sets. PEs of individual cell lines were as follows: SNB19–69±11%; SF188–70±10%; KNS42–63±7%; DAOY–65±13%; UW228-3–85±9%.

Results show that radiation exposure causes a dose-dependent cytotoxic effect on all cell lines and that radiosensitivity varies significantly between cell lines. SNB19 and DAOY were the most radioresistant, with SF2 values of 0.48 ± 0.05 and 0.57 ± 0.09, respectively. SF188 and UW228-3 were moderately resistant with SF2 values of 0.46 ± 0.08 and 0.35 ± 0.07, respectively, whereas KNS42 was highly radiosensitive with an SF2 of 0.18 ± 0.02.

**Table 4.1 Radiobiologic parameters of different brain cancer cell lines in 2D cultures.**

| Cell line | α ($Gy^{-1}$) | β ($Gy^{-2}$) | α/β (Gy) | SF2 |
|---|---|---|---|---|
| **SNB19** | 0.28±0.06 | 0.06±0.01 | 4.53±1.31 | 0.48±0.05 |
| **SF188** | 0.19±0.11 | 0.10±0.02 | 2.03±1.47 | 0.46±0.08 |
| **KNS42** | 0.72±0.08 | 0.07±0.01 | 11.00±3.85 | 0.18±0.02 |
| **DAOY** | 0.12±0.04 | 0.09±0.02 | 1.54±0.89 | 0.57±0.09 |
| **UW228-3** | 0.39±0.14 | 0.07±0.02 | 6.87±3.37 | 0.35±0.07 |

Parameters were calculated from clonogenic data fitted to a LQ model. Data represent the mean ± SD of at least three independent experiments. Abbreviation: SF2, surviving fraction at 2Gy.

The impact of hypoxic exposure on cellular radiosensitivity was evaluated using DAOY and UW228-3 cells. Cells were incubated under normoxia or hypoxia (1% $O_2$) for 48 h before irradiation. As expected, both cells lines became more resistant to radiation under hypoxic conditions compared to that of normoxic culture conditions (Figure 4.2), with SF2 values increasing

from 0.59 ± 0.10 to 0.69 ± 0.08 for DAOY (*P*=0.24) and from 0.35 ± 0.03 to 0.56 ± 0.12 (*P*=0.04) for UW228-3.

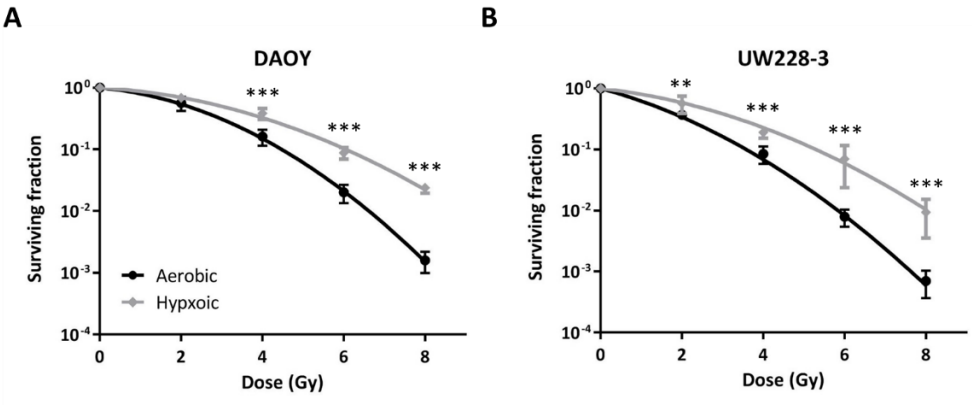



**Figure 4.2 Radiosensitivity of brain cancer cells under aerobic or hypoxic conditions.** Cell survival curves for (A) DAOY and (B) UW228-3 were fitted by the L-Q model. PEs for DAOY and UW228-3 cells cultured in normoxia were 76% and 93% (±2% and 3%), respectively; PEs in hypoxia were 65% and 86% (±12% and 8%), respectively. Data represent the mean SF ± SD of at least three independent experiments, with each experiment containing six parallel data sets, which are analysed using the Student's *t*-test. ** *P*<0.01, *** *P*<0.001 hypoxic cells *vs.* normoxic control cells.

The dose required to achieve a 1 log cell kill (SF=0.1) in hypoxia was 6.0 and 5.3 Gy in DAOY and UW228-3 cells respectively, while under aerobic conditions the same effect was observed at 4.4 and 3.5 Gy. The mean OERs (at a SF of 0.1) were 1.36 ± 0.03 and 1.51 ± 0.21 for DAOY and UW228-3 cells, respectively. These values were lower than a previous report which suggests that the OERs of x-rays are usually between 2.5 and 3.5 at irradiation doses of 0-30 Gy (Hall and Giaccia., 2012), but the significantly increased SFs of the hypoxic cells in this study still suggest that exposure to moderate hypoxia (1%) increases radioresistance of brain cancer cells.

#### 4.3.1.2 3D spheroids

Spheroid cultures have, given the impact of hypoxia on the efficacy of radiation response, been a highly useful model for understanding these tumour-microenvironmental relationships. Clonogenic survival assays were performed to compare the effect of 2D *vs.* 3D cultures on radiation responses of DAOY and UW228-3 cells. PEs for both cell lines were slightly lower in spheroids than from conventional 2D cultures (detailed in Section 3.3.4). As shown in Figure 4.3, both DAOY and UW228-3 cells in 3D spheroids were,

somewhat unexpectedly, significantly more sensitive to radiation than cells grown in 2D culture and this effect became more obvious as the irradiation dose increased.

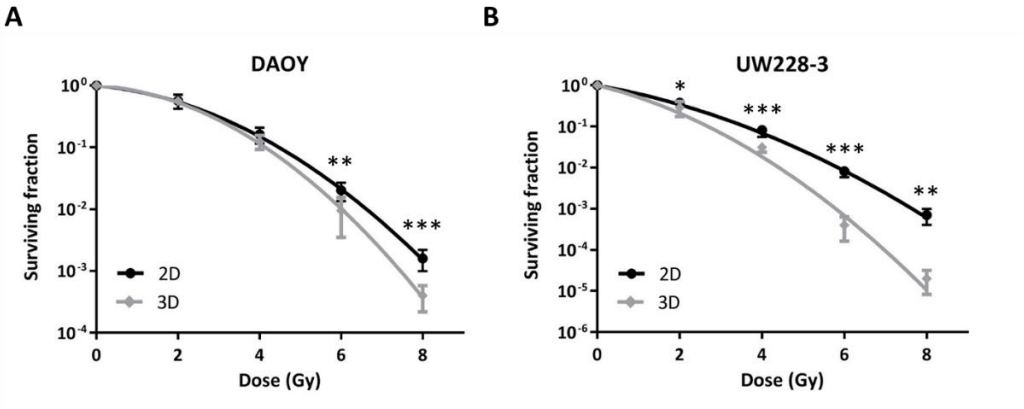



**Figure 4.3 Radiation response of DAOY (A) and UW228-3 (B) in 2D and 3D spheroid culture systems.** PEs for DAOY and UW228-3 cells cultured in 2D were 69% and 86% (± 4% and 1%), respectively; PEs for spheroids were 59% and 61% (± 5% and 15%), respectively. Data represent the mean SF ± SD of at least three independent experiments, with each experiment containing six parallel data sets, which are analysed using the Student's *t*-test. **P*<0.05, ***P*<0.01, ****P*<0.001 2D *vs.* 3D.

The SF2s for DAOY and UW228-3 spheroids were 0.56 ± 0.05 and 0.30 ± 0.06, respectively, which were slightly lower than the values of 0.57 ± 0.08 and 0.34 ± 0.06 in 2D cultures. When comparing the radiosensitivity between spheroids, UW228-3 was more sensitive to radiation than DAOY (SF2s of UW228-3 *vs.* DAOY; 0.30 ± 0.06 *vs.* 0.56 ± 0.05; *P*=0.0008), which is consistent with the data from 2D cultures as shown above.

### 4.3.2 Effect of IQ10 on radiosensitivity of brain cancer cells

#### 4.3.2.1 IQ10 radiosensitisation of brain cancer cells cultured in 2D aerobic conditions.

The radiosensitising effects of IQ10 were investigated, using the clonogenic survival assay, across a panel of 4 brain cancer cell lines using 2D culture. Cancer cells were treated with 1 µM of IQ10 for 4 h and subsequently exposed to various radiation doses under aerobic conditions. As shown in Figure 4.4, IQ10 substantially increased radiosensitivity in all but KNS42 cells with the radiosensitising effect most pronounced in UW228-3 cells.

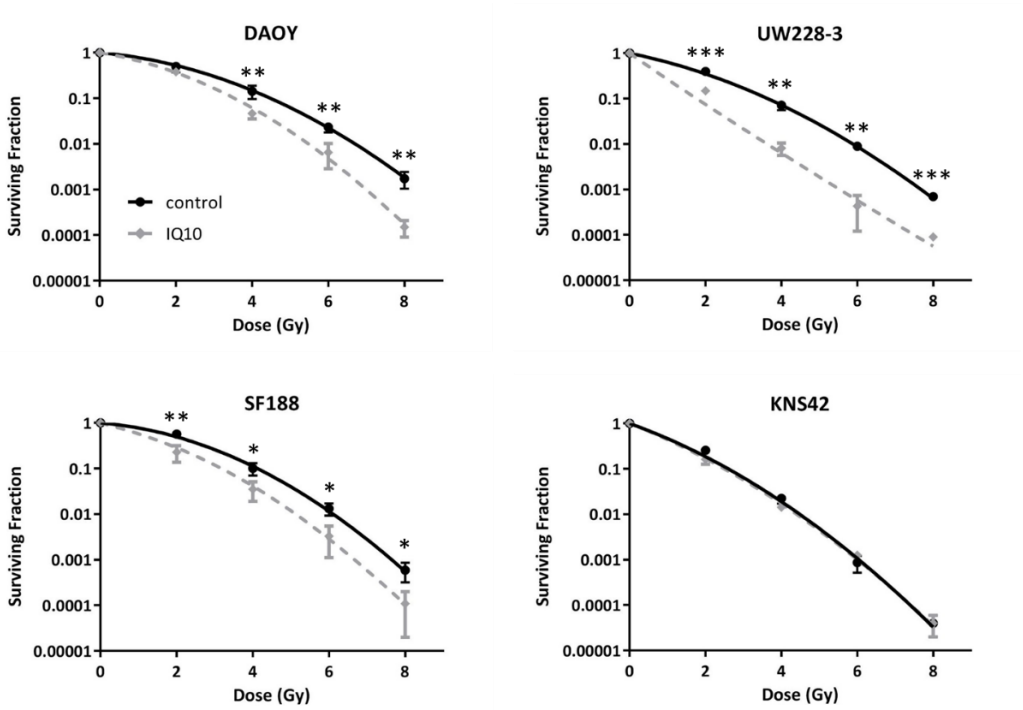



**Figure 4.4 Effects of IQ10 on radiosensitivity of brain cancer cells in 2D culture.** Linear quadratic survival curves compared the effects of IQ10 plus radiation versus radiation alone on DAOY, UW228-3, SF188 and KNS42 cells. PEs for DAOY, UW228-3, SF188 and KNS42 cells were 63% (±14%), 79% (±16%), 81% (±2%) and 64% (±5%), respectively. Data represent the mean SF ± SD of at least three independent experiments, with each experiment containing six parallel data sets, which are analysed using the Student's *t*-test. **P*< 0.05, ***P*< 0.01 and ****P*< 0.001 control *vs.* IQ10.

In addition, the SF2 values of DAOY, UW228-3 and SF188 cells were significantly reduced by IQ10, further confirming the radiosensitising effect of IQ10 (*P*=0.017, *P*=0.001, and *P*=0.048, respectively). Mean SF2 values for DAOY, UW228-3, and SF188 control cells were 0.50 ± 0.05, 0.35 ± 0.05, and 0.50 ± 0.05, respectively, compared to 0.35 ± 0.07, 0.07 ± 0.03, and 0.29 ± 0.12 for IQ10 treated cells. The mean SERs of IQ10 at 1% survival ($SER_{0.01}$) were 1.25 ± 0.03, 1.68 ± 0.25, 1.22 ± 0.04, and 1.02 ± 0.02 for DAOY, UW228-3, SF188 and KNS42 cells, respectively (Table 4.2). Other radiobiologic parameters including α, β, and α/β ratios are summarised in Table 4.2.

**Table 4.2 Radiobiologic parameters of brain cancer cells treated with IQ10 and/or radiation in 2D culture.**

| Cell line | α ($Gy^{-1}$) | β ($Gy^{-2}$) | α/β (Gy) | SF2 | $SER_{0.01}$ |
|---|---|---|---|---|---|
| DAOY | | | | | |
| IR alone | 0.21±0.07 | 0.07±0.01 | 3.01±1.28 | 0.50±0.05 | 1.25±0.03 |
| IR+IQ10 | 0.34±0.14 | 0.10±0.02 | 3.81±2.09 | 0.35±0.07 | |
| *t* test | *P*=0.142 | *P*=0.059 | *P*=0.535 | ***P*=0.017** | |
| UW228-3 | | | | | |
| IR alone | 0.40±0.10 | 0.07±0.01 | 6.58±3.53 | 0.35±0.05 | 1.68±0.25 |
| IR+IQ10 | 1.36±0.28 | 0.00±0.00 | 548.84±65.54 | 0.07±0.03 | |
| *t* test | ***P*=0.005** | ***P*=0.002** | ***P*<0.001** | ***P*=0.001** | |
| SF188 | | | | | |
| IR alone | 0.15±0.05 | 0.10±0.00 | 1.56±0.50 | 0.50±0.05 | 1.22±0.04 |
| IR+IQ10 | 0.48±0.27 | 0.08±0.04 | 8.22±8.39 | 0.29±0.12 | |
| *t* test | *P*=0.111 | *P*=0.552 | *P*=0.242 | ***P*=0.048** | |
| KNS42 | | | | | |
| IR alone | 0.69±0.06 | 0.08±0.00 | 9.25±1.44 | 0.19±0.02 | 1.02±0.02 |
| IR+IQ10 | 0.76±0.05 | 0.07±0.01 | 11.80±1.97 | 0.17±0.01 | |
| *t* test | *P*=0.212 | *P*=0.122 | *P*=0.143 | *P*=0.265 | |

Parameters were calculated from clonogenic data fitted to a linear quadratic model. Data represent the mean ± SD of at least three independent experiments. Statistical significance was determined by Student's *t*-test. The *P*-values are bold where they are ≤ 0.05. Abbreviations: IR, irradiation; $SER_{0.01}$, sensitiser enhancement ratio at 1% survival; SF2, surviving fraction at 2Gy.

α and β are experimentally derived parameters for the linear and quadratic terms of L-Q formula, respectively. The initial slope of cell survival curves and the effectiveness at low doses is determined by α, while β represents the increasing contribution from cumulative damage. The α/β ratio represents the dose at which the two terms contribute equally to the total effect (Franken et al., 2013). IQ10 treatment significantly increased the α-value while decreased the β-value with cell line UW228-3. Increase of the α-value and decrease of the β-value consequently raised the α/β ratio, indicating the efficacy of IQ10-induced radiosensitisation. In contrast, these parameters were not significantly altered in any other line, suggesting a smaller or insignificant radiosensitising effect of IQ10. Taken together, IQ10 treatment significantly enhanced in most cases the radiosensitivity of brain cancer cells cultured in 2D aerobic conditions.

#### 4.3.2.2 IQ10 does not radiosensitise hypoxic cancer cells

In order to examine whether IQ10 could enhance radiosensitivity of hypoxic DAOY or UW228-3's each cell line was treated with the clonogenic IC50 dose of IQ10 and incubated under aerobic or hypoxic conditions for 48 h prior to irradiation. Such a longer incubation time, of 48 h, was used to ensure cells were hypoxic at the time of irradiation. In line with the results from 4-h IQ10 treatment (Figure 4.4), under aerobic conditions, a 48-h IQ10 exposure (IC50 dose) also significantly sensitised both DAOY and UW228-3 cells to radiation (Figure 4.5). Following IQ10 treatment, the SFs at 6 Gy were reduced from 1.96% to 0.93% (± 0.49% and 0.34%, *P*=0.005) and from 1.05% to 0.58% (± 0.04% and 0.23%, *P*=0.03) for DAOY and UW228-3, respectively. However, under hypoxic conditions, no enhanced radiosensitivity of either line could be detected after IQ10 treatment (Figure 4.5), suggesting that IQ10 is effective in enhancing radiosensitivity in normoxia, and that radiosensitising effects are not maintained in hypoxia.

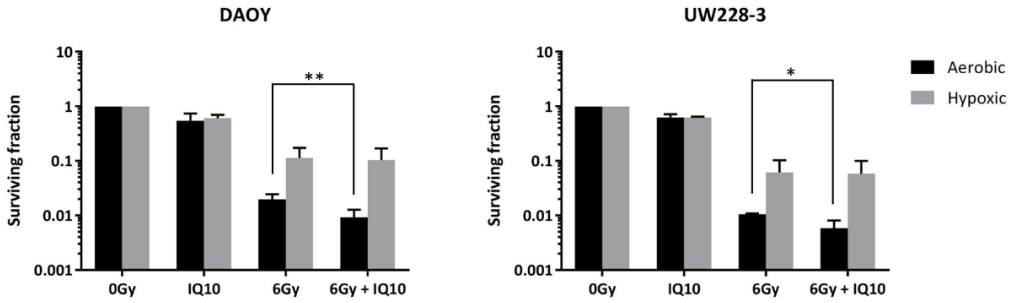



**Figure 4.5 Effects of IQ10 on radiosensitivity of brain cancer cells in normoxic *vs.* hypoxic conditions.** DAOY and UW228-3 cells were treated with clonogenic IC50 dose of IQ10 for 48 h under aerobic or hypoxic conditions. Cells were then irradiated with a single dose of 6 Gy and plated for clonogenic assay. PEs for DAOY and UW228-3 cells cultured in normoxia were 64% and 91% (±11% and 5%), respectively; PEs in hypoxia were 62% and 87% (±10% and 6%), respectively. Data represent the mean ± SD of three independent experiments, with each experiment containing six parallel data sets. Statistical significance was determined by Student's *t*-test. **P*< 0.05 and ***P*< 0.01 6 Gy *vs.* 6 Gy + IQ10.

It should be noted, however, that no radiosensitisation was observed after 48-h contact with IQ10 under hypoxia. Ideally it would have been useful to assess the radiosensitising effect of IQ10 after a 4-h drug exposure at a concentration of 1 μM as these were the treatment conditions that already

exhibited significant radiosensitising effect under 2D aerobic conditions (Section 4.3.2.1).

### 4.3.2.3 IQ10 radiosensitised brain cancer spheroids

To examine if 3D growth of cell lines influenced the radiosensitising effects of IQ10 spheroids were pretreated with IQ10 for 4 h, irradiated then immediately disaggregated and plated for clonogenic survival. As shown in Figure 4.6, IQ10 significantly enhanced the radioresponse of both DAOY and UW228-3 spheroids, with $SER_{0.01}$ values of 1.38 ± 0.31 and 1.16 ± 0.01, respectively.

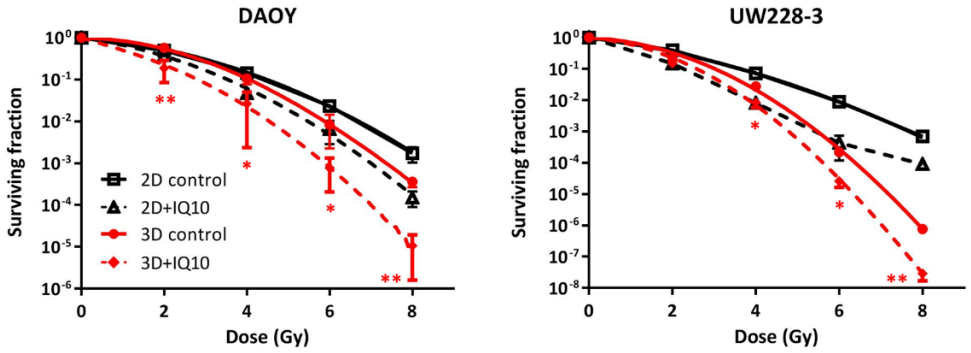



**Figure 4.6 Effects of IQ10 on radiosensitivity of brain cancer cells in 2D *vs.* 3D spheroid cultures.** Clonogenic survival curves comparing the radiosensitising effects of IQ10 on DAOY and UW228-3 cells in 2D *vs.* 3D cultures. PEs for DAOY and UW228-3 cells cultured in 2D were 63% (±14%) and 79% (±16%), respectively; PEs for 3D spheroids were 59% (±5%) and 28% (±7%), respectively. Data represent the mean SF ± SD of at least three independent experiments, with each experiment containing six parallel data sets, which are analysed using the Student's t-test. Asterisk indicates significance (*$P$< 0.05 and **$P$< 0.01).

Table 4.3 summarises other radiobiologic parameters calculated from linear-quadratic survival curves. When comparing the radiosensitising efficacy of IQ10 between 2D and 3D spheroid cultures (Figure 4.6), IQ10 seems more effective in 3D spheroid culture than in 2D culture for DAOY cells ($SER_{3D}$ = 1.38 ± 0.31 > $SER_{2D}$ = 1.25 ± 0.03, $P$=0.446), whereas IQ10 became less effective for UW228-3 spheroids ($SER_{3D}$ = 1.16 ± 0.01 < $SER_{2D}$ = 1.68 ± 0.25, $P$=0.002) (Table 4.2 and Table 4.3).

**Table 4.3 Radiobiologic parameters of brain cancer spheroids treated with IQ10 and/or radiation.**

| Spheroids | α ($Gy^{-1}$) | β ($Gy^{-2}$) | α/β (Gy) | SF2 | $SER_{0.01}$ |
|---|---|---|---|---|---|
| DAOY | | | | | |
| IR alone | 0.08±0.06 | 0.13±0.03 | 0.66±0.55 | 0.55±0.04 | 1.38±0.31 |
| IR+IQ10 | 0.68±0.62 | 0.10±0.06 | 14.26±19.46 | 0.23±0.17 | |
| *t* test | *P*=0.100 | *P*=0.421 | *P*=0.208 | ***P*=0.013** | |
| UW228-3 | | | | | |
| IR alone | 0.17±0.15 | 0.20±0.03 | 0.90±0.82 | 0.33±0.07 | 1.16±0.01 |
| IR+IQ10 | 0.28±0.30 | 0.24±0.06 | 1.41±1.74 | 0.23±0.08 | |
| *t* test | *P*=0.599 | *P*=0.303 | *P*=0.669 | *P*=0.166 | |

Parameters were calculated from clonogenic data fitted to a linear quadratic model. Data represent the mean ± SD of at least three independent experiments. Statistical significance was determined by Student's *t*-test. The *P*-values are bold where they are ≤ 0.05. Abbreviations: IR, irradiation; $SER_{0.01}$, sensitiser enhancement ratio at 1% survival; SF2, surviving fraction at 2 Gy.

The SF2 values of DAOY were significantly reduced by IQ10 from 0.55 ± 0.04 for controls to 0.23 ± 0.17 for IQ10 treated spheroids (*P*=0.013), further confirming the radiosensitising effect of IQ10. The SF2s of UW228-3 were also reduced by IQ10, but this did not achieve statistical significance (*P*=0.166). IQ10 treatment appeared to increase the α-value while decrease the β-value in DAOY spheroids with consequently increased α/β ratio; UW228-3 spheroids showed some increased α- and β-values and also increased α/β ratio after IQ10 treatment. None of these alterations of the L-Q parameters achieved statistical significance in either cell line, suggesting that IQ10 is probably not effective enough to induce any significant changes of L-Q parameters in brain cancer spheroids, but enhanced radiosensitisation obviously existed as discussed above. Collectively, irrespective of the system used (2D or 3D) it can be concluded that IQ10 sensitises DAOY and UW228-3 cells to radiation.

### 4.3.3 Downregulation of TrxR protein expression radiosensitises brain cancer cells

Data thus far strongly suggested that, via the radiosensitising effect observed with IQ10, that TrxR was an important target protein that mediates such effects. To fully evaluate the role of TrxR in regulating the radiosensitivity of brain cancer cells, TrxR siRNA was used to downregulate TrxR expression. As shown in Section 3.3.5, TrxR expression was, as determined by Western

blotting, markedly decreased (~65% reduction of control for DAOY and ~77% for SF188) in the TrxR siRNA group compared with the siRNA control group. Clonogenic data revealed that knocking down TrxR in DAOY and SF188 cells and irradiating at maximal knockdown resulted in enhanced sensitivity to radiation (Figure 4.7). The SF2s values were 0.66 ± 0.04 and 0.53 ± 0.02 for DAOY and SF188 control cells, respectively; when the cells transfected with TrxR siRNA, the SF2s were reduced to 0.53 ± 0.03 ($P$=0.012) and to 0.39 ± 0.02 ($P$<0.01), respectively (Table 4.4). However, the magnitude of the radiosensitising effect of TrxR siRNA was smaller than that of IQ10, i.e. the $SER_{0.01}$ values for cells treated with TrxR siRNA were 1.11 ± 0.04 and 1.13 ± 0.03 for DAOY and SF188 cells, respectively, which were less than the $SER_{0.01}$ values of 1.25 ± 0.03 and 1.22 ± 0.04 for cells treated with IQ10 (Table 4.2 and Table 4.4). Such differences may be due to the residual, functional, protein still present at maximal knock down (i.e. ~35% and 23% of control TrxR expression were present for DAOY and SF188 respectively) or may indicate that IQ10 affects other proteins, that influence radiosensitivity, other than solely TrxR.

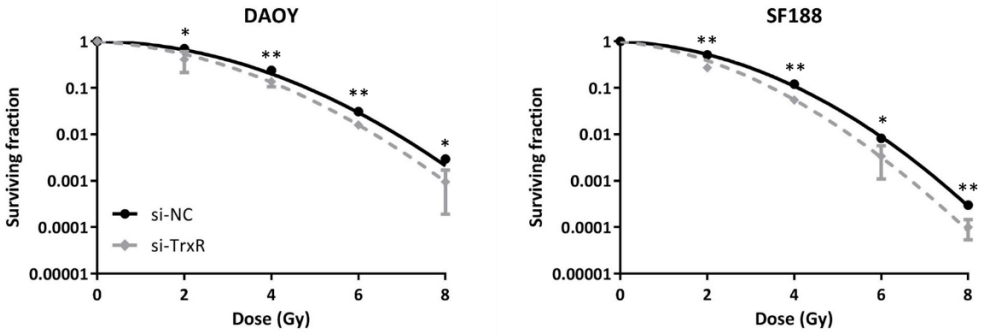



**Figure 4.7 TrxR knockdown enhances the radiosensitivity of DAOY and SF188 cells.** Clonogenic survival of DAOY and SF188 cells transfected with either TrxR siRNA or negative siRNA control for 48 h before irradiation were investigated after a range of radiation doses. The PEs of cells were as follows: si-NC DAOY - 56 ± 12%; si-TrxR DAOY - 65 ± 8%; si-NC SF188 – 52 ± 6%; si-TrxR SF188 – 55 ± 11%. Data represent the mean SF ± SD of three independent experiments, with each experiment containing six parallel data sets, which are analysed using the Student's *t*-test. *$P$<0.05 and **$P$<0.01, si-NC *vs.* si-TrxR. Abbreviations: NC, negative control.

**Table 4.4 Radiobiologic parameters of brain cancer cells transfected with TrxR siRNA or negative siRNA control.**

| Cell line | α ($Gy^{-1}$) | β ($Gy^{-2}$) | α/β (Gy) | SF2 | $SER_{0.01}$ |
|---|---|---|---|---|---|
| DAOY | | | | | |
| si-NC | 0.01±0.01 | 0.09±0.00 | 0.15±0.10 | 0.66±0.04 | 1.11±0.04 |
| si-TrxR | 0.13±0.06 | 0.09±0.01 | 1.53±0.96 | 0.53±0.03 | |
| t test | ***P*=0.027** | *P*=0.806 | *P*=0.068 | ***P*=0.012** | |
| SF188 | | | | | |
| si-NC | 0.09±0.02 | 0.12±0.00 | 0.76±0.18 | 0.53±0.02 | 1.13±0.03 |
| si-TrxR | 0.23±0.08 | 0.12±0.03 | 2.01±1.00 | 0.39±0.02 | |
| t test | ***P*=0.046** | *P*=0.685 | *P*=0.101 | ***P*<0.01** | |

Parameters were calculated from clonogenic data fitted to a linear quadratic model. Data represent the mean ± SD of three independent experiments. Abbreviations: IR, irradiation; si-NC, siRNA negative control; $SER_{0.01}$, sensitiser enhancement ratio at 1% survival.

Although the radiosensitising effect of TrxR siRNA was modest, data suggest that TrxR does exert some effects on radiosensitivity of brain cancer cells. To more fully evaluate this, in a more robust fashion, shRNA or CRISPR systems may have to be considered in future work.

### 4.3.4 IQ10 induced ROS production

To understand the potential mechanisms responsible for the enhanced radiosensitisation by IQ10, the intracellular ROS levels in brain cancer cells were examined by FACS using a $H_2$DCFDA probe. The baseline ROS level in DAOY cells was higher than that in UW228-3 cells (Figure 4.8). The MFI of ROS production for DAOY control group was 50.2 ± 6.2, whereas a lower MFI of 36.5 ± 4.8 was observed in UW228-3 control group (*P*=0.03).

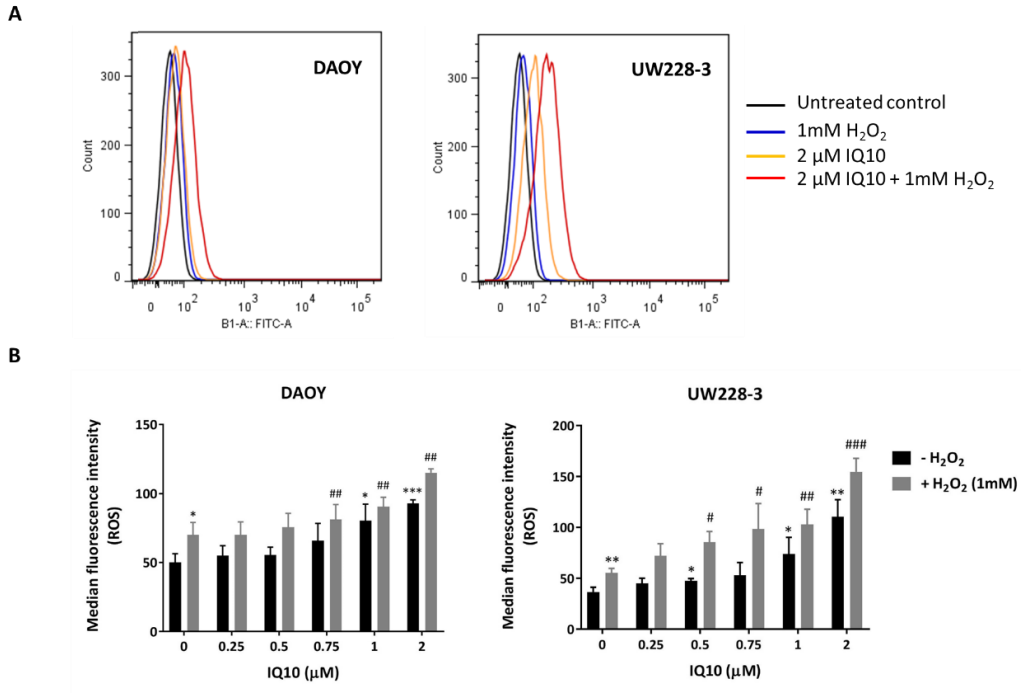



**Figure 4.8 Effect of IQ10 on intracellular ROS levels of brain cancer cells.** Cells treated with varying concentrations of IQ10 for 4 h with or without subsequent 1 mM of $H_2O_2$ for 1 h (cells without drug treatment were set as control) were collected and subjected to intracellular ROS level analysis by FACS. (A) Representative histogram of intracellular ROS of DAOY and UW228-3 cells treated with 2 µM IQ10 ± 1 mM $H_2O_2$, positive control ($H_2O_2$) and negative control cells. (B) The median fluorescence intensity (MFI) was calculated and plotted. Data represent the mean ± SD of three independent experiments, which are analysed using the ANOVA one-way tests. * $P$<0.05, ** $P$<0.01, *** $P$<0.001, IQ10/ $H_2O_2$ *vs.* untreated control. # $P$<0.05, ## $P$<0.01, ### $P$<0.001, IQ10 + $H_2O_2$ *vs.* $H_2O_2$ alone.

Both cell lines responded similarly to the positive control, $H_2O_2$, with ROS levels increasing to 1.4-fold of control in DAOY cells ($P$=0.01) and 1.5-fold of control in UW228-3 cells ($P$=0.008). Following IQ10 or IQ10 + $H_2O_2$ treatment, a dose-dependent increase in the intracellular ROS levels was observed in both cell lines (Figure 4.8B). The intracellular ROS levels were elevated to 1.8- or 2.2-fold of controls in DAOY cells after 2 µM IQ10 or 2 µM IQ10 + 1 mM $H_2O_2$ treatment ($P$<0.001 or $P$=0.003). In contrast to DAOY cells, the effect of IQ10 on increasing intracellular ROS levels was more pronounced in UW228-3 cells. Treatment with 1µM IQ10 or 1µM IQ10 + 1mM $H_2O_2$ resulted in a 2.0- or 2.9-fold increase in ROS levels compared to untreated controls in UW228-3 cells ($P$=0.02 or $P$=0.006). When the concentration of IQ10 was increased to 2µM, the intracellular ROS levels were elevated further to 3.0- or 4.3-fold of controls ($P$=0.002 or $P$<0.001). The results listed above suggest that IQ10 significantly impairs the cells ability to cope with oxidative stress, especially

that induced by $H_2O_2$. As ROS are super active chemical species and can cause detrimental effects to cells through reaction with various cellular components, including DNA, proteins and lipids. It was therefore of interest to assess if the IQ10-induced ROS elevation could lead to DNA damage, particularly DSBs.

### 4.3.5 IQ10 increases γH2AX formation alone and in response to radiation

The analysis of induction of DNA DSBs was measured by immunofluorescent detection of γH2AX foci formation. H2AX is known to be phosphorylated rapidly in response to DNA DSBs, leading to the formation of nuclear foci that can be visualised by immunocytochemical detection. Analysis of this fluorescent marker allows for a quantitative measure of DNA damage. As shown in Figure 4.9 and Appendix B-Figure B1, spontaneous DNA DSBs were found in untreated control cells (~2-4 γH2AX foci/nucleus in both DAOY and UW228-3). Following IQ10 or irradiation treatment, the γH2AX foci generation was significantly increased in both cell lines as compared to the controls, and the increase was significantly higher in the 2Gy irradiated group than in IQ10 treatment group ($P<0.01$). Furthermore, when combining IQ10 with radiation, the number of γH2AX foci was increased to an even greater extent than achieved by irradiation alone. The average γH2AX foci number was increased from 33.6 ± 0.13 in irradiation alone group to 39.2 ± 3.3 in irradiation and IQ10 combined group for DAOY cells ($P=0.01$), and from 30.0 ± 3.0 to 46.8 ± 6.5 for UW228-3 cells ($P=0.04$). When comparing between cell lines, the effects of this combination treatment on γH2AX foci formation were more pronounced in UW228-3 cells, but overall the same response was seen. Such results demonstrate that IQ10 treatment can cause DNA DSBs in brain cancer cells, either directly or indirectly, and enhance the extent of DNA damage induced by radiation, which may be one of the underlying mechanisms responsible for the IQ10-mediated radiosensitising effects seen in DAOY and UW228-3 cells. Taken together, data indicate a possible mechanistic link between radiosensitisation, DNA damage and ROS production induced by IQ10 through TrxR inactivation.

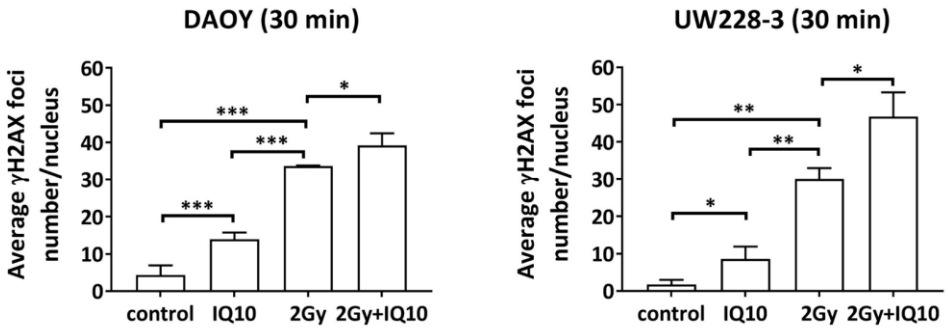



**Figure 4.9 Quantification of γH2AX foci in DAOY and UW228-3 cells following treatment with IQ10, radiation or combination of IQ10 plus radiation.** DAOY and UW228-3 cells were treated with or without IQ10 (1 µM) for 4 h prior to irradiation (2 Gy). γH2AX foci in DAOY and UW228-3 cells were quantified 30 min after treatment with IQ10 (1 µM), radiation (2Gy), or IQ10 plus radiation. Average number of γH2AX foci/nucleus is shown on the y-axis. More than 100 cells were analysed for each case. Data represent the mean ± SD of three independent experiments. One-way ANOVA test was used to calculate statistics: **P*<0.05, ***P*< 0.01, ****P*<0.001.

## 4.4 Discussion

In this study, the *in vitro* radiosensitising efficacy of a novel TrxR inhibitor IQ10 was investigated for the first time in brain cancer cells in normoxic *vs.* hypoxic and in 2D *vs.* 3D conditions. Data demonstrate that IQ10 sensitises brain cancer cells to irradiation in both 2D and 3D spheroid cultures with preliminary data suggesting that there was, unexpectedly, no enhanced radiation sensitisation under hypoxia. The mechanisms underlying the radiosensitising effect of IQ10 is possibly linked to the increased DNA damage, induced by upregulated ROS production due to the inhibition of TrxR activity by IQ10.

To determine if any difference existed in the radioresponses of different cell types, the intrinsic radiosensitivity of a panel of five brain cancer cell lines was first compared by clonogenic survival assay. The results demonstrate that the radiosensitivity varies significantly between cell lines, with the SF2 values ranging from 0.18 to 0.57. The paediatric GBM cell line KNS42 had the highest radiosensitivity, followed by another paediatric GBM line SF188 and medulloblastoma line UW228-3, and then the adult GBM line SNB19 and medulloblastoma line DAOY. From previous radiosensitivity data, SF2 values for SNB19 cell line ranged from 0.36 to 0.66 (Grabenbauer et al., 2018,

Niewidok et al., 2012, Mirjolet et al., 2013, Djuzenova et al., 2012, Stingl et al., 2010). In the present study, the SF2 for SNB19 was 0.48, which was within the reported range. SF2s for DAOY and UW228-3 cells in the present study, i.e. 0.57 and 0.35, respectively, were lower than the values reported by Zhukova et al. (2014), in which SF2s were 0.67 and 0.76, respectively. The *in vitro* radiation response of cancer cells can sometimes vary a lot between different studies due to the different cell culture conditions and growth status. One study noted that the cell growth state played an important role in radiation sensitivity, and the survival and growth rate of glioma cells was influenced by serum content of culture media but not so much by culture media type (Raaphorst et al., 1989). In addition, the degree of confluency also affects cellular radiosensitivity as cells grown to confluency before treatment show increased radiation resistance at low doses (Raaphorst et al., 1989). Therefore, careful consideration should be given to culture and growth conditions when attempting to compare the *in vitro* radiosensitivity of cells between different studies.

Hypoxia, as a result of an imbalance between oxygen supply and consumption, is a common feature of the tumour microenvironment and a well-defined factor for clinical radioresistance (Overgaard, 2007). Tumour cells in a hypoxic environment may be as much as 2-3 times more resistant to radiation than those in a normal environment (Harrison et al., 2002). As expected, the results from this study showed that hypoxia significantly increased the cell resistance to ionising radiation in both DAOY and UW228-3 cells as compared with normoxic controls, which are consistent with the published evidence (Marampon et al., 2014). Brain tumours such as glioblastoma and medulloblastoma are often characterised by intra-tumoural hypoxia (Pistollato et al., 2010) and tumour hypoxia is considered as one of the most important causes for radiotherapy failure (Wang et al., 2019). Numerous strategies have been developed over the last six decades to overcome hypoxia-induced radioresistance, but their clinical use is restricted by both limited efficacy and side effects (Wang et al., 2019).

Previous studies have reported that 3D cell culture models have diverse regions including necrotic, hypoxic and normoxic areas which react differently towards radiotherapy and chemotherapy (Koosha et al., 2017). Therefore, a 3D spheroid model was introduced in the present study to investigate and compare the radiosensitivity between 2D and 3D *in vitro* cultures in brain cancer cell lines, DAOY and UW228-3. Intriguingly, in 3D spheroid cultures, both cell lines became more sensitive to radiation compared to conventional 2D cultures. This finding is in contrast to a previous study, in which human HNSCC and lung carcinoma cells were shown to be more resistant to radiation in 3D culture (Storch et al., 2010a). However, the radiosensitivities of patient-derived GBM lines were reported as similar between 2D and 3D cultures (Gomez-Roman et al., 2017). Such discrepant results obtained from different studies might be due to cells originating from different organs responding differently to irradiation in 3D culture, as each organ has distinct structure, function and genetic features. What's more, the approach applied by Storch et al. (2010a) and Gomez-Roman et al. (2017) to examine the radioresponse of cancer cells in 3D culture is different from the current study. The present study, as described in the methodology section, used conventional 2D clonogenic assay to assess the radioresponses of brain cancer cells from both 3D spheroids and 2D monolayers. However, Storch et al. (2010a) and Gomez-Roman et al. (2017) applied an alternative 3D colony formation assay to evaluate cell survival in 3D culture - they grow cells in a laminin-rich extracellular matrix for 24 h or 8 h prior to irradiation, leaving colonies to grow for 11 days or 2-3 weeks prior to staining, and counting colony numbers according to the 2D definition for clonogenicity. As such, this 3D colony formation assay incubates cells in ECM as 3D format throughout the entire assay whereas in the current methodology cells are treated whilst in 3D spheroids but then immediately disaggregated into single cells after irradiation and plated in conventional 2D tissue-culture plastics without cell-ECM interaction. As suggested by Gomez-Roman et al. (2017) ECM concentrations can affect ligand binding and effects of ligands on signalling and cell behaviour, which might have a great influence on radiation response.

Unfortunately, time did not allow to apply this form of assessment in the present study. Although it may be a more appropriate model to better mimic the *in vivo* microenvironment of tumours, the above findings including the current data suggest that 3D culture is a much more complicated system to assess radioresponse in, with many factors needing to be considered. Further studies and an agreed set of assessment procedures are required to fully understand radioresponse of cells in 3D culture.

Radiosensitivity can be influenced by factors intrinsic and extrinsic to the cancer cells (Karar and Maity, 2009). Intrinsic factors include the cell cycle position, activation of apoptotic programmes, DNA damage repair proficiency, energy metabolism, and accumulation of genetic mutations in oncogenes and tumour-suppressor genes etc. The extrinsic factors comprise oxygen, nutrients and metabolic-waste elimination (Bernier et al., 2004). In addition, a large number of studies clearly show that radiation-induced cell signalling effects amongst adjacent cells, commonly known as radiation-induced bystander effects, have key roles in modulating overall radiation response (Butterworth et al., 2013). Some of these factors may be potential explanations for the differential radiosensitivity seen in different brain cancer cells and in different culture conditions (2D *vs.* 3D and normoxic *vs.* hypoxic). The increased understanding of both intrinsic and extrinsic factors has identified molecular targets that could be manipulated pharmacologically to increase tumour-cell killing and minimise normal-tissue toxicity (Bernier et al., 2004).

One of the major mechanisms of radiation-induced cell death is based on the generation of intracellular ROS (Hall and Giaccia, 2012) and the potential adverse effects of ROS are prevented by different cellular antioxidant defence systems, which help cells in scavenging ROS and salvaging biomolecules from oxidative damage (Mehta et al., 2016). One of the antioxidant enzymes is TrxR, which plays a key role in regulating redox balance and maintaining redox-regulated cellular functions, including transcription, proliferation, apoptosis, DNA damage recognition and repair (Arner and Holmgren, 2006, Mustacich and Powis, 2000). TrxR is often overexpressed in many aggressive tumours

and inhibition of TrxR activity can increase cellular radiation sensitivity (Urig and Becker, 2006, Smart et al., 2004, Karimpour et al., 2002). In addition, inhibitors that selectively target TrxR have shown promising results as anticancer drugs in both preclinical and clinical studies when used alone or in combination with radiation (Karimpour et al., 2002, Carde et al., 2001, Rockwell et al., 2002). MGd, a potent TrxR inhibitor, has been shown to enhance cancer cell response to radiation by forming ROS (Rockwell et al., 2002, Magda et al., 2001b) and when combining with prompt whole brain radiotherapy, MGd prolonged time to neurologic progression in lung cancer patients with brain metastases in a phase III trial (Mehta et al., 2009). A study by Smart et al. (2004) reported that Hela cells overexpressing the wild-type TrxR were more resistant to radiation-induced cytotoxicity. While knocking down TrxR in Hela and FaDu cells resulted in enhanced sensitivity to radiation (Javvadi et al., 2010a), further supporting the role of TrxR as a key determinant of intrinsic cancer cell radiosensitivity. Therefore, in the present study, the clonogenic survival assay was used to investigate whether TrxR could serve as a potential radiotherapeutic target and whether inhibition of TrxR activity by IQ10 could radiosensitise brain cancer cells. The results demonstrated that IQ10 significantly improved the response of DAOY, UW228-3 and SF188 cells to radiation, with the SER of up to 1.68 at 1% SF in conventional 2D culture. Moreover, downregulation of TrxR levels using siRNA also caused a significant increase in radiosensitivity of DAOY and SF188 cells. Such data are in agreement with previous findings (Liang et al., 2014, Javvadi et al., 2010a), in which TrxR inhibitors (i.e. selenadiazole and curcumin) significantly enhanced the sensitivity of cancer cells to radiation and stable knockdown of TrxR in both Hela and Fadu cells nearly abolished curcumin-mediated radiosensitisation (Javvadi et al., 2010b). These studies, including the current one, demonstrate TrxR as a promising target for novel radiosensitising agents.

Although IQ10 exhibited significant radiosensitising effects on the majority of brain cancer cell lines investigated, it had almost no effect on the

radiosensitivity of the paediatric GBM cell line KNS42. One of the possible reasons for this is that different brain cancer cell lines differ in their responses when exposed to IQ10. From the cytotoxicity results shown in Section 3.3.3, KNS42 cells were relatively more resistant to IQ10 than other brain cancer cell lines, therefore, in radiation-drug combination experiment, treating all cell lines with the identical dose of IQ10 (1 μM), rather than equitoxic doses, would cause less killing in KNS42 as compared to other cell lines - this decreased level of cell killing may indicate that the drug dose was insufficient to cause any changes in radiosensitivity. In addition, the intrinsic radiosensitivity may be another factor contributes to the radiosensitising effect of IQ10. Among the five brain cancer cell lines evaluated, KNS42 was the most radiosensitive line and it might be possible that IQ10 was more effective in enhancing radioresponse of inherently radioresistant cells than those that are already inherently radiosensitive. This potential explanation has some basis as a study suggested that the nature of cisplatin (also a TrxR inhibitor)-induced changes in radiosensitivity may be dependent upon the intrinsic radiosensitivity of the cell lines, with radiosensitisation only occurring in the most radioresistant cell lines (Britten et al., 1996). Franken et al. (2013) also reported that radiosensitisation was appeared to be more effective in radioresistant cell lines than in radiosensitive cell lines. Other potential mechanisms underlining the differential radiosensitising effects of IQ10 on different brain cancer cells were not followed due to time limitations. If time had allowed, the TrxR activity, intracellular ROS levels, cell cycle and apoptosis characteristics of KNS42 cells following IQ10 treatment could be assessed to further understand this phenomenon.

Antioxidant systems play a central role in maintaining the redox balance in cancer cells, and their dysregulation contributes to both normoxic and hypoxic radioresistance. Inhibition of antioxidant proteins such as TrxR could therefore be effective to reduce hypoxia-mediated radioresistance (Wang et al., 2019). Indeed, in breast cancer cells, the well-characterised TrxR inhibitor auranofin was found to overcome hypoxic radioresistance with mechanisms

linked to ROS-mediated mitochondria dysfunction, DNA damage, and apoptosis (Wang et al., 2017a, Rodman et al., 2016). Experiments investigating hypoxia radiosensitisation were limited to only one radiation dose and therefore care must be taken not to over interpret however, in the current study, no significant radiosensitising effect of the novel TrxR inhibitor IQ10 on the hypoxic brain cancer cells was observed, indicating that IQ10 may not be an ideal candidate for radiosensitising hypoxic cells. Much further work is required to investigate this, including a full radiation-dose response characterisation but a possible interpretation of this finding is that IQ10, unlike other hypoxia-activated cytotoxins, did not exhibit increased hypoxic cytotoxicity towards the brain cancer cells (results shown in Section 3.3.3). In addition, the treatment schedule of IQ10 in the hypoxic experiments was much different from the one applied in normoxic experiments (i.e. clonogenic IC50 for 48 h in hypoxia *vs.* 1 μM for 4 h in normoxia). In hypoxic experiments, cells were treated with the clonogenic IC50 dose of IQ10 for 48 h prior to irradiation. This extended incubation time and relatively lower drug concentrations might impair the potency of IQ10 so as to affect its radiosensitising effect. New hypoxia equipment is now available locally in the research group, adjacent to irradiation facilities, and so in future experiments it might be worthwhile to pre-incubate the cells under hypoxia for 24 h and treat the cells with 1 μM of IQ10 for 4 h (the treatment setting used in normoxic experiment) prior to radiation.

The 3D spheroid culture of cancer cells is considered to more closely reflect the *in vivo* tumour conditions than conventional 2D culture and therefore represents a promising system for chemosensitivity and radiosensitivity testing. In the current study, the radiosensitising effects of IQ10 were evaluated in both 2D and 3D spheroid cultures. Consistent with the 2D data, IQ10 also sensitised DAOY and UW228-3 spheroids to radiation but, under similar conditions, the combination of IQ10 and radiation was more effective on 3D spheroids than on 2D monolayers for DAOY. While in UW228-3, the radiosensitising efficacy of IQ10 was less effective in 3D spheroids. Although

drug penetration was assessed (using doxorubicin) such inconsistent radiosensitising effects of IQ10 in different spheroid models might be due to differences in drug penetration and the microenvironment of various layers within the spheroids. UW228-3 generally forms larger spheroids than DAOY, it might be more difficult for the drug to penetrate through completely, thus resulting in the decreased efficacy of radiosensitisation but nothing is known regarding the hypoxic fractions and if this differs between models. Although cells from spheroids are often more resistant than monolayers, to drugs and radiation, IQ10 still remained effective on radiosensitisation of both DAOY and UW228-3 spheroids, indicating that IQ10 treatment may improve the radiotherapy treatments of brain tumours *in vivo*. However, the 3D model used here lacks important factors of the tumour microenvironment that are known to contribute to drug and radiation response such as vasculature, fibroblasts or immune cells. Therefore, an orthotopic mouse model would be ideal to address the *in vivo* efficacy of IQ10 combined with radiation in the future.

Based on the above results, the potential molecular mechanisms of IQ10's radiosensitising effects were then investigated. It is well documented that cancer cells harbour high levels of ROS and are constantly under oxidative stress (Calaf et al., 2018). Maintenance of an appropriate level of intracellular ROS is important in retaining redox homeostasis and cellular signalling (Kumar et al., 2008); however, overproduction of ROS would result in a significant increase of intracellular oxidative stress, leading to oxidative damage and ultimately cause cell death (Javvadi et al., 2008). Redox enzymes such as TrxR are essential to many cellular processes, particularly in modulating the intracellular ROS (Roder and Thomson, 2015). Inhibition of redox enzymes alters the redox state of cells, which can lead to increased production of ROS that causes cellular oxidative stress (Fiskus et al., 2014). A large number of studies have indicated the possibility of using compounds that promote cellular ROS accumulation to effectively kill cancer cells and enhance the treatment responses *in vitro* (Trachootham et al., 2006). Results from the

present study showed that treatment with the novel TrxR inhibitor IQ10 resulted in elevated levels of ROS in both DAOY and UW228-3 cells with further increase when combined with $H_2O_2$, suggesting that IQ10 was able to induce ROS-mediated oxidative stress and cells treated with IQ10 were less capable to deal with the oxidative stress induced by $H_2O_2$. Moreover, at the concentration (1 µM IQ10) where the radiosensitising effects of IQ10 was observed, an increased ROS production either with IQ10 treatment alone or with IQ10 and $H_2O_2$ combination was also revealed. Thus, IQ10 can be considered as an appropriate drug to be combined with oxidative stress-inducing cytotoxins such as ionising radiation and the observed radiosensitising effects of IQ10 may be partly due to the decreased antioxidant buffering induced by IQ10. Previous studies have also reported the role of IQs in regulating intracellular ROS levels. In pancreatic cancer cells, IQs did not induce generalised oxidative stress; however, shifted the Trx redox state from reduced form to the oxidised form and induced radical-free oxidative stress (Jones, 2008, Yan et al., 2012). In addition, the TrxR inhibitors auranofin and curcumin, have been shown to significantly increase the intracellular ROS levels in breast and cervical cancer cells, respectively (Javvadi et al., 2008, Wang et al., 2017a).

Since increased levels of intracellular ROS can directly interact with DNA to induce oxidative DNA damage (Higgs et al., 2014), it was therefore of interest to evaluate whether IQ10-induced oxidative stress could result in DNA damage or increase the DNA damage caused by radiation. γH2AX immunofluorescence staining was employed to detect DNA DSBs at an early stage as an indicator of oxidative DNA damage. H2AX is a variant form of the nucleosome protein, histone H2A, which upon phosphorylation on its Ser 139 site (γH2AX) by ATM in response to DNA DSBs can be detected as 'γH2AX foci' using antibodies specific for γH2AX (Rogakou et al., 1998). γH2AX has been established as a highly sensitive and specific indicator of DNA DSBs after the action of different genotoxic stresses, including ionising radiation and chemotherapy drugs (Solovjeva et al., 2017). Yan et al. (2009a) have detected

DNA strand breaks in pancreatic cancer cells after a 4-h treatment of relatively high concentrations of IQs (above IC50 values). In agreement with this study, current data showed that treatment with IQ10 or radiation alone caused a significant increase in γH2AX foci expression, and the γH2AX levels were further increased after the combined treatment. Taken together, these results suggest that the radiosensitising effect of IQ10 is likely attributable to the induction of the ROS-mediated oxidative damage to DNA. Finally, it should be noted that the γH2AX foci evaluations were preliminary and detected at only a 30 mins post-irradiation time point. It is clear that more extensive evaluation is required in future work, i.e. different doses and different times, to monitor repair rather than only damage induction.

Although the ROS overproduction and subsequent DNA damage may be primary mechanisms underlying the IQ10's radiosensitising effect, other signalling pathways activated by ROS or other cellular events (e.g. apoptosis and cell cycle arrest) might also be implicated in IQ10-induced radiosensitisation, which deserves further investigation. Previous studies have reported that the IQ-induced cytotoxicity in pancreatic cancer cell lines was potentially mediated by apoptotic cell death. IQs were found to induce time- and dose-dependent apoptosis in pancreatic cancer cells with an increase in the amount of the cleaved form of caspase-3,-7,-8, and -9 (Yan et al., 2009a). In addition, inhibition of TrxR by IQs resulted in a shift of Trx redox state to the oxidised form and activation of the p38/c-Jun NH2-terminal kinase (JNK) mitogen-activated protein kinase (MAPK) signalling pathway (Yan et al., 2012). Oxidised Trx is known to activate ASK1, an upstream activator of p38/JNK in the MAPK signalling pathway (Yan et al., 2012). It is likely that AKS1 is the mechanistic link between the oxidised Trx and the activation of p38 and JNK (Saitoh et al., 1998b) and the activated p38 and JNK has been shown to signal to mitochondria and induce apoptosis through the intrinsic pathway (Ortiz et al., 2001). These observations suggested that IQs induced cell death via a mitochondria-mediated apoptotic death pathway (Yan et al., 2009a). However, whether IQ10 exhibited its cytotoxicity and radiosensitising effects through

inducing apoptosis on brain cancer cells were not investigated in the present study due to time limitation. Future experiments are needed to determine apoptotic cell death after IQ10 treatment. Plans and suggestions for future work are expanded upon in Section 6.2.

Taken together, although the molecular mechanisms of the radiosensitising effect of IQ10 is not yet fully understood, based on the findings presented here, a possible mechanism is proposed: IQ10 irreversibly inhibits TrxR activity, making the cells unable to deal with oxidative stress induced by radiation, thereby causing increased intracellular ROS levels and subsequent DNA damage, which ultimately leads to radiosensitisation of brain cancer cells.

## 4.5 Conclusions

1. The five brain cancer cell lines exhibited varying intrinsic radiosensitivities.
2. Hypoxic brain cancer cells were more radioresistant than normoxic controls but cells cultured in 3D spheroids were more sensitive to radiation than 2D cultured cells.
3. The redox enzyme TrxR is a promising radiobiological target and treatment with the TrxR inhibitor IQ10 results in a significant increase in radiosensitivity of brain cancer cells in both 2D and 3D cell culture models, but not in hypoxic conditions.
4. The TrxR inhibition by IQ10 treatment generates ROS production and subsequent oxidative DNA damage.

# Chapter 5 Effect of IQ10 on EMT-related gene expression

## 5.1 Introduction

### 5.1.1 Epithelial-mesenchymal transition (EMT)

EMT is considered as one of the hallmarks of cancer and is a crucial step in the invasion and metastasis of various cancers including brain cancers (Škovierová et al., 2018). GBMs are frequently invasive and MBs especially group 3 and 4 are often metastatic, resulting in a poor prognosis for the patients. Given that IQ10 has potent cytotoxic and radiosensitising effects against brain cancer cells, it was thought worthwhile to explore IQ10's other anticancer effects such as inhibition of cancer metastasis via EMT.

EMT is a reversible molecular process through which epithelial cells transiently undergo transdifferentiation into a mesenchymal phenotype (Kalluri and Weinberg, 2009). During this process, epithelial cells lose their cell polarity and cell-cell adhesion to acquire migratory and invasive capabilities (Kang and Massague, 2004). The resulting mesenchymal cells can revert back to an epithelial state in the reverse process, known as the mesenchymal-epithelial transition (MET), which appears to be essential for colonisation by tumour cells at distant sites, a key step in the metastatic process (Figure 5.1). EMT has important roles in specific steps of embryogenesis and wound healing. Moreover, malignant progression of many types of carcinoma also depends on EMT activation. EMT confers increased tumour-initiating and metastatic potential and greater resistance to multiple treatment modalities (Dongre and Weinberg, 2019).

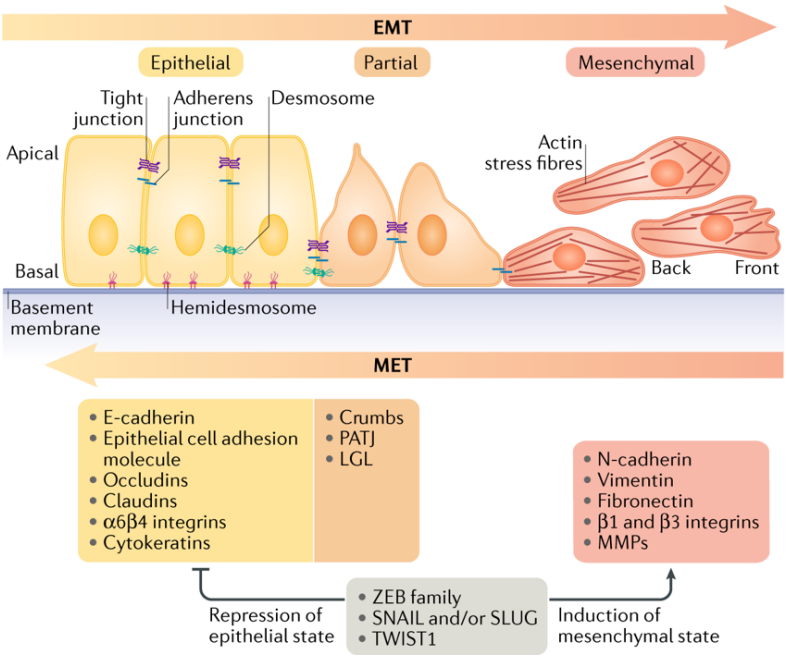



**Figure 5.1 Outline of a typical EMT programme.** Reproduced from (Dongre and Weinberg, 2019), Nat Rev Mol Cell Biol, 20, 69-84; Copyright© 2019 by Springer Nature with permission conveyed through Copyright Clearance Centre Inc.

Normally, epithelial cells display apical-basal polarity and are held together laterally by tight junctions, desmosomes and adherens junctions (Figure 5.1), the latter of which are formed by cell surface epithelial cadherin (E-cadherin) molecules. Upon activation of EMT, E-cadherin expression is inhibited, resulting in the loss of the typical polygonal morphology of epithelial cells. The cells acquire a spindle-shaped mesenchymal morphology and express markers that are associated with the mesenchymal cell status, notably neural cadherin (N-cadherin), vimentin and fibronectin (Figure 5.1) (Dongre and Weinberg, 2019). In general, tumour cells with mesenchymal characteristics have been associated with tumour progression, metastasis, chemo-resistance, and worse clinical prognosis (Ye and Weinberg, 2015). The initiation of EMT and maintenance of a mesenchymal phenotype is regulated by several families of transcriptional factors through multiple context-dependent signalling pathways (Nieto and Cano, 2012). Several key transcription factors, i.e. Zeb, Twist and Snail, have been identified to regulate EMT by interacting with each other and through responding to TGF-β and NF-κB pathways (Lamouille et al., 2014b). EMT can also be induced by growth factors, including EGF and VEGF when binding to tyrosine kinase receptors (Thiery and Sleeman, 2006).

Besides, the enhanced production of protease, particularly matrix metalloproteases (MMP), facilitates the EMT via degrading extracellular matrix (Zhang et al., 2012, Zhao et al., 2011).

EMT has been largely studied in various types of carcinomas (epithelial cells) but much less is known about the role of EMT-related process in nonepithelial tumour types such as brain tumours (e.g. gliomas and medulloblastomas) (Kahlert et al., 2017). Among all brain tumours, the involvement of EMT has been most extensively investigated in GBM. The invasive characteristic of GBM is, at least in part, due to their high migratory potential to invade the surrounding tissue. EMT has been identified as one of the key mechanisms that confer the invasive property to GBM cells (Kahlert et al., 2017, Iser et al., 2017). Several EMT-related transcription factors have been shown to play critical roles in the mesenchymal transformation of GBM including SNAI1/2, and Twist-1 (Karsy et al., 2016). Lower expression of a mesenchymal signature in GBM has been reported to correlate with longer time to recurrence and improved response to therapy (Cheng et al., 2012). In MB cells, hypoxia is shown to induce expression of mesenchymal markers (i.e. SNAI1, vimentin, and N-cadherin) and reduces expression of epithelial markers (i.e Zo-1, E-cadherin), leading to enhanced cell invasion and migration (Gupta et al., 2011). It has been reported that SHH activation in MB cells induces the expression of SNAI1, consequently activating the proto-oncogene N-MYC to induce cellular proliferation and transformation (Wanshura et al., 2011). Moreover, the expression of ZEB1 is elevated in SHH MB subgroup and inhibits granular zone exit, which eventually contributes to tumour formation (Singh et al., 2016). Thus, although not extensively studied as yet, EMT appears to play a role in brain tumours.

### 5.1.2 Role of Trx system in EMT

Previous studies have suggested that the Trx system can enhance the invasion and metastasis of cancer cells. In salivary adenoid cystic carcinoma (SACC) cells, for example, overexpression of Trx increased N-cadherin and downregulated E-cadherin expression. Trx facilitated the invasion and

metastasis of SACC cells through mediating TGF-β-induced EMT in a xenograft mouse model (Jiang et al., 2015). Bhatia et al. (2016b) have proved that overexpression of Trx in breast cancer cells enhanced cell invasion and migration *in vitro.* Targeting the TrxR with auranofin or other specific inhibitors might provide improved breast cancer patient outcomes through inhibition of cancer invasion and migration (Bhatia et al., 2016b, Cadenas et al., 2010). In colorectal cancer cells, Trx also promoted EMT as well as migration and invasion by up-regulating S100A4 through AKT activation (Zuo et al., 2018). As a negative regulator of Trx, TxNIP is downregulated in various types of human cancer and its deficiency could enhance TGF-β signalling and promote TGF-β-induced EMT (Masaki et al., 2012). In addition, a significant decrease of tumour progression and metastasis was observed in mice injected with TrxR knockdown lung carcinoma cells. It was suggested that TrxR might drive the cancer progression by catalysing Trx along with its related EMT processes (Yoo et al., 2006). Inhibition of TrxR by BBSKE was shown to reverse EMT phenotypes, inhibit migration and invasion of breast cancer cells both *in vitro* and *in vivo* (Zheng et al., 2019, Dong et al., 2016). The link between Trx system and EMT has been investigated in various cancer types, however, how the Trx system affects the EMT process in brain tumours is unclear.

### 5.1.3 Hypotheses and Aims

#### 5.1.3.1 Hypotheses

In addition to its cytotoxic and radiosensitising effects, IQ10 exhibits potential anti-invasive and anti-metastatic abilities shown by inhibition of EMT characteristics.

#### 5.1.3.2 Aims

Investigate potential anti-migratory/metastatic abilities of IQ10 by quantifying changes in expression of EMT related genes following drug exposure.

## 5.2 Materials and Methods

### 5.2.1 RNA isolation

Following seeding and overnight incubation DAOY and UW228-3 cells were treated with DMSO or 1 µM IQ10 for 4 h and incubated with the drug-free

medium for another 4 or 20 h prior to RNA extraction. Total RNA from treated cells was stabilised with RNA Protect Cell Reagent (Qiagen) and purified using the RNeasy Plus Mini Kit (Qiagen) according to the manufacturer's instructions. RNA samples from three independent experiments were pooled together. RNA quantity and purity were determined using a Nanodrop Spectrophotometer (Thermo Scientific).

### 5.2.2 cDNA synthesis

Total RNA was reverse-transcribed to cDNA with the $RT^2$ First Strand cDNA Kit (Qiagen). Genomic DNA elimination mix was prepared by adding 500 ng of RNA to buffer GE and a variable amount of RNase-free water to make up to a 10µl total volume. The mix was incubated at 42 °C for 5 min, then placed immediately on ice for at least 1 min. 10 µl of reverse-transcription mix was prepared according to Table 5.1 and added to each tube containing 10µl genomic DNA elimination mix. The mix was incubated at 42°C for 15 min following by 95°C for 5 min to stop the reaction. 91 µl of RNase-free water was then added to each reaction to make cDNA synthesis reaction.

**Table 5.1 Reverse-transcription mix.**

| Reagents | Volume for 1 reaction (µl) |
|---|---|
| 5x Buffer BC3 | 4 |
| Control P2 | 1 |
| RE3 Reverse Transcriptase Mix | 2 |
| RNase-free water | 3 |
| Total volume | 10 |

### 5.2.3 Real-time EMT PCR array

Real-time PCR was conducted using the Human Epithelial to Mesenchymal Transition (EMT) $RT^2$ Profiler™ PCR Array (PAHS-090Z, Qiagen) and $RT^2$ SYBR Green Mastermixes (Qiagen). The PCR array profiles the expression of 84 key genes associated with the EMT process. All PCR components (Table 5.2) were combined to prepare a total volume of 2700 µl mix in a 5 ml tube. The PCR

component mix was dispensed into a 96-well plate at 25 µl/well. The plate was tightly sealed with adhesive film before loaded into ABI-7500 Fast real-time PCR system (Applied Biosystems). The amplification condition was as follows: 95°C for 10 min, followed by 40 cycles of 95°C for 15 sec, and 60°C for 1 min.

**Table 5.2 PCR components mix.**

| Reagents | Volume (µl) |
|---|---|
| 2x $RT^2$ SYBR Green Mastermix | 1350 |
| cDNA synthesis reaction | 102 |
| RNase-free water | 1248 |
| Total volume | 2700 |

### 5.2.4 Statistical analysis

Data analysis of the PCR array was performed using the online GeneGlobe Data Analysis Centre (https://www.qiagen.com/gb/shop/genes-and-pathways/data-analysis-center-overview-page/). Fold-change of target genes against the reference gene was calculated from $2^{-\Delta\Delta Ct}$ values. The $C_T$ cut-off value was set at 35. Gene expression differences greater than 2-fold were considered as differentially transcribed.

## 5.3 Results

The potential role for IQ10 in the regulation of EMT was determined by using $RT^2$ Profiler PCR Arrays, which profiled the expression of 84 EMT-related genes in DAOY and UW228-3 cells. The gene expression patterns were first examined in vehicle control DAOY and UW228-3 cells at 4-h/24-h time points; and then the vehicle control group data was compared against the respective IQ10-treated group at each time point in each cell line. When comparing UW228-3 with DAOY, a total of 47 genes were differentially expressed. MMP3 and SPP1 genes were amongst those shown to be highly overexpressed in UW228-3 relative to DAOY (MMP3: 167.11 fold at 4 h and 57.41 fold at 24 h, respectively; SPP1: 61.01 fold at 4 h and 44.92 fold at 24 h, respectively),

whereas CAV2 and IGFBP4 genes were expressed in extremely low levels in UW228-3 (CAV2: -7022.89 fold at 4 h and -5153.72 fold at 24 h, respectively; IGFBP4: -11539.35 and -7702.94 fold, respectively). Other differently expressed genes are listed in Table 5.3.

**Table 5.3 Profiler PCR array results (vehicle control UW228-3 cells vs. DAOY cells).**

| Gene | Description | Fold-change | | | |
|---|---|---|---|---|---|
| | | 4h | | 24h | |
| BMP7 | Bone morphogenetic protein 7 | -380.55 | A | -281.72 | A |
| CALD1 | Caldesmon 1 | -2.15 | \ | \ | \ |
| CAMK2N1 | Calcium/calmodulin-dependent protein kinase II inhibitor 1 | -13.52 | \ | -25.07 | A |
| CAV2 | Caveolin 2 | -7022.89 | A | -5153.72 | A |
| CDH1 | Cadherin 1, type 1, E-cadherin (epithelial) | 2.59 | B | \ | \ |
| CDH2 | Cadherin 2, type 1, N-cadherin (neuronal) | -2.22 | \ | \ | \ |
| COL1A2 | Collagen, type I, alpha 2 | \ | \ | 2.39 | \ |
| COL3A1 | Collagen, type III, alpha 1 | -2.03 | \ | \ | \ |
| COL5A2 | Collagen, type V, alpha 2 | 11.04 | \ | 11.6 | \ |
| CTNNB1 | Catenin (cadherin-associated protein), beta 1, 88kDa | -2.18 | \ | -3.35 | \ |
| DSC2 | Desmocollin 2 | -27.74 | A | -21.27 | A |
| DSP | Desmoplakin | -3290.25 | A | -1776.31 | A |
| EGFR | Epidermal growth factor receptor | -6.01 | \ | -4.41 | \ |
| ERBB3 | V-erb-b2 erythroblastic leukemia viral oncogene homolog 3 (avian) | 2.69 | A | 13.09 | A |
| ESR1 | Estrogen receptor 1 | \ | \ | -3.3 | B |
| F11R | F11 receptor | \ | \ | 2.58 | \ |
| FGFBP1 | Fibroblast growth factor binding protein 1 | -4.26 | B | -10.77 | B |
| FN1 | Fibronectin 1 | -12.64 | \ | -15.22 | \ |
| FOXC2 | Forkhead box C2 (MFH-1, mesenchyme forkhead 1) | -1794.19 | A | -824.68 | A |
| FZD7 | Frizzled family receptor 7 | -4.41 | \ | -3.75 | \ |
| GNG11 | Guanine nucleotide binding protein (G protein), gamma 11 | -2.13 | \ | \ | \ |
| GSC | Goosecoid homeobox | -156.79 | A | -196.15 | A |
| GSK3B | Glycogen synthase kinase 3 beta | -2.66 | \ | -2.27 | \ |
| IGFBP4 | Insulin-like growth factor binding protein 4 | -11539.35 | A | -7702.94 | A |
| IL1RN | Interleukin 1 receptor antagonist | -95.04 | A | -15.92 | A |
| ILK | Integrin-linked kinase | -2.49 | \ | \ | \ |
| ITGA5 | Integrin, alpha 5 (fibronectin receptor, alpha polypeptide) | 3.51 | \ | 3.85 | \ |
| KRT14 | Keratin 14 | -11.10 | A | -6.21 | A |
| KRT19 | Keratin 19 | 20.94 | A | 8.3 | B |
| KRT7 | Keratin 7 | \ | \ | -2.67 | B |
| MMP2 | Matrix metallopeptidase 2 (gelatinase A, 72kDa gelatinase, 72kDa type IV collagenase) | -20.86 | \ | -15.57 | \ |
| MMP3 | Matrix metallopeptidase 3 (stromelysin 1, progelatinase) | 167.11 | A | 57.41 | A |

**Table 5.3 (continued).**

| | | | | | |
|---|---|---|---|---|---|
| MMP9 | Matrix metallopeptidase 9 (gelatinase B, 92kDa gelatinase, 92kDa type IV collagenase) | -51.41 | A | -55.45 | A |
| MST1R | Macrophage stimulating 1 receptor (c-met-related tyrosine kinase) | 2.96 | B | -16.34 | A |
| NODAL | Nodal homolog (mouse) | -27.81 | B | -19.77 | B |
| NOTCH1 | Notch 1 | \ | \ | 2.85 | A |
| NUDT13 | Nudix (nucleoside diphosphate linked moiety X)-type motif 13 | -5.86 | A | -4.26 | A |
| OCLN | Occludin | -11.90 | | -8.10 | \ |
| PDGFRB | Platelet-derived growth factor receptor, beta polypeptide | -13.37 | B | -13.65 | B |
| PLEK2 | Pleckstrin 2 | -88.98 | A | -269.41 | A |
| PTK2 | PTK2 protein tyrosine kinase 2 | -3.01 | \ | -2.95 | \ |
| SERPINE1 | Serpin peptidase inhibitor, clade E (nexin, plasminogen activator inhibitor type 1), member 1 | -3.57 | \ | -8.62 | \ |
| GEMIN2 | Survival of motor neuron protein interacting protein 1 | -2.45 | \ | -2.52 | \ |
| SNAI1 | Snail homolog 1 (Drosophila) | -79.23 | A | -72.45 | A |
| SNAI2 | Snail homolog 2 (Drosophila) | -4.33 | \ | -4.49 | \ |
| SNAI3 | Snail homolog 3 (Drosophila) | -6.62 | B | -11.02 | B |
| SPARC | Secreted protein, acidic, cysteine-rich (osteonectin) | 2.21 | \ | 2.67 | \ |
| SPP1 | Secreted phosphoprotein 1 | 61.01 | \ | 44.92 | \ |
| STEAP1 | Six transmembrane epithelial antigen of the prostate 1 | -2.84 | \ | -2.28 | \ |
| TFPI2 | Tissue factor pathway inhibitor 2 | -99.82 | \ | -134.92 | \ |
| TGFB2 | Transforming growth factor, beta 2 | 8.44 | \ | 6.52 | \ |
| TGFB3 | Transforming growth factor, beta 3 | 5.50 | \ | 6.07 | \ |
| TMEFF1 | Transmembrane protein with EGF-like and two follistatin-like domains 1 | -6.24 | \ | -4.63 | \ |
| TMEM132A | Transmembrane protein 132A | -4.43 | \ | -3.42 | \ |
| TSPAN13 | Tetraspanin 13 | -4.23 | \ | -2.79 | \ |
| TWIST1 | Twist homolog 1 (Drosophila) | -6.22 | \ | -4.78 | \ |
| VCAN | Versican | 2.65 | \ | 2.65 | \ |
| VIM | Vimentin | -2.02 | \ | \ | \ |
| WNT5A | Wingless-type MMTV integration site family, member 5A | -32.64 | \ | -26.38 | \ |
| ZEB2 | Zinc finger E-box binding homeobox 2 | -2.14 | \ | \ | \ |

A: This gene's expression is relatively low (threshold cycle> 30) in one sample and reasonably detected (threshold cycle < 30) in the other sample suggesting that the actual fold-change value is at least as large as the calculated and reported fold-change result.

B: This gene's average relative expression level is low (threshold cycle> 30) in both control and test samples.

To investigate the anti-migratory/metastatic potential of IQ10, EMT-related gene expression between vehicle control groups and IQ10-treated groups were compared at 4-h and 24-h post-treatment time points. For the DAOY cell line, a full list of the differentially expressed (≥ 2-fold) EMT-related genes is presented in Table 5.4. IQ10 treatment significantly induced expression of 2 genes whilst repressing 18 genes at 4-h. The largest changes in gene expression upon IQ10 treatment was observed with KRT19 (9.49 fold) and SNAI3 (-5.75 fold). At the 24-h time point, IQ10 significantly upregulated 3 genes and downregulated 17 genes. ERBB3 (5.94-fold) and MST1R (-69.07-fold) showed the largest changes in gene expression with IQ10 treatment. Of the genes upregulated by IQ10, KRT19, an epithelial marker, is known to be usually downregulated during EMT or metastasis (Nozato et al., 2012). Amongst those genes significantly downregulated by IQ10, fourteen are commonly upregulated during EMT (COL1A2, FN1, FOXC2, FZD7, ITGA5, SERPINE1, SNAI3, TCF4, TWIST1, VPS13A, WNT5A, WNT5B, ZEB1 and ZEB2) (Gröger et al., 2012, Venkov et al., 2011).

**Table 5.4 Profiler PCR array results for DAOY cells (IQ10-treated group *vs.* vehicle control group at two time points).**

| Gene | Description | Fold-change | |
|---|---|---|---|
| **Up-regulated gene expression in DAOY** | | **4h** | **24h** |
| **ERBB3** | V-erb-b2 erythroblastic leukemia viral oncogene homolog 3 (avian) | \ | 5.94 (B) |
| **GNG11** | Guanine nucleotide binding protein (G protein), gamma 11 | \ | 2.16 |
| **JAG1** | Jagged 1 | \ | 2.85 |
| **KRT19** | Keratin 19 | 9.49 | \ |
| **SNAI1** | Snail homolog 1 (Drosophila) | 2.37 | \ |
| **Down-regulated gene expression in DAOY** | | **4h** | **24h** |
| **COL1A2** | Collagen, type I, alpha 2 | \ | -2.79 |
| **COL3A1** | Collagen, type III, alpha 1 | \ | -2.06 |
| **DSP** | Desmoplakin | -2.05 | \ |
| **EGFR** | Epidermal growth factor receptor | -2.34 | \ |
| **ERBB3** | V-erb-b2 erythroblastic leukemia viral oncogene homolog 3 (avian) | -2.98 (B) | \ |
| **ESR1** | Estrogen receptor 1 | \ | -2.69 (B) |
| **FGFBP1** | Fibroblast growth factor binding protein 1 | -3.85 (B) | -3.46 (B) |
| **FN1** | Fibronectin 1 | \ | -2.23 |
| **FOXC2** | Forkhead box C2 (MFH-1, mesenchyme forkhead 1) | \ | -2.39 |
| **FZD7** | Frizzled family receptor 7 | \ | -2.19 |
| **GSK3B** | Glycogen synthase kinase 3 beta | -2.27 | -2.00 |
| **IL1RN** | Interleukin 1 receptor antagonist | -2.01 | -6.02 (A) |
| **ITGA5** | Integrin, alpha 5 (fibronectin receptor, alpha polypeptide) | -2.02 | \ |
| **ITGB1** | Integrin, beta 1 (fibronectin receptor, beta polypeptide, antigen CD29 includes MDF2, MSK12) | \ | -2.51 |
| **KRT7** | Keratin 7 | \ | -9.25 (B) |
| **MAP1B** | Microtubule-associated protein 1B | -2.13 | \ |
| **MST1R** | Macrophage stimulating 1 receptor (c-met-related tyrosine kinase) | \ | -69.07 (A) |
| **NOTCH1** | Notch 1 | -2.40 (A) | \ |
| **NUDT13** | Nudix (nucleoside diphosphate linked moiety X)-type motif 13 | \ | -11.39 (A) |
| **PDGFRB** | Platelet-derived growth factor receptor, beta polypeptide | \ | -8.17 (B) |
| **PTK2** | PTK2 protein tyrosine kinase 2 | -2.23 | \ |
| **SERPINE1** | Serpin peptidase inhibitor, clade E (nexin, plasminogen activator inhibitor type 1), member 1 | \ | -3.46 |
| **SNAI3** | Snail homolog 3 (Drosophila) | -5.75 (B) | \ |
| **TCF4** | Transcription factor 4 | -4.27 | \ |
| **TGFB2** | Transforming growth factor, beta 2 | -4.21 | \ |
| **TWIST1** | Twist homolog 1 (Drosophila) | -2.02 | \ |

**Table 5.4 (continued)**

| | | | |
|---|---|---|---|
| **VPS13A** | Vacuolar protein sorting 13 homolog A (S. cerevisiae) | \ | -2.87 |
| **WNT5A** | Wingless-type MMTV integration site family, member 5A | -2.3 | -2.25 |
| **WNT5B** | Wingless-type MMTV integration site family, member 5B | -5.52 | \ |
| **ZEB1** | Zinc finger E-box binding homeobox 1 | -2.40 | \ |
| **ZEB2** | Zinc finger E-box binding homeobox 2 | -2.70 | \ |

A: This gene's expression is relatively low (threshold cycle> 30) in one sample and reasonably detected (threshold cycle < 30) in the other sample suggesting that the actual fold-change value is at least as large as the calculated and reported fold-change result.

B: This gene's average relative expression level is low (threshold cycle> 30) in both control and test samples.

For the UW228-3 cell line, a full list of the differentially expressed (≥ 2-fold) EMT-related genes is presented in Table 5.5. IQ10 treatment significantly induced expression of 8 genes whilst repressing 14 genes at the 4-h time point. The largest changes in gene expression upon IQ10 treatment were seen with SNAI3 (4.72 fold) and KRT19 (-4.38 fold). At the 24-h time point, IQ10 significantly upregulated 5 genes and downregulated 39 genes. PLEK2 (7.01 fold) and KRT19 (-18.77 fold) had the largest changes in gene expression after IQ10 treatment. Of those genes upregulated by IQ10, two (DSP and RGS2) are known to be downregulated during EMT or metastasis. In addition, among those genes significantly downregulated by IQ10, fourteen are usually upregulated during EMT (CALD1, CDH2, COL1A2, COL5A2, FZD7, IL1RN, ITGA5, ITGAV, SPARC, TCF4, TMEFF1, VIM, VPS13A and ZEB2) (Gröger et al., 2012, Venkov et al., 2011).

**Table 5.5 Profiler PCR array results for UW228-3 cells (IQ10-treated group *vs.* vehicle control group at two time points).**

| Gene | Description | Fold-change | |
|---|---|---|---|
| **Up-regulated gene expression in UW228-3** | | **4h** | **24h** |
| **BMP2** | Bone morphogenetic protein 2 | \ | 5.43 (A) |
| **CAMK2N1** | Calcium/calmodulin-dependent protein kinase II inhibitor 1 | \ | 4.56 (A) |
| **DSP** | Desmoplakin | 2.11 (B) | \ |
| **ESR1** | Estrogen receptor 1 | 2.55(B) | \ |
| **FOXC2** | Forkhead box C2 (MFH-1, mesenchyme forkhead 1) | 3.39 (B) | \ |
| **IGFBP4** | Insulin-like growth factor binding protein 4 | 3.34 (B) | \ |
| **JAG1** | Jagged 1 | \ | 2.31 |
| **KRT14** | Keratin 14 | 2.23 (B) | \ |
| **MMP3** | Matrix metallopeptidase 3 (stromelysin 1, progelatinase) | \ | 2.23 |
| **PLEK2** | Pleckstrin 2 | \ | 7.01 |
| **RGS2** | Regulator of G-protein signalling 2, 24kDa | 2.20 | \ |
| **SNAI2** | Snail homolog 2 (Drosophila) | 2.87 | \ |
| **SNAI3** | Snail homolog 3 (Drosophila) | 4.72 (B) | \ |
| **Down-regulated gene expression in UW228-3** | | **4h** | **24h** |
| **AKT1** | V-akt murine thymoma viral oncogene homolog 1 | \ | -2.22 |
| **CALD1** | Caldesmon 1 | \ | -5.50 |
| **CDH1** | Cadherin 1, type 1, E-cadherin (epithelial) | -3.07 (B) | \ |
| **CDH2** | Cadherin 2, type 1, N-cadherin (neuronal) | \ | -3.73 |
| **COL1A2** | Collagen, type I, alpha 2 | \ | -8.40 |
| **COL3A1** | Collagen, type III, alpha 1 | \ | -3.03 |
| **COL5A2** | Collagen, type V, alpha 2 | \ | -5.50 |
| **CTNNB1** | Catenin (cadherin-associated protein), beta 1, 88kDa | \ | -2.13 |
| **DSC2** | Desmocollin 2 | \ | -9.71 (B) |
| **ERBB3** | V-erb-b2 erythroblastic leukemia viral oncogene homolog 3 (avian) | -2.50 (A) | -2.33 (A) |
| **F11R** | F11 receptor | \ | -3.84 |
| **FZD7** | Frizzled family receptor 7 | -2.17 | -2.95 |
| **GEMIN2** | Survival of motor neuron protein interacting protein 1 | \ | -2.43 |
| **GSK3B** | Glycogen synthase kinase 3 beta | -2.17 | -2.55 |
| **IL1RN** | Interleukin 1 receptor antagonist | \ | -2.43 |
| **ILK** | Integrin-linked kinase | \ | -2.39 |
| **ITGA5** | Integrin, alpha 5 (fibronectin receptor, alpha polypeptide) | \ | -2.35 |
| **ITGAV** | Integrin, alpha V (vitronectin receptor, alpha polypeptide, antigen CD51) | \ | -3.07 |
| **ITGB1** | Integrin, beta 1 (fibronectin receptor, beta polypeptide, antigen CD29 includes MDF2, MSK12) | \ | -2.75 |

**Table 5.5 (continued).**

| | | | |
|---|---|---|---|
| **KRT19** | Keratin 19 | -4.38 (A) | -18.77 (B) |
| **MAP1B** | Microtubule-associated protein 1B | -2.55 | -2.22 |
| **MSN** | Moesin | \ | -2.46 |
| **MST1R** | Macrophage stimulating 1 receptor (c-met-related tyrosine kinase) | -3.51 (B) | \ |
| **NOTCH1** | Notch 1 | -4.32 (A) | -6.68 (A) |
| **NUDT13** | Nudix (nucleoside diphosphate linked moiety X)-type motif 13 | \ | -2.85 |
| **OCLN** | Occludin | \ | -7.62 |
| **PTK2** | PTK2 protein tyrosine kinase 2 | -2.08 | \ |
| **RAC1** | Ras-related C3 botulinum toxin substrate 1 (rho family, small GTP binding protein Rac1) | \ | -2.57 |
| **SMAD2** | SMAD family member 2 | \ | -2.19 |
| **SPARC** | Secreted protein, acidic, cysteine-rich (osteonectin) | \ | -2.08 |
| **STAT3** | Signal transducer and activator of transcription 3 (acute-phase response factor) | \ | -2.81 |
| **TCF3** | Transcription factor 3 (E2A immunoglobulin enhancer binding factors E12/E47) | \ | -3.07 |
| **TCF4** | Transcription factor 4 | -2.16 | -2.19 |
| **TGFB1** | Transforming growth factor, beta 1 | \ | -2.14 |
| **TGFB2** | Transforming growth factor, beta 2 | \ | -2.97 |
| **TGFB3** | Transforming growth factor, beta 3 | -2.10 | -8.57 |
| **TMEFF1** | Transmembrane protein with EGF-like and two follistatin-like domains 1 | \ | -4.96 |
| **TWIST1** | Twist homolog 1 (Drosophila) | -4.29 | -2.45 |
| **VIM** | Vimentin | \ | -2.14 |
| **VPS13A** | Vacuolar protein sorting 13 homolog A (S. cerevisiae) | \ | -2.51 |
| **WNT5A** | Wingless-type MMTV integration site family, member 5A | -2.89 | \ |
| **WNT5B** | Wingless-type MMTV integration site family, member 5B | -4.00 | -4.92 |
| **ZEB2** | Zinc finger E-box binding homeobox 2 | \ | -2.68 |

A: This gene's expression is relatively low (threshold cycle> 30) in one sample and reasonably detected (threshold cycle < 30) in the other sample suggesting that the actual fold-change value is at least as large as the calculated and reported fold-change result.

B: This gene's average relative expression level is low (threshold cycle> 30) in both control and test samples.

In both DAOY and UW228-3 cell lines, 21 EMT-related genes were concordantly altered by IQ10, at more than 2-fold following treatment. IQ10 had an appreciable effect on the expression of several key EMT effectors, including N-cadherin (CDH2), vimentin (VIM), snail (SNAI) and zinc finger E-box-binding (ZEB). Such data suggest that IQ10 may play an important role on the expression of a variety of genes involved in EMT, suggesting that IQ10

treatment in DAOY and UW228-3 cells may be able to inhibit tumour invasion and metastasis by modulating a set of genes required for EMT. However, additional validation studies are required to confirm the changes seen in the arrays by measuring gene expression of the top genes (> 5 fold) or concordant altered genes using qRT-PCR, by conducting Western-based experiments to examine protein expression of the genes, and potentially by validating data in patient tumour specimens (either via RNA-CISH or standard IHC).

## 5.4 Discussion

EMT is characterised by the loss of cell-cell adhesion and an increase in cell motility. It is a key process in cancer progression and metastasis, making EMT inhibition an attractive therapeutic strategy (Lim and Thiery, 2012). Recent studies have suggested that the Trx system may play an important role in the process of EMT. In breast cancer cells, for example, overexpression of Trx was shown to enhance cell invasion, and treatment with auranofin inhibited the TrxR activity and cell migration (Bhatia et al., 2016b). In another study, Trx was shown to play a key role in SACC invasion and metastasis through the modulation of TGF-β-Akt/GSK-3β on EMT (Jiang et al., 2015). Current IHC data described in Chapter 2 suggest that the overexpression of Trx or TrxR is associated with poor prognosis of brain tumour patients, therefore, the role of Trx system in the regulation of EMT was assessed by expression profiling as alterations to this process may be associated with the decreased OS seen in the patient samples.

EMT array results revealed that TrxR inhibition by IQ10 markedly down-regulated a large number of EMT-related genes in DAOY and UW228-3 cell lines, including several master EMT effectors N-cadherin, Snail, Twist, Vimentin, and Zeb, which are usually increased during EMT (Dongre and Weinberg, 2019). N-cadherin, encoded by CDH2, is a calcium-dependent cell adhesion glycoprotein. Overexpression of N-cadherin is associated with mesenchymal transition and metastatic activity of cancer cells (Nakajima et al., 2004). Snail belongs to a family of zinc-finger transcription factors that is essential for embryonic development and well-known to induce EMT

(Barrallo-Gimeno and Nieto, 2005). Twist is a key transcription factor involved in embryonic morphogenesis and development, and also functions to induce EMT and migration (Je et al., 2013). Like Snail and Twist, ZEBs bind E-boxes and function as transcriptional repressors and activators, thereby repressing some epithelial junction and polarity genes and activating mesenchymal genes that define the EMT phenotypes (Lamouille et al., 2014a). Vimentin is an intermediate filament which is characteristically upregulated in cells undergoing EMT. Vimentin acts as a positive regulator of EMT and upregulation of Vimentin appears to be a prerequisite for EMT induction (Ivaska, 2011).

While a large number of EMT-related genes were down-regulated by TrxR inhibition with IQ10, several genes (i.e. KRT19, DSP and RGS2) were upregulated during treatment. Keratin (KRT) is an epithelial marker, and downregulation of keratin is associated with EMT. Dysregulation of keratin expression has long been recognised as a feature of epithelial tumour progression (Nozato et al., 2012). Desmoplakin (DSP) is an obligate component of functional desmosomes that anchors intermediate filaments of desmosomal plaques and desmosome components. A decrease in the expression of DSP has been associated with the reduction of cell-cell adhesion, which is key to EMT (Kubelt et al., 2015). Regulator of G-protein signalling 2 (RGS2) is a member of a larger family of RGS proteins that control signalling through G-protein coupled receptors (Linder et al., 2018). Decreased levels of RGS2 has been reported for several cancer types in association with tumour progression and EMT (Linder et al., 2018).

While DAOY has been suggested to belong to the SHH subtype of MB, the exact UW228-3 subtype is not yet clearly established. Thus, identifying protein markers and pathways in relation to EMT would also help elucidate their subtype classification. In this study, a large number of EMT-related genes were differentially expressed between the two cell lines, which may provide greater insight into the differences in their biological behaviour. Among the genes with differential expression between the two cell lines, the

upregulation of DSP and EGFR in DAOY relative to UW228-3 is consistent with a previous report that profiled the total transcriptome and proteome of these two lines (Higdon et al., 2017). Moreover, a comparative expression analysis of signature proteins and key components of signalling pathways indicated SHH as the primary signalling pathway in DAOY, and WNT as the main signalling pathway involved in UW228 (Higdon et al., 2017).

To our knowledge, few studies have been conducted to explore the relevance between the Trx system and EMT in brain cancers. This study identified for the first time that targeting TrxR by IQ10 might inhibit the migration and invasion of brain cancer cells through inhibiting pivotal EMT-related genes. However, as the data obtained from EMT arrays were not confirmed by repeat using single gene qRT-PCR or Western blotting, further verification of the link between Trx system inhibition and EMT-related gene expression needs to be conducted.

## 5.5 Conclusions

In addition to its cytotoxic and radiosensitising effects, IQ10 treatment significantly downregulated a number of pivotal EMT associated gene expression in brain cancer cells, suggesting that IQ10 might be a potential anti-migratory agent.

# Chapter 6 General discussion

## 6.1 General discussion

Brain tumours are the 9th most common cancer in the UK, accounting for 3% of all new cancer cases (Cancer Research UK, 2016a). Among all types of malignant brain tumours, GBM is the most common and aggressive type in adults; while in children the most prevalent type is MB. Despite the use of multimodal treatment strategies, including surgery, radiation and chemotherapy, the prognosis of malignant brain tumours remains poor (Zhang et al., 2017c), indicating the need for further understanding of disease onset, progression and response to treatments. Unfortunately, the potential molecular mechanisms underlying brain tumour carcinogenesis and progression remain unclear. Hence, identification and characterisation of the key clinicopathological factors underlying brain tumour progression and prognosis are needed to increase the efficacy of medical treatments so as to improve patient outcomes.

The Trx system is a key antioxidant pathway involved in defence against oxidative stress, and participates in various cellular processes including transcription, DNA damage recognition and repair, proliferation and apoptosis (reviewed in (Powis and Montfort, 2001, Biaglow and Miller, 2005, Gromer et al., 2004, Nguyen et al., 2006)). Elevated expression of Trx and TrxR are found in many human cancers including breast (Bhatia et al., 2016b), lung (Selenius et al., 2012), colon (Raffel et al., 2003), hepatoma (Choi et al., 2002), and pancreas (Powis and Kirkpatrick, 2007), and are associated with poor patient prognosis and treatment resistance. The protein expression of Trx system in brain tumour patients has also been reported, (Gollapalli et al., 2017, Jarvela et al., 2006, Haapasalo et al., 2003, Esen et al., 2015, Kemerdere et al., 2013, Zhang et al., 2017b), but almost all such studies focused on adult gliomas with, to the best of our knowledge, no studies having been conducted in paediatric brain tumours such as paediatric gliomas and MB. Moreover, among the limited studies that have been conducted very few assessed the prognostic/predictive value of Trx system proteins. Therefore, the clinical

importance of Trx system in brain tumours, especially paediatric gliomas and MB, is still largely understudied.

The current study assessed the expression of Trx system proteins, namely TrxR, Trx and TxNIP, in four independent brain tumour cohorts (i.e. adult GBM, paediatric LGG, paediatric HGG, and MB); and the association between protein expression and patient prognosis or clinicopathological variables was analysed. This is the first study to report upon the expression of all three members of Trx system proteins together in such a broad variety of brain tumour types and to evaluate their prognostic values. The results showed that all three members of the Trx system were expressed in all brain tumour types tested and significant variations in their expression between different tumour types/grades/regions were observed. Although some mixed results from survival analysis existed between different cohorts, there was a consistent finding that high levels of cytoplasmic TrxR equated to a worse prognosis in all tumour types studied, suggesting that it is potentially a very important therapeutic target in brain cancers generally. Therefore, using small molecules to specifically target TrxR might enhance the treatment efficacy in brain tumours.

There are a number of TrxR inhibitors that have been developed as potential anti-cancer agents, or as adjuncts to existing therapy, over the years (Gandin and Fernandes, 2015). Prof. Chris Moody's research group (School of Chemistry, University of Nottingham) developed a series of novel TrxR inhibitors, namely IQs, which exhibited potent anti-tumour activity against several types of human cancers both *in vitro* and *in vivo* (Yan et al., 2009a). However, the efficacy of these novel IQs had never before been examined in brain cancer cells. Hence, IQ10, one of the most potent IQs, was examined in the current study as a single agent and as a potential radiosensitiser. IQs were previously found to be potent inhibitors of TrxR activity both in pancreatic cancer cells and in cell-free systems (Yan et al., 2009a) so the insulin reduction assay was first conducted in the current study to assess whether IQ10 could also inhibit TrxR activity in brain cancer cells. As expected, data showed that

IQ10 potently inhibited TrxR activity in a dose-dependent manner at both 4 and 48-h post-treatment in different types of brain cancer cells. The inhibitory potency of IQ10 was equivalent to the well-characterised TrxR inhibitor auranofin, used as a positive control.

Having confirmed the effect of IQ10 on TrxR activity, the role of IQ10 in regulating TrxR expression was assessed by Western blotting. After 48 hours' IQ10 treatment, no significant alterations of TrxR expression was observed in brain cancer cells. Such data are consistent with a study conducted by Yan et al. (2009a), which also found that total TrxR protein levels were not altered after IQ treatment, albeit IQ3, in pancreatic cancer cells. Taking TrxR expression data together with activity results suggests that IQ10 potently inhibits TrxR activity but does not affect its expression in brain cancer cells, suggesting that IQ10 works by inhibiting TrxR function rather than regulating TrxR expression.

The current study then went on to assess the cytotoxicity of IQ10 in brain cancer cells in normoxic *vs.* hypoxic conditions and in 2D *vs.* 3D cultures. Results demonstrate that IQ10 substantially decreases proliferation and clonogenic survival of brain cancer cells under both normoxic and hypoxic conditions with the IC50s in the sub- to low micromolar range. In comparison to TMZ, a standard chemotherapeutic treatment for brain tumours, IQ10 was much more potent at decreasing proliferation and survival. The growth inhibitory and cytotoxic activity of IQs has also been assessed in previous studies (Yan et al., 2009a, 2012), in which they found that IQs displayed potent cytotoxicity against pancreatic cancer cell lines with growth inhibitory IC50s in the low nanomolar range. In addition, selected IQs were screened against the NCI-60 panel and were found to be particularly effective against colon, renal, and melanoma cancer cells (Yan et al., 2009a). Moreover, two of the most potent IQs, i.e. IQ9 and IQ10, have been shown to exert significant cytotoxic effects on breast and pancreatic cancer cells in studies conducted by Nurul Abdullah and Khaled Alhadyan, previous PhD students, in our research group. Taken together, all these findings including the current one suggest

that IQs may exhibit potent anticancer activity against a wide range of cancer types.

Tumour hypoxia is a well-established biological phenomenon that affects the curability of solid tumours, regardless of treatment modality (Walsh et al., 2014). In brain tumours, especially GBM, hypoxia is strongly linked to tumour progression, chemoradiotherapy resistance and poor patient outcomes (Cavazos and Brenner, 2016). Hence, agents capable of overcoming hypoxia resistance would be beneficial for brain tumour treatment. Since TrxR has been reported to be upregulated during hypoxia (Berggren et al., 1996), it was of interest to know whether IQ10 would be more effective under hypoxic conditions. Data show that IQ10 is equally effective in both normoxic and hypoxic conditions. An enhanced cytotoxicity of IQ10 under hypoxia was however, and somewhat unexpectedly, not observed with the underlying causes for such results remaining unclear. The cellular reductases such as NQO1, NQO2 and P450 may contribute to the hypoxic bioactivation and cytotoxicity of IQ10 in brain cancer cells but further experiments are needed to assess the changes in the reductase enzyme activities following IQ10 treatment under both normoxic and hypoxic conditions, to firmly confirm the activation mechanism in brain cancer cells. The mechanism of action of the IQs in pancreatic cancer cells has been proposed to involve metabolic reduction by cellular reductases, loss of a leaving group to generate a reactive electrophile resulting in alkylation of the selenocysteine residue in the active site of TrxR (Yan et al., 2009a). Dehn et al. (2006) reported that IQ1 exhibited its antitumour activity via inhibiting NQO1 in pancreatic cancer cell lines. In addition, NQO2 was shown to be able to activate IQs in cell-free systems (Yan et al., 2012). NQO1 and P450 were capable of reducing the indolequinone-based compound EO9 (Phillips et al., 2013). These findings suggest that the two electron reductases NQO1 and NQO2 and the one-electron reductase P450 may be involved in the reduction step of IQ10.

The traditional, and still widely used, 2D cell culture model used in the current investigation cannot fully mimic *in vivo* cellular microenvironments with

conclusions made from such 2D models requiring careful interpretation. In order to make *in vitro* models potentially more clinically applicable, 3D culture models have been developed and are being increasingly utilised in preclinical studies. Currently, multicellular tumour spheroids are considered as one of the most promising and popular 3D models for preclinical evaluation of novel anticancer agents (Ferreira et al., 2018, Li and Kumacheva, 2018). Therefore, the current study used a 3D spheroid model to compare the efficacy of IQ10 on brain cancer cells in 2D and 3D side by side. Compared with the 2D data, brain cancer cells cultured in 3D spheroids became more resistant to IQ10. Consistent with such data, a number of studies have also found that cells cultured in 3D systems are more refractory to anticancer drugs than cells grown in 2D cultures (Lovitt et al., 2014, Cox et al., 2015, Loessner et al., 2010, Karlsson et al., 2012). Such changes in drug sensitivity between 2D and 3D culture models are likely to be driven by various factors, including the cell-cell interactions, signalling pathway activations, cellular microenvironment and also drug uptake rate (Lee et al., 2013, Håkanson et al., 2010, Imamura et al., 2015b).

It has been reported that TrxR is often overexpressed in many aggressive cancers and that inhibition of TrxR can sensitise cancer cells to radiation (Urig and Becker, 2006, Smart et al., 2004, Karimpour et al., 2002). TrxR inhibitors such as MGd (Rockwell et al., 2002), auranofin (Wang et al., 2017a), and curcumin (Javvadi et al., 2010b) have been shown to act as promising radiosensitisers in the treatment of various cancer types. Therefore, in this study, IQ10 was assessed as a potential radiosensitiser in brain cancer cells. Clonogenic survival data demonstrate that, in normoxic conditions, IQ10 significantly increases radiosensitivity in all but the KNS42 cell line. The somewhat aberrant KNS42 paediatric GBM cell line data may be a reflection of the experiment using a uniform, and rather low, concentration of IQ10 (1 μM) for KNS42s, that might not be sufficient to cause any changes in its radiosensitivity – using equitoxic doses in the future would be of interest. In addition, the intrinsic radiosensitivity might be another factor affecting the

radiosensitising effect of IQ10 as radiosensitisation is appeared to be more effective in radioresistant cell lines than in radiosensitive lines (Franken et al., 2013). Thus, as the most radiosensitive line among all the brain cancer cell lines evaluated, KNS42 was more difficult to be radiosensitised by IQ10 as it is already very sensitive to the killing effects of ionising radiation. Other potential mechanisms underlining such results were not followed due to time limitations. If time had allowed, the TrxR activity, intracellular ROS levels, cell cycle and apoptosis characteristics of KNS42 cells could be assessed to further understand this phenomenon. In a previous study reported by de Andrade et al. (2016), KNS42 was rather radioresistant with only 20% reduction of colony formation after 4-Gy of irradiation; however there was a 98% reduction in the current study. Moreover, KNS42 was able to be significantly radiosensitised by chemotherapeutic agents such as the PARP inhibitor olaparib (van Vuurden et al., 2011). Such conflicting data on the *in vitro* radiation response of KNS42 cell line between different studies may lie with the different cell culture conditions and growth status (Raaphorst et al., 1989).

Hypoxic cancer cells are well recognised to be more resistant to radiotherapy and to represent the most aggressive fraction of a tumour. It is therefore important to develop effective therapeutic strategies to directly target hypoxic cancer cells in attempt to improve treatment (Pires et al., 2012). It was thought that inhibition of TrxR could be an effective way to sensitise hypoxic cancer cells to radiotherapy. Thus, the potential of IQ10 as a hypoxic radiosensitiser was evaluated in brain cancer cells. Unexpectedly, no radiosensitising effect induced by IQ10 was detected in brain cancer cells under hypoxic conditions, but such data are very preliminary and that much more work needs to be done to draw any firm conclusions as only one radiation dose was used and the drug treatment schedule was not ideal, making interpretation difficult and comparisons to normoxic data almost impossible. New hypoxia equipment is now available locally, adjacent to irradiation facilities, and so in future experiments it might be worthwhile to treat the hypoxic cells with 1 μM of IQ10 for 4 h (the treatment setting used in

normoxic experiment) prior to radiation. Since the hypoxic radiosensitising effect of IQ10 was evaluated based on two MB cell lines in the present study which may not be representative enough, more brain cancer cell lines including adult/paediatric glioma lines should be tested in the future work to verify the current findings.

As the behaviour of 3D cultured cells is more reflective of *in vivo* cellular responses (Edmondson et al., 2014), the 3D spheroid model was introduced to investigate and compare the radiosensitivity in 2D and 3D *in vitro* cultures of brain cancer cell lines. Interestingly, brain cancer cells cultured in spheroids became more sensitive to irradiation than cells grown in 2D monolayers – this finding is in contrast to others as cancer cells are generally found to be more radioresistant in 3D cell culture (Lin et al., 2009). The reason for these divergent results remains unclear. Possible explanations could include different methodological approaches and/or individual characteristics of the cell lines. These issues are discussed in greater detail in Section 4.4.

The effects of IQ10 on radioresponses of brain cancer cells was also evaluated using 3D spheroid model. Consistent with the results from 2D cultures, IQ10 also significantly sensitised brain cancer spheroids to irradiation. Although cells from spheroids are generally more resistant than monolayers to drugs and radiation, IQ10 still maintained its potent radiosensitising effect on spheroids, further suggesting that IQ10 may be a valuable radiosensitiser candidate for brain cancer treatment. As radiotherapy is conventionally delivered by fractionation, it would be interesting, in the future, to examine the radioresponse of IQ10 in 3D to fractionated irradiation, to further confirm its radiosensitising effects.

An important component of the present study was to evaluate and validate whether or not TrxR is the target for IQ10 to exert its cytotoxic and radiosensitising effects. A siRNA approach was used to knockdown TrxR expression in brain cancer cells, and the current results indicate that the cytotoxic and radiosensitising effects of IQ10 are due, in part, to functional inhibition of TrxR. In addition, TrxR is suggested to be one of the main targets

for IQ10 and targeting TrxR by IQ10 can be considered as a promising strategy to improve radioresponse. However, other targets and mechanisms may also be involved in IQ10's anticancer activity.

After confirming the role of TrxR as a regulator of radiosensitivity in brain cancer cells, the current study further investigated potential mechanisms underlying the radiosensitising effects of IQ10. The results from Chapter 4 showed that treatment with IQ10 resulted in elevated levels of ROS in brain cancer cells with a further increase when combined with $H_2O_2$, suggesting that IQ10 is able to increase oxidative stress and cells treated with IQ10 are less capable to deal with the oxidative stress induced by $H_2O_2$. In line with this result, IQ10 was found to increase the radiation-induced DNA damage as assessed by the γH2AX foci formation assay. Taken together, current results suggest that IQ10 inhibits TrxR activity, which induces intracellular ROS production and subsequent oxidative DNA damage, and ultimately allows the radiosensitisation of brain cancer cells. Additional mechanisms may also operate, for example, apoptosis and cell cycle progression might be induced by IQ10 and contribute to the radiosensitisation.

Additional experiments, in the present study, found that IQ10 markedly down-regulated a large number of EMT-related genes in brain cancer cells, indicating that targeting TrxR by IQ10 might inhibit the migration and invasion of brain cancer cells through inhibiting pivotal EMT-related genes. To the best of our knowledge, this is the first high-throughput screening study that has been conducted to explore the relevance between the Trx system and EMT in brain cancers, but further studies are needed to confirm current findings.

## 6.2 Limitations and suggestions for future work

Although the IHC study offers several strengths, there are also some limitations. The study did not compare the protein levels of Trx system in brain tumours with that found in corresponding normal tissues. It would be useful to include normal brain tissue as a comparator in the future to better understand the function of Trx system. In addition, a large amount of

important data was missing from the clinical database, due to the challenges facing data retrieval (the cases were collected as early as 1950s from multiple hospitals across England), and a proportion of cores within the TMAs could not be assessed due to missing tissue, cancer necrosis, or insufficient cancer cells, which reduced the number of cases that could be used for statistical analyses. Furthermore, the sample size of the cohorts, particularly the adult GBM cohort, was relatively small (n=18), but even so, with the interesting results presented, further investigation of these observations in larger cohorts are warranted. Finally, the expression of all three members of the Trx system proteins, i.e. TrxR, Trx, and TxNIP, were separately analysed in each tumour cohort, while the future work can be conducted using a bioinformatic approach to combine all markers to get a Trx system score.

It has been reported that certain TrxR inhibitors can preferentially kill cancer cells and spare normal cells. In order to investigate whether IQ10 also possesses such preference, MRC5 fibroblast cells were used to assess its cytotoxicity against normal cells. The results demonstrated that IQ10 seemed less toxic to MRC5 cells than to the majority of brain cancer cell lines tested. However, due to time limitations, the present study did not assess the cytotoxic and radiosensitising effects of IQ10 on a normal brain cell line (e.g. normal human astrocytes). As patients with brain tumours are particularly at risk for adverse late brain effects after (chemo)-radiotherapy, further experiments are required to explore the neurotoxic effects of IQ10 and radiation on at least one normal brain cell line.

To better understand the bioactivation of IQ10 against brain cancer cells, in this study, alterations in the protein expression of three reductases, namely NQO1, NQO2 and cytochrome P450, were evaluated following IQ10 treatment under both normoxic and hypoxic conditions. Results demonstrated that IQ10 did not affect expression levels of these reductases, except for NQO2, which was downregulated by IQ10 but only in DAOY cells under hypoxia. The current study only evaluated the function of reductases at protein level, the changes in their enzymatic activity were not measured due to time limitations. Since

protein levels may not necessarily reflect the corresponding enzyme activity, more experiments are required to measure the enzymatic activity of these reductases and search for other possible molecular targets to better understand the mechanism of action of IQ10 (upstream activators and downstream signalling pathways). Reducing enzymes such as cytochrome b5 reductase (b5R) and xanthine oxidase/xanthine dehydrogenase (XO/XDH) may also contribute to the bioreduction or cytotoxicity of IQ10 in cancer cells (Yan et al., 2008), therefore, it might be useful to include these reductases in future experiments. It is interesting to additionally assess IQ10 toxicity in a panel of reductase deficient cell lines, or in lines over-expressing specific reductase enzymes to identify the activation mechanism.

It should be noted that complete knockdown is often difficult to achieve by siRNA or shRNA methodologies with some residual protein, and therefore enzymatic activity, potentially remaining. In line with this, the TrxR activity, in the present study, could not be completely blocked by siRNA, thus causing data to be interpreted with some caution. To obtain entire removal of the protein CRISPR-Cas9 technology should to be considered even though the technique is time-consuming, laborious and expensive, particularly when applied to cancer cells that usually have a large number of chromosomal abnormalities.

As introduced in Section 1.2.2, Trx system regulates multiple cellular functions through interactions with different signalling molecules. Thus, TrxR inhibitor IQ10 may be expected to affect various downstream signalling pathways. Inhibition of such downstream functions, affected by IQ10, could be examined in future assays to confirm the specificity and mode of action, such as measuring protein and mRNA expression of Prx system by Western blotting and qRT-PCR, assessing apoptosis by annexin V-FITC apoptosis assay, examining transcription factors binding activities by inserting reporter gene and detecting enzyme by Luciferase assay, and determining the cell cycle block by propidium iodide staining and flow cytometry.

The BBB is a selective barrier formed by the endothelial cells that line cerebral microvessels (Abbott et al., 2006). It is estimated that >98% of drugs with molecular weights as low as 500 Da cannot pass through the BBB (Sarkar et al., 2014). While the presence of brain tumours compromises the integrity of BBB, the brain-tumour barrier is still a major obstacle to effective drug delivery into brain tumours (Karathanasis and Ghaghada, 2016). Indeed, poor drug penetration across the BBB is one of the largest barriers to effective treatments in brain tumours (Chornenkyy et al., 2015). Therefore, determination of drug's BBB permeability is a prerequisite for screening drugs which could take effects in CNS (Gao et al., 2017). For molecules to penetrate the BBB, a polar surface area (PSA) < 90 and a molecular weight <500 Da are usually needed (Hitchcock and Pennington, 2006). With a PSA of 68.31 and a molecular weight of 450.41, IQ10 may have the potential to cross the BBB. As such, experiments were conducted to predict the BBB penetration ability of IQ10 using caco-2 *in vitro* system with preliminary data suggesting that IQ10 was reasonably permeable and was not a substrate for efflux transporters (experiments were carried out by the contract research company Sygnature Discovery). TMZ, a standard chemotherapeutic treatment for various brain tumours and a control drug used in the present study, can efficiently cross the BBB due to its small molecular weight (194 Da) and lipophilicity (Schreck and Grossman, 2018). TMZ is a substrate for efflux transporter p-glycoprotein (PGP) and breast cancer related protein (BCRP) but not multidrug resistance protein 1 (MRP1) (Tivnan et al., 2015). Based upon the *in vitro* data discussed above, a further study to assess the BBB penetration of IQ10 in male CD-1 mice is ongoing (experiments are being conducted by Axis Bioservices, a Belfast based contract research company), with such data generated in the future, the BBB penetration ability of IQ10 will be better understood. If BBB penetration limits drug delivery there are other potential delivery strategies that could be considered, such as direct intratumoural delivery via convection-enhanced delivery (Hdeib and Sloan, 2011), ultrasound-mediated delivery (Choi et al., 2010), peptide carrier-mediated delivery (Sarkar et al., 2014),

nanoparticle delivery or intracerebral implants (Lu et al., 2014), intrathecal delivery (Nailor et al., 2016), and hydrogel-based delivery (Basso et al., 2018).

Apart from the IHC data, all results in this study were obtained using established *in vitro* cell line models; therefore, additional studies may wish to consider using primary, patient derived cells (e.g. the locally available GIN lines, which were derived from the invasive edge of the adult GBM tumours by a research group in Nottingham), tumour xenografts or ideally orthotopic mouse models to confirm the current findings and to further link experimental studies with the clinical setting. More importantly, the pharmacokinetic (PK, concentration *vs.* time) and pharmacodynamic (PD, effect *vs.* time) parameters of IQ10 should be examined in animal models, as PK/PD profiles are crucial for the prediction of drug efficacy in humans. In addition, the PK/PD data can help to guide the subsequent study design of the *in vivo* drug-radiation combination and fractionation experiments.

Data from the current study suggest that targeting TrxR by IQ10 might inhibit the EMT process in brain cancer cells. However, as the data obtained from EMT arrays were not confirmed by independent repeats (a single analysis of pooled mRNA from three independent experiments was conducted), further verification experiments such as qRT-PCR on specific genes or Western blotting should be conducted. It would also be useful to assess whether such changes in gene expression translate into a phenotypic difference in cell migration and/or invasion by conducting appropriate endpoint assays such as scratch wound migration and transwell invasion assays (Justus et al., 2014). Although the correlation between the Trx system and invasion/migration has been investigated in various cancer types (Farina et al., 2001, Farina et al., 2003, Wang et al., 2015a, Bhatia et al., 2016b, Yoo et al., 2006, Goldberg et al., 2003), few studies have been conducted with brain cancer lines, so it would be interesting to examine, in future work, the role that the Trx system plays in modulating brain cancer cell migration and invasion and whether this can be modulated by IQ10.

## 6.3 Final conclusions

The results of the current study are summarised in Table 6.1. In conclusion, the retrospective histopathology IHC based study demonstrates that Trx system proteins, namely TrxR, Trx and TxNIP, are widely expressed across a variety of brain tumour types with high cytoplasmic TrxR expression consistently associated with a worse prognosis in all brain tumour types studied, suggesting that TrxR is potentially a very important therapeutic target in brain cancers generally. The *in vitro* results show that IQ10 is a very potent TrxR inhibitor exhibiting single agent anti-proliferative and cytotoxic effects under both normoxic and hypoxic conditions and in both 2D and 3D culture systems. IQ10 was up to 1000 fold more potent than TMZ, the agent used clinically to treat brain tumours and used as a comparator in the current study. TrxR was confirmed as an important target of IQ10 and inhibition of it by IQ10 substantially sensitised both 2D and 3D cultured brain cancer cells to radiation, with this radiosensitising effect due, in part, to functional inhibition of TrxR activity, making cells less able to deal with oxidative stress with this leading to increased oxidative DNA damage and cell killing. In addition to its cytotoxic and radiosensitising effects, IQ10 might be a potential anti-migratory agent as treatment significantly downregulated pivotal EMT associated gene expression in brain cancer cells. Collectively, although further confirmation is required both *in vitro* and *in vivo*, the current study highlights TrxR as a potential therapeutic target and suggests that IQ10 could be a promising agent, either single or combined with radiation, to improve outcome in brain tumours.

**Table 6.1 Results summary.**

| | **Biomarkers** | **Adult GBM** | **pLGG** | **pHGG** | **MB** |
|---|---|---|---|---|---|
| **IHC (OS)** | Cytoplasmic TrxR | √ | √ | √ | √ |
| | Nuclear TrxR | x | √ | x | x |
| | Cytoplasmic Trx | x | √ | √ | √ |
| | Nuclear Trx | x | √ | x | √ |
| | TxNIP | x | √ | x | x |
| ***In vitro*** | **Endogenous expression of Trx proteins** | **SNB19** | **SF188** | **KNS42** | **DAOY** | **UW228-3** |
| | TrxR | KNS42 > SF188 > UW228-3 > SNB19 > DAOY | | | | |
| | Trx | KNS42 > UW228-3 > SNB19 > DAOY > SF188 | | | | |
| | TxNIP | UW228-3 > SNB19 > KNS42 > SF188 > DAOY | | | | |
| | **Intrinsic Radiosensitivity** | **SNB19** | **SF188** | **KNS42** | **DAOY** | **UW228-3** |
| | 2D | KNS42 > SF188≈UW228-3 > SNB19≈DAOY | | | | |
| | 3D | UW228-3 > DAOY | | | | |
| | Hypoxia | UW228-3 > DAOY | | | | |
| | **Response to IQ10** | **SNB19** | **SF188** | **KNS42** | **DAOY** | **UW228-3** |
| | TrxR activity | | — — | | — — | — — |
| | TrxR expression | | | | O | O |
| | Trx expression | | | | O | O |
| | TxNIP expression | | | | O | O |
| | Toxicity | | | | | |
| | 2D | + | + + | + | + + | + + |
| | 3D | | | | + + | + + |
| | Hypoxia | | | | + + | + + |
| | EMT | | | | — — | — — |
| | Radiosensitivity | | | | | |
| | 2D | | + + | O | + + | + + |
| | 3D | | | | + + | + + |
| | Hypoxia | | | | O | O |
| | ROS level | | | | + + | + + |
| | γH2AX foci | | | | + + | + + |
| | **TrxR knockdown** | **SNB19** | **SF188** | **KNS42** | **DAOY** | **UW228-3** |
| | Toxicity of IQ10 | | + | | + | |
| | Radiosensitivity | | + | | + | |

Abbreviations: "√" significant association; "x" no association. "– –" significant decrease; "+ +" significant increase; "– " moderate decrease; "+" moderate increase; "O" no change.

# References


ABBOTT, N. J., RONNBACK, L. & HANSSON, E. 2006. Astrocyte-endothelial interactions at the blood-brain barrier. *Nat Rev Neurosci,* 7**,** 41-53.

ABOIAN, M. S., SOLOMON, D. A., FELTON, E., MABRAY, M. C., VILLANUEVA-MEYER, J. E., MUELLER, S. & CHA, S. 2017. Imaging Characteristics of Pediatric Diffuse Midline Gliomas with Histone H3 K27M Mutation. *AJNR Am J Neuroradiol,* 38**,** 795-800.

AHLBOM, A., GREEN, A., KHEIFETS, L., SAVITZ, D. & SWERDLOW, A. 2004. Epidemiology of health effects of radiofrequency exposure. *Environ Health Perspect,* 112**,** 1741-54.

AHMAD, F., GHOSH, S., SINHA, S., JOSHI, S. D., MEHTA, V. S. & SEN, E. 2015. TGF-β-induced hCG-β regulates redox homeostasis in glioma cells. *Molecular and cellular biochemistry,* 399**,** 105-112.

AHMADI, M., AHMADIHOSSEINI, Z., ALLISON, S. J., BEGUM, S., ROCKLEY, K., SADIQ, M., . . . PHILLIPS, R. M. 2014. Hypoxia modulates the activity of a series of clinically approved tyrosine kinase inhibitors. *British journal of pharmacology,* 171**,** 224-236.

AHMED, E. M., BANDOPADHYAY, G., COYLE, B. & GRABOWSKA, A. 2018. A HIF-independent, CD133-mediated mechanism of cisplatin resistance in glioblastoma cells. *Cell Oncol (Dordr),* 41**,** 319-328.

AHMED, S. U., CARRUTHERS, R., GILMOUR, L., YILDIRIM, S., WATTS, C. & CHALMERS, A. J. 2015. Selective inhibition of parallel DNA damage response pathways optimizes radiosensitization of glioblastoma stem-like cells. *Cancer research,* 75**,** 4416-4428.

AHN, K. J., LEE, H. S., BAI, S. K. & SONG, C. W. 2013. Enhancement of radiation effect using beta-lapachone and underlying mechanism. *Radiation oncology journal,* 31**,** 57.

ALBERTELLA, M. R., LOADMAN, P. M., JONES, P. H., PHILLIPS, R. M., RAMPLING, R., BURNET, N., . . . DUNK, C. R. 2008. Hypoxia-selective targeting by the bioreductive prodrug AQ4N in patients with solid tumors: results of a phase I study. *Clinical cancer research,* 14**,** 1096-1104.

ALBRIGHT, A. L., SPOSTO, R., HOLMES, E., ZELTZER, P. M., FINLAY, J. L., WISOFF, J. H., . . . POLLACK, I. F. 2000. Correlation of neurosurgical subspecialization with outcomes in children with malignant brain tumors. *Neurosurgery,* 47**,** 879-85; discussion 885-7.

ALDAPE, K., ZADEH G FAU - MANSOURI, S., MANSOURI S FAU - REIFENBERGER, G., REIFENBERGER G FAU - VON DEIMLING, A. & VON DEIMLING, A. 2015. Glioblastoma: pathology, molecular mechanisms and markers.

AMIR ASLANI, B. & GHOBADI, S. 2016. Studies on oxidants and antioxidants with a brief glance at their relevance to the immune system. *Life Sci,* 146**,** 163-73.

AN, Z., AKSOY, O., ZHENG, T., FAN, Q.-W. & WEISS, W. A. 2018. Epidermal growth factor receptor and EGFRvIII in glioblastoma: signaling pathways and targeted therapies. *Oncogene,* 37**,** 1561-1575.

ANAND, P., KUNNUMAKKARA, A. B., NEWMAN, R. A. & AGGARWAL, B. B. 2007. Bioavailability of curcumin: problems and promises. *Molecular pharmaceutics,* 4**,** 807-818.

ANESTAL, K. & ARNER, E. S. 2003. Rapid induction of cell death by selenium-compromised thioredoxin reductase 1 but not by the fully active enzyme containing selenocysteine. *J Biol Chem,* 278**,** 15966-72.

ANGAJI, S. A., MOUSAVI, S. F. & BABAPOUR, E. 2012. Antioxidants: A few key points. *Annals of Biological Research,* 3**,** 3968-77.

ANTONENKOV, V. D., GRUNAU, S., OHLMEIER, S. & HILTUNEN, J. K. 2010. Peroxisomes are oxidative organelles. *Antioxid Redox Signal,* 13**,** 525-37.

ARAI, R. J., MASUTANI, H., YODOI, J., DEBBAS, V., LAURINDO, F. R., STERN, A. & MONTEIRO, H. P. 2006. Nitric oxide induces thioredoxin-1 nuclear translocation: possible association with the p21Ras survival pathway. *Biochem Biophys Res Commun,* 348**,** 1254-60.

ARNER, E. S. & HOLMGREN, A. 2000. Physiological functions of thioredoxin and thioredoxin reductase. *Eur J Biochem,* 267**,** 6102-9.

ARNER, E. S. & HOLMGREN, A. 2006. The thioredoxin system in cancer. *Semin Cancer Biol,* 16**,** 420-6.

ARNER, E. S., NAKAMURA, H., SASADA, T., YODOI, J., HOLMGREN, A. & SPYROU, G. 2001. Analysis of the inhibition of mammalian thioredoxin, thioredoxin reductase, and glutaredoxin by cis-diamminedichloroplatinum (II) and its major metabolite, the glutathione-platinum complex. *Free Radic Biol Med,* 31**,** 1170-8.

ASHBY, L. S., SMITH, K. A. & STEA, B. 2016. Gliadel wafer implantation combined with standard radiotherapy and concurrent followed by adjuvant temozolomide for treatment of newly diagnosed high-grade glioma: a systematic literature review. *World J Surg Oncol,* 14**,** 225.

ASHCRAFT, K. A., BOSS, M.-K., TOVMASYAN, A., CHOUDHURY, K. R., FONTANELLA, A. N., YOUNG, K. H., . . . PARK, W. 2015. Novel manganese-porphyrin superoxide dismutase-mimetic widens the therapeutic margin in a preclinical head and neck cancer model. *International Journal of Radiation Oncology* Biology* Physics,* 93**,** 892-900.

ASHWELL, S. & ZABLUDOFF, S. 2008. DNA damage detection and repair pathways--recent advances with inhibitors of checkpoint kinases in cancer therapy. *Clin Cancer Res,* 14**,** 4032-7.

ASSISTANCE PUBLIQUE. 2015. *gliomasPCV Only in 1p/19q Codeleted Anaplastic Gliomas* [Online]. Available: https://ClinicalTrials.gov/show/NCT02444000 [Accessed 10/12/2018].

AUM, D. J., KIM, D. H., BEAUMONT, T. L., LEUTHARDT, E. C., DUNN, G. P. & KIM, A. H. 2014. Molecular and cellular heterogeneity: the hallmark of glioblastoma. *Neurosurg Focus,* 37**,** E11.

AVERY, S. V. 2011. Molecular targets of oxidative stress. *Biochem J,* 434**,** 201-10.

BAAN, R., GROSSE, Y., LAUBY-SECRETAN, B., EL GHISSASSI, F., BOUVARD, V., BENBRAHIM-TALLAA, L., . . . STRAIF, K. 2011. Carcinogenicity of radiofrequency electromagnetic fields. *Lancet Oncol,* 12**,** 624-6.

BABIKER, H. M., MCBRIDE, A., COOKE, L. S. & MAHADEVAN, D. 2017. Therapeutic potential of investigational CHK-1 inhibitors for the treatment of solid tumors. *Expert Opin Investig Drugs,* 26**,** 1063-1072.

BABIOR, B. M. 1999. NADPH oxidase: an update. *Blood,* 93**,** 1464-76.

BAILEY, S. M., LEWIS, A. D., PATTERSON, L. H., FISHER, G. R., KNOX, R. J. & WORKMAN, P. 2001. Involvement of NADPH: cytochrome P450 reductase in the activation of indoloquinone EO9 to free radical and DNA damaging species5. *Biochemical pharmacology,* 62**,** 461-468.

BAKER, A., PAYNE, C. M., BRIEHL, M. M. & POWIS, G. 1997a. Thioredoxin, a gene found overexpressed in human cancer, inhibits apoptosis in vitro and in vivo. *Cancer research,* 57**,** 5162-5167.

BAKER, A., PAYNE, C. M., BRIEHL, M. M. & POWIS, G. 1997b. Thioredoxin, a gene found overexpressed in human cancer, inhibits apoptosis in vitro and in vivo. *Cancer Res,* 57**,** 5162-7.

BALBOUS, A., CORTES, U., GUILLOTEAU, K., RIVET, P., PINEL, B., DUCHESNE, M., . . . BENSADOUN, R. J. 2016. A radiosensitizing effect of RAD51 inhibition in glioblastoma stem-like cells. *BMC cancer,* 16**,** 604.

BARNEY, C. L., BROWN, A. P., GROSSHANS, D. R., MCALEER, M. F., DE GROOT, J. F., PUDUVALLI, V., . . . MAHAJAN, A. 2014. Technique, outcomes, and acute toxicities in adults treated with proton beam craniospinal irradiation. *Neuro-oncology,* 16**,** 303-309.

BARNHOLTZ-SLOAN, J. S., OSTROM, Q. T. & COTE, D. 2018. Epidemiology of Brain Tumors. *Neurol Clin,* 36**,** 395-419.

BARRALLO-GIMENO, A. & NIETO, M. A. 2005. The Snail genes as inducers of cell movement and survival: implications in development and cancer. *Development,* 132**,** 3151-3161.

BARTLETT, F., KORTMANN, R. & SARAN, F. 2013. Medulloblastoma. *Clin Oncol (R Coll Radiol),* 25**,** 36-45.

BASKAR, R. 2010. Emerging role of radiation induced bystander effects: Cell communications and carcinogenesis. *Genome Integr,* 1**,** 13.

BASKAR, R., LEE, K. A., YEO, R. & YEOH, K.-W. 2012. Cancer and radiation therapy: current advances and future directions. *International journal of medical sciences,* 9**,** 193-199.

BASSO, J., MIRANDA, A., NUNES, S., COVA, T., SOUSA, J., VITORINO, C. & PAIS, A. 2018. Hydrogel-Based Drug Delivery Nanosystems for the Treatment of Brain Tumors. *Gels,* 4.

BAST, A. 1986. Is formation of reactive oxygen by cytochrome P-450 perilous and predictable? *Trends in Pharmacological Sciences,* 7**,** 266-270.

BATCHALA, P. P., MUTTIKKAL, T. J. E., DONAHUE, J. H., PATRIE, J. T., SCHIFF, D., FADUL, C. E., . . . PATEL, S. H. 2019. Neuroimaging-Based Classification Algorithm for Predicting 1p/19q-Codeletion Status in IDH-Mutant Lower Grade Gliomas. *AJNR Am J Neuroradiol,* 40**,** 426-432.

BAUMERT, B. G., HEGI, M. E., VAN DEN BENT, M. J., VON DEIMLING, A., GORLIA, T., HOANG-XUAN, K., . . . STUPP, R. 2016. Temozolomide

chemotherapy versus radiotherapy in high-risk low-grade glioma (EORTC 22033-26033): a randomised, open-label, phase 3 intergroup study. *Lancet Oncol,* 17**,** 1521-1532.

BAX, D. A., LITTLE, S. E., GASPAR, N., PERRYMAN, L., MARSHALL, L., VIANA-PEREIRA, M., . . . VASSAL, G. 2009. Molecular and phenotypic characterisation of paediatric glioma cell lines as models for preclinical drug development. *PloS one,* 4**,** e5209.

BECKER, D., DICKMAN, M., GLADYSHEV, V. & RAGSDALE, S. 2007. *Redox biochemistry*, John Wiley & Sons.

BEIER, D., SCHULZ, J. B. & BEIER, C. P. 2011. Chemoresistance of glioblastoma cancer stem cells--much more complex than expected. *Mol Cancer,* 10**,** 128.

BENSON, V. S., PIRIE, K., SCHUZ, J., REEVES, G. K., BERAL, V. & GREEN, J. 2013. Mobile phone use and risk of brain neoplasms and other cancers: prospective study. *Int J Epidemiol,* 42**,** 792-802.

BEPPU, T., KAMADA, K., NAKAMURA, R., OIKAWA, H., TAKEDA, M., FUKUDA, T., . . . OGAWA, A. 2003. A phase II study of radiotherapy after hyperbaric oxygenation combined with interferon-beta and nimustine hydrochloride to treat supratentorial malignant gliomas. *J Neurooncol,* 61**,** 161-70.

BERGGREN, M., GALLEGOS, A., GASDASKA, J. R., GASDASKA, P. Y., WARNEKE, J. & POWIS, G. 1996. Thioredoxin and thioredoxin reductase gene expression in human tumors and cell lines, and the effects of serum stimulation and hypoxia. *Anticancer Res,* 16**,** 3459-66.

BERNIER, J., HALL, E. J. & GIACCIA, A. 2004. Radiation oncology: a century of achievements. *Nat Rev Cancer,* 4**,** 737-47.

BERTE, N., PIÉE-STAFFA, A., PIECHA, N., WANG, M., BORGMANN, K., KAINA, B. & NIKOLOVA, T. 2016. Targeting homologous recombination by pharmacological inhibitors enhances the killing response of glioblastoma cells treated with alkylating drugs. *Molecular cancer therapeutics,* 15**,** 2665-2678.

BHARDWAJ, R., SHARMA, P. K., JADON, S. P. & VARSHNEY, R. 2012. A combination of 2-deoxy-D-glucose and 6-aminonicotinamide induces cell cycle arrest and apoptosis selectively in irradiated human malignant cells. *Tumour Biol,* 33**,** 1021-30.

BHATIA, M., LOVITT, C. J., RANINGA, P. V., AVERY, V. M., DI TRAPANI, G. & TONISSEN, K. F. 2016a. Expression of the thioredoxin system in an in vivo-like cancer cell environment upon auranofin treatment. *Eur J Cell Biol,* 95**,** 378-388.

BHATIA, M., MCGRATH, K. L., DI TRAPANI, G., CHAROENTONG, P., SHAH, F., KING, M. M., . . . TONISSEN, K. F. 2016b. The thioredoxin system in breast cancer cell invasion and migration. *Redox Biol,* 8**,** 68-78.

BHATIA, M., MCGRATH, K. L., DI TRAPANI, G., CHAROENTONG, P., SHAH, F., KING, M. M., . . . TONISSEN, K. F. 2016c. The thioredoxin system in breast cancer cell invasion and migration. *Redox biology,* 8**,** 68-78.

BHATT, A. N., CHAUHAN, A., KHANNA, S., RAI, Y., SINGH, S., SONI, R., . . . DWARAKANATH, B. S. 2015. Transient elevation of glycolysis confers radio-resistance by facilitating DNA repair in cells. *BMC Cancer,* 15**,** 335.

BIAGLOW, J. E. & MILLER, R. A. 2005. The thioredoxin reductase/thioredoxin system: novel redox targets for cancer therapy. *Cancer biology & therapy,* 4**,** 13-20.

BINDOLI, A., RIGOBELLO, M. P., SCUTARI, G., GABBIANI, C., CASINI, A. & MESSORI, L. 2009. Thioredoxin reductase: a target for gold compounds acting as potential anticancer drugs. *Coordination Chemistry Reviews,* 253**,** 1692-1707.

BINDRA, R. S., CHALMERS, A. J., EVANS, S. & DEWHIRST, M. 2017. GBM radiosensitizers: dead in the water...or just the beginning? *J Neurooncol,* 134**,** 513-521.

BISHOP, A. J., GREENFIELD, B., MAHAJAN, A., PAULINO, A. C., OKCU, M. F., ALLEN, P. K., . . . GROSSHANS, D. R. 2014. Proton beam therapy versus conformal photon radiation therapy for childhood craniopharyngioma: multi-institutional analysis of outcomes, cyst dynamics, and toxicity. *International journal of radiation oncology, biology, physics,* 90**,** 354-361.

BLOKHINA, O., VIROLAINEN, E. & FAGERSTEDT, K. V. 2003. Antioxidants, oxidative damage and oxygen deprivation stress: a review. *Annals of botany,* 91**,** 179-194.

BLOMSTRAND, M., BRODIN, N. P., MUNCK AF ROSENSCHOLD, P., VOGELIUS, I. R., SANCHEZ MERINO, G., KIIL-BERTHLESEN, A., . . . BJORK-ERIKSSON, T. 2012. Estimated clinical benefit of protecting neurogenesis in the developing brain during radiation therapy for pediatric medulloblastoma. *Neuro Oncol,* 14**,** 882-9.

BLOOMFIELD, K. L., OSBORNE, S. A., KENNEDY, D. D., CLARKE, F. M. & TONISSEN, K. F. 2003. Thioredoxin-mediated redox control of the transcription factor Sp1 and regulation of the thioredoxin gene promoter. *Gene,* 319**,** 107-116.

BOBOLA, M. S., SILBER, J. R., ELLENBOGEN, R. G., GEYER, J. R., BLANK, A. & GOFF, R. D. 2005. O6-methylguanine-DNA methyltransferase, O6-benzylguanine, and resistance to clinical alkylators in pediatric primary brain tumor cell lines. *Clinical Cancer Research,* 11**,** 2747-2755.

BODGI, L., BAHMAD, H. F., ARAJI, T., AL CHOBOQ, J., BOU-GHARIOS, J., CHEAITO, K., . . . ABOU-KHEIR, W. 2019. Assessing Radiosensitivity of Bladder Cancer In Vitro: A 2D vs 3D Approach. *Frontiers in Oncology,* 9**,** 153.

BOULANGER, J. M. & LARBRISSEAU, A. 2005. Neurofibromatosis type 1 in a pediatric population: Ste-Justine's experience. *Can J Neurol Sci,* 32**,** 225-31.

BRACHMAN, D. G., PUGH, S. L., ASHBY, L. S., THOMAS, T. A., DUNBAR, E. M., NARAYAN, S., . . . CURRAN, W. P. 2015a. Phase 1/2 Trials of Temozolomide, Motexafin Gadolinium, and 60-Gy Fractionated Radiation for Newly Diagnosed Supratentorial Glioblastoma

Multiforme: Final Results of RTOG 0513. *International Journal of Radiation Oncology*Biology*Physics,* 91**,** 961-967.

BRACHMAN, D. G., PUGH, S. L., ASHBY, L. S., THOMAS, T. A., DUNBAR, E. M., NARAYAN, S., . . . CURRAN, W. P. 2015b. Phase 1/2 trials of Temozolomide, Motexafin Gadolinium, and 60-Gy fractionated radiation for newly diagnosed supratentorial glioblastoma multiforme: final results of RTOG 0513. *Int J Radiat Oncol Biol Phys,* 91**,** 961-7.

BRAGANZA, M. Z., KITAHARA, C. M., BERRINGTON DE GONZALEZ, A., INSKIP, P. D., JOHNSON, K. J. & RAJARAMAN, P. 2012. Ionizing radiation and the risk of brain and central nervous system tumors: a systematic review. *Neuro Oncol,* 14**,** 1316-24.

BRAJŠA, K., VUJASINOVIĆ, I., JELIĆ, D., TRZUN, M., ZLATAR, I., KARMINSKI-ZAMOLA, G. & HRANJEC, M. 2016. Antitumor activity of amidino-substituted benzimidazole and benzimidazo [1, 2-a] quinoline derivatives tested in 2D and 3D cell culture systems. *Journal of enzyme inhibition and medicinal chemistry,* 31**,** 1139-1145.

BRANDES, A. A. & PARIS, M. K. 2004. Review of the prognostic factors in medulloblastoma of children and adults. *Crit Rev Oncol Hematol,* 50**,** 121-8.

BRAT, D. J., VERHAAK, R. G., ALDAPE, K. D., YUNG, W. K., SALAMA, S. R., COOPER, L. A., . . . ZHANG, J. 2015. Comprehensive, Integrative Genomic Analysis of Diffuse Lower-Grade Gliomas. *N Engl J Med,* 372**,** 2481-98.

BRAY, F., FERLAY, J., SOERJOMATARAM, I., SIEGEL, R. L., TORRE, L. A. & JEMAL, A. 2018. Global cancer statistics 2018: GLOBOCAN estimates of incidence and mortality worldwide for 36 cancers in 185 countries. *CA Cancer J Clin*.

BRENNAN, C. W., VERHAAK, R. G., MCKENNA, A., CAMPOS, B., NOUSHMEHR, H., SALAMA, S. R., . . . CHIN, L. 2013. The somatic genomic landscape of glioblastoma. *Cell,* 155**,** 462-77.

BRENNER, A. V., LINET, M. S., FINE, H. A., SHAPIRO, W. R., SELKER, R. G., BLACK, P. M. & INSKIP, P. D. 2002. History of allergies and autoimmune diseases and risk of brain tumors in adults. *Int J Cancer,* 99**,** 252-9.

BRESLIN, S. & O'DRISCOLL, L. 2016. The relevance of using 3D cell cultures, in addition to 2D monolayer cultures, when evaluating breast cancer drug sensitivity and resistance. *Oncotarget,* 7**,** 45745-45756.

BRITTEN, R. A., EVANS, A. J., ALLALUNIS-TURNER, M. J. & PEARCEY, R. G. 1996. Effect of cisplatin on the clinically relevant radiosensitivity of human cervical carcinoma cell lines. *Int J Radiat Oncol Biol Phys,* 34**,** 367-74.

BROWN, J. M. & WILSON, W. R. 2004. Exploiting tumour hypoxia in cancer treatment. *Nature Reviews Cancer,* 4**,** 437.

BROWN, P. D., BUCKNER, J. C., O'FALLON, J. R., ITURRIA, N. L., BROWN, C. A., O'NEILL, B. P., . . . SHAW, E. G. 2004. Adult patients with supratentorial pilocytic astrocytomas: a prospective multicenter clinical trial. *Int J Radiat Oncol Biol Phys,* 58**,** 1153-60.

BUCKNER, J. C., SHAW, E. G., PUGH, S. L., CHAKRAVARTI, A., GILBERT, M. R., BARGER, G. R., . . . CURRAN, W. J., JR. 2016. Radiation plus

Procarbazine, CCNU, and Vincristine in Low-Grade Glioma. *N Engl J Med,* 374**,** 1344-55.

BURD, R., LAVORGNA, S. N., LENAZ, L., REDDY, G., KONG, X., WACHSBERGER, P. R. & DICKER, A. P. 2005. Radiosensitization of hypoxic tumors by the bioreductive agent apaziquone (EO9, EOquin (TM)). *Clin Cancer Res,* 11**,** 9008s.

BURKHARD, C., DI PATRE, P. L., SCHULER, D., SCHULER, G., YASARGIL, M. G., YONEKAWA, Y., . . . OHGAKI, H. 2003. A population-based study of the incidence and survival rates in patients with pilocytic astrocytoma. *J Neurosurg,* 98**,** 1170-4.

BUSH, N. A. & BUTOWSKI, N. 2017. The Effect of Molecular Diagnostics on the Treatment of Glioma. *Curr Oncol Rep,* 19**,** 26.

BUTLER, L. M., ZHOU, X., XU, W.-S., SCHER, H. I., RIFKIND, R. A., MARKS, P. A. & RICHON, V. M. 2002. The histone deacetylase inhibitor SAHA arrests cancer cell growth, up-regulates thioredoxin-binding protein-2, and down-regulates thioredoxin. *Proceedings of the National Academy of Sciences,* 99**,** 11700-11705.

BUTOWSKI, N. A. 2015. Epidemiology and diagnosis of brain tumors. *Continuum (Minneap Minn),* 21**,** 301-13.

BUTTERWORTH, K. T., MCMAHON, S. J., HOUNSELL, A. R., O'SULLIVAN, J. M. & PRISE, K. M. 2013. Bystander signalling: exploring clinical relevance through new approaches and new models. *Clin Oncol (R Coll Radiol),* 25**,** 586-92.

CADENAS, C., FRANCKENSTEIN, D., SCHMIDT, M., GEHRMANN, M., HERMES, M., GEPPERT, B., . . . HENGSTLER, J. G. 2010. Role of thioredoxin reductase 1 and thioredoxin interacting protein in prognosis of breast cancer. *Breast Cancer Res,* 12**,** R44.

CAI, W., ZHANG, B., DUAN, D., WU, J. & FANG, J. 2012a. Curcumin targeting the thioredoxin system elevates oxidative stress in HeLa cells. *Toxicol Appl Pharmacol,* 262**,** 341-8.

CAI, W., ZHANG, L., SONG, Y., WANG, B., ZHANG, B., CUI, X., . . . FANG, J. 2012b. Small molecule inhibitors of mammalian thioredoxin reductase. *Free Radical Biology and Medicine,* 52**,** 257-265.

CAIRNCROSS, G., WANG, M., SHAW, E., JENKINS, R., BRACHMAN, D., BUCKNER, J., . . . MEHTA, M. 2013. Phase III trial of chemoradiotherapy for anaplastic oligodendroglioma: long-term results of RTOG 9402. *J Clin Oncol,* 31**,** 337-43.

CALAF, G. M., URZUA, U., TERMINI, L. & AGUAYO, F. 2018. Oxidative stress in female cancers. *Oncotarget,* 9**,** 23824-23842.

CALBOLI, F. C. F., COX, D. G., BURING, J. E., GAZIANO, J. M., MA, J., STAMPFER, M., . . . MICHAUD, D. S. 2011. Prediagnostic plasma IgE levels and risk of adult glioma in four prospective cohort studies. *Journal of the National Cancer Institute,* 103**,** 1588-1595.

CAMP, R. L., DOLLED-FILHART, M. & RIMM, D. L. 2004. X-tile: a new bio-informatics tool for biomarker assessment and outcome-based cut-point optimization. *Clinical cancer research,* 10**,** 7252-7259.

CANCER RESEARCH UK. 2015. *Brain, other CNS and intracranial tumours risk factors* [Online]. Available: https://www.cancerresearchuk.org/health-professional/cancer-statistics/statistics-by-cancer-type/brain-other-cns-and-intracranial-tumours/risk-factors#heading-Four [Accessed 29 Oct 2018].

CANCER RESEARCH UK. 2016a. *Brain, other CNS and intracranial tumours statistics* [Online]. Available: https://www.cancerresearchuk.org/health-professional/cancer-statistics/statistics-by-cancer-type/brain-other-cns-and-intracranial-tumours#heading-One [Accessed 29 Oct 2018].

CANCER RESEARCH UK. 2016b. *Survival for different types of brain tumour* [Online]. Available: https://www.cancerresearchuk.org/about-cancer/brain-tumours/survival [Accessed 29 Oct 2018].

CARAMES MASANA, F. & DE REIJKE, T. M. 2017. The efficacy of Apaziquone in the treatment of bladder cancer. *Expert Opin Pharmacother,* 18**,** 1781-1788.

CARDE, P., TIMMERMAN, R., MEHTA, M. P., KOPROWSKI, C. D., FORD, J., TISHLER, R. B., . . . RENSCHLER, M. F. 2001. Multicenter phase Ib/II trial of the radiation enhancer motexafin gadolinium in patients with brain metastases. *J Clin Oncol,* 19**,** 2074-83.

CARETTI, V., HIDDINGH, L., LAGERWEIJ, T., SCHELLEN, P., KOKEN, P. W., HULLEMAN, E., . . . NOSKE, D. P. 2013. WEE1 kinase inhibition enhances the radiation response of diffuse intrinsic pontine gliomas. *Molecular cancer therapeutics,* 12**,** 141-150.

CARLSON, B. A., YOO, M.-H., TOBE, R., MUELLER, C., NARANJO-SUAREZ, S., HOFFMANN, V. J., . . . HATFIELD, D. L. 2012. Thioredoxin reductase 1 protects against chemically induced hepatocarcinogenesis via control of cellular redox homeostasis. *Carcinogenesis,* 33**,** 1806-1813.

CARRUTHERS, R., AHMED, S. U., STRATHDEE, K., GOMEZ-ROMAN, N., AMOAH-BUAHIN, E., WATTS, C. & CHALMERS, A. J. 2015a. Abrogation of radioresistance in glioblastoma stem-like cells by inhibition of ATM kinase. *Molecular oncology,* 9**,** 192-203.

CARRUTHERS, R., AHMED, S. U., STRATHDEE, K., GOMEZ-ROMAN, N., AMOAH-BUAHIN, E., WATTS, C. & CHALMERS, A. J. 2015b. Abrogation of radioresistance in glioblastoma stem-like cells by inhibition of ATM kinase. *Mol Oncol,* 9**,** 192-203.

CASTEL, D., PHILIPPE, C., CALMON, R., LE DRET, L., TRUFFAUX, N., BODDAERT, N., . . . DEBILY, M. A. 2015. Histone H3F3A and HIST1H3B K27M mutations define two subgroups of diffuse intrinsic pontine gliomas with different prognosis and phenotypes. *Acta Neuropathol,* 130**,** 815-27.

CAVAZOS, D. A. & BRENNER, A. J. 2016. Hypoxia in astrocytic tumors and implications for therapy. *Neurobiol Dis,* 85**,** 227-233.

CENAS, N., NIVINSKAS, H., ANUSEVICIUS, Z., SARLAUSKAS, J., LEDERER, F. & ARNER, E. S. 2004. Interactions of quinones with thioredoxin reductase: a challenge to the antioxidant role of the mammalian selenoprotein. *J Biol Chem,* 279**,** 2583-92.

CENAS, N., PRAST, S., NIVINSKAS, H., SARLAUSKAS, J. & ARNÉR, E. S. 2006. Interactions of nitroaromatic compounds with the mammalian selenoprotein thioredoxin reductase and the relation to induction of apoptosis in human cancer cells. *Journal of biological chemistry,* 281**,** 5593-5603.

CENTRE LEON BERARD. 2012. *Study of Vismodegib in Combination With Temozolomide Versus Temozolomide Alone in Patients With Medulloblastomas With an Activation of the Sonic Hedgehog Pathway* [Online]. Available: https://ClinicalTrials.gov/show/NCT01601184 [Accessed 06/12/2018].

CHAKRAVARTI, A., BERKEY, B., ROBINS, H. I., GUHA, A., CURRAN, W. J., BRACHMAN, D., . . . MEHTA, M. 2006. An update of phase II results from RTOG 0211: A phase I/II study of gefitinib with radiotherapy in newly diagnosed glioblastoma. *Journal of Clinical Oncology,* 24**,** 1527-1527.

CHALMERS, A. J. 2010. Overcoming resistance of glioblastoma to conventional cytotoxic therapies by the addition of PARP inhibitors. *Anticancer Agents Med Chem,* 10**,** 520-33.

CHAMBERLAIN, M. C. 2010. Temozolomide: therapeutic limitations in the treatment of adult high-grade gliomas. *Expert Rev Neurother,* 10**,** 1537-44.

CHAN, A. K., YAO, Y., ZHANG, Z., CHUNG, N. Y., LIU, J. S., LI, K. K., . . . NG, H. K. 2015. TERT promoter mutations contribute to subset prognostication of lower-grade gliomas. *Mod Pathol,* 28**,** 177-86.

CHANG, C. H., HOUSEPIAN, E. M. & HERBERT, C. 1969. An operative staging system and a megavoltage radiotherapeutic technic for cerebellar medulloblastomas. *Radiology,* 93**,** 1351-1359.

CHANG, J. E., KHUNTIA, D., ROBINS, H. I. & MEHTA, M. P. 2007. Radiotherapy and radiosensitizers in the treatment of glioblastoma multiforme. *Clin Adv Hematol Oncol,* 5**,** 894-902.

CHAUTARD, E., LOUBEAU, G., TCHIRKOV, A., CHASSAGNE, J., VERMOT-DESROCHES, C., MOREL, L. & VERRELLE, P. 2010. Akt signaling pathway: a target for radiosensitizing human malignant glioma. *Neuro-oncology,* 12**,** 434-443.

CHELIKANI, P., FITA, I. & LOEWEN, P. C. 2004. Diversity of structures and properties among catalases. *Cell Mol Life Sci,* 61**,** 192-208.

CHEN, S.-J., ZHOU, G.-B., ZHANG, X.-W., MAO, J.-H. & CHEN, Z. 2011. From an old remedy to a magic bullet: molecular mechanisms underlying the therapeutic effects of arsenic in fighting leukemia. *Blood,* 117**,** 6425-6437.

CHEN, Y., CAI, J., MURPHY, T. J. & JONES, D. P. 2002. Overexpressed human mitochondrial thioredoxin confers resistance to oxidant-induced apoptosis in human osteosarcoma cells. *J Biol Chem,* 277**,** 33242-8.

CHEN, Y. D., FENG, J., FANG, T., YANG, M., QIU, X. G. & JIANG, T. 2013. Effect of intensity-modulated radiotherapy versus three-dimensional conformal radiotherapy on clinical outcomes in patients with glioblastoma multiforme. *Chin Med J (Engl),* 126**,** 2320-4.

CHENDIL, D., RANGA, R. S., MEIGOONI, D., SATHISHKUMAR, S. & AHMED, M. M. 2004. Curcumin confers radiosensitizing effect in prostate cancer cell line PC-3. *Oncogene,* 23**,** 1599-607.

CHENG, W.-Y., KANDEL, J. J., YAMASHIRO, D. J., CANOLL, P. & ANASTASSIOU, D. 2012. A multi-cancer mesenchymal transition gene expression signature is associated with prolonged time to recurrence in glioblastoma. *PloS one,* 7**,** e34705.

CHENG, Y. & QI, Y. 2017. Current progresses in metal-based anticancer complexes as mammalian TrxR inhibitors. *Anti-Cancer Agents in Medicinal Chemistry (Formerly Current Medicinal Chemistry-Anti-Cancer Agents),* 17**,** 1046-1069.

CHERNIKOVA, S. B., GAME, J. C. & BROWN, J. M. 2012. Inhibiting homologous recombination for cancer therapy. *Cancer biology & therapy,* 13**,** 61-68.

CHEW, E.-H., LU, J., BRADSHAW, T. D. & HOLMGREN, A. 2008. Thioredoxin reductase inhibition by antitumor quinols: a quinol pharmacophore effect correlating to antiproliferative activity. *The FASEB Journal,* 22**,** 2072-2083.

CHINOT, O. L., WICK, W., MASON, W., HENRIKSSON, R., SARAN, F., NISHIKAWA, R., . . . CERNEA, D. 2014. Bevacizumab plus radiotherapy–temozolomide for newly diagnosed glioblastoma. *New England Journal of Medicine,* 370**,** 709-722.

CHISTIAKOV, D. A., CHEKHONIN, I. V. & CHEKHONIN, V. P. 2017. The EGFR variant III mutant as a target for immunotherapy of glioblastoma multiforme. *Eur J Pharmacol,* 810**,** 70-82.

CHOI, J. H., KIM, T., KIM, S., BAEK, S.-H., KIM, J., LEE, S.-R. & KIM, J.-R. 2002. Overexpression of mitochondrial thioredoxin reductase and peroxiredoxin III in hepatocellular carcinomas. *Anticancer research,* 22**,** 3331-3335.

CHOI, J. J., FESHITAN, J. A., BASERI, B., WANG, S., TUNG, Y. S., BORDEN, M. A. & KONOFAGOU, E. E. 2010. Microbubble-size dependence of focused ultrasound-induced blood-brain barrier opening in mice in vivo. *IEEE Trans Biomed Eng,* 57**,** 145-54.

CHOI, Y.-M., KIM, H.-K., SHIM, W., ANWAR, M. A., KWON, J.-W., KWON, H.-K., . . . CHOI, S. 2015. Mechanism of Cisplatin-Induced Cytotoxicity Is Correlated to Impaired Metabolism Due to Mitochondrial ROS Generation. *PloS one,* 10**,** e0135083-e0135083.

CHORNENKYY, Y., AGNIHOTRI, S., YU, M., BUCZKOWICZ, P., RAKOPOULOS, P., GOLBOURN, B., . . . HAWKINS, C. 2015. Poly-ADP-Ribose Polymerase as a Therapeutic Target in Pediatric Diffuse Intrinsic Pontine Glioma and Pediatric High-Grade Astrocytoma. *Molecular Cancer Therapeutics,* 14**,** 2560.

CHOUDRY, G. A., STEWART, P. H., DOUBLE, J. A., KRUL, M., NAYLOR, B., FLANNIGAN, G. M., . . . PHILLIPS, R. M. 2001. A novel strategy for NQO1 (NAD (P) H: quinone oxidoreductase, EC 1.6. 99.2) mediated therapy of bladder cancer based on the pharmacological properties of EO9. *British journal of cancer,* 85**,** 1137.

CLARKE, J. L., MOLINARO, A. M., PHILLIPS, J. J., BUTOWSKI, N. A., CHANG, S. M., PERRY, A., . . . PRADOS, M. D. 2014. A single-institution phase II trial of radiation, temozolomide, erlotinib, and bevacizumab for initial treatment of glioblastoma. *Neuro Oncol,* 16**,** 984-90.

CLAUS, E. B., CALVOCORESSI, L., BONDY, M. L., SCHILDKRAUT, J. M., WIEMELS, J. L. & WRENSCH, M. 2012. Dental x-rays and risk of meningioma. *Cancer,* 118**,** 4530-4537.

COCKLE, J. V., PICTON, S., LEVESLEY, J., ILETT, E., CARCABOSO, A. M., SHORT, S., . . . BRUNING-RICHARDSON, A. 2015. Cell migration in paediatric glioma; characterisation and potential therapeutic targeting. *Br J Cancer,* 112**,** 693-703.

CORSO, C. D. & BINDRA, R. S. 2016. Success and Failures of Combined Modalities in Glioblastoma Multiforme: Old Problems and New Directions. *Semin Radiat Oncol,* 26**,** 281-98.

COX, A. G., BROWN, K. K., ARNER, E. S. & HAMPTON, M. B. 2008. The thioredoxin reductase inhibitor auranofin triggers apoptosis through a Bax/Bak-dependent process that involves peroxiredoxin 3 oxidation. *Biochem Pharmacol,* 76**,** 1097-109.

COX, M. C., REESE, L. M., BICKFORD, L. R. & VERBRIDGE, S. S. 2015. Toward the Broad Adoption of 3D Tumor Models in the Cancer Drug Pipeline. *ACS Biomaterials Science & Engineering,* 1**,** 877-894.

CURATOLO, P., BOMBARDIERI, R. & JOZWIAK, S. 2008. Tuberous sclerosis. *Lancet,* 372**,** 657-68.

CURTIN, N. J. 2012. DNA repair dysregulation from cancer driver to therapeutic target. *Nature Reviews Cancer,* 12**,** 801.

DA MOTTA, L. L., LEDAKI, I., PURSHOUSE, K., HAIDER, S., DE BASTIANI, M. A., BABAN, D., . . . MCINTYRE, A. 2017. The BET inhibitor JQ1 selectively impairs tumour response to hypoxia and downregulates CA9 and angiogenesis in triple negative breast cancer. *Oncogene,* 36**,** 122-132.

DAI, Y.-F. & ZHAO, X.-M. 2015. A survey on the computational approaches to identify drug targets in the postgenomic era. *BioMed research international,* 2015.

DANG, M. & PHILLIPS, P. C. 2017. Pediatric Brain Tumors. *Continuum (Minneap Minn),* 23**,** 1727-1757.

DANIELS, T. B., BROWN, P. D., FELTEN, S. J., WU, W., BUCKNER, J. C., ARUSELL, R. M., . . . SHAW, E. G. 2011. Validation of EORTC prognostic factors for adults with low-grade glioma: a report using intergroup 86-72-51. *Int J Radiat Oncol Biol Phys,* 81**,** 218-24.

DE ANDRADE, P. V., ANDRADE, A. F., DE PAULA QUEIROZ, R. G., SCRIDELI, C. A., TONE, L. G. & VALERA, E. T. 2016. The histone deacetylase inhibitor PCI-24781 as a putative radiosensitizer in pediatric glioblastoma cell lines. *Cancer Cell Int,* 16**,** 31.

DE BRAGANCA, K. C. & PACKER, R. J. 2013. Treatment Options for Medulloblastoma and CNS Primitive Neuroectodermal Tumor (PNET). *Curr Treat Options Neurol,* 15**,** 593-606.

DE GROOT, J. F. 2015. High-grade gliomas. *Continuum (Minneap Minn),* 21**,** 332-44.

DEHN, D. L., SIEGEL, D., ZAFAR, K. S., REIGAN, P., SWANN, E., MOODY, C. J. & ROSS, D. 2006. 5-Methoxy-1, 2-dimethyl-3-[(4-nitrophenoxy) methyl] indole-4, 7-dione, a mechanism-based inhibitor of NAD (P) H: quinone oxidoreductase 1, exhibits activity against human pancreatic cancer in vitro and in vivo. *Molecular cancer therapeutics,* 5**,** 1702-1709.

DELMORE, J. E., ISSA, G. C., LEMIEUX, M. E., RAHL, P. B., SHI, J., JACOBS, H. M., . . . MITSIADES, C. S. 2011. BET bromodomain inhibition as a therapeutic strategy to target c-Myc. *Cell,* 146**,** 904-17.

DEMIZU, Y., SASAKI, R., TRACHOOTHAM, D., PELICANO, H., COLACINO, J. A., LIU, J. & HUANG, P. 2008. Alterations of cellular redox state during NNK-induced malignant transformation and resistance to radiation. *Antioxid Redox Signal,* 10**,** 951-61.

DENKO, N. C., FONTANA, L. A., HUDSON, K. M., SUTPHIN, P. D., RAYCHAUDHURI, S., ALTMAN, R. & GIACCIA, A. J. 2003. Investigating hypoxic tumor physiology through gene expression patterns. *Oncogene,* 22**,** 5907.

DESOUKY, O., DING, N. & ZHOU, G. 2015. Targeted and non-targeted effects of ionizing radiation. *Journal of Radiation Research and Applied Sciences,* 8**,** 247-254.

DESOUZA, R. M., JONES, B. R., LOWIS, S. P. & KURIAN, K. M. 2014. Pediatric medulloblastoma - update on molecular classification driving targeted therapies. *Front Oncol,* 4**,** 176.

DI MEO, S., REED, T. T., VENDITTI, P. & VICTOR, V. M. 2016. Role of ROS and RNS Sources in Physiological and Pathological Conditions. *Oxidative medicine and cellular longevity,* 2016**,** 1245049-1245049.

DILLON, M. T., BARKER, H. E., PEDERSEN, M., HAFSI, H., BHIDE, S. A., NEWBOLD, K. L., . . . HARRINGTON, K. J. 2017. Radiosensitization by the ATR Inhibitor AZD6738 through Generation of Acentric Micronuclei. *Mol Cancer Ther,* 16**,** 25-34.

DJUZENOVA, C. S., BLASSL, C., ROLOFF, K., KUGER, S., KATZER, A., NIEWIDOK, N., . . . FLENTJE, M. 2012. Hsp90 inhibitor NVP-AUY922 enhances radiation sensitivity of tumor cell lines under hypoxia. *Cancer Biol Ther,* 13**,** 425-34.

DO, K., DOROSHOW, J. H. & KUMMAR, S. 2013. Wee1 kinase as a target for cancer therapy. *Cell cycle,* 12**,** 3348-3353.

DOKTOROVA, H., HRABETA, J., KHALIL, M. A. & ECKSCHLAGER, T. 2015. Hypoxia-induced chemoresistance in cancer cells: The role of not only HIF-1. *Biomed Pap Med Fac Univ Palacky Olomouc Czech Repub,* 159**,** 166-77.

DONG, C., ZHANG, L., SUN, R., LIU, J., YIN, H., LI, X., . . . ZENG, H. 2016. Role of thioredoxin reductase 1 in dysplastic transformation of human breast epithelial cells triggered by chronic oxidative stress. *Sci Rep,* 6**,** 36860.

DONGRE, A. & WEINBERG, R. A. 2019. New insights into the mechanisms of epithelial-mesenchymal transition and implications for cancer. *Nat Rev Mol Cell Biol,* 20**,** 69-84.

DOUW, L., KLEIN, M., FAGEL, S. S., VAN DEN HEUVEL, J., TAPHOORN, M. J., AARONSON, N. K., . . . HEIMANS, J. J. 2009. Cognitive and radiological

effects of radiotherapy in patients with low-grade glioma: long-term follow-up. *Lancet Neurol,* 8**,** 810-8.

DURANT, S. T., ZHENG, L., WANG, Y., CHEN, K., ZHANG, L., ZHANG, T., . . . FOK, J. H. 2018. The brain-penetrant clinical ATM inhibitor AZD1390 radiosensitizes and improves survival of preclinical brain tumor models. *Science advances,* 4**,** eaat1719.

DURANTE, M., BRAUER-KRISCH, E. & HILL, M. 2018. Faster and safer? FLASH ultra-high dose rate in radiotherapy. *Br J Radiol,* 91**,** 20170628.

EBERHART, C. G., KRATZ, J., WANG, Y., SUMMERS, K., STEARNS, D., COHEN, K., . . . BURGER, P. C. 2004. Histopathological and molecular prognostic markers in medulloblastoma: c-myc, N-myc, TrkC, and anaplasia. *J Neuropathol Exp Neurol,* 63**,** 441-9.

ECKEL-PASSOW, J. E., LACHANCE, D. H., MOLINARO, A. M., WALSH, K. M., DECKER, P. A., SICOTTE, H., . . . JENKINS, R. B. 2015. Glioma Groups Based on 1p/19q, IDH, and TERT Promoter Mutations in Tumors. *New England Journal of Medicine,* 372**,** 2499-2508.

EDMONDSON, R., BROGLIE, J. J., ADCOCK, A. F. & YANG, L. 2014. Three-dimensional cell culture systems and their applications in drug discovery and cell-based biosensors. *Assay and drug development technologies,* 12**,** 207-218.

EMADI, A. & GORE, S. D. 2010. Arsenic trioxide—an old drug rediscovered. *Blood reviews,* 24**,** 191-199.

ENDLICH, B., RADFORD, I. R., FORRESTER, H. B. & DEWEY, W. C. 2000. Computerized video time-lapse microscopy studies of ionizing radiation-induced rapid-interphase and mitosis-related apoptosis in lymphoid cells. *Radiat Res,* 153**,** 36-48.

ERDI, F., KAYA, B., ESEN, H., KARATAS, Y., FINDIK, S., KESKIN, F., . . . KALKAN, E. 2018. New Clues in the Malignant Progression of Glioblastoma: Can the Thioredoxin System Play a Role? *Turk Neurosurg,* 28**,** 7-12.

ERIKSSON, S. E., PRAST-NIELSEN, S., FLABERG, E., SZEKELY, L. & ARNÉR, E. S. J. 2009. High levels of thioredoxin reductase 1 modulate drug-specific cytotoxic efficacy. *Free Radical Biology and Medicine,* 47**,** 1661-1671.

ESBENSHADE, A. J., KOCAK, M., HERSHON, L., ROUSSEAU, P., DECARIE, J.-C., SHAW, S., . . . MOGHRABI, A. 2017. A Phase II feasibility study of oral etoposide given concurrently with radiotherapy followed by dose intensive adjuvant chemotherapy for children with newly diagnosed high-risk medulloblastoma (protocol POG 9631): A report from the Children's Oncology Group. *Pediatric blood & cancer,* 64**,** 10.1002/pbc.26373.

ESEN, H., ERDI, F., KAYA, B., FEYZIOGLU, B., KESKIN, F. & DEMIR, L. S. 2015. Tissue thioredoxin reductase-1 expression in astrocytomas of different grades. *Journal of neuro-oncology,* 121**,** 451-458.

FALCHI, L., VERSTOVSEK, S., RAVANDI‐KASHANI, F. & KANTARJIAN, H. M. 2016. The evolution of arsenic in the treatment of acute promyelocytic leukemia and other myeloid neoplasms: Moving toward an effective oral, outpatient therapy. *Cancer,* 122**,** 1160-1168.

FANG, J., LU, J. & HOLMGREN, A. 2005. Thioredoxin reductase is irreversibly modified by curcumin: a novel molecular mechanism for its anticancer activity. *J Biol Chem,* 280**,** 25284-90.

FAORO, D., VON BUEREN, A. O., SHALABY, T., SCIUSCIO, D., HURLIMANN, M. L., ARNOLD, L., . . . GROTZER, M. A. 2011. Expression of O(6)-methylguanine-DNA methyltransferase in childhood medulloblastoma. *J Neurooncol,* 103**,** 59-69.

FARINA, A. R., TACCONELLI, A., CAPPABIANCA, L., DESANTIS, G., GULINO, A. & MACKAY, A. R. 2003. Thioredoxin inhibits microvascular endothelial capillary tubule formation. *Exp Cell Res,* 291**,** 474-83.

FARINA, A. R., TACCONELLI, A., CAPPABIANCA, L., MASCIULLI, M. P., HOLMGREN, A., BECKETT, G. J., . . . MACKAY, A. R. 2001. Thioredoxin alters the matrix metalloproteinase/tissue inhibitors of metalloproteinase balance and stimulates human SK-N-SH neuroblastoma cell invasion. *Eur J Biochem,* 268**,** 405-13.

FATTMAN, C. L., SCHAEFER, L. M. & OURY, T. D. 2003. Extracellular superoxide dismutase in biology and medicine. *Free Radic Biol Med,* 35**,** 236-56.

FELSBERG, J., HENTSCHEL, B., KAULICH, K., GRAMATZKI, D., ZACHER, A., MALZKORN, B., . . . WELLER, M. 2017. Epidermal Growth Factor Receptor Variant III (EGFRvIII) Positivity in EGFR-Amplified Glioblastomas: Prognostic Role and Comparison between Primary and Recurrent Tumors. *Clin Cancer Res,* 23**,** 6846-6855.

FERLAY, J., SOERJOMATARAM, I., DIKSHIT, R., ESER, S., MATHERS, C., REBELO, M., . . . BRAY, F. 2015. Cancer incidence and mortality worldwide: sources, methods and major patterns in GLOBOCAN 2012. *Int J Cancer,* 136**,** E359-86.

FERNANDES, A. P. & HOLMGREN, A. 2004. Glutaredoxins: glutathione-dependent redox enzymes with functions far beyond a simple thioredoxin backup system. *Antioxid Redox Signal,* 6**,** 63-74.

FERREIRA, L., GASPAR, V. & MANO, J. 2018. Design of spherically structured 3D in vitro tumor models-Advances and prospects. *Acta biomaterialia*.

FERRER-FONT, L., ARIAS-RAMOS, N., LOPE-PIEDRAFITA, S., JULIA-SAPE, M., PUMAROLA, M., ARUS, C. & CANDIOTA, A. P. 2017. Metronomic treatment in immunocompetent preclinical GL261 glioblastoma: effects of cyclophosphamide and temozolomide. *NMR Biomed,* 30.

FESTUCCIA, C., MANCINI, A., COLAPIETRO, A., GRAVINA, G. L., VITALE, F., MARAMPON, F., . . . MEHRLING, T. 2018. The first-in-class alkylating deacetylase inhibitor molecule tinostamustine shows antitumor effects and is synergistic with radiotherapy in preclinical models of glioblastoma. *J Hematol Oncol,* 11**,** 32.

FISHER, J. L., SCHWARTZBAUM, J. A., WRENSCH, M. & WIEMELS, J. L. 2007. Epidemiology of brain tumors. *Neurol Clin,* 25**,** 867-90, vii.

FISKUS, W., SABA, N., SHEN, M., GHIAS, M., LIU, J., GUPTA, S. D., . . . SCHORNO, K. 2014. Auranofin induces lethal oxidative and endoplasmic reticulum stress and exerts potent preclinical activity against chronic lymphocytic leukemia. *Cancer research***,** canres. 2033.2013.

FOKAS, E., PREVO, R., POLLARD, J., REAPER, P., CHARLTON, P., CORNELISSEN, B., . . . MCKENNA, W. G. 2012. Targeting ATR in vivo using the novel inhibitor VE-822 results in selective sensitization of pancreatic tumors to radiation. *Cell death & disease,* 3**,** e441.

FORD, J. M., SEIFERHELD, W., ALGER, J. R., WU, G., ENDICOTT, T. J., MEHTA, M., . . . PHAN, S.-C. 2007. Results of the Phase I Dose-Escalating Study of Motexafin Gadolinium With Standard Radiotherapy in Patients With Glioblastoma Multiforme. *International Journal of Radiation Oncology*Biology*Physics,* 69**,** 831-838.

FORRESTER, H. B., VIDAIR, C. A., ALBRIGHT, N., LING, C. C. & DEWEY, W. C. 1999. Using computerized video time lapse for quantifying cell death of X-irradiated rat embryo cells transfected with c-myc or c-Ha-ras. *Cancer Res,* 59**,** 931-9.

FORSYTH, P. A., SHAW, E. G., SCHEITHAUER, B. W., O'FALLON, J. R., LAYTON, D. D., JR. & KATZMANN, J. A. 1993. Supratentorial pilocytic astrocytomas. A clinicopathologic, prognostic, and flow cytometric study of 51 patients. *Cancer,* 72**,** 1335-42.

FRANKEN, N. A., OEI, A. L., KOK, H. P., RODERMOND, H. M., SMINIA, P., CREZEE, J., . . . BARENDSEN, G. W. 2013. Cell survival and radiosensitisation: modulation of the linear and quadratic parameters of the LQ model (Review). *Int J Oncol,* 42**,** 1501-15.

FREI, P., POULSEN, A. H., JOHANSEN, C., OLSEN, J. H., STEDING-JESSEN, M. & SCHUZ, J. 2011. Use of mobile phones and risk of brain tumours: update of Danish cohort study. *BMJ,* 343**,** d6387.

FRIEDMANN-MORVINSKI, D. 2014. Glioblastoma heterogeneity and cancer cell plasticity. *Crit Rev Oncog,* 19**,** 327-36.

FURY, M. G., LEE, N. Y., SHERMAN, E., LISA, D., KELLY, K., LIPSON, B., . . . SHEN, R. 2012. A phase 2 study of bevacizumab with cisplatin plus intensity‐modulated radiation therapy for stage III/IVB head and neck squamous cell cancer. *Cancer,* 118**,** 5008-5014.

GAD, S. C., SULLIVAN, D. W., JR., SPASOJEVIC, I., MUJER, C. V., SPAINHOUR, C. B. & CRAPO, J. D. 2016. Nonclinical Safety and Toxicokinetics of MnTnBuOE-2-PyP5+ (BMX-001). *Int J Toxicol,* 35**,** 438-53.

GAJJAR, A., CHINTAGUMPALA, M., ASHLEY, D., KELLIE, S., KUN, L. E., MERCHANT, T. E., . . . GILBERTSON, R. J. 2006. Risk-adapted craniospinal radiotherapy followed by high-dose chemotherapy and stem-cell rescue in children with newly diagnosed medulloblastoma (St Jude Medulloblastoma-96): long-term results from a prospective, multicentre trial. *Lancet Oncol,* 7**,** 813-20.

GAJJAR, A. J. & ROBINSON, G. W. 2014. Medulloblastoma-translating discoveries from the bench to the bedside. *Nat Rev Clin Oncol,* 11**,** 714-22.

GANDIN, V. & FERNANDES, A. 2015. Metal-and semimetal-containing inhibitors of thioredoxin reductase as anticancer agents. *Molecules,* 20**,** 12732-12756.

GAO, Z., CHEN, Y., CAI, X. & XU, R. 2017. Predict drug permeability to blood-brain-barrier from clinical phenotypes: drug side effects and drug indications. *Bioinformatics (Oxford, England),* 33**,** 901-908.

GARCIA-BARROS, M., PARIS, F., CORDON-CARDO, C., LYDEN, D., RAFII, S., HAIMOVITZ-FRIEDMAN, A., . . . KOLESNICK, R. 2003. Tumor response to radiotherapy regulated by endothelial cell apoptosis. *Science,* 300**,** 1155-9.

GASPAR, N., MARSHALL, L., PERRYMAN, L., BAX, D. A., LITTLE, S. E., VIANA-PEREIRA, M., . . . JONES, C. 2010. MGMT-independent temozolomide resistance in pediatric glioblastoma cells associated with a PI3-kinase-mediated HOX/stem cell gene signature. *Cancer Res,* 70**,** 9243-52.

GHAFFARI, S. H., YOUSEFI, M., DIZAJI, M. Z., MOMENY, M., BASHASH, D., ZEKRI, A., . . . GHAVAMZADEH, A. 2016. Arsenic Trioxide Induces Apoptosis and Incapacitates Proliferation and Invasive Properties of U87MG Glioblastoma Cells through a Possible NF-kappaB-Mediated Mechanism. *Asian Pac J Cancer Prev,* 17**,** 1553-64.

GHIA, A. J. 2018. Fractionated Radiotherapy of Intracranial Gliomas. *Prog Neurol Surg,* 31**,** 38-47.

GILBERT, M. R., DIGNAM, J. J., ARMSTRONG, T. S., WEFEL, J. S., BLUMENTHAL, D. T., VOGELBAUM, M. A., . . . WON, M. 2014. A randomized trial of bevacizumab for newly diagnosed glioblastoma. *New England Journal of Medicine,* 370**,** 699-708.

GILES, G. I. 2006. The redox regulation of thiol dependent signaling pathways in cancer. *Curr Pharm Des,* 12**,** 4427-43.

GLOD, J., RAHME, G. J., KAUR, H., E, H. R., HWANG, E. I. & ISRAEL, M. A. 2016. Pediatric Brain Tumors: Current Knowledge and Therapeutic Opportunities. *J Pediatr Hematol Oncol,* 38**,** 249-60.

GOEL, A. & AGGARWAL, B. B. 2010. Curcumin, the golden spice from Indian saffron, is a chemosensitizer and radiosensitizer for tumors and chemoprotector and radioprotector for normal organs. *Nutr Cancer,* 62**,** 919-30.

GOGLIA, A. G., DELSITE, R., LUZ, A. N., SHAHBAZIAN, D., SALEM, A. F., SUNDARAM, R. K., . . . JASIN, M. 2015. Identification of novel radiosensitizers in a high-throughput, cell-based screen for DSB repair inhibitors. *Molecular cancer therapeutics,* 14**,** 326-342.

GOLDBERG, S. F., MIELE, M. E., HATTA, N., TAKATA, M., PAQUETTE-STRAUB, C., FREEDMAN, L. P. & WELCH, D. R. 2003. Melanoma Metastasis Suppression by Chromosome 6. *Cancer Research,* 63**,** 432.

GOLDSTEIN, M. & KASTAN, M. B. 2015. The DNA damage response: implications for tumor responses to radiation and chemotherapy. *Annual review of medicine,* 66**,** 129-143.

GOLLAPALLI, K., GHANTASALA, S., ATAK, A., RAPOLE, S., MOIYADI, A., EPARI, S. & SRIVASTAVA, S. 2017. Tissue Proteome Analysis of Different Grades of Human Gliomas Provides Major Cues for Glioma Pathogenesis. *Omics,* 21**,** 275-284.

GOMEZ-ROMAN, N., STEVENSON, K., GILMOUR, L., HAMILTON, G. & CHALMERS, A. J. 2017. A novel 3D human glioblastoma cell culture

system for modeling drug and radiation responses. *Neuro Oncol,* 19**,** 229-241.

GORLIA, T., DELATTRE, J. Y., BRANDES, A. A., KROS, J. M., TAPHOORN, M. J., KOUWENHOVEN, M. C., . . . VAN DEN BENT, M. J. 2013a. New clinical, pathological and molecular prognostic models and calculators in patients with locally diagnosed anaplastic oligodendroglioma or oligoastrocytoma. A prognostic factor analysis of European Organisation for Research and Treatment of Cancer Brain Tumour Group Study 26951. *Eur J Cancer,* 49**,** 3477-85.

GORLIA, T., WU, W., WANG, M., BAUMERT, B. G., MEHTA, M., BUCKNER, J. C., . . . VAN DEN BENT, M. J. 2013b. New validated prognostic models and prognostic calculators in patients with low-grade gliomas diagnosed by central pathology review: a pooled analysis of EORTC/RTOG/NCCTG phase III clinical trials. *Neuro Oncol,* 15**,** 1568-79.

GRABENBAUER, F., KATZER, A., SISARIO, D., MEMMEL, S., FLENTJE, M., SUKHORUKOV, V. L. & DJUZENOVA, C. S. 2018. MEK-inhibitor PD184352 enhances the radiosensitizing effect of the Hsp90 inhibitor NVP-AUY922: the role of cell type and drug-irradiation schedule. *Oncotarget,* 9**,** 37379-37392.

GRAHAM, K. & UNGER, E. 2018. Overcoming tumor hypoxia as a barrier to radiotherapy, chemotherapy and immunotherapy in cancer treatment. *International journal of nanomedicine,* 13**,** 6049-6058.

GRÖGER, C. J., GRUBINGER, M., WALDHÖR, T., VIERLINGER, K. & MIKULITS, W. 2012. Meta-analysis of gene expression signatures defining the epithelial to mesenchymal transition during cancer progression. *PloS one,* 7**,** e51136.

GROMER, S., URIG, S. & BECKER, K. 2004. The thioredoxin system—from science to clinic. *Medicinal research reviews,* 24**,** 40-89.

GUPTA, R., CHETTY, C., BHOOPATHI, P., LAKKA, S., MOHANAM, S., RAO, J. S. & DINH, D. E. 2011. Downregulation of uPA/uPAR inhibits intermittent hypoxia-induced epithelial-mesenchymal transition (EMT) in DAOY and D283 medulloblastoma cells. *Int J Oncol,* 38**,** 733-44.

HAAPASALO, H., KYLANIEMI, M., PAUNUL, N., KINNULA, V. L. & SOINI, Y. 2003. Expression of antioxidant enzymes in astrocytic brain tumors. *Brain Pathol,* 13**,** 155-64.

HAAS, B., SCHUTTE, L., WOS-MAGANGA, M., WEICKHARDT, S., TIMMER, M. & ECKSTEIN, N. 2018a. Thioredoxin Confers Intrinsic Resistance to Cytostatic Drugs in Human Glioma Cells. *Int J Mol Sci,* 19.

HAAS, B., SCHÜTTE, L., WOS-MAGANGA, M., WEICKHARDT, S., TIMMER, M. & ECKSTEIN, N. 2018b. Thioredoxin Confers Intrinsic Resistance to Cytostatic Drugs in Human Glioma Cells. *International journal of molecular sciences,* 19**,** 2874.

HÅKANSON, M., TEXTOR, M. & CHARNLEY, M. 2010. Engineered 3D environments to elucidate the effect of environmental parameters on drug response in cancer. *Integrative Biology,* 3**,** 31-38.

HALASZ, L. M., BUSSIERE, M. R., DENNIS, E. R., NIEMIERKO, A., CHAPMAN, P. H., LOEFFLER, J. S. & SHIH, H. A. 2011. Proton stereotactic radiosurgery

for the treatment of benign meningiomas. *Int J Radiat Oncol Biol Phys,* 81**,** 1428-35.

HALL, E. J. & GIACCIA, A. J. 2012. *Radiobiology for the Radiologist*, Wolters Kluwer Health/Lippincott Williams & Wilkins.

HALL, E. J. & GIACCIA., A. J. 2012. *Radiobiology for the Radiologist*, Philadelphia: Lippincott Williams & Wilkins.

HALLIWELL, B. 1992. Reactive oxygen species and the central nervous system. *J Neurochem,* 59**,** 1609-23.

HAN, H., BEARSS, D. J., BROWNE, L. W., CALALUCE, R., NAGLE, R. B. & VON HOFF, D. D. 2002. Identification of differentially expressed genes in pancreatic cancer cells using cDNA microarray. *Cancer research,* 62**,** 2890-2896.

HAN, S. H., JEON, J. H., JU, H. R., JUNG, U., KIM, K. Y., YOO, H. S., . . . NA, Y. S. 2003a. VDUP1 upregulated by TGF-β1 and 1, 25-dihydorxyvitamin D 3 inhibits tumor cell growth by blocking cell-cycle progression. *Oncogene,* 22**,** 4035.

HAN, S. H., JEON, J. H., JU, H. R., JUNG, U., KIM, K. Y., YOO, H. S., . . . CHOI, I. 2003b. VDUP1 upregulated by TGF-beta1 and 1,25-dihydorxyvitamin D3 inhibits tumor cell growth by blocking cell-cycle progression. *Oncogene,* 22**,** 4035-46.

HARDELL, L., CARLBERG, M., SODERQVIST, F. & MILD, K. H. 2013. Case-control study of the association between malignant brain tumours diagnosed between 2007 and 2009 and mobile and cordless phone use. *Int J Oncol,* 43**,** 1833-45.

HARGREAVES, R., HARTLEY, J. A. & BUTLER, J. 2000. Mechanisms of action of quinone-containing alkylating agents: DNA alkylation by aziridinylquinones. *Front Biosci,* 5**,** E172-E180.

HARRIS, A. L. 2002a. Hypoxia—a key regulatory factor in tumour growth. *Nature Reviews Cancer,* 2**,** 38.

HARRIS, A. L. 2002b. Hypoxia — a key regulatory factor in tumour growth. *Nature Reviews Cancer,* 2**,** 38.

HARRISON, L. B., CHADHA, M., HILL, R. J., HU, K. & SHASHA, D. 2002. Impact of tumor hypoxia and anemia on radiation therapy outcomes. *The oncologist,* 7**,** 492-508.

HARTMANN, C., HENTSCHEL, B., SIMON, M., WESTPHAL, M., SCHACKERT, G., TONN, J. C., . . . WELLER, M. 2013. Long-term survival in primary glioblastoma with versus without isocitrate dehydrogenase mutations. *Clin Cancer Res,* 19**,** 5146-57.

HARTMANN, C., HENTSCHEL, B., WICK, W., CAPPER, D., FELSBERG, J., SIMON, M., . . . VON DEIMLING, A. 2010. Patients with IDH1 wild type anaplastic astrocytomas exhibit worse prognosis than IDH1-mutated glioblastomas, and IDH1 mutation status accounts for the unfavorable prognostic effect of higher age: implications for classification of gliomas. *Acta Neuropathol,* 120**,** 707-18.

HASHEMY, S. I., UNGERSTEDT, J. S., ZAHEDI AVVAL, F. & HOLMGREN, A. 2006. Motexafin gadolinium, a tumor-selective drug targeting thioredoxin reductase and ribonucleotide reductase. *J Biol Chem,* 281**,** 10691-7.

HATWALNE, M. S. 2012. Free radical scavengers in anaesthesiology and critical care. *Indian journal of anaesthesia,* 56**,** 227-233.

HDEIB, A. & SLOAN, A. E. 2011. Convection-enhanced delivery of 131I-chTNT-1/B mAB for treatment of high-grade adult gliomas. *Expert Opin Biol Ther,* 11**,** 799-806.

HE, L., HE, T., FARRAR, S., JI, L., LIU, T. & MA, X. 2017. Antioxidants Maintain Cellular Redox Homeostasis by Elimination of Reactive Oxygen Species. *Cell Physiol Biochem,* 44**,** 532-553.

HEDLEY, D., PINTILIE, M., WOO, J., NICKLEE, T., MORRISON, A., BIRLE, D., . . . HILL, R. 2004. Up-regulation of the redox mediators thioredoxin and apurinic/apyrimidinic excision (APE)/Ref-1 in hypoxic microregions of invasive cervical carcinomas, mapped using multispectral, wide-field fluorescence image analysis. *The American journal of pathology,* 164**,** 557-565.

HEGI, M. E., DISERENS, A. C., GORLIA, T., HAMOU, M. F., DE TRIBOLET, N., WELLER, M., . . . STUPP, R. 2005. MGMT gene silencing and benefit from temozolomide in glioblastoma. *N Engl J Med,* 352**,** 997-1003.

HELLEDAY, T., PETERMANN, E., LUNDIN, C., HODGSON, B. & SHARMA, R. A. 2008. DNA repair pathways as targets for cancer therapy. *Nature Reviews Cancer,* 8**,** 193.

HEMMINKI, K., TRETLI, S., OLSEN, J. H., TRYGGVADOTTIR, L., PUKKALA, E., SUNDQUIST, J. & GRANSTROM, C. 2010. Familial risks in nervous system tumours: joint Nordic study. *Br J Cancer,* 102**,** 1786-90.

HEMMINKI, K., TRETLI, S., SUNDQUIST, J., JOHANNESEN, T. B. & GRANSTROM, C. 2009. Familial risks in nervous-system tumours: a histology-specific analysis from Sweden and Norway. *Lancet Oncol,* 10**,** 481-8.

HERMANTO, U., FRIJA, E. K., LII, M. J., CHANG, E. L., MAHAJAN, A. & WOO, S. Y. 2007. Intensity-modulated radiotherapy (IMRT) and conventional three-dimensional conformal radiotherapy for high-grade gliomas: does IMRT increase the integral dose to normal brain? *Int J Radiat Oncol Biol Phys,* 67**,** 1135-44.

HERMS, J., NEIDT, I., LUSCHER, B., SOMMER, A., SCHURMANN, P., SCHRODER, T., . . . KRETZSCHMAR, H. A. 2000. C-MYC expression in medulloblastoma and its prognostic value. *Int J Cancer,* 89**,** 395-402.

HERST, P. M., BROADLEY, K. W., HARPER, J. L. & MCCONNELL, M. J. 2012. Pharmacological concentrations of ascorbate radiosensitize glioblastoma multiforme primary cells by increasing oxidative DNA damage and inhibiting G2/M arrest. *Free Radic Biol Med,* 52**,** 1486-93.

HIGDON, R., KALA, J., WILKINS, D., YAN, J. F., SETHI, M. K., LIN, L., . . . FANAYAN, S. 2017. Integrated Proteomic and Transcriptomic-Based Approaches to Identifying Signature Biomarkers and Pathways for Elucidation of Daoy and UW228 Subtypes. *Proteomes,* 5**,** 5.

HIGGS, M. R., CHOUTEAU, P. & LERAT, H. 2014. 'Liver let die': oxidative DNA damage and hepatotropic viruses. *Journal of General Virology,* 95**,** 991-1004.

HILL, R., RICHARDSON, S., LINDSEY, J. & CROSIER, S. 2017. Medu-16. Time, Pattern And Outcome Of Medulloblastoma Relapse Is Biology And Therapy-dependent. *Neuro-oncology,* 19**,** iv41.

HIROTA, K., MATSUI, M., IWATA, S., NISHIYAMA, A., MORI, K. & YODOI, J. 1997. AP-1 transcriptional activity is regulated by a direct association between thioredoxin and Ref-1. *Proceedings of the National Academy of Sciences,* 94**,** 3633-3638.

HIRSCHHAEUSER, F., MENNE, H., DITTFELD, C., WEST, J., MUELLER-KLIESER, W. & KUNZ-SCHUGHART, L. A. 2010. Multicellular tumor spheroids: An underestimated tool is catching up again. *Journal of Biotechnology,* 148**,** 3-15.

HITCHCOCK, S. A. & PENNINGTON, L. D. 2006. Structure− brain exposure relationships. *Journal of medicinal chemistry,* 49**,** 7559-7583.

HOLMGREN, A. 1985. Thioredoxin. *Annu Rev Biochem,* 54**,** 237-71.

HOLMGREN, A. & BJORNSTEDT, M. 1995. Thioredoxin and thioredoxin reductase. *Methods Enzymol,* 252**,** 199-208.

HOLMGREN, A. & LU, J. 2010. Thioredoxin and thioredoxin reductase: current research with special reference to human disease. *Biochemical and biophysical research communications,* 396**,** 120-124.

HOONJAN, M., JADHAV, V. & BHATT, P. 2018. Arsenic trioxide: insights into its evolution to an anticancer agent. *J Biol Inorg Chem,* 23**,** 313-329.

HORNING, J. L., SAHOO, S. K., VIJAYARAGHAVALU, S., DIMITRIJEVIC, S., VASIR, J. K., JAIN, T. K., . . . LABHASETWAR, V. 2008. 3-D tumor model for in vitro evaluation of anticancer drugs. *Molecular pharmaceutics,* 5**,** 849-862.

HOSHIKAWA, H., INDO, K., MORI, T. & MORI, N. 2011. Enhancement of the radiation effects by D-allose in head and neck cancer cells. *Cancer Lett,* 306**,** 60-6.

HOSHIKAWA, H., KAMITORI, K., INDO, K., MORI, T., KAMATA, M., TAKAHASHI, T. & TOKUDA, M. 2018. Combined treatment with D-allose, docetaxel and radiation inhibits the tumor growth in an in vivo model of head and neck cancer. *Oncol Lett,* 15**,** 3422-3428.

HOTTINGER, A. F. & KHAKOO, Y. 2007. Update on the management of familial central nervous system tumor syndromes. *Curr Neurol Neurosci Rep,* 7**,** 200-7.

HOTTINGER, A. F., PACHECO, P. & STUPP, R. 2016. Tumor treating fields: a novel treatment modality and its use in brain tumors. *Neuro-oncology,* 18**,** 1338-1349.

HUANG, B., DESAI, A., TANG, S., THOMAS, T. P. & BAKER, J. R., JR. 2010. The synthesis of a c(RGDyK) targeted SN38 prodrug with an indolequinone structure for bioreductive drug release. *Org Lett,* 12**,** 1384-7.

HUANG, B., TANG, S., DESAI, A., CHENG, X. M., KOTLYAR, A., VAN DER SPEK, A., . . . BAKER, J. R., JR. 2009. Human plasma-mediated hypoxic activation of indolequinone-based naloxone pro-drugs. *Bioorg Med Chem Lett,* 19**,** 5016-20.

HUBER, J. M., AMANN, A., KOECK, S., LORENZ, E., KELM, J. M., OBEXER, P., . . . GAMERITH, G. 2016. Evaluation of assays for drug efficacy in a three-

dimensional model of the lung. *Journal of cancer research and clinical oncology,* 142**,** 1955-1966.

IMAMURA, Y., MUKOHARA, T., SHIMONO, Y., FUNAKOSHI, Y., CHAYAHARA, N., TOYODA, M., . . . NAKATSURA, T. 2015a. Comparison of 2D-and 3D-culture models as drug-testing platforms in breast cancer. *Oncology reports,* 33**,** 1837-1843.

IMAMURA, Y., MUKOHARA, T., SHIMONO, Y., FUNAKOSHI, Y., CHAYAHARA, N., TOYODA, M., . . . MINAMI, H. 2015b. Comparison of 2D- and 3D-culture models as drug-testing platforms in breast cancer. *Oncol Rep,* 33**,** 1837-43.

INGHAM, P. W. & PLACZEK, M. 2006. Orchestrating ontogenesis: variations on a theme by sonic hedgehog. *Nat Rev Genet,* 7**,** 841-50.

INMAN, M., VISCONTI, A., YAN, C., SIEGEL, D., ROSS, D. & MOODY, C. J. 2014. Antitumour indolequinones: synthesis and activity against human pancreatic cancer cells. *Organic & biomolecular chemistry,* 12**,** 4848-4861.

INTERPHONE STUDY GROUP 2010. Brain tumour risk in relation to mobile telephone use: results of the INTERPHONE international case-control study. *Int J Epidemiol,* 39**,** 675-94.

ISER, I. C., PEREIRA, M. B., LENZ, G. & WINK, M. R. 2017. The Epithelial-to-Mesenchymal Transition-Like Process in Glioblastoma: An Updated Systematic Review and In Silico Investigation. *Med Res Rev,* 37**,** 271-313.

ISLAM, M. T. 2017. Radiation interactions with biological systems. *Int J Radiat Biol,* 93**,** 487-493.

IVANOV, D. P., PARKER, T. L., WALKER, D. A., ALEXANDER, C., ASHFORD, M. B., GELLERT, P. R. & GARNETT, M. C. 2014a. Multiplexing spheroid volume, resazurin and acid phosphatase viability assays for high-throughput screening of tumour spheroids and stem cell neurospheres. *PloS one,* 9**,** e103817-e103817.

IVANOV, D. P., PARKER, T. L., WALKER, D. A., ALEXANDER, C., ASHFORD, M. B., GELLERT, P. R. & GARNETT, M. C. 2014b. Multiplexing spheroid volume, resazurin and acid phosphatase viability assays for high-throughput screening of tumour spheroids and stem cell neurospheres. *PLoS One,* 9**,** e103817.

IVANOV, D. P., PARKER, T. L., WALKER, D. A., ALEXANDER, C., ASHFORD, M. B., GELLERT, P. R. & GARNETT, M. C. 2015. In vitro co-culture model of medulloblastoma and human neural stem cells for drug delivery assessment. *Journal of Biotechnology,* 205**,** 3-13.

IVASCU, A. & KUBBIES, M. 2006. Rapid generation of single-tumor spheroids for high-throughput cell function and toxicity analysis. *J Biomol Screen,* 11**,** 922-32.

IVASKA, J. 2011. Vimentin: Central hub in EMT induction? *Small GTPases,* 2**,** 51-53.

JACKSON, R. K., LIEW, L. P. & HAY, M. P. 2019. Overcoming Radioresistance: Small Molecule Radiosensitisers and Hypoxia-activated Prodrugs. *Clinical Oncology*.

JAECKLE, K., VOGELBAUM, M., BALLMAN, K., ANDERSON, S. K., GIANNINI, C., ALDAPE, K., . . . BROWN, P. 2016. CODEL (Alliance-N0577; EORTC-26081/22086; NRG-1071; NCIC-CEC-2): Phase III Randomized Study of RT vs. RT+TMZ vs. TMZ for Newly Diagnosed 1p/19q-Codeleted Anaplastic Oligodendroglial Tumors. Analysis of Patients Treated on the Original Protocol Design (PL02.005). *Neurology,* 86**,** PL02.005.

JAKOLA, A. S., SKJULSVIK, A. J., MYRMEL, K. S., SJAVIK, K., UNSGARD, G., TORP, S. H., . . . SOLHEIM, O. 2017. Surgical resection versus watchful waiting in low-grade gliomas. *Ann Oncol,* 28**,** 1942-1948.

JANSS, A. J., LEVOW, C., BERNHARD, E. J., MUSCHEL, R. J., MCKENNA, W. G., SUTTON, L. & PHILLIPS, P. C. 1998. Caffeine and staurosporine enhance the cytotoxicity of cisplatin and camptothecin in human brain tumor cell lines. *Experimental cell research,* 243**,** 29-38.

JARVELA, S., BRAGGE, H., PAUNU, N., JARVELA, T., PALJARVI, L., KALIMO, H., . . . HAAPASALO, H. 2006. Antioxidant enzymes in oligodendroglial brain tumors: association with proliferation, apoptotic activity and survival. *J Neurooncol,* 77**,** 131-40.

JAVVADI, P., HERTAN, L., KOSOFF, R., DATTA, T., KOLEV, J., MICK, R., . . . KOUMENIS, C. 2010a. Thioredoxin reductase-1 mediates curcumin-induced radiosensitization of squamous carcinoma cells. *Cancer research,* 70**,** 1941-1950.

JAVVADI, P., HERTAN, L., KOSOFF, R., DATTA, T., KOLEV, J., MICK, R., . . . KOUMENIS, C. 2010b. Thioredoxin reductase-1 mediates curcumin-induced radiosensitization of squamous carcinoma cells. *Cancer Res,* 70**,** 1941-50.

JAVVADI, P., SEGAN, A. T., TUTTLE, S. W. & KOUMENIS, C. 2008. The chemopreventive agent curcumin is a potent radiosensitizer of human cervical tumor cells via increased reactive oxygen species production and overactivation of the mitogen-activated protein kinase pathway. *Mol Pharmacol,* 73**,** 1491-501.

JAYAKUMAR, S., PATWARDHAN, R. S., PAL, D., SHARMA, D. & SANDUR, S. K. 2016. Dimethoxycurcumin, a metabolically stable analogue of curcumin enhances the radiosensitivity of cancer cells: Possible involvement of ROS and thioredoxin reductase. *Biochem Biophys Res Commun,* 478**,** 446-454.

JE, E.-C., LCA, B. S. & GA, G. A. 2013. The role of transcription factor TWIST in cancer cells. *J Genet Syndr Gene Ther,* 4**,** 1-7.

JIANG, Y., FENG, X., ZHENG, L., LI, S. L., GE, X. Y. & ZHANG, J. G. 2015. Thioredoxin 1 mediates TGF-beta-induced epithelial-mesenchymal transition in salivary adenoid cystic carcinoma. *Oncotarget,* 6**,** 25506-19.

JIMENEZ, A., ZU, W., RAWE, V. Y., PELTO-HUIKKO, M., FLICKINGER, C. J., SUTOVSKY, P., . . . MIRANDA-VIZUETE, A. 2004. Spermatocyte/spermatid-specific thioredoxin-3, a novel Golgi apparatus-associated thioredoxin, is a specific marker of aberrant spermatogenesis. *J Biol Chem,* 279**,** 34971-82.

JOHANSSON, C., LILLIG, C. H. & HOLMGREN, A. 2004. Human mitochondrial glutaredoxin reduces S-glutathionylated proteins with high affinity accepting electrons from either glutathione or thioredoxin reductase. *J Biol Chem,* 279**,** 7537-43.

JOHNSON, D. R., BROWN, P. D., GALANIS, E. & HAMMACK, J. E. 2012. Pilocytic astrocytoma survival in adults: analysis of the Surveillance, Epidemiology, and End Results Program of the National Cancer Institute. *J Neurooncol,* 108**,** 187-93.

JOHNSON, D. R. & GALANIS, E. 2013. Incorporation of prognostic and predictive factors into glioma clinical trials. *Curr Oncol Rep,* 15**,** 56-63.

JOINER, M. C. & VAN DER KOGEL, A. 2016. *Basic clinical radiobiology*, CRC press.

JONES, D. P. 2008. Radical-free biology of oxidative stress. *American Journal of Physiology-Cell Physiology,* 295**,** C849-C868.

JOŚKO, J. & MAZUREK, M. 2004. Transcription factors having impact on vascular endothelial growth factor (VEGF) gene expression in angiogenesis. *Medical Science Monitor,* 10**,** RA89-RA98.

JUNN, E., HAN, S. H., IM, J. Y., YANG, Y., CHO, E. W., UM, H. D., . . . CHOI, I. 2000. Vitamin D3 up-regulated protein 1 mediates oxidative stress via suppressing the thioredoxin function. *J Immunol,* 164**,** 6287-95.

JUSTUS, C. R., LEFFLER, N., RUIZ-ECHEVARRIA, M. & YANG, L. V. 2014. In vitro cell migration and invasion assays. *Journal of visualized experiments : JoVE***,** 51046.

KAHLERT, U. D., JOSEPH, J. V. & KRUYT, F. A. E. 2017. EMT- and MET-related processes in nonepithelial tumors: importance for disease progression, prognosis, and therapeutic opportunities. *Mol Oncol,* 11**,** 860-877.

KAHLOS, K., SOINI, Y., SÄILY, M., KOISTINEN, P., KAKKO, S., PÄÄKKÖ, P., . . . KINNULA, V. L. 2001. Up‐regulation of thioredoxin and thioredoxin reductase in human malignant pleural mesothelioma. *International journal of cancer,* 95**,** 198-204.

KAKOLYRIS, S., GIATROMANOLAKI, A., KOUKOURAKIS, M., POWIS, G., SOUGLAKOS, J., SIVRIDIS, E., . . . HARRIS, A. L. 2001. Thioredoxin expression is associated with lymph node status and prognosis in early operable non-small cell lung cancer. *Clinical cancer research,* 7**,** 3087-3091.

KALIA, V. K., PRABHAKARA, S. & NARAYANAN, V. 2009. Modulation of cellular radiation responses by 2-deoxy-D-glucose and other glycolytic inhibitors: implications for cancer therapy. *J Cancer Res Ther,* 5 Suppl 1**,** S57-60.

KALLURI, R. & WEINBERG, R. A. 2009. The basics of epithelial-mesenchymal transition. *The Journal of clinical investigation,* 119**,** 1420-1428.

KANG, Y. & MASSAGUE, J. 2004. Epithelial-mesenchymal transitions: twist in development and metastasis. *Cell,* 118**,** 277-9.

KARAR, J. & MAITY, A. 2009. Modulating the tumor microenvironment to increase radiation responsiveness. *Cancer Biol Ther,* 8**,** 1994-2001.

KARATHANASIS, E. & GHAGHADA, K. B. 2016. Crossing the barrier: treatment of brain tumors using nanochain particles. *Wiley interdisciplinary reviews. Nanomedicine and nanobiotechnology,* 8**,** 678-695.

KARIMPOUR, S., LOU, J., LIN, L. L., RENE, L. M., LAGUNAS, L., MA, X., . . . GIUS, D. 2002. Thioredoxin reductase regulates AP-1 activity as well as thioredoxin nuclear localization via active cysteines in response to ionizing radiation. *Oncogene,* 21**,** 6317-27.

KARLENIUS, T. C. & TONISSEN, K. F. 2010. Thioredoxin and Cancer: A Role for Thioredoxin in all States of Tumor Oxygenation. *Cancers,* 2**,** 209-232.

KARLSSON, H., FRYKNÄS, M., LARSSON, R. & NYGREN, P. 2012. Loss of cancer drug activity in colon cancer HCT-116 cells during spheroid formation in a new 3-D spheroid cell culture system. *Experimental cell research,* 318**,** 1577-1585.

KARSH, L., SHORE, N., SOLOWAY, M., BHAT, G., REDDY, G., LEU, S. Y. & WITJES, J. A. 2018. Double-Blind, Randomized, Placebo-controlled Studies Evaluating Apaziquone (E09, Qapzola) Intravesical Instillation Post Transurethral Resection of Bladder Tumors for the Treatment of Low-risk Non-Muscle Invasive Bladder Cancer. *Bladder Cancer,* 4**,** 293-301.

KARSY, M., GUAN, J., JENSEN, R., HUANG, L. E. & COLMAN, H. 2016. The Impact of Hypoxia and Mesenchymal Transition on Glioblastoma Pathogenesis and Cancer Stem Cells Regulation. *World Neurosurg,* 88**,** 222-36.

KAST, R. E. 2010. Glioblastoma invasion, cathepsin B, and the potential for both to be inhibited by auranofin, an old anti-rheumatoid arthritis drug. *Cent Eur Neurosurg,* 71**,** 139-42.

KAWATA, M., OGI, K., NISHIYAMA, K., MIYAMOTO, S., NAKAGAKI, T., SHIMANISHI, M., . . . HIRATSUKA, H. 2017. Additive effect of radiosensitization by 2-deoxy-D-glucose delays DNA repair kinetics and suppresses cell proliferation in oral squamous cell carcinoma. *J Oral Pathol Med,* 46**,** 979-985.

KAYA, B., CICEK, O., ERDI, F., FINDIK, S., KARATAS, Y., ESEN, H., . . . KALKAN, E. 2016. Intratumoral hemorrhage-related differences in the expression of vascular endothelial growth factor, basic fibroblast growth factor and thioredoxin reductase 1 in human glioblastoma. *Mol Clin Oncol,* 5**,** 343-346.

KAZDA, T., JANCALEK, R., POSPISIL, P., SEVELA, O., PROCHAZKA, T., VRZAL, M., . . . LAACK, N. N. 2014. Why and how to spare the hippocampus during brain radiotherapy: the developing role of hippocampal avoidance in cranial radiotherapy. *Radiat Oncol,* 9**,** 139.

KELLER, S. & SCHMIDT, M. H. H. 2017. EGFR and EGFRvIII Promote Angiogenesis and Cell Invasion in Glioblastoma: Combination Therapies for an Effective Treatment. *Int J Mol Sci,* 18.

KELLEY, K., KNISELY, J., SYMONS, M. & RUGGIERI, R. 2016. Radioresistance of Brain Tumors. *Cancers (Basel),* 8.

KEMERDERE, R., KACIRA, T., HANIMOGLU, H., KUCUR, M., TANRIVERDI, T. & CANBAZ, B. 2013. Tissue and plasma thioredoxin reductase

expressions in patients with glioblastoma multiforme. *J Neurol Surg A Cent Eur Neurosurg,* 74**,** 234-8.

KENNY, P. A., LEE, G. Y., MYERS, C. A., NEVE, R. M., SEMEIKS, J. R., SPELLMAN, P. T., . . . PETERSEN, O. W. 2007. The morphologies of breast cancer cell lines in three ‐ dimensional assays correlate with their profiles of gene expression. *Molecular oncology,* 1**,** 84-96.

KHOUJA, M. H., BAEKELANDT, M., SARAB, A., NESLAND, J. M. & HOLM, R. 2010. Limitations of tissue microarrays compared with whole tissue sections in survival analysis. *Oncology letters,* 1**,** 827-831.

KIDD, E. A., MANSUR, D. B., LEONARD, J. R., MICHALSKI, J. M., SIMPSON, J. R. & PERRY, A. 2006. The efficacy of radiation therapy in the management of grade I astrocytomas. *J Neurooncol,* 76**,** 55-8.

KIEBERT, G. M., CURRAN, D., AARONSON, N. K., BOLLA, M., MENTEN, J., RUTTEN, E. H., . . . KARIM, A. B. 1998. Quality of life after radiation therapy of cerebral low-grade gliomas of the adult: results of a randomised phase III trial on dose response (EORTC trial 22844). EORTC Radiotherapy Co-operative Group. *Eur J Cancer,* 34**,** 1902-9.

KIJIMA, N. & KANEMURA, Y. 2016. Molecular Classification of Medulloblastoma. *Neurol Med Chir (Tokyo),* 56**,** 687-697.

KIM, H., CHAE, H.-Z., KIM, Y.-J., KIM, Y., HWANG, T.-S., PARK, E.-M. & PARK, Y.-M. 2003a. Preferential elevation of Prx I and Trx expression in lung cancer cells following hypoxia and in human lung cancer tissues. *Cell biology and toxicology,* 19**,** 285-298.

KIM, H. J., CHAE, H. Z., KIM, Y. J., KIM, Y. H., HWANGS, T. S., PARK, E. M. & PARK, Y. M. 2003b. Preferential elevation of Prx I and Trx expression in lung cancer cells following hypoxia and in human lung cancer tissues. *Cell Biol Toxicol,* 19**,** 285-98.

KIM, S. J., MIYOSHI, Y., TAGUCHI, T., TAMAKI, Y., NAKAMURA, H., YODOI, J., . . . NOGUCHI, S. 2005. High thioredoxin expression is associated with resistance to docetaxel in primary breast cancer. *Clin Cancer Res,* 11**,** 8425-30.

KIM, S. Y., SUH, H.-W., CHUNG, J. W., YOON, S.-R. & CHOI, I. 2007. Diverse functions of VDUP1 in cell proliferation, differentiation, and diseases. *Cell Mol Immunol,* 4**,** 345-351.

KIM, W., CHOY, W., DYE, J., NAGASAWA, D., SAFAEE, M., FONG, B. & YANG, I. 2011. The tumor biology and molecular characteristics of medulloblastoma identifying prognostic factors associated with survival outcomes and prognosis. *J Clin Neurosci,* 18**,** 886-90.

KLEIN, J., JURATLI, T. A., RADEV, Y., DAUBNER, D., SOUCEK, S., SCHACKERT, G. & KREX, D. 2017. Safety and Effectiveness of Bis-Chloroethylnitrosourea Wafer Chemotherapy in Elderly Patients with Recurrent Glioblastoma. *Oncology,* 93**,** 43-50.

KOHSAKA, S., WANG, L., YACHI, K., MAHABIR, R., NARITA, T., ITOH, T., . . . TANAKA, S. 2012. STAT3 Inhibition Overcomes Temozolomide Resistance in Glioblastoma by Downregulating MGMT Expression. *Molecular Cancer Therapeutics,* 11**,** 1289-1299.

KOHSHI, K., BEPPU, T., TANAKA, K., OGAWA, K., INOUE, O., KUKITA, I. & CLARKE, R. E. 2013. Potential roles of hyperbaric oxygenation in the treatments of brain tumors. *Undersea Hyperb Med,* 40**,** 351-62.

KOMINSKY, S., JOHNSON, H. M., BRYAN, G., TANABE, T., HOBEIKA, A. C., SUBRAMANIAM, P. S. & TORRES, B. 1998. IFNγ inhibition of cell growth in glioblastomas correlates with increased levels of the cyclin dependent kinase inhibitor p21 WAF1/CIP1. *Oncogene,* 17**,** 2973.

KONDZIOLKA, D., MATHIEU, D., LUNSFORD, L. D., MARTIN, J. J., MADHOK, R., NIRANJAN, A. & FLICKINGER, J. C. 2008. Radiosurgery as definitive management of intracranial meningiomas. *Neurosurgery,* 62**,** 53-8; discussion 58-60.

KOOL, M., KORSHUNOV, A., REMKE, M., JONES, D. T., SCHLANSTEIN, M., NORTHCOTT, P. A., . . . PFISTER, S. M. 2012. Molecular subgroups of medulloblastoma: an international meta-analysis of transcriptome, genetic aberrations, and clinical data of WNT, SHH, Group 3, and Group 4 medulloblastomas. *Acta Neuropathol,* 123**,** 473-84.

KOOSHA, F., NESHASTEH-RIZ, A., TAKAVAR, A., EYVAZZADEH, N., MAZAHERI, Z., EYNALI, S. & MOUSAVI, M. 2017. The combination of A-966492 and Topotecan for effective radiosensitization on glioblastoma spheroids. *Biochem Biophys Res Commun,* 491**,** 1092-1097.

KOSCHMANN, C., BLOOM, K., UPADHYAYA, S., GEYER, J. R. & LEARY, S. E. 2016. Survival After Relapse of Medulloblastoma. *J Pediatr Hematol Oncol,* 38**,** 269-73.

KRISHNAMURTHY, P. & WADHWANI, A. 2012. Antioxidant enzymes and human health. *Antioxidant enzyme.* InTech.

KRISHNAN, S., RAO, R. D., JAMES, C. D. & SARKARIA, J. N. 2003. Combination of epidermal growth factor receptor targeted therapy with radiation therapy for malignant gliomas. *Front Biosci,* 8**,** e1-13.

KROCK, B. L., SKULI, N. & SIMON, M. C. 2011. Hypoxia-induced angiogenesis: good and evil. *Genes Cancer,* 2**,** 1117-33.

KUBELT, C., HATTERMANN, K., SEBENS, S., MEHDORN, H. M. & HELD-FEINDT, J. 2015. Epithelial-to-mesenchymal transition in paired human primary and recurrent glioblastomas. *International journal of oncology,* 46**,** 2515-2525.

KUMAR, B., KOUL, S., KHANDRIKA, L., MEACHAM, R. B. & KOUL, H. K. 2008. Oxidative stress is inherent in prostate cancer cells and is required for aggressive phenotype. *Cancer Res,* 68**,** 1777-85.

KUNNUMAKKARA, A. B., BORDOLOI, D., HARSHA, C., BANIK, K., GUPTA, S. C. & AGGARWAL, B. B. 2017. Curcumin mediates anticancer effects by modulating multiple cell signaling pathways. *Clin Sci (Lond),* 131**,** 1781-1799.

KWON, H. J., WON, Y. S., SUH, H. W., JEON, J. H., SHAO, Y., YOON, S. R., . . . CHOI, I. 2010. Vitamin D3 upregulated protein 1 suppresses TNF-alpha-induced NF-kappaB activation in hepatocarcinogenesis. *J Immunol,* 185**,** 3980-9.

LACROIX, M., ABI-SAID, D., FOURNEY, D. R., GOKASLAN, Z. L., SHI, W., DEMONTE, F., . . . SAWAYA, R. 2001. A multivariate analysis of 416

patients with glioblastoma multiforme: prognosis, extent of resection, and survival. *J Neurosurg,* 95**,** 190-8.

LAI, S. F., WANG, C. W., CHEN, Y. H., LAN, K. H., CHENG, J. C., CHENG, A. L. & KUO, S. H. 2012. Medulloblastoma in adults. Treatment outcome, relapse patterns, and prognostic factors. *Strahlenther Onkol,* 188**,** 878-86.

LAMMERING, G., VALERIE, K., LIN, P. S., MIKKELSEN, R. B., CONTESSA, J. N., FEDEN, J. P., . . . SCHMIDT-ULLRICH, R. K. 2001. Radiosensitization of malignant glioma cells through overexpression of dominant-negative epidermal growth factor receptor. *Clin Cancer Res,* 7**,** 682-90.

LAMOUILLE, S., XU, J. & DERYNCK, R. 2014a. Molecular mechanisms of epithelial-mesenchymal transition. *Nature reviews. Molecular cell biology,* 15**,** 178-196.

LAMOUILLE, S., XU, J. & DERYNCK, R. 2014b. Molecular mechanisms of epithelial-mesenchymal transition. *Nat Rev Mol Cell Biol,* 15**,** 178-96.

LAPOINTE, S., PERRY, A. & BUTOWSKI, N. A. 2018. Primary brain tumours in adults. *Lancet,* 392**,** 432-446.

LARSEN, J., WHARTON, S. B., MCKEVITT, F., ROMANOWSKI, C., BRIDGEWATER, C., ZAKI, H. & HOGGARD, N. 2017. 'Low grade glioma': an update for radiologists. *Br J Radiol,* 90**,** 20160600.

LAURENT, T. C., MOORE, E. C. & REICHARD, P. 1964. ENZYMATIC SYNTHESIS OF DEOXYRIBONUCLEOTIDES. IV. ISOLATION AND CHARACTERIZATION OF THIOREDOXIN, THE HYDROGEN DONOR FROM ESCHERICHIA COLI B. *J Biol Chem,* 239**,** 3436-44.

LEE, C. Y. 2017. Strategies of temozolomide in future glioblastoma treatment. *OncoTargets and therapy,* 10**,** 265-270.

LEE, J. M., MHAWECH-FAUCEGLIA, P., LEE, N., PARSANIAN, L. C., LIN, Y. G., GAYTHER, S. A. & LAWRENSON, K. 2013. A three-dimensional microenvironment alters protein expression and chemosensitivity of epithelial ovarian cancer cells in vitro. *Lab Invest,* 93**,** 528-42.

LEECE, R., XU, J., OSTROM, Q. T., CHEN, Y., KRUCHKO, C. & BARNHOLTZ-SLOAN, J. S. 2017. Global incidence of malignant brain and other central nervous system tumors by histology, 2003-2007. *Neuro-oncology,* 19**,** 1553-1564.

LEEK, R., GRIMES, D. R., HARRIS, A. L. & MCINTYRE, A. 2016. Methods: using three-dimensional culture (spheroids) as an in vitro model of tumour hypoxia. *Tumor Microenvironment.* Springer.

LESTER-COLL, N. H., SUPKO, J. G., KLUYTENAAR, J., PAVLIK, K. F., YU, J. B., MOLITERNO, J., . . . BINDRA, R. 2018. Mibefradil dihydrochoride with hypofractionated radiation for recurrent glioblastoma: A phase I dose expansion trial. *Journal of Clinical Oncology,* 36**,** e14046-e14046.

LESUEUR, P., CHEVALIER, F., EL-HABR, E. A., JUNIER, M.-P., CHNEIWEISS, H., CASTERA, L., . . . SAINTIGNY, Y. 2018. Radiosensitization Effect of Talazoparib, a Parp Inhibitor, on Glioblastoma Stem Cells Exposed to Low and High Linear Energy Transfer Radiation. *Scientific Reports,* 8**,** 3664.

LEVIN, W. P., KOOY, H., LOEFFLER, J. S. & DELANEY, T. F. 2005. Proton beam therapy. *British Journal Of Cancer,* 93**,** 849.

LI, X., LI, Y., CAO, Y., LI, P., LIANG, B., SUN, J. & FENG, E. 2017. Safety and efficacy of fractionated stereotactic radiotherapy and stereotactic radiosurgery for treatment of pituitary adenomas: A systematic review and meta-analysis. *J Neurol Sci,* 372**,** 110-116.

LI, Y. & KUMACHEVA, E. 2018. Hydrogel microenvironments for cancer spheroid growth and drug screening. *Science advances,* 4**,** eaas8998.

LIANG, Y. W., ZHENG, J., LI, X., ZHENG, W. & CHEN, T. 2014. Selenadiazole derivatives as potent thioredoxin reductase inhibitors that enhance the radiosensitivity of cancer cells. *Eur J Med Chem,* 84**,** 335-42.

LICHTENFELS, R., KELLNER, R., ATKINS, D., BUKUR, J., ACKERMANN, A., BECK, J., . . . SELIGER, B. 2003. Identification of metabolic enzymes in renal cell carcinoma utilizing PROTEOMEX analyses. *Biochimica et Biophysica Acta (BBA)-Proteins and Proteomics,* 1646**,** 21-31.

LIEBERMAN, F. S., CLOUGHESY, T., FINE, H., KUHN, J., LAMBORN, K., MALKIN, M., . . . PRADOS, M. 2004. NABTC phase I/II trial of ZD-1839 for recurrent malignant gliomas and unresectable meningiomas. *Journal of Clinical Oncology,* 22**,** 1510-1510.

LILLIG, C. H., BERNDT, C. & HOLMGREN, A. 2008. Glutaredoxin systems. *Biochim Biophys Acta,* 1780**,** 1304-17.

LIM, J. & THIERY, J. P. 2012. Epithelial-mesenchymal transitions: insights from development. *Development,* 139**,** 3471-3486.

LIN, Y.-F., NAGASAWA, H., PENG, Y., CHUANG, E. Y. & BEDFORD, J. S. 2009. Comparison of several radiation effects in human MCF10A mammary epithelial cells cultured as 2D monolayers or 3D acinar stuctures in matrigel. *Radiation research,* 171**,** 708-715.

LINAM, J. & YANG, L.-X. 2015. Recent developments in radiosensitization. *Anticancer research,* 35**,** 2479-2485.

LINCOLN, D. T., ALI, E. E., TONISSEN, K. F. & CLARKE, F. M. 2003a. The thioredoxin-thioredoxin reductase system: over-expression in human cancer. *Anticancer research,* 23**,** 2425-2433.

LINCOLN, D. T., ALI EMADI, E. M., TONISSEN, K. F. & CLARKE, F. M. 2003b. The thioredoxin-thioredoxin reductase system: over-expression in human cancer. *Anticancer Res,* 23**,** 2425-33.

LINDER, A., HAGBERG THULIN, M., DAMBER, J.-E. & WELÉN, K. 2018. Analysis of regulator of G-protein signalling 2 (RGS2) expression and function during prostate cancer progression. *Scientific Reports,* 8**,** 17259.

LINET, M. S., SLOVIS, T. L., MILLER, D. L., KLEINERMAN, R., LEE, C., RAJARAMAN, P. & BERRINGTON DE GONZALEZ, A. 2012. Cancer risks associated with external radiation from diagnostic imaging procedures.

LIU, J., HINKHOUSE, M. M., SUN, W., WEYDERT, C. J., RITCHIE, J. M., OBERLEY, L. W. & CULLEN, J. J. 2004. Redox regulation of pancreatic cancer cell growth: role of glutathione peroxidase in the suppression of the malignant phenotype. *Hum Gene Ther,* 15**,** 239-50.

LIU, K. W., PAJTLER, K. W., WORST, B. C., PFISTER, S. M. & WECHSLER-REYA, R. J. 2017. Molecular mechanisms and therapeutic targets in pediatric brain tumors. *Sci Signal,* 10.

LOESSNER, D., STOK, K. S., LUTOLF, M. P., HUTMACHER, D. W., CLEMENTS, J. A. & RIZZI, S. C. 2010. Bioengineered 3D platform to explore cell–ECM interactions and drug resistance of epithelial ovarian cancer cells. *Biomaterials,* 31**,** 8494-8506.

LOGSDON, D. P., GRIMARD, M., LUO, M., SHAHDA, S., JIANG, Y., TONG, Y., . . . FISHEL, M. L. 2016. Regulation of HIF1α under Hypoxia by APE1/Ref-1 Impacts CA9 Expression: Dual Targeting in Patient-Derived 3D Pancreatic Cancer Models. *Molecular cancer therapeutics,* 15**,** 2722-2732.

LOGSDON, D. P., SHAH, F., CARTA, F., SUPURAN, C. T., KAMOCKA, M., JACOBSEN, M. H., . . . FISHEL, M. L. 2018. Blocking HIF signaling via novel inhibitors of CA9 and APE1/Ref-1 dramatically affects pancreatic cancer cell survival. *Scientific reports,* 8**,** 13759-13759.

LOUIS, D. N., OHGAKI, H., WIESTLER, O. D., CAVENEE, W. K., BURGER, P. C., JOUVET, A., . . . KLEIHUES, P. 2007. The 2007 WHO classification of tumours of the central nervous system. *Acta neuropathologica,* 114**,** 97-109.

LOUIS, D. N., PERRY, A., REIFENBERGER, G., VON DEIMLING, A., FIGARELLA-BRANGER, D., CAVENEE, W. K., . . . ELLISON, D. W. 2016. The 2016 World Health Organization Classification of Tumors of the Central Nervous System: a summary. *Acta Neuropathol,* 131**,** 803-20.

LOVITT, C. J., SHELPER, T. B. & AVERY, V. M. 2014. Advanced cell culture techniques for cancer drug discovery. *Biology (Basel),* 3**,** 345-67.

LOVITT, C. J., SHELPER, T. B. & AVERY, V. M. 2015. Evaluation of chemotherapeutics in a three-dimensional breast cancer model. *Journal of cancer research and clinical oncology,* 141**,** 951-959.

LU, C.-T., ZHAO, Y.-Z., WONG, H. L., CAI, J., PENG, L. & TIAN, X.-Q. 2014. Current approaches to enhance CNS delivery of drugs across the brain barriers. *International journal of nanomedicine,* 9**,** 2241-2257.

LU, J., CHEW, E. H. & HOLMGREN, A. 2007. Targeting thioredoxin reductase is a basis for cancer therapy by arsenic trioxide. *Proc Natl Acad Sci U S A,* 104**,** 12288-93.

LU, J. & HOLMGREN, A. 2012. Thioredoxin system in cell death progression. *Antioxid Redox Signal,* 17**,** 1738-47.

LU, J. & HOLMGREN, A. 2014. The thioredoxin antioxidant system. *Free Radic Biol Med,* 66**,** 75-87.

LV, W., BUDKE, B., PAWLOWSKI, M., CONNELL, P. P. & KOZIKOWSKI, A. P. 2016. Development of small molecules that specifically inhibit the D-loop activity of RAD51. *Journal of medicinal chemistry,* 59**,** 4511-4525.

MACAULAY, R. J., WANG, W., DIMITROULAKOS, J., BECKER, L. E. & YEGER, H. 1999. Lovastatin-induced apoptosis of human medulloblastoma cell lines in vitro. *Journal of neuro-oncology,* 42**,** 1-11.

MACDONALD, T. J., AGUILERA, D. & CASTELLINO, R. C. 2014. The rationale for targeted therapies in medulloblastoma. *Neuro Oncol,* 16**,** 9-20.

MAGDA, D., LEPP, C., GERASIMCHUK, N., LEE, I., SESSLER, J. L., LIN, A., . . . MILLER, R. A. 2001a. Redox cycling by motexafin gadolinium enhances cellular response to ionizing radiation by forming reactive oxygen species. *Int J Radiat Oncol Biol Phys,* 51**,** 1025-36.

MAGDA, D., LEPP, C., GERASIMCHUK, N., LEE, I., SESSLER, J. L., LIN, A., . . . MILLER, R. A. 2001b. Redox cycling by motexafin gadolinium enhances cellular response to ionizing radiation by forming reactive oxygen species. *International Journal of Radiation Oncology* Biology* Physics,* 51**,** 1025-1036.

MAGDA, D. & MILLER, R. A. 2006. Motexafin gadolinium: a novel redox active drug for cancer therapy. *Semin Cancer Biol,* 16**,** 466-76.

MAHMOOD, D. F., ABDERRAZAK, A., EL HADRI, K., SIMMET, T. & ROUIS, M. 2013. The thioredoxin system as a therapeutic target in human health and disease. *Antioxid Redox Signal,* 19**,** 1266-303.

MALHOTRA, J. D. & KAUFMAN, R. J. 2007. Endoplasmic reticulum stress and oxidative stress: a vicious cycle or a double-edged sword? *Antioxid Redox Signal,* 9**,** 2277-93.

MALMSTROM, A., GRONBERG, B. H., MAROSI, C., STUPP, R., FRAPPAZ, D., SCHULTZ, H., . . . HENRIKSSON, R. 2012. Temozolomide versus standard 6-week radiotherapy versus hypofractionated radiotherapy in patients older than 60 years with glioblastoma: the Nordic randomised, phase 3 trial. *Lancet Oncol,* 13**,** 916-26.

MARAMPON, F., GRAVINA, G. L., ZANI, B. M., POPOV, V. M., FRATTICCI, A., CERASANI, M., . . . FESTUCCIA, C. 2014. Hypoxia sustains glioblastoma radioresistance through ERKs/DNA-PKcs/HIF-1alpha functional interplay. *Int J Oncol,* 44**,** 2121-31.

MARIANI, L., DEIANA, G., VASSELLA, E., FATHI, A. R., MURTIN, C., ARNOLD, M., . . . REINERT, M. M. 2006. Loss of heterozygosity 1p36 and 19q13 is a prognostic factor for overall survival in patients with diffuse WHO grade 2 gliomas treated without chemotherapy. *J Clin Oncol,* 24**,** 4758-63.

MARTIN, J. L. 1995. Thioredoxin--a fold for all reasons. *Structure,* 3**,** 245-50.

MARTINDALE, J. L. & HOLBROOK, N. J. 2002. Cellular response to oxidative stress: signaling for suicide and survival. *J Cell Physiol,* 192**,** 1-15.

MARZANO, C., GANDIN, V., FOLDA, A., SCUTARI, G., BINDOLI, A. & RIGOBELLO, M. P. 2007. Inhibition of thioredoxin reductase by auranofin induces apoptosis in cisplatin-resistant human ovarian cancer cells. *Free Radic Biol Med,* 42**,** 872-81.

MASAKI, S., MASUTANI, H., YOSHIHARA, E. & YODOI, J. 2012. Deficiency of Thioredoxin Binding Protein-2 (TBP-2) Enhances TGF-β Signaling and Promotes Epithelial to Mesenchymal Transition. *PLOS ONE,* 7**,** e39900.

MASELLA, R. & MAZZA, G. 2009. *Glutathione and sulfur amino acids in human health and disease*, John Wiley & Sons.

MATHEMA, V. B., KOH, Y. S., THAKURI, B. C. & SILLANPAA, M. 2012. Parthenolide, a sesquiterpene lactone, expresses multiple anti-cancer and anti-inflammatory activities. *Inflammation,* 35**,** 560-5.

MATSUZAWA, A. 2017. Thioredoxin and redox signaling: Roles of the thioredoxin system in control of cell fate. *Arch Biochem Biophys,* 617**,** 101-105.

MAYER, B., KLEMENT, G., KANEKO, M., MAN, S., JOTHY, S., RAK, J. & KERBEL, R. S. 2001. Multicellular gastric cancer spheroids recapitulate growth pattern and differentiation phenotype of human gastric carcinomas. *Gastroenterology,* 121**,** 839-52.

MCCARTHY, B. J., RANKIN, K., IL'YASOVA, D., ERDAL, S., VICK, N., ALI-OSMAN, F., . . . DAVIS, F. 2011. Assessment of type of allergy and antihistamine use in the development of glioma. *Cancer Epidemiol Biomarkers Prev,* 20**,** 370-8.

MCDONALD, P. C., WINUM, J.-Y., SUPURAN, C. T. & DEDHAR, S. 2012. Recent developments in targeting carbonic anhydrase IX for cancer therapeutics. *Oncotarget,* 3**,** 84.

MCINTYRE, A. & HARRIS, A. L. 2015. Metabolic and hypoxic adaptation to anti‐angiogenic therapy: a target for induced essentiality. *EMBO Molecular Medicine,* 7**,** 368-379.

MCNEILL, K. A. 2016. Epidemiology of Brain Tumors. *Neurol Clin,* 34**,** 981-998.

MCSHANE, L. M., ALTMAN, D. G., SAUERBREI, W., TAUBE, S. E., GION, M. & CLARK, G. M. 2005. REporting recommendations for tumour MARKer prognostic studies (REMARK). *Br J Cancer,* 93**,** 387-91.

MEHTA, M., BASALINGAPPA, K., GRIFFITH, J. N., ANDRADE, D., BABU, A., AMREDDY, N., . . . MUNSHI, A. 2016. HuR silencing elicits oxidative stress and DNA damage and sensitizes human triple-negative breast cancer cells to radiotherapy. *Oncotarget,* 7**,** 64820-64835.

MEHTA, M. P., RODRIGUS, P., TERHAARD, C., RAO, A., SUH, J., ROA, W., . . . KOMAKI, R. 2003. Survival and neurologic outcomes in a randomized trial of motexafin gadolinium and whole-brain radiation therapy in brain metastases. *Journal of Clinical Oncology,* 21**,** 2529-2536.

MEHTA, M. P., SHAPIRO, W. R., GLANTZ, M. J., PATCHELL, R. A., WEITZNER, M. A., MEYERS, C. A., . . . FORD, J. 2002. Lead-in phase to randomized trial of motexafin gadolinium and whole-brain radiation for patients with brain metastases: centralized assessment of magnetic resonance imaging, neurocognitive, and neurologic end points. *Journal of clinical oncology,* 20**,** 3445-3453.

MEHTA, M. P., SHAPIRO, W. R., PHAN, S. C., GERVAIS, R., CARRIE, C., CHABOT, P., . . . RENSCHLER, M. F. 2009. Motexafin gadolinium combined with prompt whole brain radiotherapy prolongs time to neurologic progression in non-small-cell lung cancer patients with brain metastases: results of a phase III trial. *Int J Radiat Oncol Biol Phys,* 73**,** 1069-76.

MEHTA, S. K. & GOWDER, S. J. T. 2015. Members of antioxidant machinery and their functions. *Basic Principles and Clinical Significance of Oxidative Stress.* InTech.

MEISTER, A. 1994. Glutathione-ascorbic acid antioxidant system in animals. *J Biol Chem,* 269**,** 9397-400.

MERCHANT, T. E., HUA, C. H., SHUKLA, H., YING, X., NILL, S. & OELFKE, U. 2008. Proton versus photon radiotherapy for common pediatric brain tumors: comparison of models of dose characteristics and their relationship to cognitive function. *Pediatr Blood Cancer,* 51**,** 110-7.

MICHAELS, H. B. & HUNT, J. W. 1978. A model for radiation damage in cells by direct effect and by indirect effect: a radiation chemistry approach. *Radiat Res,* 74**,** 23-34.

MILLER, R. A., WOODBURN, K., FAN, Q., RENSCHLER, M. F., SESSLER, J. L. & KOUTCHER, J. A. 1999. In vivo animal studies with gadolinium (III) texaphyrin as a radiation enhancer. *International Journal of Radiation Oncology* Biology* Physics,* 45**,** 981-989.

MINCHINTON, A. I. & TANNOCK, I. F. 2006. Drug penetration in solid tumours. *Nature Reviews Cancer,* 6**,** 583.

MINNITI, G., ESPOSITO, V., AMICHETTI, M. & ENRICI, R. M. 2009. The role of fractionated radiotherapy and radiosurgery in the management of patients with craniopharyngioma. *Neurosurg Rev,* 32**,** 125-32; discussion 132.

MIRAB, F., KANG, Y. J. & MAJD, S. 2019. Preparation and characterization of size-controlled glioma spheroids using agarose hydrogel microwells. *PLoS One,* 14**,** e0211078.

MIRJOLET, C., PAPA, A. L., CREHANGE, G., RAGUIN, O., SEIGNEZ, C., PAUL, C., . . . MILLOT, N. 2013. The radiosensitization effect of titanate nanotubes as a new tool in radiation therapy for glioblastoma: a proof-of-concept. *Radiother Oncol,* 108**,** 136-42.

MISRA, K., DHILLON, G. S., BRAR, S. K. & VERMA, M. 2014. Antioxidants. *Biotransformation of Waste Biomass into High Value Biochemicals.* Springer.

MISTRY, I. N., THOMAS, M., CALDER, E. D. D., CONWAY, S. J. & HAMMOND, E. M. 2017. Clinical Advances of Hypoxia-Activated Prodrugs in Combination With Radiation Therapy. *International Journal of Radiation Oncology*Biology*Physics,* 98**,** 1183-1196.

MITCHELL, D. A. & MARLETTA, M. A. 2005. Thioredoxin catalyzes the S-nitrosation of the caspase-3 active site cysteine. *Nat Chem Biol,* 1**,** 154-8.

MITCHELL, J. B., CHOUDHURI, R., FABRE, K., SOWERS, A. L., CITRIN, D., ZABLUDOFF, S. D. & COOK, J. A. 2010. In vitro and in vivo radiation sensitization of human tumor cells by a novel checkpoint kinase inhibitor, AZD7762. *Clinical cancer research,* 16**,** 2076-2084.

MIYAZAKI, K., NODA, N., OKADA, S., HAGIWARA, Y., MIYATA, M., SAKURABAYASHI, I., . . . WAKASUGI, H. 1998. EIevated serum level of Thioredoxin in patients with Hepatocellular Carcinoma. *Biotherapy,* 11**,** 277-288.

MIZUMOTO, M., OSHIRO, Y., YAMAMOTO, T., KOHZUKI, H. & SAKURAI, H. 2017. Proton Beam Therapy for Pediatric Brain Tumor. *Neurol Med Chir (Tokyo),* 57**,** 343-355.

MOCHIZUKI, M., KWON, Y. W., YODOI, J. & MASUTANI, H. 2009. Thioredoxin regulates cell cycle via the ERK1/2-cyclin D1 pathway. *Antioxid Redox Signal,* 11**,** 2957-71.

MOHINDRA, P., SINHA, R. N., ANDREWS, R. J. & KHUNTIA, D. 2012. Non-cytotoxic radiosensitizers in brain radiotherapy: journey till the first decade of this millennium. *Curr Cancer Drug Targets,* 12**,** 260-78.

MOREL, K. L., ORMSBY, R. J., BEZAK, E., SWEENEY, C. J. & SYKES, P. J. 2017. Parthenolide Selectively Sensitizes Prostate Tumor Tissue to Radiotherapy while Protecting Healthy Tissues In Vivo. *Radiat Res,* 187**,** 501-512.

MORGAN, B., EZERINA, D., AMOAKO, T. N., RIEMER, J., SEEDORF, M. & DICK, T. P. 2013. Multiple glutathione disulfide removal pathways mediate cytosolic redox homeostasis. *Nat Chem Biol,* 9**,** 119-25.

MORRIS, G., ANDERSON, G., DEAN, O., BERK, M., GALECKI, P., MARTIN-SUBERO, M. & MAES, M. 2014. The glutathione system: a new drug target in neuroimmune disorders. *Mol Neurobiol,* 50**,** 1059-84.

MOTHERSILL, C. & SEYMOUR, C. B. 2004. Radiation-induced bystander effects--implications for cancer. *Nat Rev Cancer,* 4**,** 158-64.

MUKHERJEE, A., HUBER, K., EVANS, H., LAKHANI, N. & MARTIN, S. 2007. A cellular and molecular investigation of the action of PMX464, a putative thioredoxin inhibitor, in normal and colorectal cancer cell lines. *British journal of pharmacology,* 151**,** 1167-1175.

MUKHERJEE, A., WESTWELL, A. D., BRADSHAW, T. D., STEVENS, M. F., CARMICHAEL, J. & MARTIN, S. G. 2005. Cytotoxic and antiangiogenic activity of AW464 (NSC 706704), a novel thioredoxin inhibitor: an in vitro study. *Br J Cancer,* 92**,** 350-8.

MURPHY, E. S. & SUH, J. H. 2011. Radiotherapy for vestibular schwannomas: a critical review. *Int J Radiat Oncol Biol Phys,* 79**,** 985-97.

MUSTACICH, D. & POWIS, G. 2000. Thioredoxin reductase. *Biochemical Journal,* 346**,** 1-8.

MUZ, B., DE LA PUENTE, P., AZAB, F. & AZAB, A. K. 2015. The role of hypoxia in cancer progression, angiogenesis, metastasis, and resistance to therapy. *Hypoxia (Auckland, N.Z.),* 3**,** 83-92.

NAILOR, A., WALKER, D. A., JACQUES, T. S., WARREN, K. E., BREM, H., KEARNS, P. R., . . . KILDAY, J.-P. 2016. Highlights of Children with Cancer UK's Workshop on Drug Delivery in Paediatric Brain Tumours. *Ecancermedicalscience,* 10**,** 630-630.

NAKAJIMA, S., DOI, R., TOYODA, E., TSUJI, S., WADA, M., KOIZUMI, M., . . . MORI, T. 2004. N-cadherin expression and epithelial-mesenchymal transition in pancreatic carcinoma. *Clinical cancer research,* 10**,** 4125-4133.

NARANJO-SUAREZ, S., CARLSON, B. A., TOBE, R., YOO, M. H., TSUJI, P. A., GLADYSHEV, V. N. & HATFIELD, D. L. 2013. Regulation of HIF-1alpha activity by overexpression of thioredoxin is independent of thioredoxin reductase status. *Mol Cells,* 36**,** 151-7.

NARANJO-SUAREZ, S., CARLSON, B. A., TSUJI, P. A., YOO, M.-H., GLADYSHEV, V. N. & HATFIELD, D. L. 2012. HIF-independent regulation of thioredoxin

reductase 1 contributes to the high levels of reactive oxygen species induced by hypoxia. *PLoS One,* 7**,** e30470.

NATIONAL COMPREHENSIVE CANCER NETWORK. 2018. *Central Nervous System Cancers (version 2.2018)* [Online]. Available: https://www.nccn.org/professionals/physician_gls/pdf/cns.pdf [Accessed 05/12/2018].

NEWLANDS, E. S., BLACKLEDGE, G. R., SLACK, J. A., RUSTIN, G. J., SMITH, D. B., STUART, N. S., . . . ET AL. 1992. Phase I trial of temozolomide (CCRG 81045: M&B 39831: NSC 362856). *Br J Cancer,* 65**,** 287-91.

NGUYEN, P., AWWAD, R. T., SMART, D. D., SPITZ, D. R. & GIUS, D. 2006. Thioredoxin reductase as a novel molecular target for cancer therapy. *Cancer Lett,* 236**,** 164-74.

NIEDER, C., ANDRATSCHKE, N. H. & GROSU, A. L. 2016. Re-irradiation for Recurrent Primary Brain Tumors. *Anticancer Res,* 36**,** 4985-4995.

NIETO, M. A. & CANO, A. 2012. The epithelial-mesenchymal transition under control: global programs to regulate epithelial plasticity. *Semin Cancer Biol,* 22**,** 361-8.

NIEWIDOK, N., WACK, L.-J., SCHIESSL, S., STINGL, L., KATZER, A., POLAT, B., . . . DJUZENOVA, C. S. 2012. Hsp90 Inhibitors NVP-AUY922 and NVP-BEP800 May Exert a Significant Radiosensitization on Tumor Cells along with a Cell Type-Specific Cytotoxicity. *Translational oncology,* 5**,** 356-369.

NIMSE, S. B. & PAL, D. 2015. Free radicals, natural antioxidants, and their reaction mechanisms. *Rsc Advances,* 5**,** 27986-28006.

NIRMALANANDHAN, V. S., DUREN, A., HENDRICKS, P., VIELHAUER, G. & SITTAMPALAM, G. S. 2010. Activity of anticancer agents in a three-dimensional cell culture model. *Assay and drug development technologies,* 8**,** 581-590.

NISHIYAMA, A., MATSUI, M., IWATA, S., HIROTA, K., MASUTANI, H., NAKAMURA, H., . . . YODOI, J. 1999. Identification of thioredoxin-binding protein-2/vitamin D(3) up-regulated protein 1 as a negative regulator of thioredoxin function and expression. *J Biol Chem,* 274**,** 21645-50.

NITA, M. & GRZYBOWSKI, A. 2016. The Role of the Reactive Oxygen Species and Oxidative Stress in the Pathomechanism of the Age-Related Ocular Diseases and Other Pathologies of the Anterior and Posterior Eye Segments in Adults. *Oxid Med Cell Longev,* 2016**,** 3164734.

NOLAN, K. A., DUNSTAN, M. S., CARAHER, M. C., SCOTT, K. A., LEYS, D. & STRATFORD, I. J. 2012. In silico screening reveals structurally diverse, nanomolar inhibitors of NQO2 that are functionally active in cells and can modulate NF-κB signaling. *Molecular cancer therapeutics,* 11**,** 194-203.

NONN, L., WILLIAMS, R. R., ERICKSON, R. P. & POWIS, G. 2003. The absence of mitochondrial thioredoxin 2 causes massive apoptosis, exencephaly, and early embryonic lethality in homozygous mice. *Mol Cell Biol,* 23**,** 916-22.

NORDBERG, J. & ARNER, E. S. 2001. Reactive oxygen species, antioxidants, and the mammalian thioredoxin system. *Free Radic Biol Med,* 31**,** 1287-312.

NOZATO, M., KANEKO, S., NAKAGAWARA, A. & KOMURO, H. 2012. Epithelial-mesenchymal transition-related gene expression as a new prognostic marker for neuroblastoma. *International journal of oncology,* 42**,** 134-140.

O'BRIEN, P. 1991. Molecular mechanisms of quinone cytotoxicity. *Chemico-biological interactions,* 80**,** 1-41.

OGAWA, K., ISHIUCHI, S., INOUE, O., YOSHII, Y., SAITO, A., WATANABE, T., . . . MURAYAMA, S. 2012. Phase II trial of radiotherapy after hyperbaric oxygenation with multiagent chemotherapy (procarbazine, nimustine, and vincristine) for high-grade gliomas: long-term results. *Int J Radiat Oncol Biol Phys,* 82**,** 732-8.

OLADGHAFFARI, M., SHABESTANI MONFARED, A., FARAJOLLAHI, A., BARADARAN, B., MOHAMMADI, M., SHANEHBANDI, D., . . . PIRAYESH ISLAMIAN, J. 2017. MLN4924 and 2DG combined treatment enhances the efficiency of radiotherapy in breast cancer cells. *Int J Radiat Biol,* 93**,** 590-599.

OOSTERWIJK, E. 2014. Carbonic anhydrase expression in kidney and renal cancer: implications for diagnosis and treatment. *Carbonic Anhydrase: Mechanism, Regulation, Links to Disease, and Industrial Applications.* Springer.

ORTIZ, M. A., LOPEZ-HERNANDEZ, F. J., BAYON, Y., PFAHL, M. & PIEDRAFITA, F. J. 2001. Retinoid-related molecules induce cytochrome c release and apoptosis through activation of c-Jun NH2-terminal kinase/p38 mitogen-activated protein kinases. *Cancer Research,* 61**,** 8504-8512.

OSTROM, Q. T., GITTLEMAN, H., DE BLANK, P. M., FINLAY, J. L., GURNEY, J. G., MCKEAN-COWDIN, R., . . . BARNHOLTZ-SLOAN, J. S. 2016a. American Brain Tumor Association Adolescent and Young Adult Primary Brain and Central Nervous System Tumors Diagnosed in the United States in 2008-2012. *Neuro Oncol,* 18 Suppl 1**,** i1-i50.

OSTROM, Q. T., GITTLEMAN, H., FULOP, J., LIU, M., BLANDA, R., KROMER, C., . . . BARNHOLTZ-SLOAN, J. S. 2015. CBTRUS Statistical Report: Primary Brain and Central Nervous System Tumors Diagnosed in the United States in 2008-2012. *Neuro Oncol,* 17 Suppl 4**,** iv1-iv62.

OSTROM, Q. T., GITTLEMAN, H., LIAO, P., VECCHIONE-KOVAL, T., WOLINSKY, Y., KRUCHKO, C. & BARNHOLTZ-SLOAN, J. S. 2017. CBTRUS Statistical Report: Primary brain and other central nervous system tumors diagnosed in the United States in 2010-2014. *Neuro Oncol,* 19**,** v1-v88.

OSTROM, Q. T., GITTLEMAN, H., XU, J., KROMER, C., WOLINSKY, Y., KRUCHKO, C. & BARNHOLTZ-SLOAN, J. S. 2016b. CBTRUS Statistical Report: Primary Brain and Other Central Nervous System Tumors Diagnosed in the United States in 2009-2013. *Neuro Oncol,* 18**,** v1-v75.

OTHMAN, R. T., KIMISHI, I., BRADSHAW, T. D., STORER, L. C., KORSHUNOV, A., PFISTER, S. M., . . . COYLE, B. 2014. Overcoming multiple drug resistance mechanisms in medulloblastoma. *Acta Neuropathol Commun,* 2**,** 57.

OVERGAARD, J. 2007. Hypoxic radiosensitization: adored and ignored. *Journal of Clinical Oncology,* 25**,** 4066-4074.

PABLA, N., HUANG, S., MI, Q.-S., DANIEL, R. & DONG, Z. 2008. ATR-Chk2 signaling in p53 activation and DNA damage response during cisplatin-induced apoptosis. *Journal of Biological Chemistry,* 283**,** 6572-6583.

PACKER, R. J., GAJJAR, A., VEZINA, G., RORKE-ADAMS, L., BURGER, P. C., ROBERTSON, P. L., . . . SPOSTO, R. 2006. Phase III study of craniospinal radiation therapy followed by adjuvant chemotherapy for newly diagnosed average-risk medulloblastoma. *J Clin Oncol,* 24**,** 4202-8.

PACKER, R. J., MACDONALD, T. & VEZINA, G. 2010. Central nervous system tumors. *Hematol Oncol Clin North Am,* 24**,** 87-108.

PAL, M., MISRA, K., DHILLON, G., KAUR BRAR, S. & VERMA, M. 2014. Antioxidants.

PANG, L. Y., SAUNDERS, L. & ARGYLE, D. J. 2017. Epidermal growth factor receptor activity is elevated in glioma cancer stem cells and is required to maintain chemotherapy and radiation resistance. *Oncotarget,* 8**,** 72494-72512.

PARK, K.-J., KIM, Y.-J., CHOI, E. J., PARK, N. K., KIM, G. H., KIM, S. M., . . . KIM, D.-W. 2010. Expression pattern of the thioredoxin system in human endothelial progenitor cells and endothelial cells under hypoxic injury. *Korean circulation journal,* 40**,** 651-658.

PARK, S. H., WON, J., KIM, S. I., LEE, Y., PARK, C. K., KIM, S. K. & CHOI, S. H. 2017. Molecular Testing of Brain Tumor. *J Pathol Transl Med,* 51**,** 205-223.

PASCIAK, A. S., BRADLEY, Y. & MCKINNEY, J. M. 2016. *Handbook of Radioembolization: Physics, Biology, Nuclear Medicine, and Imaging*, CRC Press.

PATTERSON, A. V., BARHAM, H. M., CHINJE, E. C., ADAMS, G. E., HARRIS, A. L. & STRATFORD, I. J. 1995. Importance of P450 reductase activity in determining sensitivity of breast tumour cells to the bioreductive drug, tirapazamine (SR 4233). *Br J Cancer,* 72**,** 1144-50.

PATWARDHAN, R. S., SHARMA, D., CHECKER, R., THOH, M. & SANDUR, S. K. 2015. Spatio-temporal changes in glutathione and thioredoxin redox couples during ionizing radiation-induced oxidative stress regulate tumor radio-resistance. *Free Radic Res,* 49**,** 1218-32.

PEARCE, M. S., SALOTTI, J. A., LITTLE, M. P., MCHUGH, K., LEE, C., KIM, K. P., . . . BERRINGTON DE GONZALEZ, A. 2012. Radiation exposure from CT scans in childhood and subsequent risk of leukaemia and brain tumours: a retrospective cohort study. *Lancet,* 380**,** 499-505.

PEI, Y., LIU, K. W., WANG, J., GARANCHER, A., TAO, R., ESPARZA, L. A., . . . WECHSLER-REYA, R. J. 2016. HDAC and PI3K Antagonists Cooperate to Inhibit Growth of MYC-Driven Medulloblastoma. *Cancer Cell,* 29**,** 311-323.

PEKMEZCI, M., RICE, T., MOLINARO, A. M., WALSH, K. M., DECKER, P. A., HANSEN, H., . . . WRENSCH, M. R. 2017. Adult infiltrating gliomas with WHO 2016 integrated diagnosis: additional prognostic roles of ATRX and TERT. *Acta Neuropathol,* 133**,** 1001-1016.

PENNEY, R. B. & ROY, D. 2013. Thioredoxin-mediated redox regulation of resistance to endocrine therapy in breast cancer. *Biochimica et Biophysica Acta (BBA)-Reviews on Cancer,* 1836**,** 60-79.

PERAZZOLI, G., PRADOS, J., ORTIZ, R., CABA, O., CABEZA, L., BERDASCO, M., . . . MELGUIZO, C. 2015. Temozolomide Resistance in Glioblastoma Cell Lines: Implication of MGMT, MMR, P-Glycoprotein and CD133 Expression. *PLoS One,* 10**,** e0140131.

PERRY, J. R., LAPERRIERE, N., O'CALLAGHAN, C. J., BRANDES, A. A., MENTEN, J., PHILLIPS, C., . . . MASON, W. P. 2017. Short-Course Radiation plus Temozolomide in Elderly Patients with Glioblastoma. *N Engl J Med,* 376**,** 1027-1037.

PESSETTO, Z. Y., WEIR, S. J., SETHI, G., BROWARD, M. A. & GODWIN, A. K. 2013. Drug repurposing for gastrointestinal stromal tumor. *Molecular cancer therapeutics*.

PFISTER, S., REMKE, M., BENNER, A., MENDRZYK, F., TOEDT, G., FELSBERG, J., . . . KORSHUNOV, A. 2009. Outcome prediction in pediatric medulloblastoma based on DNA copy-number aberrations of chromosomes 6q and 17q and the MYC and MYCN loci. *J Clin Oncol,* 27**,** 1627-36.

PHAM, A., LEE, B. & CHANG, E. L. 2017. Stereotactic Radiosurgery for Multiple Brain Metastases: Two Cases of Preserved Quality of Life. *Cureus,* 9**,** e1995-e1995.

PHILIPS, A., HENSHAW, D. L., LAMBURN, G. & O'CARROLL, M. J. 2018. Brain tumours: rise in Glioblastoma Multiforme incidence in England 1995–2015 suggests an adverse environmental or lifestyle factor. *Journal of environmental and public health,* 2018**,** 7910754.

PHILLIPS, R. M., HENDRIKS, H. R., PETERS, G. J., EORTC ‐ PHARMACOLOGY & GROUP, M. M. 2013. EO9 (Apaziquone): from the clinic to the laboratory and back again. *British journal of pharmacology,* 168**,** 11-18.

PHILLIPS, R. M., HENDRIKS, H. R., SWEENEY, J. B., REDDY, G. & PETERS, G. J. 2017. Efficacy, pharmacokinetic and pharmacodynamic evaluation of apaziquone in the treatment of non-muscle invasive bladder cancer. *Expert Opin Drug Metab Toxicol,* 13**,** 783-791.

PICHANDI, A., GANESH, K. M., JERRIN, A., BALAJI, K., SRIDHAR, P. S. & SUREGA, A. 2015. Cranio Spinal Irradiation of Medulloblastoma Using High Precision Techniques - A Dosimetric Comparison. *Technol Cancer Res Treat,* 14**,** 491-6.

PIGNATTI, F., VAN DEN BENT, M., CURRAN, D., DEBRUYNE, C., SYLVESTER, R., THERASSE, P., . . . KARIM, A. B. 2002. Prognostic factors for survival in adult patients with cerebral low-grade glioma. *J Clin Oncol,* 20**,** 2076-84.

PIRAYESH ISLAMIAN, J., HATAMIAN, M., AVAL, N. A., RASHIDI, M. R., MESBAHI, A., MOHAMMADZADEH, M. & ASGHARI JAFARABADI, M. 2017. Targeted superparamagnetic nanoparticles coated with 2-deoxy-d-gloucose and doxorubicin more sensitize breast cancer cells to ionizing radiation. *Breast,* 33**,** 97-103.

PIRES, I. M., OLCINA, M. M., ANBALAGAN, S., POLLARD, J. R., REAPER, P. M., CHARLTON, P. A., . . . HAMMOND, E. M. 2012. Targeting radiation-resistant hypoxic tumour cells through ATR inhibition. *British Journal Of Cancer,* 107**,** 291.

PISTOLLATO, F., RAMPAZZO, E., PERSANO, L., ABBADI, S., FRASSON, C., DENARO, L., . . . BASSO, G. 2010. Interaction of hypoxia-inducible factor-1α and Notch signaling regulates medulloblastoma precursor proliferation and fate. *Stem cells (Dayton, Ohio),* 28**,** 1918-1929.

PLUMB, J. A., GERRITSEN, M., MILROY, R., THOMSON, P. & WORKMAN, P. 1994. Relative importance of DT-diaphorase and hypoxia in the bioactivation of E09 by human lung tumor cell lines. *International Journal of Radiation Oncology* Biology* Physics,* 29**,** 295-299.

PLUMB, J. A. & WORKMAN, P. 1994. Unusually marked hypoxic sensitization to indoloquinone E09 and mitomycin C in a human colon‐tumour cell line that lacks DT‐diaphorase activity. *International journal of cancer,* 56**,** 134-139.

POLKINGHORN, W. R., DUNKEL, I. J., SOUWEIDANE, M. M., KHAKOO, Y., LYDEN, D. C., GILHEENEY, S. W., . . . WOLDEN, S. L. 2011. Disease control and ototoxicity using intensity-modulated radiation therapy tumor-bed boost for medulloblastoma. *Int J Radiat Oncol Biol Phys,* 81**,** e15-20.

POWIS, G. & KIRKPATRICK, D. L. 2007. Thioredoxin signaling as a target for cancer therapy. *Current opinion in pharmacology,* 7**,** 392-397.

POWIS, G., KIRKPATRICK, D. L., ANGULO, M. & BAKER, A. 1998. Thioredoxin redox control of cell growth and death and the effects of inhibitors. *Chem Biol Interact,* 111-112**,** 23-34.

POWIS, G. & MONTFORT, W. R. 2001. Properties and biological activities of thioredoxins. *Annu Rev Pharmacol Toxicol,* 41**,** 261-95.

POWIS, G., MUSTACICH, D. & COON, A. 2000. The role of the redox protein thioredoxin in cell growth and cancer. *Free Radic Biol Med,* 29**,** 312-22.

POWIS, G., WIPF, P., LYNCH, S. M., BIRMINGHAM, A. & KIRKPATRICK, D. L. 2006. Molecular pharmacology and antitumor activity of palmarumycin-based inhibitors of thioredoxin reductase. *Molecular cancer therapeutics,* 5**,** 630-636.

PRASAD, G. & HAAS-KOGAN, D. A. 2009. Radiation-induced gliomas. *Expert review of neurotherapeutics,* 9**,** 1511-1517.

PRAST-NIELSEN, S., HUANG, H.-H. & WILLIAMS, D. L. 2011. Thioredoxin glutathione reductase: its role in redox biology and potential as a target for drugs against neglected diseases. *Biochimica et biophysica acta,* 1810**,** 1262-1271.

QIU, L., ZHANG, F., SHI, Y., BAI, Z., WANG, J., LI, Y., . . . YANG, X. 2016. Gliomas: Motexafin Gadolinium-enhanced Molecular MR Imaging and Optical Imaging for Potential Intraoperative Delineation of Tumor Margins. *Radiology,* 279**,** 400-9.

QU, Y., WANG, J., RAY, P. S., GUO, H., HUANG, J., SHIN-SIM, M., . . . CUI, X. 2011. Thioredoxin-like 2 regulates human cancer cell growth and metastasis via redox homeostasis and NF-kappaB signaling. *J Clin Invest,* 121**,** 212-25.

QUINLAN, A. & RIZZOLO, D. 2017. Understanding medulloblastoma. *Jaapa,* 30**,** 30-36.

RAAPHORST, G. P., FEELEY, M. M., DA SILVA, V. F., DANJOUX, C. E. & GERIG, L. H. 1989. A comparison of heat and radiation sensitivity of three human glioma cell lines. *International Journal of Radiation Oncology • Biology • Physics,* 17**,** 615-622.

RAFFEL, J., BHATTACHARYYA, A. K., GALLEGOS, A., CUI, H., EINSPAHR, J. G., ALBERTS, D. S. & POWIS, G. 2003. Increased expression of thioredoxin-1 in human colorectal cancer is associated with decreased patient survival. *Journal of Laboratory and Clinical Medicine,* 142**,** 46-51.

RAGONESE, M., RACIOPPI, M., BASSI, P. F., DI GIANFRANCESCO, L., LENCI, N., FILIANOTI, A. & RECUPERO, S. M. 2016. Mitomycin C: new strategies to improve efficacy of a well-known therapy. *Urologia,* 83**,** 24-28.

RAMASWAMY, V., NOR, C. & TAYLOR, M. D. 2015. p53 and Meduloblastoma. *Cold Spring Harb Perspect Med,* 6**,** a026278.

RAMASWAMY, V., REMKE, M., BOUFFET, E., BAILEY, S., CLIFFORD, S. C., DOZ, F., . . . POMEROY, S. L. 2016. Risk stratification of childhood medulloblastoma in the molecular era: the current consensus. *Acta Neuropathol,* 131**,** 821-31.

RAMASWAMY, V. & TAYLOR, M. D. 2017. Medulloblastoma: From Myth to Molecular. *J Clin Oncol,* 35**,** 2355-2363.

RAMKISSOON, L. A., BRITT, N., GUEVARA, A., WHITT, E., SEVERSON, E., SATHYAN, P., . . . RAMKISSOON, S. H. 2018. Precision Neuro-oncology: the Role of Genomic Testing in the Management of Adult and Pediatric Gliomas. *Curr Treat Options Oncol,* 19**,** 41.

RAVIRAJ, J., BOKKASAM, V. K., KUMAR, V. S., REDDY, U. S. & SUMAN, V. 2014. Radiosensitizers, radioprotectors, and radiation mitigators. *Indian Journal of Dental Research,* 25**,** 83.

REARDON, D. A., WEN, P. Y. & MELLINGHOFF, I. K. 2014. Targeted molecular therapies against epidermal growth factor receptor: Past experiences and challenges. *Neuro-Oncology,* 16**,** viii7-viii13.

REE, A. H., BRATLAND, A., NOME, R. V., STOKKE, T., FODSTAD, O. & ANDERSSON, Y. 2004. Inhibitory targeting of checkpoint kinase signaling overrides radiation-induced cell cycle gene regulation: a therapeutic strategy in tumor cell radiosensitization? *Radiother Oncol,* 72**,** 305-10.

RIBI, K., RELLY, C., LANDOLT, M., ALBER, F., BOLTSHAUSER, E. & GROTZER, M. 2005. Outcome of medulloblastoma in children: long-term complications and quality of life. *Neuropediatrics,* 36**,** 357-365.

RIGOBELLO, M. P., SCUTARI, G., FOLDA, A. & BINDOLI, A. 2004. Mitochondrial thioredoxin reductase inhibition by gold(I) compounds and concurrent stimulation of permeability transition and release of cytochrome c. *Biochem Pharmacol,* 67**,** 689-96.

ROBERTSON, N., HAIGH, A., ADAMS, G. & STRATFORD, I. 1994. Factors affecting sensitivity to EO9 in rodent and human tumour cells in vitro: DT-diaphorase activity and hypoxia. *European Journal of Cancer,* 30**,** 1013-1019.

ROBINSON, G. W., ORR, B. A., WU, G., GURURANGAN, S., LIN, T., QADDOUMI, I., . . . GAJJAR, A. 2015. Vismodegib Exerts Targeted Efficacy Against Recurrent Sonic Hedgehog-Subgroup Medulloblastoma: Results From Phase II Pediatric Brain Tumor Consortium Studies PBTC-025B and PBTC-032. *J Clin Oncol,* 33**,** 2646-54.

ROCKWELL, S., DONNELLY, E. T., LIU, Y. & TANG, L.-Q. 2002. Preliminary studies of the effects of gadolinium texaphyrin on the growth and radiosensitivity of EMT6 cells in vitro. *International Journal of Radiation Oncology* Biology* Physics,* 54**,** 536-541.

RODER, C. & THOMSON, M. J. 2015. Auranofin: repurposing an old drug for a golden new age. *Drugs in R&D,* 15**,** 13-20.

RODMAN, S. N., SPENCE, J. M., RONNFELDT, T. J., ZHU, Y., SOLST, S. R., O'NEILL, R. A., . . . FATH, M. A. 2016. Enhancement of Radiation Response in Breast Cancer Stem Cells by Inhibition of Thioredoxin- and Glutathione-Dependent Metabolism. *Radiat Res,* 186**,** 385-395.

ROGAKOU, E. P., PILCH, D. R., ORR, A. H., IVANOVA, V. S. & BONNER, W. M. 1998. DNA double-stranded breaks induce histone H2AX phosphorylation on serine 139. *Journal of biological chemistry,* 273**,** 5858-5868.

RONG, Y., DURDEN, D. L., VAN MEIR, E. G. & BRAT, D. J. 2006. 'Pseudopalisading'necrosis in glioblastoma: a familiar morphologic feature that links vascular pathology, hypoxia, and angiogenesis. *Journal of Neuropathology & Experimental Neurology,* 65**,** 529-539.

RONG, Y. & WELSH, J. S. 2011. Dosimetric and clinical review of helical tomotherapy. *Expert Rev Anticancer Ther,* 11**,** 309-20.

RONSON, B. B., SCHULTE, R. W., HAN, K. P., LOREDO, L. N., SLATER, J. M. & SLATER, J. D. 2006. Fractionated proton beam irradiation of pituitary adenomas. *Int J Radiat Oncol Biol Phys,* 64**,** 425-34.

ROOD, B. R., MACDONALD, T. J. & PACKER, R. J. 2004. Current treatment of medulloblastoma: recent advances and future challenges. *Semin Oncol,* 31**,** 666-75.

ROULEAU, M., PATEL, A., HENDZEL, M. J., KAUFMANN, S. H. & POIRIER, G. G. 2010. PARP inhibition: PARP1 and beyond. *Nature reviews cancer,* 10**,** 293.

RUDIN, C. M. 2012. Vismodegib. *Clinical Cancer Research,* 18**,** 3218-3222.

RUDIN, C. M., HANN, C. L., LATERRA, J., YAUCH, R. L., CALLAHAN, C. A., FU, L., . . . LOW, J. A. 2009. Treatment of medulloblastoma with hedgehog pathway inhibitor GDC-0449. *N Engl J Med,* 361**,** 1173-8.

RUNDLE, S., BRADBURY, A., DREW, Y. & CURTIN, N. J. 2017. Targeting the ATR-CHK1 Axis in Cancer Therapy. *Cancers,* 9**,** 41.

RUTKA, J., GIBLIN, J., DOUGHERTY, D., LIU, H., MCCULLOCH, J., BELL, C., . . . ROSENBLUM, M. 1987. Establishment and characterization of five cell lines derived from human malignant gliomas. *Acta neuropathologica,* 75**,** 92-103.

RUTKOWSKI, S., VON HOFF, K., EMSER, A., ZWIENER, I., PIETSCH, T., FIGARELLA-BRANGER, D., . . . GRILL, J. 2010. Survival and Prognostic

Factors of Early Childhood Medulloblastoma: An International Meta-Analysis. *Journal of Clinical Oncology,* 28**,** 4961-4968.

RYU, S., BUATTI, J. M., MORRIS, A., KALKANIS, S. N., RYKEN, T. C. & OLSON, J. J. 2014. The role of radiotherapy in the management of progressive glioblastoma : a systematic review and evidence-based clinical practice guideline. *J Neurooncol,* 118**,** 489-99.

SABEL, M., FLEISCHHACK, G., TIPPELT, S., GUSTAFSSON, G., DOZ, F., KORTMANN, R., . . . RUTKOWSKI, S. 2016. Relapse patterns and outcome after relapse in standard risk medulloblastoma: a report from the HIT-SIOP-PNET4 study. *Journal of neuro-oncology,* 129**,** 515-524.

SAID, H. M., HAGEMANN, C., STAAB, A., STOJIC, J., KÜHNEL, S., VINCE, G. H., . . . VORDERMARK, D. 2007. Expression patterns of the hypoxia-related genes osteopontin, CA9, erythropoietin, VEGF and HIF-1α in human glioma in vitro and in vivo. *Radiotherapy and Oncology,* 83**,** 398-405.

SAITOH, M., NISHITOH, H., FUJII, M., TAKEDA, K., TOBIUME, K., SAWADA, Y., . . . ICHIJO, H. 1998a. Mammalian thioredoxin is a direct inhibitor of apoptosis signal-regulating kinase (ASK) 1. *Embo j,* 17**,** 2596-606.

SAITOH, M., NISHITOH, H., FUJII, M., TAKEDA, K., TOBIUME, K., SAWADA, Y., . . . ICHIJO, H. 1998b. Mammalian thioredoxin is a direct inhibitor of apoptosis signal‐regulating kinase (ASK) 1. *The EMBO journal,* 17**,** 2596-2606.

SAMKANGE-ZEEB, F. & BLETTNER, M. 2009. Emerging aspects of mobile phone use. *Emerging health threats journal,* 2**,** e5-e5.

SANAI, N., POLLEY, M. Y., MCDERMOTT, M. W., PARSA, A. T. & BERGER, M. S. 2011. An extent of resection threshold for newly diagnosed glioblastomas. *J Neurosurg,* 115**,** 3-8.

SANDALOVA, T., ZHONG, L., LINDQVIST, Y., HOLMGREN, A. & SCHNEIDER, G. 2001. Three-dimensional structure of a mammalian thioredoxin reductase: implications for mechanism and evolution of a selenocysteine-dependent enzyme. *Proc Natl Acad Sci U S A,* 98**,** 9533-8.

SARCAR, B., KAHALI, S., PRABHU, A. H., SHUMWAY, S. D., XU, Y., DEMUTH, T. & CHINNAIYAN, P. 2011. Targeting radiation-induced G2 checkpoint activation with the Wee-1 inhibitor MK-1775 in glioblastoma cell lines. *Molecular cancer therapeutics,* 10**,** 2405-2414.

SARKAR, G., CURRAN, G. L., SARKARIA, J. N., LOWE, V. J. & JENKINS, R. B. 2014. Peptide carrier-mediated non-covalent delivery of unmodified cisplatin, methotrexate and other agents via intravenous route to the brain. *PLoS One,* 9**,** e97655.

SAROWAR, S. 2016. *Treatment with Bortezomib Sensitizes Glioblastoma Cells to Temozolomide.* The University of Bergen.

SASADA, T., NAKAMURA, H., UEDA, S., SATO, N., KITAOKA, Y., GON, Y., . . . YODOI, J. 1999. Possible involvement of thioredoxin reductase as well as thioredoxin in cellular sensitivity to cis-diamminedichloroplatinum (II). *Free radical biology & medicine,* 27**,** 504-514.

SAXENA, G., CHEN, J. & SHALEV, A. 2010. Intracellular shuttling and mitochondrial function of thioredoxin-interacting protein. *J Biol Chem,* 285**,** 3997-4005.

SCHEFTER, T., WINTER, K., KWON, J. S., STUHR, K., BALARAJ, K., YAREMKO, B. P., . . . GROUP, R. T. O. 2014. RTOG 0417: efficacy of bevacizumab in combination with definitive radiation therapy and cisplatin chemotherapy in untreated patients with locally advanced cervical carcinoma. *International Journal of Radiation Oncology* Biology* Physics,* 88**,** 101-105.

SCHEURER, M. E., AMIRIAN, E. S., DAVLIN, S. L., RICE, T., WRENSCH, M. & BONDY, M. L. 2011. Effects of antihistamine and anti-inflammatory medication use on risk of specific glioma histologies. *Int J Cancer,* 129**,** 2290-6.

SCHOENFELD, J. D., SIBENALLER, Z. A., MAPUSKAR, K. A., WAGNER, B. A., CRAMER-MORALES, K. L., FURQAN, M., . . . ALLEN, B. G. 2017. O2(-) and H2O2-Mediated Disruption of Fe Metabolism Causes the Differential Susceptibility of NSCLC and GBM Cancer Cells to Pharmacological Ascorbate. *Cancer Cell,* 31**,** 487-500.e8.

SCHRECK, K. C. & GROSSMAN, S. A. 2018. Role of Temozolomide in the Treatment of Cancers Involving the Central Nervous System. *Oncology,* 32.

SCHUZ, J., JACOBSEN, R., OLSEN, J. H., BOICE, J. D., JR., MCLAUGHLIN, J. K. & JOHANSEN, C. 2006. Cellular telephone use and cancer risk: update of a nationwide Danish cohort. *J Natl Cancer Inst,* 98**,** 1707-13.

SCOCCIANTI, S., MAGRINI, S. M., RICARDI, U., DETTI, B., KRENGLI, M., PARISI, S., . . . BITI, G. 2012. Radiotherapy and temozolomide in anaplastic astrocytoma: a retrospective multicenter study by the Central Nervous System Study Group of AIRO (Italian Association of Radiation Oncology). *Neuro-oncology,* 14**,** 798-807.

SELENIUS, M., HEDMAN, M., BRODIN, D., GANDIN, V., RIGOBELLO, M. P., FLYGARE, J., . . . FERNANDES, A. P. 2012. Effects of redox modulation by inhibition of thioredoxin reductase on radiosensitivity and gene expression. *J Cell Mol Med,* 16**,** 1593-605.

SELENIUS, M., RUNDLOF, A. K., OLM, E., FERNANDES, A. P. & BJORNSTEDT, M. 2010. Selenium and the selenoprotein thioredoxin reductase in the prevention, treatment and diagnostics of cancer. *Antioxid Redox Signal,* 12**,** 867-80.

SESHACHARYULU, P., PONNUSAMY, M. P., HARIDAS, D., JAIN, M., GANTI, A. K. & BATRA, S. K. 2012. Targeting the EGFR signaling pathway in cancer therapy. *Expert Opin Ther Targets,* 16**,** 15-31.

SEYFRIED, T. N., KIEBISH, M. A., MARSH, J., SHELTON, L. M., HUYSENTRUYT, L. C. & MUKHERJEE, P. 2011. Metabolic management of brain cancer. *Biochimica et Biophysica Acta (BBA) - Bioenergetics,* 1807**,** 577-594.

SHAH, S. S., RODRIGUEZ, G. A., MUSICK, A., WALTERS, W. M., DE CORDOBA, N., BARBARITE, E., . . . GRAHAM, R. M. 2019. Targeting Glioblastoma Stem Cells with 2-Deoxy-D-Glucose (2-DG) Potentiates Radiation-Induced Unfolded Protein Response (UPR). *Cancers (Basel),* 11.

SHAHPAR, S., MHATRE, P. V. & HUANG, M. E. 2016. Update on Brain Tumors: New Developments in Neuro-oncologic Diagnosis and Treatment, and Impact on Rehabilitation Strategies. *Pm r,* 8**,** 678-89.

SHAO, F.-Y., DU, Z.-Y., MA, D.-L., CHEN, W.-B., FU, W.-Y., RUAN, B.-B., . . . WONG, N. S. 2015. B5, a thioredoxin reductase inhibitor, induces apoptosis in human cervical cancer cells by suppressing the thioredoxin system, disrupting mitochondrion-dependent pathways and triggering autophagy. *Oncotarget,* 6**,** 30939.

SHARMA, P. K. & VARSHNEY, R. 2012. 2-Deoxy-D-glucose and 6-aminonicotinamide-mediated Nrf2 down regulation leads to radiosensitization of malignant cells via abrogation of GSH-mediated defense. *Free Radic Res,* 46**,** 1446-57.

SHAW, E., ARUSELL, R., SCHEITHAUER, B., O'FALLON, J., O'NEILL, B., DINAPOLI, R., . . . ABRAMS, R. 2002. Prospective randomized trial of low- versus high-dose radiation therapy in adults with supratentorial low-grade glioma: initial report of a North Central Cancer Treatment Group/Radiation Therapy Oncology Group/Eastern Cooperative Oncology Group study. *J Clin Oncol,* 20**,** 2267-76.

SHELAR, S. B., KAMINSKA, K. K., REDDY, S. A., KUMAR, D., TAN, C. T., YU, V. C., . . . CHEW, E. H. 2015. Thioredoxin-dependent regulation of AIF-mediated DNA damage. *Free Radic Biol Med,* 87**,** 125-36.

SHELPER, T. B., LOVITT, C. J. & AVERY, V. M. 2016. Assessing Drug Efficacy in a Miniaturized Pancreatic Cancer In Vitro 3D Cell Culture Model. *Assay Drug Dev Technol,* 14**,** 367-80.

SHEU, S. S., NAUDURI, D. & ANDERS, M. W. 2006. Targeting antioxidants to mitochondria: a new therapeutic direction. *Biochim Biophys Acta,* 1762**,** 256-65.

SHINOJIMA, N., TADA, K., SHIRAISHI, S., KAMIRYO, T., KOCHI, M., NAKAMURA, H., . . . USHIO, Y. 2003. Prognostic value of epidermal growth factor receptor in patients with glioblastoma multiforme. *Cancer Res,* 63**,** 6962-70.

SIDNEY KIMMEL COMPREHENSIVE CANCER CENTER. 2016. *Study Assessing the Feasibility of a Surgery and Chemotherapy-Only in Children With Wnt Positive Medulloblastoma* [Online]. Available: https://ClinicalTrials.gov/show/NCT02212574 [Accessed 06/12/2018].

SIEGEL, D., YAN, C. & ROSS, D. 2012. NAD(P)H:quinone oxidoreductase 1 (NQO1) in the sensitivity and resistance to antitumor quinones. *Biochemical pharmacology,* 83**,** 1033-1040.

SINGH, S., HOWELL, D., TRIVEDI, N., KESSLER, K., ONG, T., ROSMANINHO, P., . . . SOLECKI, D. J. 2016. Zeb1 controls neuron differentiation and germinal zone exit by a mesenchymal-epithelial-like transition. *Elife,* 5.

SINGHAL, S., BIRCH, J. M., KERR, B., LASHFORD, L. & EVANS, D. G. 2002. Neurofibromatosis type 1 and sporadic optic gliomas. *Arch Dis Child,* 87**,** 65-70.

ŠKOVIEROVÁ, H., OKAJČEKOVÁ, T., STRNÁDEL, J., VIDOMANOVÁ, E. & HALAŠOVÁ, E. 2018. Molecular regulation of epithelial-to-

mesenchymal transition in tumorigenesis (Review). *International journal of molecular medicine,* 41**,** 1187-1200.

SMART, D. K., ORTIZ, K. L., MATTSON, D., BRADBURY, C. M., BISHT, K. S., SIECK, L. K., . . . GIUS, D. 2004. Thioredoxin reductase as a potential molecular target for anticancer agents that induce oxidative stress. *Cancer Res,* 64**,** 6716-24.

SMITH, S. J., DIKSIN, M., CHHAYA, S., SAIRAM, S., ESTEVEZ-CEBRERO, M. A. & RAHMAN, R. 2017. The Invasive Region of Glioblastoma Defined by 5ALA Guided Surgery Has an Altered Cancer Stem Cell Marker Profile Compared to Central Tumour. *International journal of molecular sciences,* 18**,** 2452.

SOINI, Y., KAHLOS, K., NÄPÄNKANGAS, U., KAARTEENAHO-WIIK, R., SÄILY, M., KOISTINEN, P., . . . KINNULA, V. L. 2001. Widespread expression of thioredoxin and thioredoxin reductase in non-small cell lung carcinoma. *Clinical Cancer Research,* 7**,** 1750-1757.

SOLOVJEVA, L., FIRSANOV, D., PLESKACH, N. & SVETLOVA, M. 2017. Immunofluorescence Analysis of gamma-H2AX Foci in Mammalian Fibroblasts at Different Phases of the Cell Cycle. *Methods Mol Biol,* 1644**,** 187-194.

SORDILLO, L. A., SORDILLO, P. P. & HELSON, L. 2015. Curcumin for the Treatment of Glioblastoma. *Anticancer Res,* 35**,** 6373-8.

SOWA, M. B., CHRISLER, W. B., ZENS, K. D., ASHJIAN, E. J. & OPRESKO, L. K. 2010. Three-dimensional culture conditions lead to decreased radiation induced cytotoxicity in human mammary epithelial cells. *Mutation Research/Fundamental and Molecular Mechanisms of Mutagenesis,* 687**,** 78-83.

SPENCE, A. M., MUZI, M., SWANSON, K. R., O'SULLIVAN, F., ROCKHILL, J. K., RAJENDRAN, J. G., . . . YAGLE, K. J. 2008. Regional hypoxia in glioblastoma multiforme quantified with [18F] fluoromisonidazole positron emission tomography before radiotherapy: correlation with time to progression and survival. *Clinical Cancer Research,* 14**,** 2623-2630.

SREBOTNIK-KIRBIS, I. & LIMBACK-STOKIN, C. 2016. Application of brush cytology for FISH-based detection of 1p/19q codeletion in oligodendroglial tumors. *J Neurooncol,* 129**,** 415-422.

SRINIVASAN, M., RAJENDRA PRASAD, N. & MENON, V. P. 2006. Protective effect of curcumin on gamma-radiation induced DNA damage and lipid peroxidation in cultured human lymphocytes. *Mutat Res,* 611**,** 96-103.

STINGL, L., STUHMER, T., CHATTERJEE, M., JENSEN, M. R., FLENTJE, M. & DJUZENOVA, C. S. 2010. Novel HSP90 inhibitors, NVP-AUY922 and NVP-BEP800, radiosensitise tumour cells through cell-cycle impairment, increased DNA damage and repair protraction. *Br J Cancer,* 102**,** 1578-91.

STOCK, K., ESTRADA, M. F., VIDIC, S., GJERDE, K., RUDISCH, A., SANTO, V. E., . . . GRAESER, R. 2016. Capturing tumor complexity in vitro: Comparative analysis of 2D and 3D tumor models for drug discovery. *Sci Rep,* 6**,** 28951.

STORCH, K., EKE, I., BORGMANN, K., KRAUSE, M., RICHTER, C., BECKER, K., . . . CORDES, N. 2010a. Three-Dimensional Cell Growth Confers Radioresistance by Chromatin Density Modification. *Cancer Research,* 70**,** 3925.

STORCH, K., EKE, I., BORGMANN, K., KRAUSE, M., RICHTER, C., BECKER, K., . . . CORDES, N. 2010b. Three-dimensional cell growth confers radioresistance by chromatin density modification. *Cancer research,* 70**,** 3925-3934.

STUPP, R., HEGI, M. E., MASON, W. P., VAN DEN BENT, M. J., TAPHOORN, M. J., JANZER, R. C., . . . MIRIMANOFF, R. O. 2009. Effects of radiotherapy with concomitant and adjuvant temozolomide versus radiotherapy alone on survival in glioblastoma in a randomised phase III study: 5-year analysis of the EORTC-NCIC trial. *Lancet Oncol,* 10**,** 459-66.

STUPP, R., MASON, W. P., VAN DEN BENT, M. J., WELLER, M., FISHER, B., TAPHOORN, M. J., . . . BOGDAHN, U. 2005. Radiotherapy plus concomitant and adjuvant temozolomide for glioblastoma. *New England Journal of Medicine,* 352**,** 987-996.

STUPP, R., TAILLIBERT, S., KANNER, A., READ, W., STEINBERG, D., LHERMITTE, B., . . . RAM, Z. 2017. Effect of Tumor-Treating Fields Plus Maintenance Temozolomide vs Maintenance Temozolomide Alone on Survival in Patients With Glioblastoma: A Randomized Clinical Trial. *Jama,* 318**,** 2306-2316.

STUPP, R., TAILLIBERT, S., KANNER, A. A., KESARI, S., STEINBERG, D. M., TOMS, S. A., . . . RAM, Z. 2015. Maintenance Therapy With Tumor-Treating Fields Plus Temozolomide vs Temozolomide Alone for Glioblastoma: A Randomized Clinical Trial. *Jama,* 314**,** 2535-43.

SU, Y., SHRUBSOLE, M. J., NESS, R. M., CAI, Q., KATAOKA, N., WASHINGTON, K. & ZHENG, W. 2006. Immunohistochemical Expressions of Ki-67, Cyclin D1, β-Catenin, Cyclooxygenase-2, and Epidermal Growth Factor Receptor in Human Colorectal Adenoma: A Validation Study of Tissue Microarrays. *Cancer Epidemiology Biomarkers & Prevention,* 15**,** 1719-1726.

SUN, Y., ST CLAIR, D. K., XU, Y., CROOKS, P. A. & ST CLAIR, W. H. 2010. A NADPH oxidase-dependent redox signaling pathway mediates the selective radiosensitization effect of parthenolide in prostate cancer cells. *Cancer Res,* 70**,** 2880-90.

TABAYASHI, T., TANAKA, Y., TAKAHASHI, Y., KIMURA, Y., TOMIKAWA, T., SAGAWA, M., . . . KIZAKI, M. 2016. Inhibition of WEE1 Induces Cell Death of Both Bortezomib-and Lenalidomide-Resistant Multiple Myeloma Cells: A Novel Therapeutic Approach Targeting Cell-Cycle Checkpoint Kinase. Am Soc Hematology.

TAKESHITA, I., TAKAKI, T., KURAMITSU, M., NAGASAKA, S., MACHI, T., OGAWA, H., . . . KITAMURA, K. 1987. Characteristics of an established human glioma cell line, KNS-42. *Neurologia medico-chirurgica,* 27**,** 581-587.

TANABE, K., MAKIMURA, Y., TACHI, Y., IMAGAWA-SATO, A. & NISHIMOTO, S. 2005. Hypoxia-selective activation of 5-fluorodeoxyuridine prodrug

possessing indolequinone structure: radiolytic reduction and cytotoxicity characteristics. *Bioorg Med Chem Lett,* 15**,** 2321-4.

TARBELL, N. J., FRIEDMAN, H., POLKINGHORN, W. R., YOCK, T., ZHOU, T., CHEN, Z., . . . KUN, L. 2013. High-risk medulloblastoma: a pediatric oncology group randomized trial of chemotherapy before or after radiation therapy (POG 9031). *J Clin Oncol,* 31**,** 2936-41.

TAVENDER, T. J., SHEPPARD, A. M. & BULLEID, N. J. 2008. Peroxiredoxin IV is an endoplasmic reticulum-localized enzyme forming oligomeric complexes in human cells. *Biochem J,* 411**,** 191-9.

TAYLOR, M. D., NORTHCOTT, P. A., KORSHUNOV, A., REMKE, M., CHO, Y. J., CLIFFORD, S. C., . . . PFISTER, S. M. 2012. Molecular subgroups of medulloblastoma: the current consensus. *Acta Neuropathol,* 123**,** 465-72.

TAYLOR, R. E., BAILEY, C. C., ROBINSON, K., WESTON, C. L., ELLISON, D., IRONSIDE, J., . . . LASHFORD, L. S. 2003. Results of a randomized study of preradiation chemotherapy versus radiotherapy alone for nonmetastatic medulloblastoma: The International Society of Paediatric Oncology/United Kingdom Children's Cancer Study Group PNET-3 Study. *J Clin Oncol,* 21**,** 1581-91.

TENGA, A., BEARD, J. A., TAKWI, A., WANG, Y.-M. & CHEN, T. 2016. Regulation of Nuclear Receptor Nur77 by miR-124. *PloS one,* 11**,** e0148433-e0148433.

TEOH, M., CLARK, C. H., WOOD, K., WHITAKER, S. & NISBET, A. 2011. Volumetric modulated arc therapy: a review of current literature and clinical use in practice. *Br J Radiol,* 84**,** 967-96.

TEW, K. D. & TOWNSEND, D. M. 2011. Redox platforms in cancer drug discovery and development. *Current opinion in chemical biology,* 15**,** 156-161.

THIERY, J. P. & SLEEMAN, J. P. 2006. Complex networks orchestrate epithelial-mesenchymal transitions. *Nat Rev Mol Cell Biol,* 7**,** 131-42.

THOM, S. R. 2011. Hyperbaric oxygen: its mechanisms and efficacy. *Plastic and reconstructive surgery,* 127 Suppl 1**,** 131S-141S.

TICHY, A., VAVROVA, J., PEJCHAL, J. & REZACOVA, M. 2010. Ataxia-telangiectasia mutated kinase (ATM) as a central regulator of radiation-induced DNA damage response. *Acta Medica (Hradec Kralove),* 53**,** 13-7.

TIVNAN, A., ZAKARIA, Z., O'LEARY, C., KÖGEL, D., POKORNY, J. L., SARKARIA, J. N. & PREHN, J. H. 2015. Inhibition of multidrug resistance protein 1 (MRP1) improves chemotherapy drug response in primary and recurrent glioblastoma multiforme. *Frontiers in neuroscience,* 9**,** 218.

TONISSEN, K. F. & DI TRAPANI, G. 2009. Thioredoxin system inhibitors as mediators of apoptosis for cancer therapy. *Mol Nutr Food Res,* 53**,** 87-103.

TONSGARD, J. H. 2006. Clinical manifestations and management of neurofibromatosis type 1. *Semin Pediatr Neurol,* 13**,** 2-7.

TRACHOOTHAM, D., ZHOU, Y., ZHANG, H., DEMIZU, Y., CHEN, Z., PELICANO, H., . . . HUANG, P. 2006. Selective killing of oncogenically transformed

cells through a ROS-mediated mechanism by β-phenylethyl isothiocyanate. *Cancer Cell,* 10**,** 241-252.

TSENG, S. H., BOBOLA, M. S., BERGER, M. S. & SILBER, J. R. 1999. Characterization of paclitaxel (Taxol®) sensitivity in human glioma-and medulloblastoma-derived cell lines. *Neuro-oncology,* 1**,** 101-108.

TURNER, M. C., KREWSKI, D., ARMSTRONG, B. K., CHETRIT, A., GILES, G. G., HOURS, M., . . . CARDIS, E. 2013. Allergy and brain tumors in the INTERPHONE study: pooled results from Australia, Canada, France, Israel, and New Zealand. *Cancer Causes Control,* 24**,** 949-60.

TUTTLE, S., HERTAN, L., DAURIO, N., PORTER, S., KAUSHICK, C., LI, D., . . . KOUMENIS, C. 2012. The chemopreventive and clinically used agent curcumin sensitizes HPV (-) but not HPV (+) HNSCC to ionizing radiation, in vitro and in a mouse orthotopic model. *Cancer Biol Ther,* 13**,** 575-84.

UDAKA, Y. T. & PACKER, R. J. 2018. Pediatric Brain Tumors. *Neurol Clin,* 36**,** 533-556.

UENO, M., MASUTANI, H., ARAI, R. J., YAMAUCHI, A., HIROTA, K., SAKAI, T., . . . NIKAIDO, T. 1999. Thioredoxin-dependent redox regulation of p53-mediated p21 activation. *J Biol Chem,* 274**,** 35809-15.

UHM, J. H., BALLMAN, K. V., GIANNINI, C., KRAUSS, J. C., BUCKNER, J. C., JAMES, D., . . . JAECKLE, K. A. 2004. Phase II study of ZD1839 in patients with newly diagnosed grade 4 astrocytoma. *Journal of Clinical Oncology,* 22**,** 1505-1505.

URIG, S. & BECKER, K. 2006. On the potential of thioredoxin reductase inhibitors for cancer therapy. *Semin Cancer Biol,* 16**,** 452-65.

VAN DEN BENT, M. J. 2003. Can chemotherapy replace radiotherapy in low-grade gliomas? Time for randomized studies. *Semin Oncol,* 30**,** 39-44.

VAN DEN BENT, M. J., AFRA, D., DE WITTE, O., BEN HASSEL, M., SCHRAUB, S., HOANG-XUAN, K., . . . KARIM, A. B. 2005. Long-term efficacy of early versus delayed radiotherapy for low-grade astrocytoma and oligodendroglioma in adults: the EORTC 22845 randomised trial. *Lancet,* 366**,** 985-90.

VAN DEN BENT, M. J., BAUMERT, B., ERRIDGE, S. C., VOGELBAUM, M. A., NOWAK, A. K., SANSON, M., . . . KROS, J. M. 2017. Interim results from the CATNON trial (EORTC study 26053-22054) of treatment with concurrent and adjuvant temozolomide for 1p/19q non-co-deleted anaplastic glioma: a phase 3, randomised, open-label intergroup study. *Lancet,* 390**,** 1645-1653.

VAN DEN BENT, M. J., BRANDES, A. A., TAPHOORN, M. J., KROS, J. M., KOUWENHOVEN, M. C., DELATTRE, J. Y., . . . HOANG-XUAN, K. 2013. Adjuvant procarbazine, lomustine, and vincristine chemotherapy in newly diagnosed anaplastic oligodendroglioma: long-term follow-up of EORTC brain tumor group study 26951. *J Clin Oncol,* 31**,** 344-50.

VAN DEN BENT, M. J., DUBBINK, H. J., MARIE, Y., BRANDES, A. A., TAPHOORN, M. J., WESSELING, P., . . . SANSON, M. 2010. IDH1 and IDH2 mutations are prognostic but not predictive for outcome in anaplastic oligodendroglial tumors: a report of the European Organization for

Research and Treatment of Cancer Brain Tumor Group. *Clin Cancer Res,* 16**,** 1597-604.

VAN VUURDEN, D. G., HULLEMAN, E., MEIJER, O. L., WEDEKIND, L. E., KOOL, M., WITT, H., . . . KASPERS, G. J. 2011. PARP inhibition sensitizes childhood high grade glioma, medulloblastoma and ependymoma to radiation. *Oncotarget,* 2**,** 984.

VAUGHN, A. E. & DESHMUKH, M. 2008. Glucose metabolism inhibits apoptosis in neurons and cancer cells by redox inactivation of cytochrome c. *Nature cell biology,* 10**,** 1477.

VAUPEL, P. 2004. The role of hypoxia-induced factors in tumor progression. *The oncologist,* 9**,** 10-17.

VENDETTI, F. P., LEIBOWITZ, B. J., BARNES, J., SCHAMUS, S., KIESEL, B. F., ABBERBOCK, S., . . . BAKKENIST, C. J. 2017. Pharmacologic ATM but not ATR kinase inhibition abrogates p21-dependent G1 arrest and promotes gastrointestinal syndrome after total body irradiation. *Scientific Reports,* 7**,** 41892.

VENKOV, C., PLIETH, D., NI, T., KARMAKER, A., BIAN, A., GEORGE JR, A. L. & NEILSON, E. G. 2011. Transcriptional networks in epithelial-mesenchymal transition. *PLoS One,* 6**,** e25354.

VERMA, V. 2016. Relationship and interactions of curcumin with radiation therapy. *World J Clin Oncol,* 7**,** 275-83.

VOGT, A., TAMURA, K., WATSON, S. & LAZO, J. S. 2000. Antitumor imidazolyl disulfide IV-2 causes irreversible G(2)/M cell cycle arrest without hyperphosphorylation of cyclin-dependent kinase Cdk1. *J Pharmacol Exp Ther,* 294**,** 1070-5.

VON BUEREN, A. O., BACOLOD, M. D., HAGEL, C., HEINIMANN, K., FEDIER, A., KORDES, U., . . . RUTKOWSKI, S. 2012. Mismatch repair deficiency: a temozolomide resistance factor in medulloblastoma cell lines that is uncommon in primary medulloblastoma tumours. *British journal of cancer,* 107**,** 1399-1408.

VON BUEREN, A. O., KORTMANN, R. D., VON HOFF, K., FRIEDRICH, C., MYNAREK, M., MULLER, K., . . . RUTKOWSKI, S. 2016. Treatment of Children and Adolescents With Metastatic Medulloblastoma and Prognostic Relevance of Clinical and Biologic Parameters. *J Clin Oncol,* 34**,** 4151-4160.

VON HOFF, K., HINKES, B., GERBER, N. U., DEINLEIN, F., MITTLER, U., URBAN, C., . . . ZWIENER, I. 2009. Long-term outcome and clinical prognostic factors in children with medulloblastoma treated in the prospective randomised multicentre trial HIT '91. *European journal of cancer,* 45**,** 1209-1217.

WAGNER, D., CHRISTIANSEN, H., WOLFF, H. & VORWERK, H. 2009. Radiotherapy of malignant gliomas: comparison of volumetric single arc technique (RapidArc), dynamic intensity-modulated technique and 3D conformal technique. *Radiother Oncol,* 93**,** 593-6.

WALSH, J. C., LEBEDEV, A., ATEN, E., MADSEN, K., MARCIANO, L. & KOLB, H. C. 2014. The clinical importance of assessing tumor hypoxia: relationship

of tumor hypoxia to prognosis and therapeutic opportunities. *Antioxidants & redox signaling,* 21**,** 1516-1554.

WALTON, M. I., SMITH, P. J. & WORKMAN, P. 1991. The role of NAD (P) H: quinone reductase (EC 1.6. 99.2, DT-diaphorase) in the reductive bioactivation of the novel indoloquinone antitumor agent E09. *Cancer communications,* 3**,** 199-206.

WANG, D. & LIPPARD, S. J. 2005. Cellular processing of platinum anticancer drugs. *Nat Rev Drug Discov,* 4**,** 307-20.

WANG, F., LIN, F., ZHANG, P., NI, W., BI, L., WU, J. & JIANG, L. 2015a. Thioredoxin-1 inhibitor, 1-methylpropyl 2-imidazolyl disulfide, inhibits the growth, migration and invasion of colorectal cancer cell lines. *Oncol Rep,* 33**,** 967-73.

WANG, H., BOUZAKOURA, S., DE MEY, S., JIANG, H., LAW, K., DUFAIT, I., . . . DE RIDDER, M. 2017a. Auranofin radiosensitizes tumor cells through targeting thioredoxin reductase and resulting overproduction of reactive oxygen species. *Oncotarget,* 8**,** 35728-35742.

WANG, H., JIANG, H., VAN DE GUCHT, M. & DE RIDDER, M. 2019. Hypoxic Radioresistance: Can ROS Be the Key to Overcome It? *Cancers,* 11**,** 112.

WANG, H., LIU, Y., WANG, X., LIU, D., SUN, Z., WANG, C., . . . YU, S. 2015b. Randomized clinical control study of locoregional therapy combined with arsenic trioxide for the treatment of hepatocellular carcinoma. *Cancer,* 121**,** 2917-2925.

WANG, X., CHEN, J. X., LIU, J. P., YOU, C., LIU, Y. H. & MAO, Q. 2014. Gain of function of mutant TP53 in glioblastoma: prognosis and response to temozolomide. *Ann Surg Oncol,* 21**,** 1337-44.

WANG, X. & HAI, C. 2016. Novel insights into redox system and the mechanism of redox regulation. *Mol Biol Rep,* 43**,** 607-28.

WANG, Y., KONG, X., GUO, Y., WANG, R. & MA, W. 2017b. Continuous dose-intense temozolomide and cisplatin in recurrent glioblastoma patients. *Medicine (Baltimore),* 96**,** e6261.

WANSHURA, L. E. C., GALVIN, K. E., YE, H., FERNANDEZ-ZAPICO, M. E. & WETMORE, C. 2011. Sequential Activation of Snail1 and N-Myc Modulates Sonic Hedgehog–Induced Transformation of Neural Cells. *Cancer Research,* 71**,** 5336-5345.

WATANABE, T., NOBUSAWA, S., KLEIHUES, P. & OHGAKI, H. 2009. IDH1 mutations are early events in the development of astrocytomas and oligodendrogliomas. *Am J Pathol,* 174**,** 1149-53.

WEITZEL, D. H., TOVMASYAN, A., ASHCRAFT, K. A., RAJIC, Z., WEITNER, T., LIU, C., . . . YOUNG, K. H. 2015. Radioprotection of the brain white matter by Mn (III) N-butoxyethylpyridylporphyrin–based superoxide dismutase mimic MnTnBuOE-2-PyP5+. *Molecular cancer therapeutics,* 14**,** 70-79.

WELLER, M., VAN DEN BENT, M., TONN, J. C., STUPP, R., PREUSSER, M., COHEN-JONATHAN-MOYAL, E., . . . WICK, W. 2017. European Association for Neuro-Oncology (EANO) guideline on the diagnosis and treatment of adult astrocytic and oligodendroglial gliomas. *Lancet Oncol,* 18**,** e315-e329.

WELSH, S. J., BELLAMY, W. T., BRIEHL, M. M. & POWIS, G. 2002a. The redox protein thioredoxin-1 (Trx-1) increases hypoxia-inducible factor 1alpha protein expression: Trx-1 overexpression results in increased vascular endothelial growth factor production and enhanced tumor angiogenesis. *Cancer Res,* 62**,** 5089-95.

WELSH, S. J., BELLAMY, W. T., BRIEHL, M. M. & POWIS, G. 2002b. The redox protein thioredoxin-1 (Trx-1) increases hypoxia-inducible factor 1α protein expression: Trx-1 overexpression results in increased vascular endothelial growth factor production and enhanced tumor angiogenesis. *Cancer research,* 62**,** 5089-5095.

WESSELING, P., VAN DEN BENT, M. & PERRY, A. 2015. Oligodendroglioma: pathology, molecular mechanisms and markers. *Acta Neuropathol,* 129**,** 809-27.

WEYDERT, C. J. & CULLEN, J. J. 2010. Measurement of superoxide dismutase, catalase and glutathione peroxidase in cultured cells and tissue. *Nat Protoc,* 5**,** 51-66.

WICK, W., PLATTEN, M., MEISNER, C., FELSBERG, J., TABATABAI, G., SIMON, M., . . . WELLER, M. 2012. Temozolomide chemotherapy alone versus radiotherapy alone for malignant astrocytoma in the elderly: the NOA-08 randomised, phase 3 trial. *Lancet Oncol,* 13**,** 707-15.

WICK, W., ROTH, P., HARTMANN, C., HAU, P., NAKAMURA, M., STOCKHAMMER, F., . . . WELLER, M. 2016. Long-term analysis of the NOA-04 randomized phase III trial of sequential radiochemotherapy of anaplastic glioma with PCV or temozolomide. *Neuro Oncol,* 18**,** 1529-1537.

WIEMELS, J. L., WIENCKE, J. K., PATOKA, J., MOGHADASSI, M., CHEW, T., MCMILLAN, A., . . . WRENSCH, M. 2004. Reduced immunoglobulin E and allergy among adults with glioma compared with controls. *Cancer Res,* 64**,** 8468-73.

WIGERTZ, A., LONN, S., SCHWARTZBAUM, J., HALL, P., AUVINEN, A., CHRISTENSEN, H. C., . . . FEYCHTING, M. 2007. Allergic conditions and brain tumor risk. *Am J Epidemiol,* 166**,** 941-50.

WILLIAMS, K. J., ALBERTELLA, M. R., FITZPATRICK, B., LOADMAN, P. M., SHNYDER, S. D., CHINJE, E. C., . . . STRATFORD, I. J. 2009a. In vivo activation of the hypoxia-targeted cytotoxin AQ4N in human tumor xenografts. *Molecular cancer therapeutics,* 8**,** 3266-3275.

WILLIAMS, V. C., LUCAS, J., BABCOCK, M. A., GUTMANN, D. H., KORF, B. & MARIA, B. L. 2009b. Neurofibromatosis type 1 revisited. *Pediatrics,* 123**,** 124-33.

WINKLER, F., KOZIN, S. V., TONG, R. T., CHAE, S.-S., BOOTH, M. F., GARKAVTSEV, I., . . . DI TOMASO, E. 2004. Kinetics of vascular normalization by VEGFR2 blockade governs brain tumor response to radiation: role of oxygenation, angiopoietin-1, and matrix metalloproteinases. *Cancer cell,* 6**,** 553-563.

WITTE, A. B., ANESTAL, K., JERREMALM, E., EHRSSON, H. & ARNER, E. S. 2005. Inhibition of thioredoxin reductase but not of glutathione reductase by

the major classes of alkylating and platinum-containing anticancer compounds. *Free Radic Biol Med,* 39**,** 696-703.

WONG, T. T., LIU, Y. L., HO, D. M., CHANG, K. P., LIANG, M. L., CHEN, H. H., . . . CHEN, Y. W. 2015. Factors affecting survival of medulloblastoma in children: the changing concept of management. *Childs Nerv Syst,* 31**,** 1687-98.

WOOLSTON, C. & MARTIN, S. 2011a. Analysis of tumor and endothelial cell viability and survival using sulforhodamine B and clonogenic assays. *Mammalian Cell Viability.* Springer.

WOOLSTON, C. & MARTIN, S. 2011b. Analysis of tumor and endothelial cell viability and survival using sulforhodamine B and clonogenic assays. *Methods Mol Biol,* 740**,** 45-56.

WOOLSTON, C. M., DEEN, S., AL-ATTAR, A., SHEHATA, M., CHAN, S. Y. & MARTIN, S. G. 2010. Redox protein expression predicts progression-free and overall survival in ovarian cancer patients treated with platinum-based chemotherapy. *Free Radic Biol Med,* 49**,** 1263-72.

WOOLSTON, C. M., MADHUSUDAN, S., SOOMRO, I. N., LOBO, D. N., REECE-SMITH, A. M., PARSONS, S. L. & MARTIN, S. G. 2013. Thioredoxin interacting protein and its association with clinical outcome in gastro-oesophageal adenocarcinoma. *Redox Biol,* 1**,** 285-91.

WOOLSTON, C. M., STORR, S. J., ELLIS, I. O., MORGAN, D. A. & MARTIN, S. G. 2011. Expression of thioredoxin system and related peroxiredoxin proteins is associated with clinical outcome in radiotherapy treated early stage breast cancer. *Radiother Oncol,* 100**,** 308-13.

WOOLSTON, C. M., ZHANG, L., STORR, S. J., AL-ATTAR, A., SHEHATA, M., ELLIS, I. O., . . . MARTIN, S. G. 2012. The prognostic and predictive power of redox protein expression for anthracycline-based chemotherapy response in locally advanced breast cancer. *Mod Pathol,* 25**,** 1106-16.

WORKMAN, P. 1994. Enzyme-directed bioreductive drug development revisited: a commentary on recent progress and future prospects with emphasis on quinone anticancer agents and quinone metabolizing enzymes, particularly DT-diaphorase. *Oncology Research Featuring Preclinical and Clinical Cancer Therapeutics,* 6**,** 461-475.

WORKMAN, P., BINGER, M. & KOOISTRA, K. 1992. Pharmacokinetics, distribution, and metabolism of the novel bioreductive alkylating indoloquinone EO9 in rodents. *International Journal of Radiation Oncology* Biology* Physics,* 22**,** 713-716.

WYKOFF, C. C., BEASLEY, N. J., WATSON, P. H., TURNER, K. J., PASTOREK, J., SIBTAIN, A., . . . MAXWELL, P. H. 2000. Hypoxia-inducible expression of tumor-associated carbonic anhydrases. *Cancer research,* 60**,** 7075-7083.

XU, J. & ARNÉR, E. S. 2012. Pyrroloquinoline quinone modulates the kinetic parameters of the mammalian selenoprotein thioredoxin reductase 1 and is an inhibitor of glutathione reductase. *Biochemical pharmacology,* 83**,** 815-820.

XU, S., YAO, H., PEI, L., HU, M., LI, D., QIU, Y., . . . XU, J. 2017. Design, synthesis, and biological evaluation of NAD(P)H: Quinone oxidoreductase

(NQO1)-targeted oridonin prodrugs possessing indolequinone moiety for hypoxia-selective activation. *Eur J Med Chem,* 132**,** 310-321.

XU, S., ZAKIAN, K., THALER, H., MATEI, C., ALFIERI, A., CHEN, Y. & KOUTCHER, J. A. 2001. Effects of Motexafin gadolinium on tumor metabolism and radiation sensitivity. *Int J Radiat Oncol Biol Phys,* 49**,** 1381-90.

XU, Y., FANG, F., MIRIYALA, S., CROOKS, P. A., OBERLEY, T. D., CHAISWING, L., . . . CLAIR, W. H. 2013. KEAP1 is a redox sensitive target that arbitrates the opposing radiosensitive effects of parthenolide in normal and cancer cells. *Cancer Res,* 73**,** 4406-17.

YADAV, N. K., SHUKLA, P., OMER, A., SINGH, P. & SINGH, R. 2016. Alternative methods in toxicology: CFU assays application, limitation and future prospective. *Drug and chemical toxicology,* 39**,** 1-12.

YAHARA, K., OHGURI, T., UDONO, H., YAMAMOTO, J., TOMURA, K., ONODA, T., . . . KOROGI, Y. 2017. Radiotherapy using IMRT boosts after hyperbaric oxygen therapy with chemotherapy for glioblastoma. *J Radiat Res,* 58**,** 351-356.

YAMADA, M., TOMIDA, A., YOSHIKAWA, H., TAKETANI, Y. & TSURUO, T. 1996. Increased expression of thioredoxin/adult T-cell leukemia-derived factor in cisplatin-resistant human cancer cell lines. *Clin Cancer Res,* 2**,** 427-32.

YAMAGUCHI, F., TAKATA, M., KAMITORI, K., NONAKA, M., DONG, Y., SUI, L. & TOKUDA, M. 2008. Rare sugar D-allose induces specific up-regulation of TXNIP and subsequent G1 cell cycle arrest in hepatocellular carcinoma cells by stabilization of p27kip1. *Int J Oncol,* 32**,** 377-85.

YAN, C., KEPA, J. K., SIEGEL, D., STRATFORD, I. J. & ROSS, D. 2008. Dissecting the role of multiple reductases in bioactivation and cytotoxicity of the antitumor agent 2,5-diaziridinyl-3-(hydroxymethyl)-6-methyl-1,4-benzoquinone (RH1). *Molecular pharmacology,* 74**,** 1657-1665.

YAN, C., SHIEH, B., REIGAN, P., ZHANG, Z., COLUCCI, M. A., CHILLOUX, A., . . . ROSS, D. 2009a. Potent activity of indolequinones against human pancreatic cancer: identification of thioredoxin reductase as a potential target. *Mol Pharmacol,* 76**,** 163-72.

YAN, C., SIEGEL, D., NEWSOME, J., CHILLOUX, A., MOODY, C. J. & ROSS, D. 2012. Antitumor indolequinones induced apoptosis in human pancreatic cancer cells via inhibition of thioredoxin reductase and activation of redox signaling. *Mol Pharmacol,* 81**,** 401-10.

YAN, H., PARSONS, D. W., JIN, G., MCLENDON, R., RASHEED, B. A., YUAN, W., . . . BIGNER, D. D. 2009b. IDH1 and IDH2 mutations in gliomas. *N Engl J Med,* 360**,** 765-73.

YANG, H., YOON, S. J., JIN, J., CHOI, S. H., SEOL, H. J., LEE, J.-I., . . . YOO, H. Y. 2011. Inhibition of checkpoint kinase 1 sensitizes lung cancer brain metastases to radiotherapy. *Biochemical and biophysical research communications,* 406**,** 53-58.

YE, X. & WEINBERG, R. A. 2015. Epithelial-Mesenchymal Plasticity: A Central Regulator of Cancer Progression. *Trends Cell Biol,* 25**,** 675-686.

YOKOMIZO, A., ONO, M., NANRI, H., MAKINO, Y., OHGA, T., WADA, M., . . . KOHNO, K. 1995. Cellular levels of thioredoxin associated with drug

sensitivity to cisplatin, mitomycin C, doxorubicin, and etoposide. *Cancer Research,* 55**,** 4293-4296.

YOO, M. H., XU, X. M., CARLSON, B. A., GLADYSHEV, V. N. & HATFIELD, D. L. 2006. Thioredoxin reductase 1 deficiency reverses tumor phenotype and tumorigenicity of lung carcinoma cells. *J Biol Chem,* 281**,** 13005-8.

YOON, M., SHIN, D. H., KIM, J., KIM, J. W., KIM, D. W., PARK, S. Y., . . . SHIN, S. H. 2011. Craniospinal irradiation techniques: a dosimetric comparison of proton beams with standard and advanced photon radiotherapy. *Int J Radiat Oncol Biol Phys,* 81**,** 637-46.

YOSHIHARA, E., MASAKI, S., MATSUO, Y., CHEN, Z., TIAN, H. & YODOI, J. 2014. Thioredoxin/Txnip: redoxisome, as a redox switch for the pathogenesis of diseases. *Front Immunol,* 4**,** 514.

YOU, B. R., SHIN, H. R. & PARK, W. H. 2014. PX-12 inhibits the growth of A549 lung cancer cells via G2/M phase arrest and ROS-dependent apoptosis. *Int J Oncol,* 44**,** 301-8.

YUH, G. E., LOREDO, L. N., YONEMOTO, L. T., BUSH, D. A., SHAHNAZI, K., PRESTON, W., . . . SLATER, J. D. 2004. Reducing toxicity from craniospinal irradiation: using proton beams to treat medulloblastoma in young children. *Cancer J,* 10**,** 386-90.

ZANONI, M., PICCININI, F., ARIENTI, C., ZAMAGNI, A., SANTI, S., POLICO, R., . . . TESEI, A. 2016. 3D tumor spheroid models for in vitro therapeutic screening: a systematic approach to enhance the biological relevance of data obtained. *Scientific reports,* 6**,** 19103.

ZAPOTOCKY, M., MATA-MBEMBA, D., SUMERAUER, D., LIBY, P., LASSALETTA, A., ZAMECNIK, J., . . . RAMASWAMY, V. 2018. Differential patterns of metastatic dissemination across medulloblastoma subgroups. *J Neurosurg Pediatr,* 21**,** 145-152.

ZAWLIK, I., VACCARELLA, S., KITA, D., MITTELBRONN, M., FRANCESCHI, S. & OHGAKI, H. 2009. Promoter methylation and polymorphisms of the MGMT gene in glioblastomas: a population-based study. *Neuroepidemiology,* 32**,** 21-9.

ZENG, Y., MA, J., ZHAN, Y., XU, X., ZENG, Q., LIANG, J. & CHEN, X. 2018. Hypoxia-activated prodrugs and redox-responsive nanocarriers. *International journal of nanomedicine,* 13**,** 6551.

ZHANG, B., ZHANG, J., PENG, S., LIU, R., LI, X., HOU, Y., . . . FANG, J. 2017a. Thioredoxin reductase inhibitors: A patent review. *Expert opinion on therapeutic patents,* 27**,** 547-556.

ZHANG, J., ZHANG, B., LI, X., HAN, X., LIU, R. & FANG, J. 2019a. Small molecule inhibitors of mammalian thioredoxin reductase as potential anticancer agents: An update. *Medicinal research reviews,* 39**,** 5-39.

ZHANG, K., CHEN, D., JIAO, X., ZHANG, S., LIU, X., CAO, J., . . . WANG, D. 2012. Retraction. Slug enhances invasion ability of pancreatic cancer cells through upregulation of matrix metalloproteinase-9 and actin cytoskeleton remodeling. *Laboratory investigation; a journal of technical methods and pathology,* 92**,** 1801-1801.

ZHANG, P., GAO, J., WANG, X., WEN, W., YANG, H., TIAN, Y., . . . TU, Y. 2017b. A novel indication of thioredoxin-interacting protein as a tumor suppressor gene in malignant glioma. *Oncol Lett,* 14**,** 2053-2058.

ZHANG, R., AL-LAMKI, R., BAI, L., STREB, J. W., MIANO, J. M., BRADLEY, J. & MIN, W. 2004. Thioredoxin-2 inhibits mitochondria-located ASK1-mediated apoptosis in a JNK-independent manner. *Circ Res,* 94**,** 1483-91.

ZHANG, S., DEEN, S., STORR, S. J., YAO, A. & MARTIN, S. G. 2019b. Expression of Syk and MAP4 proteins in ovarian cancer. *Journal of Cancer Research and Clinical Oncology,* 145**,** 909-919.

ZHANG, X., PENG, L., LIU, A., JI, J., ZHAO, L. & ZHAI, G. 2018. The enhanced effect of tetrahydrocurcumin on radiosensitivity of glioma cells. *J Pharm Pharmacol,* 70**,** 749-759.

ZHANG, Y. 2014. *Reox protein regulation of therapeutic response in breast cancer.* PhD, University of Nottingham.

ZHANG, Y., CHEN, F., TAI, G., WANG, J., SHANG, J., ZHANG, B., . . . LIU, F. 2017c. TIGAR knockdown radiosensitizes TrxR1-overexpressing glioma in vitro and in vivo via inhibiting Trx1 nuclear transport. *Sci Rep,* 7**,** 42928.

ZHANG, Y. & MARTIN, S. G. 2014. Redox proteins and radiotherapy. *Clin Oncol (R Coll Radiol),* 26**,** 289-300.

ZHAO, X. L., SUN, T., CHE, N., SUN, D., ZHAO, N., DONG, X. Y., . . . SUN, B. C. 2011. Promotion of hepatocellular carcinoma metastasis through matrix metalloproteinase activation by epithelial-mesenchymal transition regulator Twist1. *J Cell Mol Med,* 15**,** 691-700.

ZHENG, X., CHEN, Y., BAI, M., LIU, Y., XU, B., SUN, R. & ZENG, H. 2019. The antimetastatic effect and underlying mechanisms of thioredoxin reductase inhibitor ethaselen. *Free Radic Biol Med,* 131**,** 7-17.

ZHONG, L., ARNER, E. S. & HOLMGREN, A. 2000. Structure and mechanism of mammalian thioredoxin reductase: the active site is a redox-active selenolthiol/selenenylsulfide formed from the conserved cysteine-selenocysteine sequence. *Proc Natl Acad Sci U S A,* 97**,** 5854-9.

ZHONG, L. & HOLMGREN, A. 2000. Essential role of selenium in the catalytic activities of mammalian thioredoxin reductase revealed by characterization of recombinant enzymes with selenocysteine mutations. *J Biol Chem,* 275**,** 18121-8.

ZHOU, H., RAO, J., LIN, J., YIN, B., SHENG, H., LIN, F., . . . YANG, L. 2011a. The insulin-like growth factor-I receptor kinase inhibitor NVP-ADW742 sensitizes medulloblastoma to the effects of chemotherapy. *Oncol Rep,* 25**,** 1565-71.

ZHOU, J. & CHNG, W. J. 2013. Roles of thioredoxin binding protein (TXNIP) in oxidative stress, apoptosis and cancer. *Mitochondrion,* 13**,** 163-9.

ZHOU, J., DAMDIMOPOULOS, A. E., SPYROU, G. & BRÜNE, B. 2007. Thioredoxin 1 and thioredoxin 2 have opposed regulatory functions on hypoxia inducible factor-1α. *Journal of Biological Chemistry*.

ZHOU, J., YU, Q. & CHNG, W. J. 2011b. TXNIP (VDUP-1, TBP-2): a major redox regulator commonly suppressed in cancer by epigenetic mechanisms. *Int J Biochem Cell Biol,* 43**,** 1668-73.

ZHUKOVA, N., RAMASWAMY, V., REMKE, M., MARTIN, D. C., CASTELO-BRANCO, P., ZHANG, C. H., . . . SHIH, D. J. 2014. WNT activation by lithium abrogates TP53 mutation associated radiation resistance in medulloblastoma. *Acta neuropathologica communications,* 2**,** 174.

ZOU, P., XIA, Y., CHEN, W., CHEN, X., YING, S., FENG, Z., . . . QIU, C. 2016. EF24 induces ROS-mediated apoptosis via targeting thioredoxin reductase 1 in gastric cancer cells. *Oncotarget,* 7**,** 18050.

ZUO, Z., ZHANG, P., LIN, F., SHANG, W., BI, R., LU, F., . . . JIANG, L. 2018. Interplay between Trx-1 and S100P promotes colorectal cancer cell epithelial-mesenchymal transition by up-regulating S100A4 through AKT activation. *J Cell Mol Med,* 22**,** 2430-2441.

# Appendix A: Supplementary Information for Chapter 2

**Table A1 Cell culture media formulations.**

| Cell Line | Reagents | Source | Volume |
|---|---|---|---|
| **SNB19 DAOY** | Minimum essential medium eagle (MEM) (with Earle's salts and sodium bicarbonate, without L-glutamine) | M2279, Sigma, UK | 500 ml |
| | Heat inactivated iron supplemented donor bovine serum | Gibco, Life Technologies, UK | 58 ml |
| | Penicillin/Streptomycin (10,000 units penicillin and 10 mg streptomycin/ml) | P0781, Sigma, UK | 5.8 ml |
| | L-Glutamine (200 mM) | G7513, Sigma, UK | 5.8 ml |
| | MEM non-essential amino acids solution (100x) | M7145, Sigma, UK | 5.8 ml |
| | Sodium pyruvate solution (100mM) | S8636, Sigma, UK | 5.8 ml |
| **SF188 KNS42** | Dulbecco's modified eagle medium: nutrient mixture F-12 (DMEM/F-12) | 21331-020,Gibco, Life Technologies, UK | 500 ml |
| | Heat inactivated iron supplemented donor bovine serum | Gibco, Life Technologies, UK | 57 ml |
| | Penicillin/Streptomycin (10,000 units penicillin and 10 mg streptomycin/ml) | P0781, Sigma, UK | 5.7 ml |
| | L-Glutamine (200 mM) | G7513, Sigma, UK | 5.7 ml |
| **UW228-3** | Dulbecco's modified eagle's medium/Nutrient Mixture F-12 Ham | D6421, Sigma, UK | 500 ml |
| | Heat inactivated iron supplemented donor bovine serum | Gibco, Life Technologies, UK | 91.5 ml |
| | Penicillin/Streptomycin (10,000 units penicillin and 10 mg streptomycin/ml) | G7513, Sigma, UK | 6.1 ml |
| | L-Glutamine (200 mM) | S8636, Sigma, UK | 6.1 ml |
| | Sodium pyruvate (100mM) | P0781, Sigma, UK | 6.1 ml |

**Table A1 Continued.**

| Cell Line | Reagents | Source | Volume |
|---|---|---|---|
| **MDA-MB-231** | Minimum essential medium eagle (MEM) (with Earle's salts and sodium bicarbonate, without L-glutamine) | M2279, Sigma, UK | 500 ml |
| | Heat inactivated iron supplemented donor bovine serum | Gibco, Life Technologies, UK | 57 ml |
| | Penicillin/Streptomycin (10,000 units penicillin and 10 mg streptomycin/ml) | P4333, Sigma, UK | 5.7 ml |
| | L-glutamine (200 mM) | G7513, Sigma, UK | 5.7 ml |
| | MEM non-essential amino acids solution (100x) | M7145, Sigma, UK | 5.7 ml |
| **MCF-7** | Dulbecco's Modified Eagle's Medium (DMEM) (with 4500 mg/L glucose, L-glutamine, and sodium bicarbonate, without sodium pyruvate) | D5796, Sigma, UK | 500 ml |
| | Heat inactivated iron supplemented donor bovine serum | Gibco, Life Technologies, UK | 56 ml |
| | Penicillin/Streptomycin (10,000 units penicillin and 10 mg streptomycin/ml) | P4333, Sigma, UK | 5.6 ml |
| **MRC5** | Minimum essential medium eagle (MEM) (with Earle's salts and sodium bicarbonate, without L-glutamine) | M2279, Sigma, UK | 500 ml |
| | Heat inactivated iron supplemented donor bovine serum | Gibco, Life Technologies, UK | 59 ml |
| | Penicillin/Streptomycin (10,000 units penicillin and 10 mg streptomycin/ml) | P0781, Sigma, UK | 5.9 ml |
| | L-glutamine (200 mM) | G7513, Sigma, UK | 5.9 ml |
| | MEM non-essential amino acids solution (100x) | M7145, Sigma, UK | 5.9 ml |
| | Hepes solution (1 M) | H0887, sigma, UK | 5.9 ml |
| | Sodium carbonate solution (7.5%) | S8761, Sigma, UK | 5.9 ml |
| **FB83** | RPMI-1640 medium | R8758, Sigma, UK | 500 ml |
| | Heat inactivated iron supplemented donor bovine serum | Gibco, Life Technologies, UK | 56 ml |
| | Penicillin/Streptomycin (10,000 units penicillin and 10 mg streptomycin/ml) | P4333, Sigma, UK | 5.6 ml |

**Table A2 Buffers for Western blotting.**

| Buffer | Preparation |
|---|---|
| 1X Running buffer | 50 ml 20X Bolt™ MES SDS running buffer (ThermoFisher Scientific) supplemented with 950 ml distilled $H_2O$. |
| 1X Transfer buffer | 50 ml 20X Bolt™ Transfer Buffer (ThermoFisher Scientific) mixed with 100 ml methanol to a total volume of 500 ml with distilled $H_2O$. |
| 0.1% PBS/Tween (PBS/T) | 1 ml Tween 20 (Sigma) dissolved in 1000 ml PBS. |
| Blocking buffer | 2.5 g milk powder (Marvel Original dried skimmed milk powder) dissolved in 50 ml 0.1% PBS/Tween. |

Abbreviations: SDS, sodium dodecyl sulfate; PBS, phosphate buffered saline.

**Table A3 Statistics of H-score of TrxR, Trx and TxNIP in adult GBM, paediatric LGG, paediatric HGG and MB cohorts.**

| Statistics | Adult GBM | | | | | | | | | Paediatric LGG | | | Paediatric HGG | | | MB | | |
|---|---|---|---|---|---|---|---|---|---|---|---|---|---|---|---|---|---|---|
| | Core | | | Rim | | | Invasive margin | | | | | | | | | | | |
| | TrxR | Trx | TxNIP | TrxR | Trx | TxNIP | TrxR | Trx | TxNIP | TrxR | Trx | TxNIP | TrxR | Trx | TxNIP | TrxR | Trx | TxNIP |
| **N (Valid)** | 14 | 12 | 16 | 15 | 15 | 15 | 12 | 7 | 7 | 87 | 87 | 89 | 104 | 107 | 95 | 82 | 80 | 79 |
| **N** | 4 | 6 | 2 | 3 | 3 | 3 | 5 | 10 | 10 | 49 | 49 | 47 | 63 | 60 | 72 | 32 | 34 | 35 |
| **Mean** | 100.7 | 98.1 | 152.7 | 114.4 | 101.3 | 144.3 | 80.5 | 110.0 | 158.6 | 118.9 | 100.8 | 154 | 80.6 | 117.2 | 180.6 | 130.3 | 134.5 | 148.9 |
| **SEM** | 13.5 | 19.5 | 14.4 | 8.8 | 15.4 | 14.2 | 5.6 | 6.8 | 12.0 | 5.1 | 5.7 | 7.7 | 6.3 | 6.5 | 6.7 | 5.9 | 7.1 | 7.4 |
| **Median** | 78 | 122 | 168 | 100 | 105 | 140 | 86 | 105 | 170 | 120 | 97 | 173 | 67 | 110 | 192 | 130 | 137 | 150 |
| **SD** | 50.4 | 67.6 | 57.5 | 34.2 | 59.7 | 55.1 | 19.3 | 18.0 | 31.8 | 47.8 | 53.1 | 72.8 | 64.5 | 66.8 | 65.1 | 53.4 | 63.4 | 65.8 |
| **Range** | 157 | 180 | 198 | 113 | 198 | 192 | 55 | 50 | 80 | 230 | 273 | 280 | 217 | 283 | 270 | 270 | 280 | 258 |
| **Minimum** | 30 | 5 | 30 | 77 | 0 | 30 | 50 | 90 | 115 | 5 | 0 | 0 | 0 | 0 | 10 | 0 | 0 | 12 |
| **Maximum** | 187 | 185 | 228 | 190 | 198 | 222 | 105 | 140 | 195 | 235 | 273 | 280 | 217 | 283 | 280 | 270 | 280 | 270 |

Abbreviations: SEM, standard error of mean; SD, standard deviation.

**Table A4 Statistics of nuclear score of TrxR and Trx in adult GBM, paediatric LGG, paediatric HGG and MB cohorts.**

| Statistics | Adult GBM | | | | | | Paediatric LGG | | Paediatric HGG | | MB | |
|---|---|---|---|---|---|---|---|---|---|---|---|---|
| | Core | | Rim | | Invasive | | | | | | | |
| | TrxR | Trx | TrxR | Trx | TrxR | Trx | TrxR | Trx | TrxR | Trx | TrxR | Trx |
| **N (Valid)** | 14 | 12 | 15 | 15 | 12 | 7 | 87 | 87 | 104 | 107 | 82 | 80 |
| **N (Missing)** | 4 | 6 | 3 | 3 | 5 | 10 | 49 | 49 | 63 | 60 | 32 | 34 |
| **Mean** | 47 | 35 | 72 | 34 | 79 | 52 | 55 | 19 | 36 | 30 | 64 | 38 |
| **SEM** | 7.1 | 9.8 | 6.3 | 8.4 | 5.2 | 10.1 | 3 | 2.1 | 3.1 | 2.7 | 3.3 | 3.0 |
| **Median** | 48.5 | 37.5 | 80 | 23 | 85 | 60 | 57 | 12 | 27.5 | 20 | 73 | 34 |
| **SD** | 26.4 | 33.9 | 24.0 | 32. | 18.1 | 26.7 | 28.4 | 19.2 | 31.4 | 27.9 | 30.2 | 26.7 |
| **Rang** | 88 | 90 | 85 | 90 | 53 | 75 | 95 | 88 | 100 | 98 | 100 | 99 |
| **Minimum** | 7 | 0 | 15 | 0 | 45 | 10 | 0 | 0 | 0 | 0 | 0 | 0 |
| **Maximum** | 95 | 90 | 100 | 90 | 98 | 85 | 95 | 88 | 100 | 98 | 100 | 99 |

No nuclear staining was observed for TxNIP expression. Abbreviations: SEM, standard error of mean; SD, standard deviation.

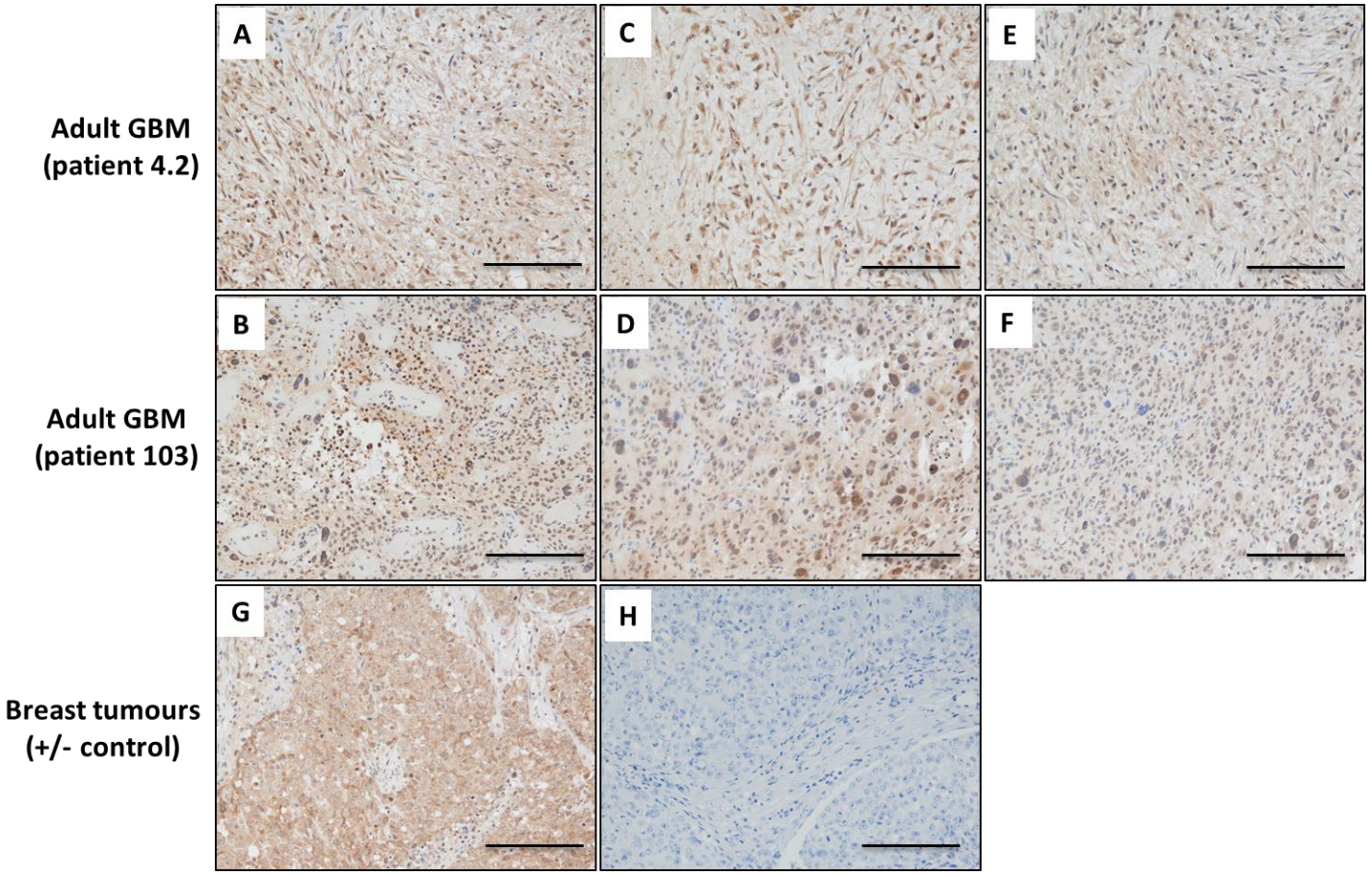



**Figure A1 Optimisation of anti-TrxR antibody on adult GBM and breast tumour tissues.** Brain and breast tissue sections were subjected to immunohistochemistry. (A and B) 1:100 dilution of primary antibody; (C and D) 1:150 dilution; (E and F) 1:300 dilution. Photomicrographs are at 10X magnification. Scale bar represents 100 µm.

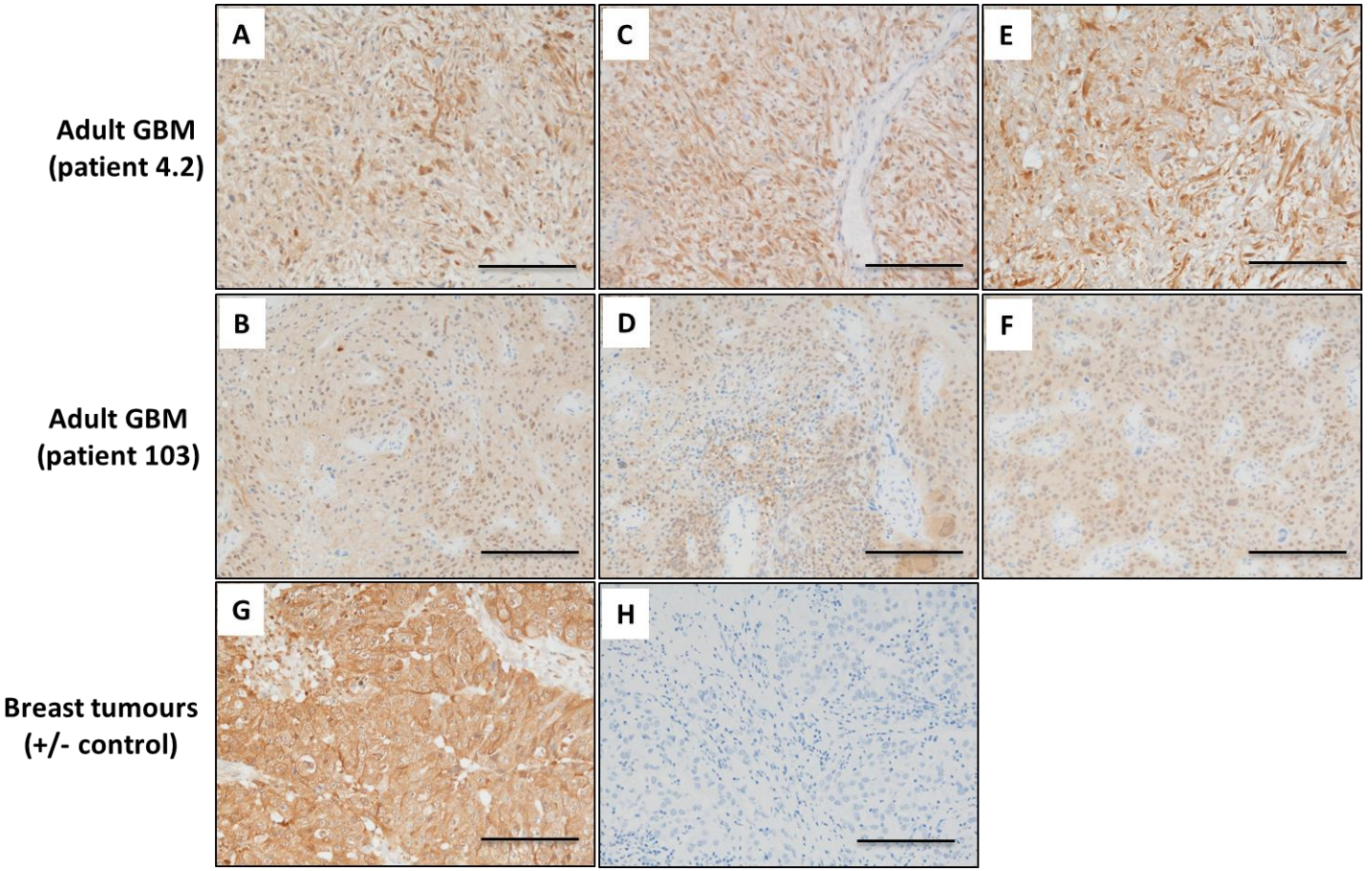



**Figure A2 Optimisation of anti-Trx antibody on adult GBM and breast tumour tissues.** Brain and breast tissue sections were subjected to immunohistochemistry. (A and B) 1:2000 dilution of primary antibody; (C and D) 1:3000 dilution; (E and F) 1:4000 dilution. Photomicrographs are at 10X magnification. Scale bar represents 100 µm.

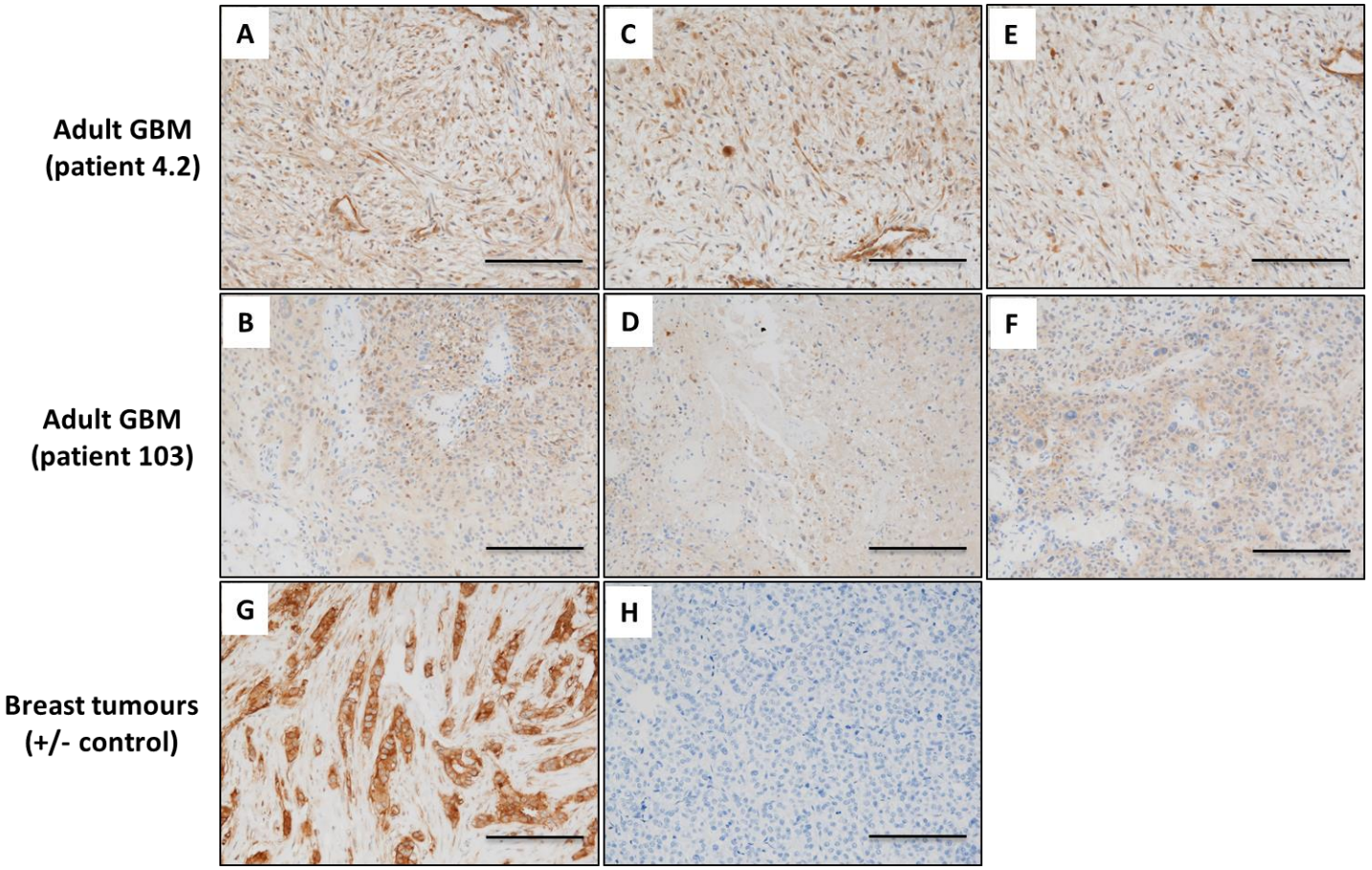



**Figure A3 Optimisation of anti-TxNIP antibody on adult GBM and breast tumour tissues.** Brain and breast tissue sections were subjected to immunohistochemistry. (A and B) 1:250 dilution of primary antibody; (C and D) 1:500 dilution; (E and F) 1:1000 dilution. Photomicrographs are at 10X magnification. Scale bar represents 100 µm.

**Table A5 Associations between TrxR expression and clinicopathological variables in adult GBM (Core).**

| Variable | Cytoplasmic TrxR | | | Nuclear TrxR | | |
|---|---|---|---|---|---|---|
| | Low | High | *P*-value | Low | High | *P*-value |
| Age (years) | | | | | | |
| ≤ 59 | 5 (35.7%) | 4 (28.6%) | 1.000 | 7 (50.0%) | 2 (14.3%) | 0.580 |
| > 59 | 2 (14.3%) | 3 (21.4%) | | 3 (21.4%) | 2 (14.3%) | |
| Gender | | | | | | |
| Male | 2 (14.3%) | 5 (35.7%) | 0.592 | 6 (42.9%) | 1 (7.1%) | 0.559 |
| Female | 4 (28.6%) | 3 (21.4%) | | 4 (28.6%) | 3 (21.4%) | |
| Tumour site | | | | | | |
| Parietal | 3 (21.4%) | 4 (28.6%) | 0.613 | 7 (50.0%) | 0 (0.0%) | **0.008** |
| Temporal | 1 (7.1%) | 2 (14.3%) | | 0 (0.0%) | 3 (21.4%) | |
| Occipital | 1 (7.1%) | 0 (0.0%) | | 1 (7.1%) | 0 (0.0%) | |
| Frontal | 2 (14.3%) | 1 (7.1%) | | 2 (14.3%) | 1 (7.1%) | |
| Resection status | | | | | | |
| Complete | 5 (35.7%) | 8 (57.1%) | 0.429 | 6 (42.9%) | 7 (50.0%) | 1.000 |
| Partial | 1 (7.1%) | 0 (0.0%) | | 1 (7.1%) | 0 (0.0%) | |
| IDH-1 status | | | | | | |
| Wild-type | 7 (50.0%) | 6 (42.9%) | 1.000 | 10 (71.4%) | 3 (21.4%) | 0.286 |
| Mutant | 0 (0.0%) | 1 (7.1%) | | 0 (0.0%) | 1 (7.1%) | |

The *P* values are resultant from the Pearson $\chi^2$ test of association or Fisher's Exact test if a cell count was less than five. Significant *P* values are indicated in bold. The number and percentage of observations for cohort is shown for each clinicopathological variable. Abbreviations: GBM, glioblastoma.

**Table A6 Associations between TrxR expression and clinicopathological variables in adult GBM (Invasive margin).**

| Variable | Cytoplasmic TrxR | | | Nuclear TrxR | | |
|---|---|---|---|---|---|---|
| | Low | High | *P*-value | Low | High | *P*-value |
| Age (years) | | | | | | |
| ≤ 59 | 5 (41.7%) | 3 (25.0%) | 0.545 | 5 (41.7%) | 3 (25.0%) | 0.545 |
| > 59 | 1 (8.3%) | 3 (25.0%) | | 1 (8.3%) | 3 (25.0%) | |
| Gender | | | | | | |
| Male | 0 (0.0%) | 5 (41.7%) | **0.015** | 1 (8.3%) | 4 (33.3%) | 0.417 |
| Female | 6 (50.0%) | 1 (8.3%) | | 0 (0.0%) | 7 (58.3%) | |
| Tumour site | | | | | | |
| Parietal | 1 (8.3%) | 3 (25.0%) | 0.096 | 3 (25.0%) | 1 (8.3%) | 0.379 |
| Temporal | 4 (33.3%) | 0 (0.0%) | | 1 (8.3%) | 3 (25.0%) | |
| Occipital | 0 (0.0%) | 1 (8.3%) | | 0 (0.0%) | 1 (8.3%) | |
| Frontal | 1 (8.3%) | 2 (16.7%) | | 1 (8.3%) | 2 (16.7%) | |
| Resection status | | | | | | |
| Complete | 2 (16.7%) | 7 (58.3%) | 0.236 | 4 (33.3%) | 5 (41.7%) | 1.000 |
| Partial | 2 (16.7%) | 1 (8.3%) | | 2 (16.7%) | 1 (8.3%) | |
| IDH-1 status | | | | | | |
| Wild-type | 5 (41.7%) | 6 (50.0%) | 1.000 | 6 (50.0%) | 5 (41.7%) | 1.000 |
| Mutant | 1 (8.3%) | 0 (0.0%) | | 0 (0.0%) | 1 (8.3%) | |

The *P* values are resultant from the Pearson $\chi^2$ test of association or Fisher's Exact test if a cell count was less than five. Significant *P* values are indicated in bold. The number and percentage of observations for cohort is shown for each clinicopathological variable. Abbreviations: GBM, glioblastoma.

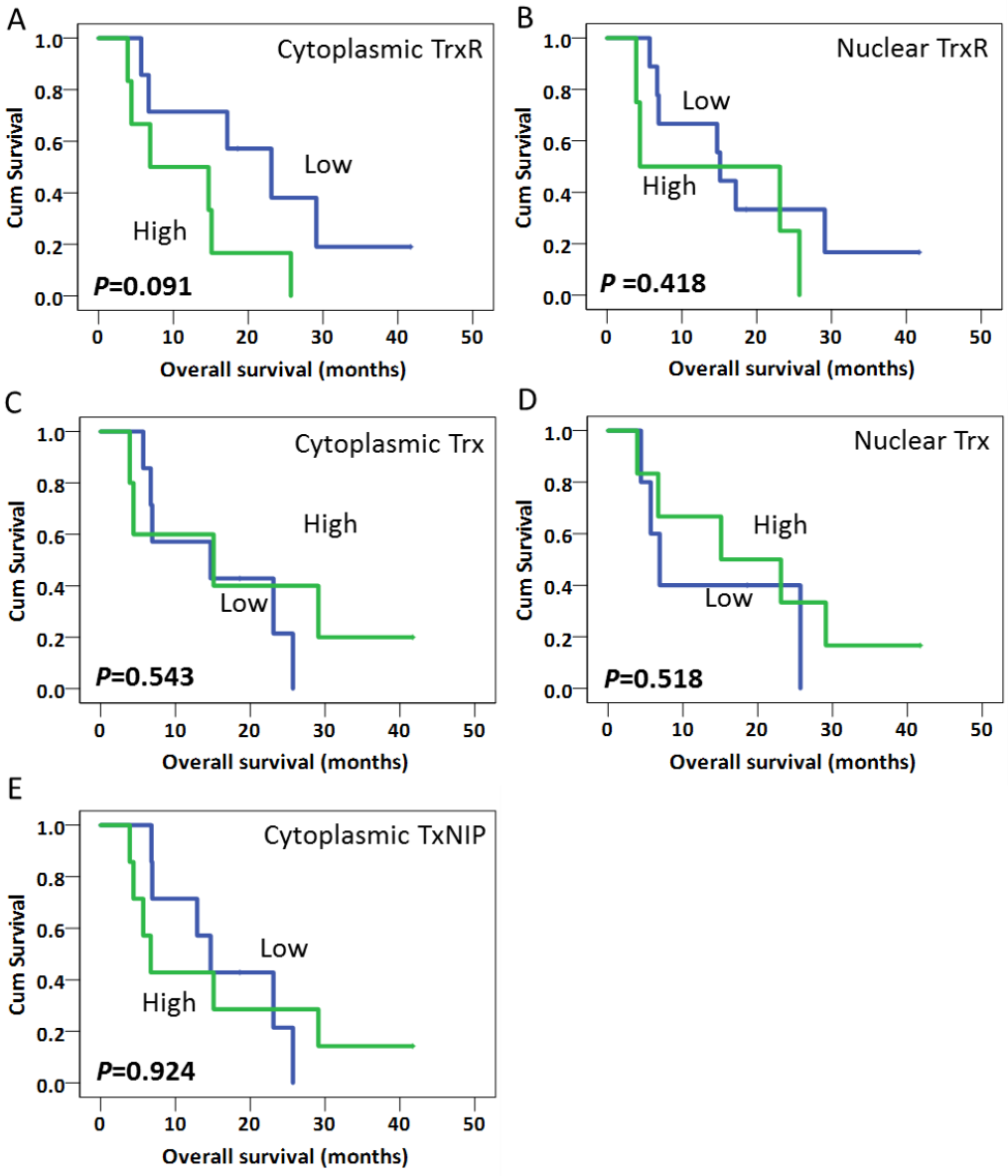



**Figure A4 Kaplan-Meier survival curves of TrxR, Trx and TxNIP expression and overall survival in the adult GBM cohort (core).** No significant associations were found between TrxR (A and B), Trx (C and D) and TxNIP (E) expression and overall survival (all *P* values > 0.05). Curves show low (blue line) and high protein expression (green line) with significance determined using the log-rank test.

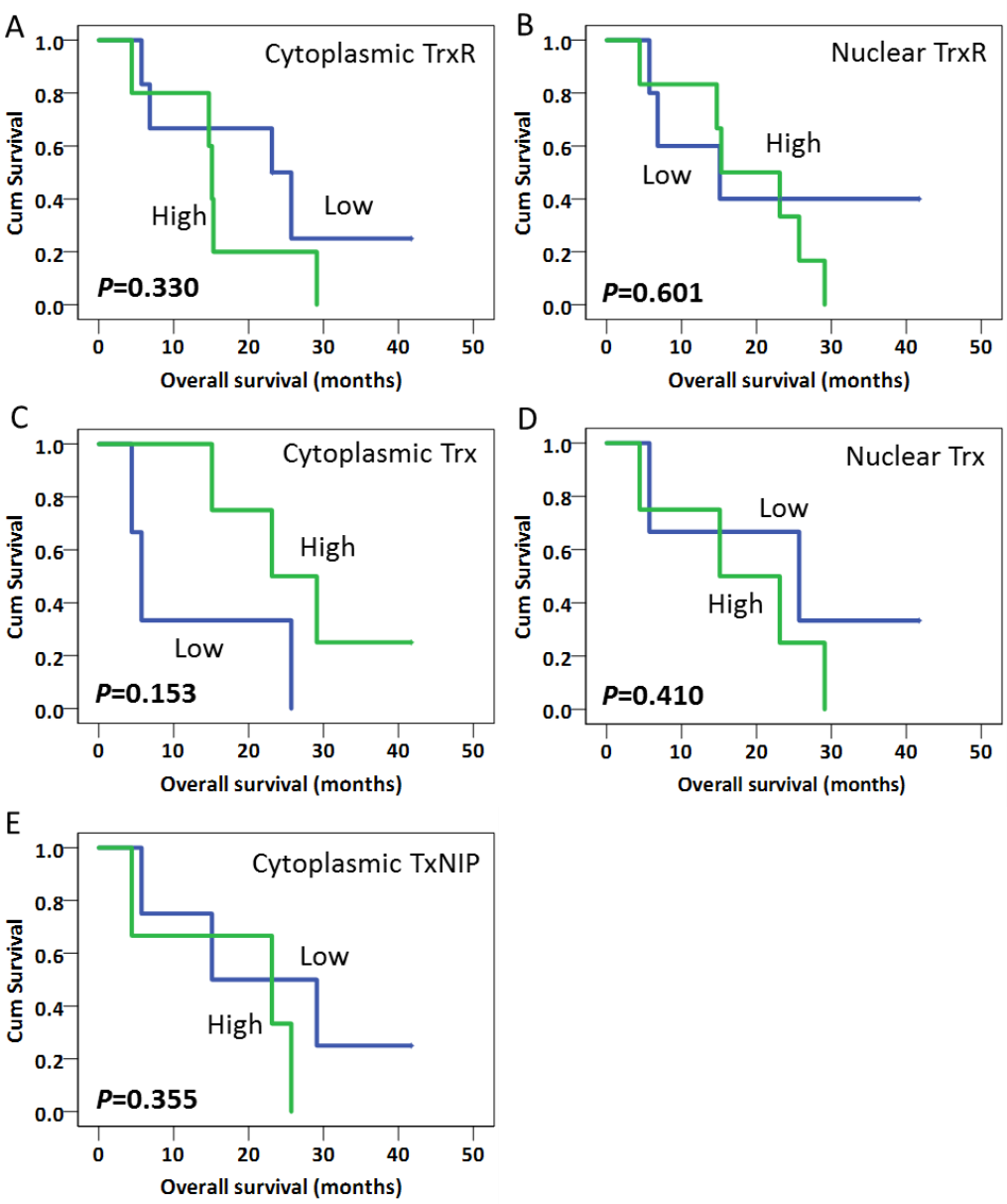



**Figure A5 Kaplan-Meier survival curves of TrxR, Trx and TxNIP expression and overall survival in the adult GBM cohort (invasive margin).** No significant associations were found between TrxR (A and B), Trx (C and D) and TxNIP (E) expression and overall survival (all *P* values > 0.05). Curves show low (blue line) and high protein expression (green line) with significance determined using the log-rank test.

**Table A7 Associations between TrxR, Trx and TxNIP expression and clinicopathological variables in paediatric LGG.**

| Variable | Cytoplasmic TrxR | | | Nuclear TrxR | | | Cytoplasmic Trx | | | Nuclear Trx | | | Cytoplasmic TxNIP | | |
|---|---|---|---|---|---|---|---|---|---|---|---|---|---|---|---|
| | **Low** | **High** | ***P*** | **Low** | **High** | ***P*** | **Low** | **High** | ***P*** | **Low** | **High** | ***P*** | **Low** | **High** | ***P*** |
| Age | | | | | | | | | | | | | | | |
| ≤3 | 13 (15.1%) | 5 (5.8%) | 0.292 | 9 (10.3%) | 10 (11.5%) | 0.752 | 3 (3.4%) | 16 (18.4%) | 0.403 | 9 (10.6%) | 9 (10.6%) | 0.778 | 3 (3.4%) | 16 (18.0%) | 0.395 |
| >3 | 58 (67.4%) | 10 (11.6%) | | 35 (40.2%) | 33 (37.9%) | | 6 (6.9%) | 62 (71.3%) | | 36 (42.4%) | 31 (36.5%) | | 6 (6.7%) | 64 (71.9%) | |
| Gender | | | | | | | | | | | | | | | |
| Male | 32 (44.4%) | 6 (8.3%) | 0.833 | 18 (24.7%) | 20 (27.4%) | 0.887 | 5 (6.8%) | 33 (44.6%) | 0.712 | 16 (22.2%) | 21 (29.2%) | 0.155 | 4 (5.3%) | 34 (44.7%) | 1.000 |
| Female | 28 (38.9%) | 6 (8.3%) | | 16 (21.9%) | 19 (26.0%) | | 3 (4.1%) | 33 (44.6%) | | 21 (29.2%)) | 14 (19.4%) | | 5 (6.6%) | 33 (43.4%) | |
| Tumour site | | | | | | | | | | | | | | | |
| Supratentorial | 12 (17.4%) | 7 (10.1%) | **0.003** | 10 (14.3%) | 10 (14.3%) | 0.649 | 2 (2.8%) | 19 (26.8%) | 1.000 | 11 (15.9%) | 10 (14.5%) | 0.733 | 7 (9.7%) | 15 (20.8%) | **0.041** |
| Infratentorial | 47 (68.1%) | 3 (4.3%) | | 22 (31.4%) | 28 (40.0%) | | 6 (8.5%) | 44 (62.0%) | | 23 (33.3%) | 25 (36.2%) | | 29 (40.3%) | 21 (29.2%) | |
| Recurrence | | | | | | | | | | | | | | | |
| No | 42 (60.0%) | 3 (4.3%) | **0.006** | 17 (23.9%) | 29 (40.8%) | **0.029** | 3 (4.2%) | 44 (61.1%) | 0.116 | 21 (30.0%) | 24 (34.3%) | 0.285 | 4 (5.4%) | 43 (58.1%) | 0.273 |
| Yes | 16 (22.9%) | 9 (12.9%) | | 16 (22.5%) | 9 (12.7%) | | 5 (6.0%) | 20 (27.8%) | | 15 (21.4%) | 10 (14.3%) | | 5 (6.8%) | 22 (29.7%) | |

The *P* values are resultant from the Pearson $\chi^2$ test of association or Fisher's Exact test if a cell count was less than five. Significant P values are indicated in bold. The number and percentage of observations for cohort is shown for each clinicopathological variable. The table does not include the number of observations where clinicopathological data or scores were not available. Abbreviations: LGG, low-grade glioma.

**Table A8 Associations between Trx expression and clinicopathological variables in paediatric HGG.**

| Variable | Cytoplasmic Trx | | | Nuclear Trx | | |
|---|---|---|---|---|---|---|
| | Low | High | *P*-value | Low | High | *P*-value |
| **Age** | | | | | | |
| **≤3** | 16 (15.0%) | 2 (1.9%) | 0.145 | 17 (15.7%) | 1 (0.9%) | 0.188 |
| **>3** | 62 (57.9%) | 27 (25.2%) | | 72 (66.7%) | 18 (16.7%) | |
| **Gender** | | | | | | |
| **Male** | 41 (51.3%) | 9 (11.3%) | 0.564 | 41 (51.3%) | 9 (11.3%) | 0.520 |
| **Female** | 23 (28.8%) | 7 (8.8%) | | 27 (33.8%) | 3 (3.8%) | |
| **Histological subtypes** | | | | | | |
| **AA** | 16 (20.8%) | 2 (2.6%) | **0.008** | 16 (20.8%) | 2 (2.6%) | 0.189 |
| **GBM** | 42 (54.5%) | 9 (11.7%) | | 44 (57.1%) | 7 (9.1%) | |
| **AO** | 3 (3.9%) | 5 (6.5%) | | 5 (6.5%) | 3 (3.9%) | |
| **Tumour site** | | | | | | |
| **Supratentorial** | 52 (67.5%) | 14 (18.2%) | 1.000 | 55 (71.4%) | 11 (14.3%) | 1.000 |
| **Infratentorial** | 9 (11.7%) | 2 (2.6%) | | 10 (13.0%) | 1 (1.3%) | |
| **WHO grade** | | | | | | |
| **III** | 19 (24.7%) | 6 (7.8%) | 0.545 | 21 (27.3%) | 4 (5.2%) | 0.741 |
| **IV** | 43 (55.8%) | 9 (11.7%) | | 45 (58.4%) | 7 (9.1%) | |
| **Extent of resection** | | | | | | |
| **Gross total** | 12 (18.5%) | 1 (1.5%) | 0.446 | 13 (20.0%) | 0 (0.0%) | 0.141 |
| **Subtotal** | 25 (38.5%) | 8 (12.3%) | | 25 (38.5%) | 8 (12.3%) | |
| **Biopsy** | 15 (23.1%) | 4 (6.2%) | | 16 (24.6%) | 3 (4.6%) | |
| **Recurrence** | | | | | | |
| **No** | 10 (14.5%) | 0 (0.0%) | 0.189 | 9 (13.0%) | 1 (1.4%) | 1.000 |
| **Yes** | 46 (66.7%) | 13 (18.8%) | | 50 (72.5%) | 9 (13.0%) | |

The *P* values are resultant from the Pearson $\chi^2$ test of association or Fisher's Exact test if a cell count was less than five. Significant P values are indicated in bold. The number and percentage of observations for cohort is shown for each clinicopathological variable. Abbreviations: HGG, high-grade glioma; AA, anaplastic astrocytoma; GBM, glioblastoma; AO, anaplastic oligodendroglioma.

**Table A9 Associations between TxNIP expression and clinicopathological variables in paediatric HGG.**

| Variable | Cytoplasmic TxNIP | | |
|---|---|---|---|
| | Low | High | *P*-value |
| **Age** | | | |
| **≤3** | 6 (6.3%) | 11 (11.6%) | 0.114 |
| **>3** | 44 (46.3%) | 34 (35.8%) | |
| **Gender** | | | |
| **Male** | 21 (30.0%) | 25 (35.7%) | 0.314 |
| **Female** | 14 (20.0%) | 10 (14.3%) | |
| **Histological subtypes** | | | |
| **AA** | 12 (17.9%) | 3 (4.5%) | **0.009** |
| **GBM** | 17 (25.4%) | 28 (41.8%) | |
| **AO** | 5 (7.5%) | 2 (3.0%) | |
| **Tumour site** | | | |
| **Supratentorial** | 25 (36.8%) | 32 (47.1%) | **0.021** |
| **Infratentorial** | 9 (13.2%) | 2 (2.9%) | |
| **WHO grade** | | | |
| **III** | 16 (23.9%) | 5 (7.5%) | **0.005** |
| **IV** | 18 (26.9%) | 28 (41.8%) | |
| **Extent of resection** | | | |
| **Gross total** | 8 (13.3%) | 4 (6.7%) | 0.333 |
| **Subtotal** | 13 (21.7%) | 18 (30.0%) | |
| **Biopsy** | 9 (15.0%) | 8 (13.3%) | |
| **Recurrence** | | | |
| **No** | 7 (11.3%) | 3 (4.8%) | 0.167 |
| **Yes** | 24 (38.7%) | 28 (45.2%) | |

The *P* values are resultant from the Pearson $\chi^2$ test of association or Fisher's Exact test if a cell count was less than five. Significant P values are indicated in bold. The number and percentage of observations for cohort is shown for each clinicopathological variable. Abbreviations: HGG, high-grade glioma; AA, anaplastic astrocytoma; GBM, glioblastoma; AO, anaplastic oligodendroglioma.

**Table A10 Association between Trx expression and clinicopathological variables in MB.**

| Variable | Cytoplasmic Trx | | | Nuclear Trx | | |
|---|---|---|---|---|---|---|
| | Low | High | *P*-value | Low | High | *P*-value |
| Age | | | | | | |
| ≤3 | 7 (8.8%) | 5 (6.3%) | 0.495 | 9 (11.3%) | 3 (3.8%) | 0.711 |
| >3 | 49 (61.3%) | 19 (23.8%) | | 54 (67.5%) | 14 (17.5%) | |
| Gender | | | | | | |
| Male | 35 (46.7%) | 15 (20.0%) | 0.859 | 40 (53.3%) | 10 (13.3%) | 0.690 |
| Female | 17 (22.7%) | 8 (10.7%) | | 19 (25.3%) | 6 (8.0%) | |
| Histological subtypes | | | | | | |
| Classic | 28 (45.2%) | 15 (24.2%) | 0.149 | 35 (56.5%) | 8 (12.9%) | **0.041** |
| Desmoplastic/nodular | 7 (11.3%) | 1 (1.6%) | | 7 (11.3%) | 1 (1.6%) | |
| MB with extensive nodularity | 0 (0.0%) | 2 (3.2%) | | 0 (0.0%) | 2 (3.2%) | |
| Large cell/ anaplastic | 5 (8.1%) | 2 (3.2%) | | 4 (6.5%) | 3 (4.8%) | |
| Medullomyoblastoma | 2 (3.2%) | 0 (0.0%) | | 2 (3.2%) | 0 (0.0%) | |
| Extent of resection | | | | | | |
| Complete | 26 (44.1%) | 11 (18.6%) | 0.559 | 20 (33.9%) | 2 (3.4%) | 0.179 |
| Partial | 17 (28.8%) | 5 (8.5%) | | 27 (45.8%) | 10 (16.9%) | |
| Recurrence | | | | | | |
| Yes | 18 (28.1%) | 14 (21.9%) | **0.031** | 21 (32.8%) | 11 (17.2%) | **0.016** |
| No | 26 (40.6%) | 6 (9.4%) | | 29 (45.3%) | 3 (4.7%) | |
| Metastasis | | | | | | |
| Absence | 28 (45.9%) | 10 (16.4%) | 0.482 | 31 (50.8%) | 7 (11.5%) | 1.000 |
| Presence | 15 (24.6%) | 8 (13.1%) | | 19 (31.1%) | 4 (6.6%) | |

The *P* values are resultant from the Pearson $\chi^2$ test of association or Fisher's Exact test if a cell count was less than five. Significant *P* values are indicated in bold. The number and percentage of observations for cohort is shown for each clinicopathological variable. Abbreviations: MB, medulloblastoma.

# Appendix B: Supplementary Information for Chapter 4

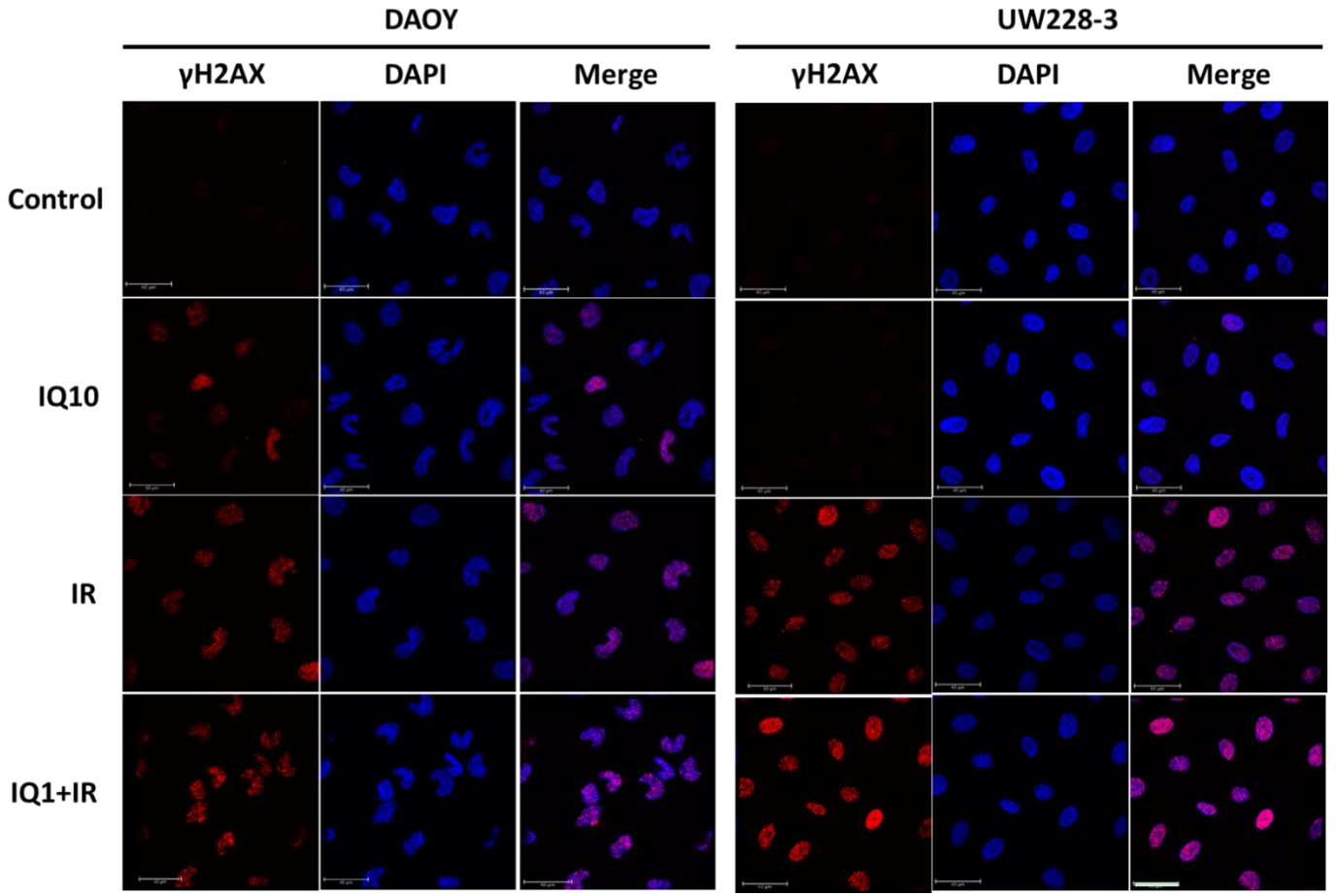



**Figure B1 Representative images of γH2AX immunofluorescent staining in DAOY and UW228-3 cells (63X).** Red, γH2AX; Blue, DAPI fluorescent stain. Scale bar = 40 µm.